МІНІСТЕРСТВО ОСВІТИ ТА НАУКИ УКРАЇНИ

НАЦІОНАЛЬНИЙ ТЕХНІЧНИЙ УНІВЕРСИТЕТ
«ХАРКІВСЬКИЙ ПОЛІТЕХНІЧНИЙ ІНСТИТУТ»

Ministry of Education & Science of Ukraine
National Technical University
«Kharkiv Polytechnic Institute»

РІЗАННЯ ТА ІНСТРУМЕНТИ в технологічних системах

CUTTING & TOOLS IN TECHNOLOGICAL SYSTEM

Міжнародний науково-технічний збірник
International Scientific-Technical Collection

Заснований у 1966 р. М. Ф. Семко
Found by M. F. Semko in 1966

ВИПУСК № 99
Edition № 99

Харків НТУ «ХПІ» – 2023 – Kharkiv NTU «KhPI»

ББК 34.63
УДК 621.91

Державне видання
Свідоцтво Державного комітету телебачення і радіомовлення України
КВ № 7840 від 8 вересня 2003 року
Друкується за рішенням Вченої Ради НТУ "ХПІ",
протокол № 10 від 01 грудня 2023 р.

У збірнику представлені наукові статті, в яких розглядаються актуальні питання в області механічної обробки різних сучасних матеріалів із застосуванням високопродуктивних технологій, нових методик, вимірювальних приладів для контролю якості оброблених поверхонь і високоефективних різальних інструментів. Розглядаються аспекти оптимізації та математичного моделювання на різних етапах технологічного процесу.

Для інженерів і наукових співробітників, що працюють в області технології машинобудування, різання матеріалів, проектування різальних інструментів в технологічних системах.

Науковий збірник «Різання та інструменти в технологічних системах» включений в Перелік фахових видань України категорії «Б», наказ МОН України від 17.03.2020 р., № 409

Р34 Резание и инструменты в технологических системах: Междунар. науч.- техн. сб. – Харьков: НТУ «ХПИ», 2023. – Вып. 99. – 166 с.

Адреса редакційної колегії: вул. Кирпичова, 2, Харків, 61002, Національний технічний університет «Харківський політехнічний інститут», кафедра «Інтегровані технології машинобудування» ім. М.Ф. Семка, тел. +38 (057) 706-41-43.

ББК 34.63
Матеріали відтворені з авторських оригіналів
НТУ «ХПІ», 2023

UDC 621.914.1 **doi: 10.20998/2078-7405.2023.99.01**

ANALYSIS OF THE EFFECT OF VARYING THE CUTTING RATIO ON FORCE COMPONENTS AND SURFACE ROUGHNESS IN FACE MILLING

Csaba **Felhő** [0000-0003-0997-666X]

University of Miskolc, 3515, Miskolc - Egyetemváros, Hungary
csaba.felho@uni-miskolc.hu

Received: 15 November 2023 / Revised:20 November 2023 / Accepted: 25 November 2023 / Published: 01 December 2023

Abstract. *Traditional machining processes, such as face milling, still play a very important role in the production of machine parts and are the subject of ongoing research. One important area of research is the investigation of high-feed milling processes. However, due to the increased feed per tooth value f_z, it is advisable to reduce the depth of cut (a_p) in order to maintain the cutting forces at an appropriate level. In this way, the ratio of these two technological parameters, the so-called cutting ratio, changes and we can move into the range of inverse machining, where $a_p / f_z < 1$. In this paper, the consequences of this change is investigated on the surface roughness and the components of the cutting force, and it is discussed how the optimal cutting ratio can be found.*
Keywords: *high feed milling; cutting force components, surface roughness.*

1. INTRODUCTION

Face milling is a very frequently used process in the production of various machine parts. It is an unavoidable procedure during the production of practically all larger flat surfaces. As a consequence of this, researchers have long been interested in examining, perfecting, and pushing the limits of the process [1]. Nevertheless, it still has areas that are unexploited and still need to be investigated [2].

The topic of the paper is the experimental investigation of the effect of changing the so-called cutting ratio (which is the ratio of the depth of cut to the feed, a_p / f_z) on the components of the cutting force and the roughness of the machined surface during face milling. Traditionally, this cutting ratio is usually a value greater than one ($a_p / f_z > 1$), which means that the allowance is removed with a large layer thickness, but at a low speed. At the same time, nowadays, high-speed milling is becoming more and more a trend, where the feed is drastically increased, and a given layer is removed in much less time [2]. At the same time, due to the increase in feed, it is necessary to reduce the depth of cut, because otherwise the cutting forces may be unmanageably high due to the increase in the chip cross-section [3], [4]. Since the blank products are also manufactured according to increasingly strict tolerances, there is often no need to use more than one cuts, so the entire processing is faster

and more economical [5]. Nowadays, machining processes are designed to use the maximum possible machine power and simultaneously ensure the required surface roughness, because there is simply no time to perform roughing and smoothing operations sequentially [6], [7]. So, in fact, the problem to be solved is to remove the same chip cross-section with as much feed as possible and, correspondingly, with as little depth of cut as possible, while ensuring the appropriate performance and roughness data [8]–[10]. That is why the researchers worked on the integration of several different shaped milling inserts into one milling head [11]. At the same time, the use of so-called wiper inserts to smooth-out the milled surface can be considered a common practice [12]. However, the use of a wiper insert sometimes can have negative impact on the stability of the process, so in some cases it is more practical to use a curved invert to avoid unwanted vibrations [9]. The design of the cutting edge is also of great importance when cutting with defined edge geometry [13].

In the present paper, it was investigated what effect the removal of a constant chip cross-section with a changed cutting ratio has on the components of the cutting force, as well as on the surface roughness In particular, we have experimentally investigated the combined effect of the changed technological data on force and roughness, and we were looking for the optimum point up to which it makes sense to increase the feed rate with decreasing depth of cut.

2. MATERIALS AND METHODS

This section describes the machines and tools used, the characteristics of the specimens, and the measuring and other instruments. The setup used in the cutting experiments is shown in Figure 1. A Perfect Jet MCV-M8 type vertical three-dimensional CNC milling machine, a product of the Taiwan-based Ping Jeng Machinery company, was used for the tests. This equipment is specifically designed for high precision, high rigidity and high-speed machining.

Figure 1. The experimental setup used for the cutting tests

During the experiments, a CoroMill 200 R200-068Q27-12L face milling head was used. A CoroMill RCKT 1204M0-PM S40T grade coated carbide round insert was clamped into the milling head, but only one insert was cutting in the milling head at a time (this process variant is also known as fly-cutting, and it is often used for experimental investigations).

The careful selection of the feed and depth of cut values used during the tests was ensured that both traditional and inverse milling ratio values were included. Based on the above, it is considered conventional cutting if the cutting ratio $a_p/f_z > 1$ and inverse if $a_p / f_z < 1$. When choosing the feed values, the tool manufacturer's recommendations were first taken into account, which for this insert is between 0.1 – 0.3 mm for the used C45 steel material. However, in order to ensure the inverse chip ratio, it was also necessary to test feed values much higher than this, so the feed range used in practice was between 0.1 – 1 mm. Since, at the same time, by changing the depth of cut, the theoretical chip cross-section was kept at a constant value (A_c = 0.1 mm^2), so the larger feed could be safely used. The feed and depth of cut values selected according to the above principles are contained in Table 1.

Table 1. Feed rate and depth of cut values used during the tests

Sample No.	1.	2.	3.	4.	5.
Feed per tooth f_t [mm/tooth]	0.1	0.2	0.316	0.5	1
Depth of cut a_p [mm]	1	0.5	0.316	0.2	0.1
Cutting ratio a_p/f_z	10	2.5	1	0.4	0.1

As can be seen in the table, in addition to the two conventional and two inverse cutting ratios, in one case the depth of cut and the feed rate were the same (0.316 mm), here the cutting ratio is $a_p / f_z = 1$. This can be considered a special borderline case. Additional technological data were as follows: spindle speed n = 986 RPM, cutting speed v_c = 270 m/min, which were chosen according to the parameters of the milling machine and the recommendations of the tool manufacturer.

The dimensions of the used test specimen can be seen in Fig. 2, its material is the previously mentioned C45 material quality, the main characteristics of which are shown in Table 2. The center line of the milling head was set to the center of the workpiece.

Table 2: Chemical composition and mechanical properties of C45 steel [14]

Chemical Composition (average), [%]								
C	**Mn**	**Si**	**P**	**S**	**Cr**	**Ni**	**Mo**	**Fe**
0.48	0.74	0.36	0.011	0.01	0.09	0.02	0.002	rest
Yield Strength (min.)						Re=430MPa		
Tensile strength(min.)						Rm=740MPa		

Hardness(min.)	250HB

During milling, the components of the cutting force were measured and recorded using the force measuring instrument inserted in the machining system. The force was measured by detecting the force components in the x, y and z directions acting on the workpiece attached to the Kistler 9257A type dynamometer which was clamped to the machine table.

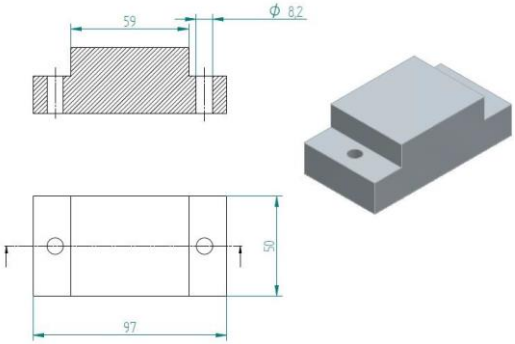

Figure 2. Main geometric characteristics of the used specimen

The dynamometer signals were transmitted by 3 Kistler 5011A charge amplifiers to the National Instruments CompactDAQ-9171 type four-channel data acquisition unit, which communicated with the connected computer via a USB port. The data obtained in this way were processed, displayed and recorded by a measuring program created in the LabView system. The milling configuration used, the main process parameters and the directions of the cutting force components acting on the workpiece are shown in Fig. 3.

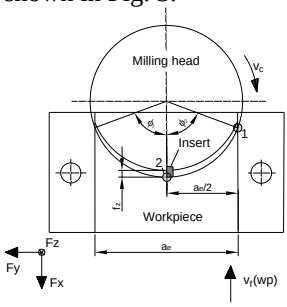

Figure 3. The milling setup and axis directions for force measurements

Two notable points are marked on Fig. 3: Point 1 is the entry point of the insert, and Point 2 is the intersection of the centre line of the tool with the tip of the insert. This is a point of interest because it is at this point that the force data were evaluated and the comparisons were made. It is well known that the surface roughness value is always highest when measured at the centre line, so the 2*D* roughness data reported in the results were also measured here, and it is useful to compare them with the corresponding force data.

The surface roughness was measured using an AltiSurf 520 three-dimensional surface roughness measuring device with a CL2 type confocal chromatic distance measuring sensor. The measuring head was also equipped with an MG140 magnifier, giving a measuring range of 300 μm and an axial resolution of 0.012 μm. The measured roughness data were evaluated using AltiMap Premium software. With respect to the roughness parameters, the parameters R_a and R_z, commonly used in industrial practice, and their three-dimensional equivalents S_a and S_z were investigated. Two-dimensional profiles were measured and evaluated according to EN ISO 4287 and 4288, three-dimensional surfaces according to EN ISO 25178-2:2012. These are not the latest versions of the relevant standards, but the version of the evaluation software used can calculate the values of these parameters, and the newer standards do not carry significant differences in interpretation.

3. RESULTS AND DISCUSSION

The results of the experiments and measurements carried out are reported below. First, the data of the roughness measurements are given in Table 3. The numbers show that the roughness values increase monotonically with increasing feed rate, which primarily affects the surface roughness. The really big jump occurs at f_z = 0.5 mm, where there are already 4.5 times higher values of R_a and 3.3 times higher values of R_z. And at 1 mm feed there is already an increase of about 18 times in R_a and nearly 12 times in R_z. For the three-dimensional roughness parameters, these values are very similar (the indicated numbers are the f_z values in mm): $Sa_{0.1\rightarrow0.5}$: 4.6; $Sa_{0.1\rightarrow1}$: 16; $Sz_{0.1\rightarrow0.5}$: 2.6; $Sz_{0.1\rightarrow1}$: 8.9.

Table 3. 2*D* and 3*D* roughness results

a_p/f_z	f_z [mm]	a_p [mm]	*Ra* [μm]	*Rz* [μm]	*Sa* [μm]	*Sz* [μm]
10	0.1	1	0.29	1.92	0.34	2.97
2.5	0.2	0.5	0.42	2.44	0.46	2.99
1	0.316	0.316	0.64	3.43	0.64	4.27
0.4	0.5	0.2	1.31	6.40	1.59	7.87
0.1	1	0.1	5.29	22.81	5.44	26.4

The measured 2*D* roughness profiles and the 3*D* surfaces are shown in Figure 4, where the significant roughness degradation starting from f_z = 0.5 mm is visually well noticeable. In the following, the force measurement data are presented, starting with the values of the force components measured at the centre line of the milling head in Table 4.

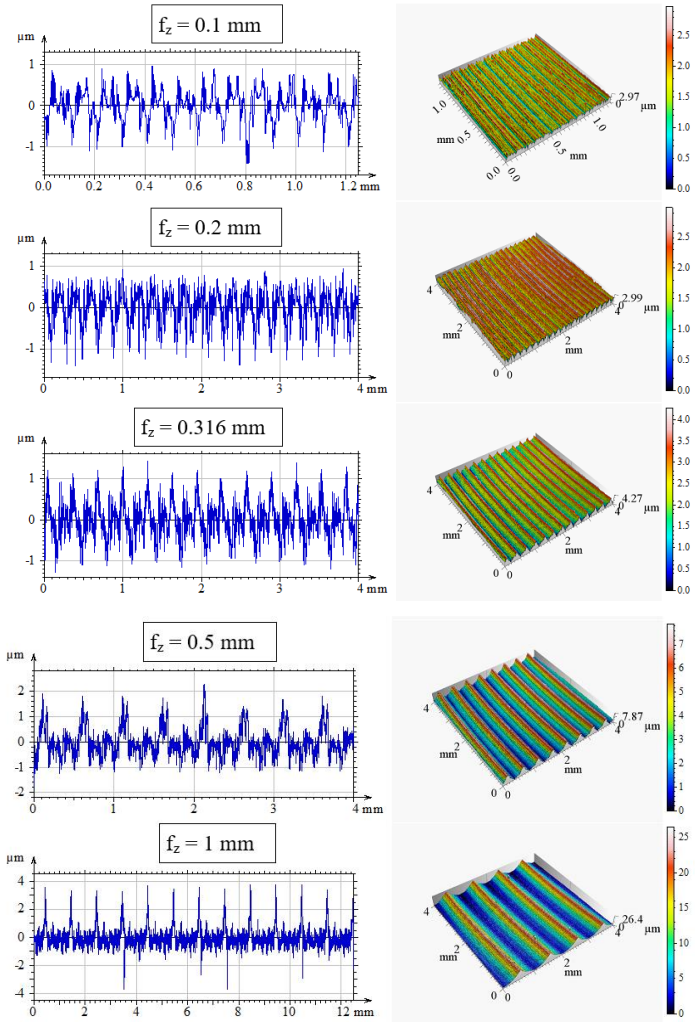

Figure 4. Measured roughness profiles and 3*D* surfaces

When interpreting the force data, it is worth noting once again that the undeformed (theoretical) chip cross section was the same in all cases while the cutting ratio was varied, so, in theory, the same amount of material should be removed in each case. It can be seen from the data that the change in all force components shows a downward trend.

Table 4. The measured force components

a_p/f_z	f_z [mm]	a_p [mm]	*Fx* [N]	*Fy* [N]	*Fz* [N]
10	0.1	1	289	389	812
2.5	0.2	0.5	231	335	659
1	0.316	0.316	201	308	587
0.4	0.5	0.2	180	287	543
0.1	1	0.1	155	264	473

Since the main aim of the investigations was to find some kind of optimum cutting ratio, it is useful to plot the roughness data and the cutting forces in one diagram, a practical implementation of which is illustrated in Figure 5.

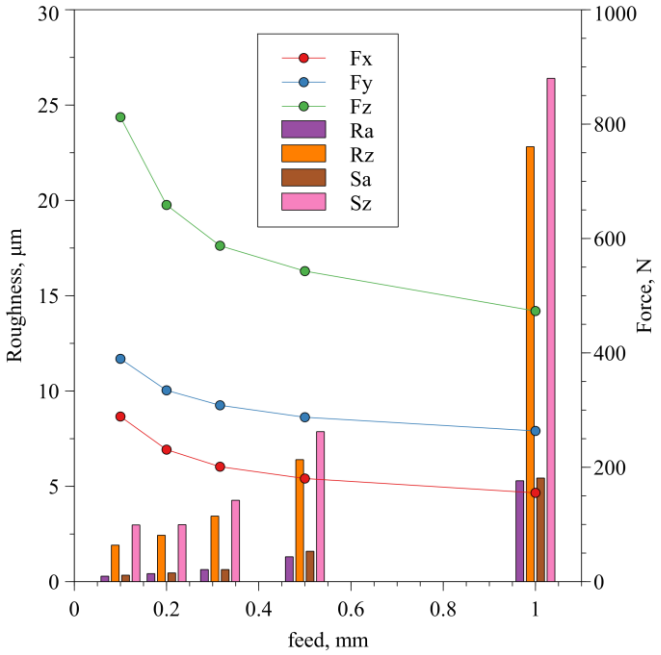

Figure 5. Variation of cutting force and surface roughness per feed change

With the help of this visual representation, the trends of the changes of the two output parameters under study and their relative positions to each other can be seen much more clearly. The values of the force components decrease significantly at low feed rates (up to f_z = 0.316 mm). At the same time, between f_z = 0.5 and 1 mm, there is only a slight decrease, and the curves of the force components Fx and Fy are almost horizontal. This means that a large increase in the feed rate no longer has a significant effect on the force components, provided that the theoretical chip cross-section is kept constant. However, the value of the applicable feed is basically limited by the value of the roughness parameters prescribed for the machined surface: above a certain feed, the roughness deteriorates to a great extent. In the present experiments, this occurs approximately after f_z = 0.316 mm. However, we must also note that the cutting of metals is a very complex process, during which an extremely large number of factors must be taken into account in order to find the optimal technological parameters, which requires great expertise and a thorough examination of the given cutting conditions.

References: 1. *Liang S. Y., Hecker R. L., Landers R. G.*: Machining Process Monitoring and Control: The State-of-the-Art. Journal of Manufacturing Science and Engineering 2004 126, 2: 297–310 https://doi.org/10.1115/1.1707035. **2.** *Kar B. C., Panda A., Kumar R., Sahoo A. K., Mishra R. R.*: Research trends in high speed milling of metal alloys: A short review. Materials Today: Proceedings 2020 26: 2657–2662 https://doi.org/10.1016/j.matpr.2020.02.559. **3.** *Henz R. O., Campos F., Araujo A. C., Fromentin G.*: Cutting Forces in High Feed Milling., presented at the 25 International Conference for Mechanical Engineering, Uberlândia, Brazil, 2019. **4.** *Kundrák J., Markopoulos A. P., Makkai T., Nagy A.*: Correlation Between Chip Ratio and Specific Forces with Increasing Feed per Tooth and Cutting Speed in Face Milling of Steel. WSEAS Transactions on Environment and Development 2018 14, 1: 338–346 **5.** *Xu J., Li L., Lin T., Gupta M. K., Chen M.*: Machinability analysis in high-speed milling of AlSi7Mg alloys under EMQL conditions: An approach toward sustainable manufacturing. Journal of Manufacturing Processes 2022 81: 1005–1017 https://doi.org/10.1016/j.jmapro.2022.07.010. **6.** *Wang Y.-C., Kim D.-W., Katayama H., Hsueh W.-C.*: Optimization of machining economics and energy consumption in face milling operations. Int J Adv Manuf Technol 2018 99, 9: 2093–2100 https://doi.org/10.1007/s00170-018-1848-6. **7.** *Sztankovics I.*: The Effect of the Circular Feed on the Surface Roughness and the Machining Time. Cutting & Tools in Technological System 94: 70–76 https://doi.org/10.20998/2078-7405.2021.94.08. **8.** *Varga G., Kundrák J.*: Effects of Technological Parameters on Surface Characteristics in Face Milling. Solid State Phenomena 2017 261: 285–292 https://doi.org/10.4028/www.scientific.net/SSP.261.285. **9.** *Borysenko D., Karpuschewski B., Welzel F., Kundrák J., Felhő C.*: Influence of cutting ratio and tool macro geometry on process characteristics and workpiece conditions in face milling. CIRP Journal of Manufacturing Science and Technology 2019 24: 1–5 https://doi.org/10.1016/j.cirpj.2018.12.003. **10.** *Sztankovics I., Kundrák J.*: Chip Removal Characteristics with Constant Chip Cross-Sectional Area and Different ap/fz Ratios in Face Milling. 2017 **11.** *Beňo J., Maňková I., Vrábel M., Karpuschewski B., Emmer T., Schmidt K.*: Operation Safety and Performance of Milling Cutters with Shank Style Holders of Tool Inserts. Procedia Engineering 2012 48: 15–23 https://doi.org/10.1016/j.proeng.2012.09.479. **12.** *Toledo J. V. R., Arruda E. M., Júnior S. S. C., Diniz A. E., Ferreira J. R.*: Performance of wiper geometry carbide tools in face milling of AISI 1045 steel. J Braz. Soc. Mech. Sci. Eng. 2018 40, 10: 478 https://doi.org/10.1007/s40430-018-1400-5. **13.** *Fedorovych V. O., Ostroverkh Y. V., Kozakova N. V.*: The Methodology of Sharpening of Blade Tools

Made of Superhard Materials. Cutting & Tools in Technological System 2019 91: no.91 https://doi.org/10.20998/2078-7405.2019.91.17. **14.** *Skoczylas A., Zaleski K.*: Studies on the Selected Properties of C45 Steel Elements Surface Layer After Laser Cutting, Finishing Milling and Burnishing. Advances in Science and Technology. Research Journal 2016 10, 32: 118–123 https://doi.org/10.12913/22998624/65127

Чаба Фелькхо, Мішкольц, Угорщина

АНАЛІЗ ВПЛИВУ ЗМІНИ КОЕФІЦІЄНТА РІЗАННЯ НА СИЛОВІ СКЛАДОВІ ТА ШОРСТКІСТЬ ПОВЕРХНІ ПРИ ТОРЦЕВОМУ ФРЕЗЕРУВАННІ

Анотація. *Традиційні процеси механічної обробки, такі як торцеве фрезерування, як і раніше, відіграють дуже важливу роль у виробництві деталей машин і є предметом постійних досліджень. Одним з важливих напрямків досліджень є вивчення процесів різання з високою подачею. Однак у зв'язку зі збільшеним значенням подачі на один зуб f_z доцільно зменшити глибину різання (a_p), щоб підтримувати зусилля різання на належному рівні. Таким чином, змінюється співвідношення цих двох технологічних параметрів, так званий коефіцієнт різання, і ми можемо перейти в діапазон зворотної обробки, де $a_p / f_z < 1$. У даній роботі досліджуються наслідки дії цієї зміни на шорсткість поверхні і складових сили різання, а також обговорюється, як можна знайти оптимальне співвідношення умов різання. Результати проведених експериментів і вимірювань показують, що значення шорсткості монотонно збільшуються зі збільшенням швидкості подачі, що в першу чергу впливає на шорсткість поверхні. По-справжньому великий стрибок відбувається при $f_z = 0.5$ мм, де вже в 4,5 рази вищі значення R_a і в 3,3 рази вищі значення R_z. А на 1 мм подачі вже спостерігається приріст приблизно в 18 разів у R_a і майже в 12 разів у R_z. Для параметрів тривимірної шорсткості ці значення дуже схожі (зазначені числа є значеннями f_z в мм): S_a 0,1→0,5: 4,6; S_a 0.1→1: 16; S_z 0,1→0,5: 2,6; S_z 0.1→1: 8.9. Значення силових складових значно зменшуються при малих швидкостях подачі (до $f_z = 0,316$ мм). При цьому між $f_z = 0,5$ і 1 мм спостерігається лише незначне зменшення, а криві силових складових F_x і F_y майже горизонтальні. Це означає, що значне збільшення швидкості подачі вже не робить істотного впливу на силові складові за умови, що теоретичний поперечний переріз стружки залишається постійним. Однак величина застосовуваної швидкості в основному обмежена величиною параметрів шорсткості, прописаних для оброблюваної поверхні: з перевищенням подачі, шорсткість в значній мірі погіршується. У цих дослідах це відбувається приблизно після $f_z = 0,316$ мм. Однак потрібно також зазначити, що різання металів є дуже складним процесом, в ході якого необхідно враховувати надзвичайно велику кількість факторів з метою пошуку оптимальних технологічних параметрів, що вимагає великих знань і ретельного вивчення заданих умов різання.*

Ключові слова: *високошвидкісне фрезерування; складові сили різання; шорсткість поверхні.*

.

UDC 621.91.01 **doi: 10.20998/2078-7405.2023.99.02**

ALTERATION OF THE CUTTING FORCE COMPONENTS IN TANGENTIAL TURNING

István **Sztankovics** [0000-0002-1147-7475], István T. **Pásztor** [0000-0002-6971-3063]

University of Miskolc, 3515, Miskolc - Egyetemváros, Hungary
istvan.sztankovics@uni-miskolc.hu

Received: 10 November 2023 / Revised:19 November 2023 / Accepted: 23 November 2023 / Published: 01 December 2023

Abstract. *In the development of cutting procedure, the study of the cutting force is important to evaluate the possible loads and elastic deformations in the machining system. The unusual relative position of the cutting tool leads to a changing characteristic of the cutting force in tangential turning. Therefore, it is particularly important to study the values and ratios of the cutting force components in different setups in this finishing procedure. In this paper the depth of cut, feed, and cutting speed are changed, and the effect of these parameters are analysed on the major cutting force, feed force and passive force. The full factorial design of experiment method is applied in the selection of setup parameters and the evaluation of the results. The maximal values and the ratio of the force components were analysed by the determination of equations.*
Keywords: *design of experiments; feed force; major cutting force; passive force; tangential turning.*

1. INTRODUCTION

The machining processes are needed to be developed continuously due to meet the prescribed requirements of achievable surface quality, obtainable efficiency, and increasing productivity [1]. The quality management of cutting tools is also an important field [2]. In turning of cylindrical surfaces, one direction of the developments is the correct selection of process parameters. Experimental examination of turning operation, analysis of the most relevant parameter, and optimization strategies is all part of the current research [3]. If material removal rate, surface roughness and tool wear are considered, the usual order of impact of these parameters are the depth of cut, the cutting speed, and the feed [4]. However, cutting speed is more important, if we consider tool life [5], and tool wear is directly related to the machined surface quality of the workpiece [6]. Moreover, the process parameters also affect the shape accuracy [7]. Process conditions should be selected with care to be able to reduce the machining time without increasing cutting forces excessively [8]. Other effects must be taken into consideration, since the depth of cut to feed ratio alters the force components [9], while the shear angle is also an important factor [10].

The application of tangential turning [11] as finish machining is spreading in the industrial application, due to the achievable surface roughness [12] and form accuracy [13], while obtaining low machining times. However, the analysis of cutting forces is needed, to study the possible elastic deformations of the machining system. In this paper, the cutting force components are studied in tangential turning by changing the cutting speed, feed, and depth of cut. The maximal values of Major cutting force, Feed force, and Passive force were measured and analysed. During the measurement, the recommended adjustment values are set.

2. EXPERIMENTAL CONDITIONS AND METHODS

The aim of this research was the evaluation of the cutting forces acting between the workpiece and tool in tangential turning. Therefore, several cutting experiments were carried out to accomplish this task on a EMAG VSC 400 DS hard machining centre. Cylindrical workpieces with 70 mm outer diameter were machined. The chosen material was 42CrMo4 grade alloyed steel, which processed by hardening heat treatment to 60 HRC hardness before the experiments. The tangentially turned surfaces were pre-machined by a standard turning tool with a SANDVIK Coromant CNMG 12 04 12-PM 4314 cutting insert. An inserted turning tool with 45° inclination angle is applied in the tangential turnings, which made by HORN Cutting Tools Ltd. and consisted of two parts: S117.0032.00 insert and H117.2530.4132 holder. The cutting edge of the tool was an uncoated carbide insert (MG12 grade).

The effect of the cutting speed (v_c), the feed per workpiece revolutions (f) and the depth of cut (a) were analysed in this study. The 2^3 factorial design method was applied in the parameter selection and analysis. A lower and an upper limit value were chosen for each studied parameter. The lower value range of the parameters are aimed in this study in the initial research of the topic. Therefore, the cutting speed was chosen to be 100 m/min and 200 m/min, the feed was set to 0.3 mm and 0.6 mm. Two kinds of depth of cut were also chosen: 0.1 mm and 0.2 mm. 8 different setups are resulted, which can be seen in Table 1.

Table 1 – Experimental setups

Setup	1	2	3	4	5	6	7	8
v_c [m/min]	100	200	100	200	100	200	100	200
f [mm]	0.3	0.3	0.6	0.6	0.3	0.3	0.6	0.6
a [mm]	0.1	0.1	0.1	0.1	0.2	0.2	0.2	0.2

The cutting forces were measured during the experiments with a Kistler 9257A three component dynamometer. The measurement setup also contained three Kistler

5011 charge amplifier, a NI-9215 data acquisition unit with cDAQ-9171 chasing and NI Labview software. The forces measured by the dynamometer are equivalent to the forces to be analysed, therefore no further calculations were needed.

In this paper, the following cutting forces are studied:

- F_c – Major cutting force, acting in the direction of cutting speed [N]
- F_f – Feed force, acting in the direction of feed [N]
- F_p – Passive force, acting perpendicular to F_c and F_f [N]

Equations were worked out for the analysis of the cutting process using the form in Equation 1 according to the 2^3 full factorial experimental design method. The y is the dependent value and k_i are the coefficients describing the effect of the different factors on the dependent value. The independent variables are the cutting speed (v_c), feed (f) and depth of cut (a)

$$y(v_c, f, a) = k_0 + k_1 v_c + k_2 f + k_3 a + k_{12} v_c f + k_{13} v_c a + k_{23} f a + k_{123} v_c f a \quad (1)$$

3. EXPERIMENTAL RESULTS

The experiments were carried out and the cutting forces are measured for each setup. The resulted force-time curves were evaluated, and the maximum value of the force components were calculated for each studied cutting force component in the constant chip cross-sectional phase. These values are shown in Table 2. Equation 2-4 shows the determined mathematical formulas, which are calculated by the application of the necessary numerical analysis.

Table 2 – Measurement results

Setup	1	2	3	4	5	6	7	8
F_c [N]	188.0	197.9	313.0	283.1	315.3	393.1	597.7	554.2
F_p [N]	137.7	205.9	238.6	298.2	202.2	463.6	369.1	457.7
F_f [N]	61.3	61.1	104.9	108.4	114.0	149.4	242.1	237.8

$$F_c(v_c, f, a) = 192.6 - 0.9953 v_c - 246.5 f - 1793.2 a + 1.387 v_c f + \\ + 14.93 v_c a + 7960.3 f a - 27.14 v_c f a \quad (2)$$

$$F_f(v_c, f, a) = 132.7 - 0.8291 v_c - 293.7 f - 1109.6 a + 1.569 v_c f + \\ + 7.897 v_c a + 4265.7 f a - 14.45 v_c f a \quad (3)$$

$$F_p(v_c, f, a) = 319.1 - 2.808 v_c - 402.8 f - 3591.1 a + 5.190 v_c f + \\ + 35.75 v_c a + 7676.4 f a - 54.76 v_c f a \quad (4)$$

During the study of the cutting forces, it is important to look at the ratio of these forces. It can tell a lot about the chip removal process, if these ratios are changing in different setups. Therefore, using the result presented in Table 2, the F_c/F_p, F_c/F_f and F_p/F_f ratios are also calculated in the 8 experimental setups. These outcomes can be seen in Table 3. Equation 5–7 present the mathematical formulas for these values, which will be used in the deeper discussion of the results.

Table 3 – Calculated ratios of the cutting forces

Setup	1	2	3	4	5	6	7	8
F_c/F_p [-]	1.37	0.96	1.31	0.95	1.56	0.85	1.62	1.21
F_c/F_f [-]	3.07	3.24	2.98	2.61	2.77	2.63	2.47	2.33
F_p/F_f [-]	2.25	3.37	2.28	2.75	1.77	3.10	1.52	1.92

$$F_c / F_f\,(v_c, f, a) = 1.657 + 0.0157v_c + 4.082f + 7.693a - 0.03626v_cf - \\ - 0.085v_ca - 25.31fa + 0.1807v_cfa \quad (5)$$

$$F_c / F_p\,(v_c, f, a) = 1.213 + 0.00124v_c + 0.1803f + 6.507a - 0.00735v_cf - \\ - 0.05695v_ca - 4.953fa + 0.08726v_cfa \quad (6)$$

$$F_p / F_f\,(v_c, f, a) = 1.125 + 0.0128v_c + 2.243f - 6.81a - 0.012146v_cf + \\ + 0.04891v_ca + 0.127fa - 0.09437v_cfa \quad (7)$$

4. DISCUSSION

The analysis of the effect of the setup parameters on the cutting forces consists of two sections. First the maximal values of each force components were analysed, which is followed by the evaluation of the ratios between those.

Figure 1 presents the cutting force in function of the feed and cutting speed on two levels of the depth of cut. Firstly, we can see, that both f and a has an increasing effect on F_c. From the two, the depth of cut has a more significant effect, because the two-fold increase of a resulted in nearly two-fold increase of the major cutting force. However, the two-fold increase of the feed has a lower impact resulting with around 1.5-1.8-fold increase. This can be explained by the fact, that the depth of cut affects the chip width, while the feed affects the chip height. Increasing the letter lowers the specific cutting force, which results in a lower increase in the cutting force

by the same increase in the chip cross-sectional area. The cutting speed has a neglectable effect on the major cutting force.

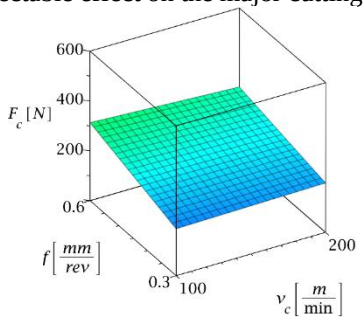

a_p = 0.1 mm

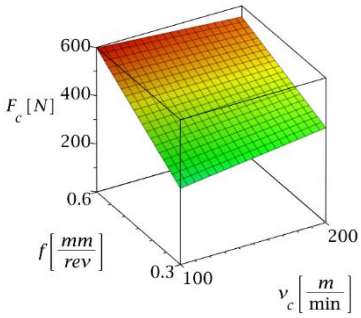

a_p = 0.2 mm

Figure 1 – Alteration of the F_c in the studied range

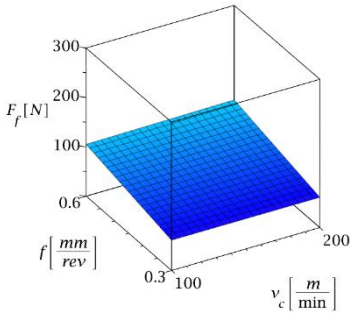

a_p = 0.1 mm

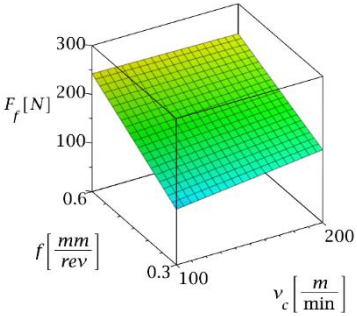

a_p = 0.2 mm

Figure 2 – Alteration of the F_f in the studied range

We can see the feed directional force in function of the feed and cutting speed in Figure 2. It can be seen, that in case of 0.1 depth of cut, the alteration of the feed has a lower (increasing) impact than in case of 0.2 depth of cut. However, the two-fold increase of the depth of cut resulted a nearly 2.5-fold increase in F_f in the studied range. This can be explained by the change in the shape of the cross-sectional area of the chip. The projection of the cutting tool in the base plane can be described with a hyperbolic function. If the depth of cut is higher, this results in the change of the direction of the resultant force in the base plane, which shifts from the direction of the tool holder to the direction of the feed. Therefore, the depth of cut has a higher impact in the studied range. The cutting speed has a low effect on this cutting force component.

In Figure 3, the alteration of the passive force can be seen. The first, and most interesting conclusion can be drawn by the analysis of the cutting speed change. The

two-fold increase of the cutting speed results in a 1.5-2-fold increase in the F_p value. This phenomenon can be explained by two suggestions. First, the increase of the cutting speed results in a different, much higher deformation rate in the workpiece material, which results in a higher plastic deformation as well. This causes a higher radial load on the tool. Secondly, higher v_c results in a greater area of material, which will be in contact with the cutting tool in a given time period. However, this phenomenon should be analysed more thoroughly in a later study. The effect of the feed on F_p is higher than its effect on F_f, while the effect of the depth of cut lowers. this can be explained by the previously mentioned change in the chip shape.

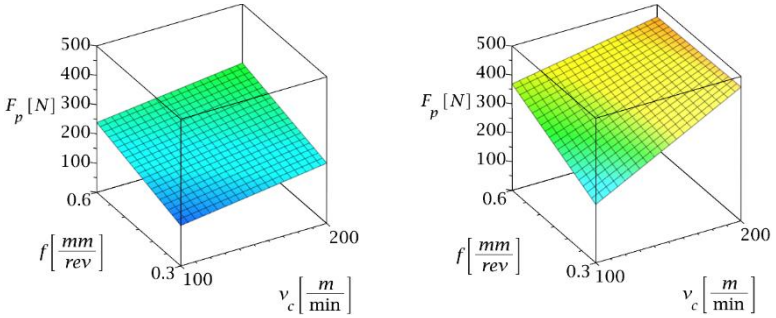

a_p = 0.1 mm a_p = 0.2 mm

Figure 3 – Alteration of the F_p in the studied range

The study continues with the evaluation of the ratios between the cutting force components. Figure 4 presents ratio between the major cutting force and the feed directional force. In this figure it can be clearly seen that the feed and cutting speed have a small effect on this ratio, however the two-fold increase of the depth of cut results in a nearly 1.3-fold increase in F_c/Ff. This means, that by the variation of the setup parameters in the studied range, the direction of the active force (the resultant from the summation of F_c and F_f) remains nearly the same. Figure 5 presents the alteration of the ratio between the major cutting force and the passive force. The effect of the cutting speed on F_p also affects the alteration of the ratio: increasing the v_c results in a lower ratio. The two-fold increase of the depth of cut increases the studied attribute by 1.2-fold, however the increase of the feed has a neglectable effect. Among the analysed setup parameters, the cutting speed has the highest effect. Finally, the ratio between the passive force and the feed directional force is analysed using Figure 6. Here we can see the increasing effect of the cutting speed on the studied ratio. This is caused by the fact that the passive force is affected by the change in v_c, however the feed directional force is unaffected. The depth of cut has also an increasing effect on this ratio: a two-fold increase in a results in a nearly 1.3-fold increase in F_p/F_f. The feed rate has a neglectable effect on the ratio.

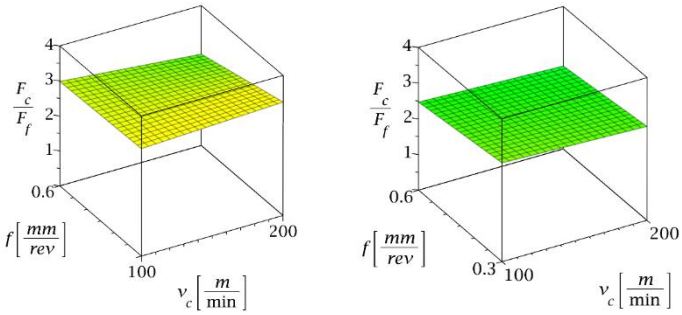

a_p = 0.1 mm a_p = 0.2 mm

Figure 4 – The ratio of F_c and F_f in the studied range

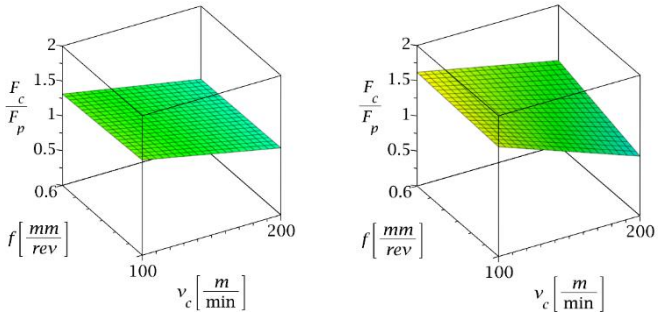

a_p = 0.1 mm a_p = 0.2 mm

Figure 5 – The ratio of F_c and F_p in the studied range

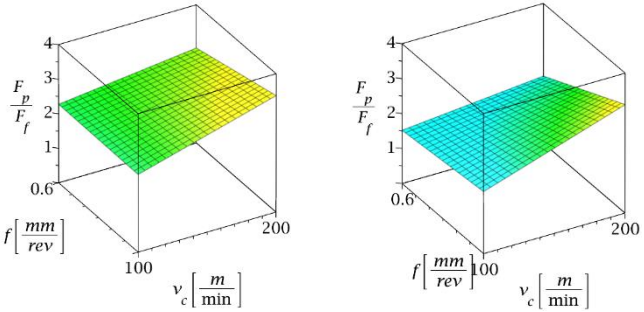

a_p = 0.1 mm a_p = 0.2 mm

Figure 6 – The ratio of F_p and F_f in the studied range

5. CONCLUSIONS

The need to improve of productivity draws the attention of researchers on machining procedures, where high feed rate can be applied, while the surface roughness can be held below the prescribed values. Tangential turning allows the creation of ground-like surfaces, however the feed rate can be set to higher values, than used to in traditional turning. In this paper, cutting experiments were carried out to study the cutting force components in tangential turning, which values play an important role in the shape correctness. In the evaluation of the resulted data the following conclusions were drawn:

- The major cutting force and the feed directional force is unaffected by the alteration of the cutting speed; yet, it has an increasing effect on the passive force.
- The change of the depth of cut changes the shape of the active section of the cutting edge, which changes the direction of the resultant cutting force.
- The ratio between the analysed cutting force components can be manipulated by the adjustment of the setup parameters.

References: 1. *Byrne, G., Dornfeld, D., Denkena, B. J. C. A.:* Advancing cutting technology. CIRP Annals, 52(2), pp. 483–507. (2003). **2.** *Klymenko, G. P., Vasylchenko, Y., & Donchenko, Y.:* Quality management of cutting tools on heavy machines. Rezanie I Instrument V Tehnologiceskikh Sistemakh/ Cutting And Tool In Technological Systems, (94), pp. 135–141. (2021). **3.** *Balwan, V. R., Dabade, B., Wankhade, L.:* Influence of hard turning parameters on cutting forces of EN 353 steel. Materials Today: Proceedings, 63, pp. 149–156. (2022). **4.** *Pathapalli, V. R., P, S. R., Basam, V. R., Doni, M. K.:* Multi Response Optimization of Turning Process by Considering its Cutting Parameters Implementing Grey Relational Analysis. International Journal of Integrated Engineering, 11(8), pp. 110–118. (2019). **5.** *Kundrak, J., Palmai, Z., Varga, G.:* Analysis of tool life functions in hard turning. Tehnički vjesnik, 27(1), pp. 166–173. (2020). **6.** *Felho, C., Varga, G.:* Theoretical roughness modeling of hard turned surfaces considering tool wear. Machines, 10(3), 188. (2022). **7.** *Nagy, A., Varga, G.:* Effect of abandonment of cooling and lubrication on surface roughness and cylindricity in turning of steel. Multidiszciplináris Tudományok, 11(4), pp. 395–407. (2021). **8.** *Kundrák, J., Markopoulos, A. P., Karkalos, N. E., Makkai, T.:* The examination of cutting force as function of depth of cut in cases with constant and changing chip cross section. In Advances in Manufacturing II: Volume 4-Mechanical Engineering (pp. 405–415). Springer International Publishing. (2019). **9.** *Felhő, C., Rakonczai, E.*: FEM investigation of cutting force components in high-feed face milling. Rezanie I Instrument V Tehnologiceskikh Sistemakh/ Cutting And Tool In Technological Systems, (91), pp. 191–199. (2019). **10.** *Manovytskyi, O., Klymenko, S., & Burykin, V.:* Calculation of shear angle when cutting with a tool of a negative rake angle. Rezanie I Instrument V Tehnologiceskikh Sistemakh/ Cutting And Tool In Technological Systems, (97), pp. 59–69. (2022). **11.** *Schreiber, L., Trott, K.:* Verfahren zur drallfreien spanenden Bearbeitung von rotationssymmetrischen Flächen. Patent DE19963897A1. (1999). **12.** *Kunstfeld, T., & Haas, W.*: Shaft surface manufacturing methods for rotary shaft lip seals. Sealing technology, 2005(7), pp. 5–9. (2005). **13.** *Nee, A. Y. C., & Venkatesh, V. C.:* Form accuracy of tangentially skived workpieces. CIRP Annals, 34(1), pp. 121–124. (1985).

Іштван Станкович, Іштван Пастор, Мішкольц, Угорщина

ЗМІННІСТЬ СКЛАДОВИХ СИЛИ РІЗАННЯ ПРИ ТАНГЕНЦІАЛЬНОМУ ТОЧІННІ

Анотація. *При розробці процедури різання важливе значення має вивчення сили різання для оцінки можливих навантажень і пружних деформацій в системі обробки. Незвичайне взаємне розташування ріжучого інструменту призводить до зміни характеристики сили різання при тангенціальному повороті. Тому особливо важливо вивчити значення та співвідношення компонентів сили різання в різних установках у цій процедурі фінішної обробки. Аналіз впливу параметрів установки на зусилля різання складається з двох розділів. Спочатку були проаналізовані максимальні значення кожної складової сили, після чого проводилась оцінка співвідношень між ними. Видно, що глибина різання має більш значний вплив, оскільки дворазове її збільшення призвело до майже дворазового збільшення основної сили різання. Однак дворазове збільшення подачі має менший вплив, що призводить до збільшення сили приблизно в 1,5-1,8 рази. Це можна пояснити тим, що глибина різання впливає на ширину стружки, в той час як подача впливає на її висоту. Збільшення швидкості знижує питому силу різання, що призводить до меншого збільшення сили різання за рахунок такого ж збільшення площі поперечного перерізу стружки. Швидкість різання незначно впливає на основну силу різання. У даній роботі змінюються глибина різання, подача і швидкість різання, а також аналізується вплив цих параметрів на основну силу різання, силу подачі і пасивну силу. Повний факторний план експерименту застосовується при виборі параметрів установки та оцінці результатів. Максимальні значення і співвідношення силових складових були проаналізовані шляхом рішення рівнянь. При оцінці отриманих даних були зроблені наступні висновки: на основну силу різання та спрямовану силу подачі не впливає зміна швидкості різання; Проте вона все більше впливає на пасивну силу; зміна глибини різання змінює форму активної ділянки ріжучої кромки, що змінює напрямок результуючої сили різання; співвідношенням між аналізованими компонентами сили різання можна маніпулювати, регулюючи параметри установки.*

Ключові слова: *планування експериментів; сила подачі; основна сила різання; пасивна сила; тангенціальний поворот.*

УДК 621.9.01 **doi: 10.20998/2078-7405.2023.99.08**

ACTUAL CONTACT AREA ON THE WORN CLEARANCE FACE OF THE CUTTER WITH THE ROUND KYBORITE INSERT

Olersandr **Manovytsky** [0000-0003-3882-7866], Sergii **Klymenko** [0000-0003-1464-3771], Serhii **Klymenko** [0000-0002-7913-5519], Maryna **Kopeikina** [0000-0002-5956-5503]

V.M. Bakul Institute for Superhard Materials of NAS of Ukraine, Kyiv, Ukraine
msm5@i.ua

Received: 11 November 2023 / Revised:18 November 2023 / Accepted: 22 November 2023 / Published: 01 December 2023

Abstract. *For a tool equipped with a circular cutting insert, a dependence is proposed for calculating the nominal area of the contact area on the back surface. It is proved that the actual area of the contact area of the tool differs significantly from the nominal one due to the presence of a system of micro-irregularities, which makes a difference in the assessment of machining process parameters. Using the example of a tool equipped with a circular cutting insert made of polycrystalline cubic boron nitride ciborite, an approach to determining the actual contact area of the back surface with the workpiece during finishing turning of hardened steel is considered. The possibility of taking into account the influence of the system of irregularities in the contact area, determined by the parameters of its topography, on the size of the actual area is shown, and the ratio of the actual and nominal areas of the contact areas of the tool is determined, and it is found that, depending on the degree of development of the microrelief, the ratio of the actual and nominal areas of the contact surface of the cutter differs by at least 20%. It is shown that the actual contact area is also related to the total length of the main and auxiliary cutting edges, determined by the maximum values of the main and auxiliary angles in the cutter plan, and the size of the wear chamfer on the back surface of the cutter.*
Keywords: *cutting tool; clearance face; Kyborite PCBN; contact area; irregularities; actual contact area.*

1. INTRODUCTION

There are many scientific publications devoted to the determination of contact stresses on the working areas of cutting tools.For example, [1,2] provides a general methodology for determining contact stresses on tool working areas, and [3] adjusts this approach to the case of using tools made of superhard materials when machining hardened steels.At the same time, when determining the stresses in these works, the distribution of cutting forces relative to the nominal contact area is considered both on the rake and clearance surfaces of the tool. It is quite clear that such a simplification is justified for approximate calculations, but can introduce significant errors in the case of the presence of a developed system of waves and icronormalities

on the contact areas of elements of any friction pair, which results in a significant discrepancy between the value of the actual contact surface area and
the nominal one [4, 5]. The formation of such a system of irregularities on the working surfaces, and, accordingly, the determination of the actual area of the contact area, should be considered as a result of wear of the cutting tool [6, 7].

This paper proposes an approach to determining the actual contact area of a tool, considered on the example of the clearance face of a cutter equipped with a round cutting insert made of a polycrystalline superhard composite (PCBN) Kyborite [8], when machining hardened steel.

2. METHODS

The study was carried out when turning hardened steel ШХ-15 with a cutter with a round insert RNMN 070300 made of Kyborite PCBN. Cutting modes: cutting speed - 120 m/min, feed - 0.08 mm/rev.

The images were obtained using a BRUKER ContourGT 3D Optical Microscope. The length of the profile was determined by the KU-A curvimeter using longitudinal and transverse profilograms with the same scale along the X, Y axes.

3. RESULTS

For a better understanding of the processes of contact between cutting tools and the workpiece, we use a predictive model, according to which, at the moment the clearance face of the cutter touches the workpiece, the processed material deforms on the cutting surface. Gradually, the deformation of the material being processed changes from elastic to plastic. Being in a deformed state, the material undergoes plastic shear and turns into chips, and both plastic and elastic deformation occurs on the clearance surface of the cutter during contact, accompanied by elastic recovery of the processed workpiece material after it leaves contact with the cutter.

It should be noted that the actual contact area of a sharp cutter in the plastic contact areas depends on the set of irregularities formed during tool manufacturing and is larger than their nominal area. The areas of elastic contact are smaller than their nominal area.

To find the nominal contact area of a tool equipped with a round cutting insert with the workpiece surface, the contact diagram shown in Fig. 1. For a simplified view of the contact surface, the part of the contact surface formed by the cutting edge with a radius of curvature is not shown.

Assuming that the radius of curvature of the cutting edge and the back angle of the cutter are the same along the entire working length of the cutting edge, we assume

that the contact surface will be limited to the *ABDC* shape, which is a truncated cone with a generic OO_1 and an angle α. However, such a solution introduces some errors, since the radius of curvature and the contact length of the elastically restored part of the deformed material are comparable values. So, let's imagine the area of this surface as a rectangle, which is a scan of the surface of a truncated cone with a part of a circle with a radius *r* equal to the radius of the top of the cutting tool and a rectangular scan of a part of a toroidal surface with a large outer radius *r* equal to the radius of the top of the cutting tool and an end radius ρ equal to the radius of curvature of the cutting edge.

In fact, such a shape is similar to a trapezoid, but in real conditions, due to the small values of the clearance angle, this distinction can be neglected by aligning the bases of the trapezoid and considering them equal to the total length of the cutting edges.

Then the contact area is defined as:

$$A_3 = h_y(b + b_1). \tag{1}$$

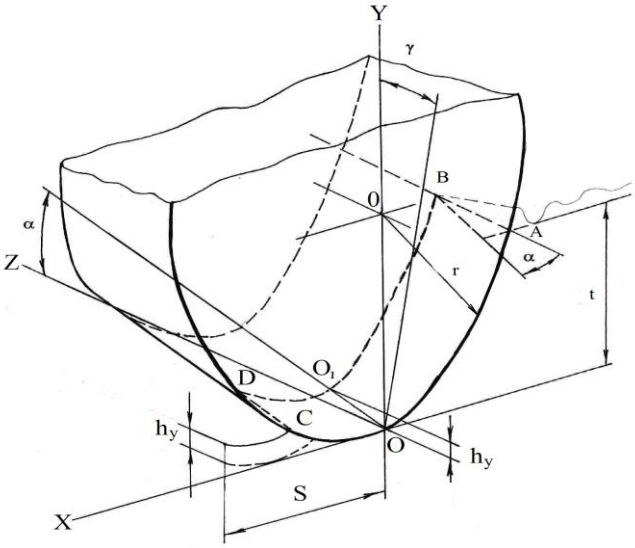

Figure 1 – Diagram for determining the contact area of the clearance face of a cutter with a radius at the tip with the machined surface

To calculate the nominal contact area of a cutting tool with a radius at the tip with the machined surface, the diagram shown in Fig. 2. According to it, we have:

$$\Psi_1 = arccos\left(1-\frac{r}{cos\,\gamma}\right), \tag{2}$$

$$\Psi_2 = arcsin\left(\frac{S+h_y}{2r}\right) \tag{3}$$

then:

$$\cup \mathrm{OA} = b = r\,arccos\left(1-\frac{t}{r\,cos\,\gamma}\right), \tag{4}$$

$$\cup \mathrm{OC} = b_1 = r\,arcsin\left(\frac{S+h_y}{2r}\right). \tag{5}$$

By summing up the individual segments of the *AC* arc, we get its length:

$$\cup \mathrm{AC} = (b+b_1) = r\left[arccos\left(1-\frac{t}{r\,cos\,\gamma}\right)+arcsin\left(\frac{S+h_y}{2r}\right)\right] \tag{6}$$

.

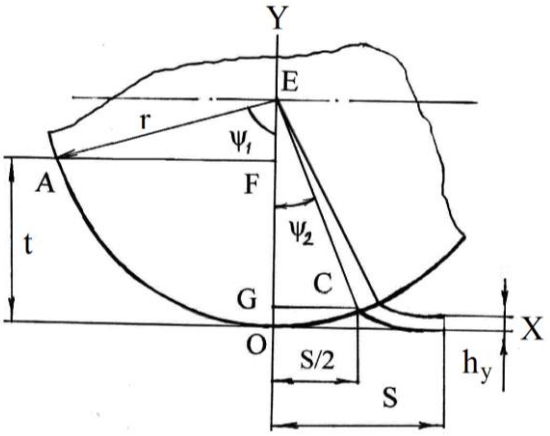

Figure 2 – Diagram for calculating the nominal contact area of a cutting tool with a radius at the tip with the surface to be machined

After substituting into equation (6) the values of the length of contact between the back surface and the machined surface from equation (5), the value of the elastic recovery height from equation (2) and the total length of the cutting edges from equation (1), we obtain the equation for calculating the nominal contact area of a sharp cutter with a radius at the apex:

$$A_3 = \rho\left[arccos\left(0{,}5 + \frac{\tau}{\sigma_T} \right) + 0{,}4\left(\frac{\sigma_T - \tau}{\sigma_T \, sin\alpha} \right) \right] \cdot , \qquad (7)$$

$$\cdot r\left\{ arccos\left(1 - \frac{t}{r\cos\gamma} \right) + arcsin\frac{1}{2r}\left[S + 0{,}4\rho\left(1 - \frac{\tau}{\sigma_T} \right) \right] \right\} .$$

During the prewear period of the tool, when the sharp edge of the cutter plunges into the workpiece, an active interaction with the workpiece occurs, accompanied by micro-crushing of particles from the tool composite, wear of the tool along the rake and clearance surfaces, which leads to an increase in the radius of curvature of the cutting edge, an increase in the contact surface and a more even distribution of thermobaric loads on the working part of the cutter, which creates the prerequisites for the transition to the period of steady-state wear.

A typical example of a worn back surface of a tool is shown in Fig. 3 [9]. It should be noted that the contact surfaces have characteristic furrows, grooves, and protrusions located in the direction of the common cutting feed – speed vector [9–11].

Fig. 4 shows optical-electronic images of the worn area on the clearance surface of a tool equipped with a round cutting insert made of Kyborite PCBN after turning ShKh-15 steel. Although the geometrical parameters of the cutting parts of the BZN6000 cutters shown in Fig. 3 and the RNMN 070300 Kiborite PCBN insert shown in Fig. 4 differ significantly, the topography of the worn surface has a similar appearance with rounding of the cutting grooves characteristic of PCBN and breakouts of crystallite blocks from the superhard tool material. Such images and the resulting profilograms by coordinates allow us to quantify the depth of depressions and the height of protrusions relative to the nominal position of the cutting edges [7].

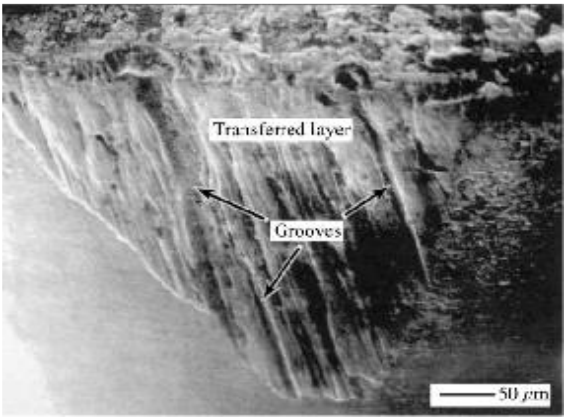

a

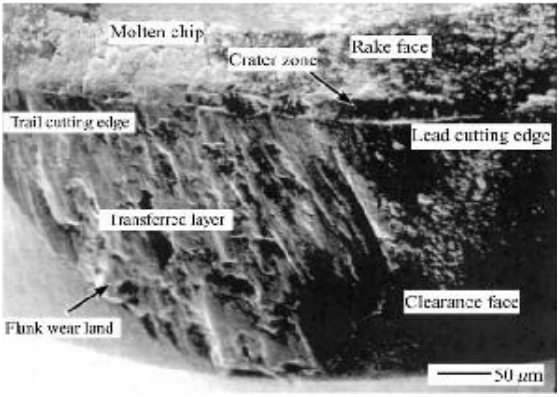

b

Figure 3 – Contact surfaces of a tool made of BZN6000 PCBN when turning hardened steel

Digital processing of the obtained images makes it possible to determine the line of protrusions and depressions on the worn surface of the tool. The 3*D* image and quantitative values of the heights of the protrusions and the depths of the depressions shown in Fig. 3, *b*, clearly demonstrate the contour of the worn area on the clearance surface of the insert and show that the actual contact area of the cutter with the workpiece is much larger than the nominal one.

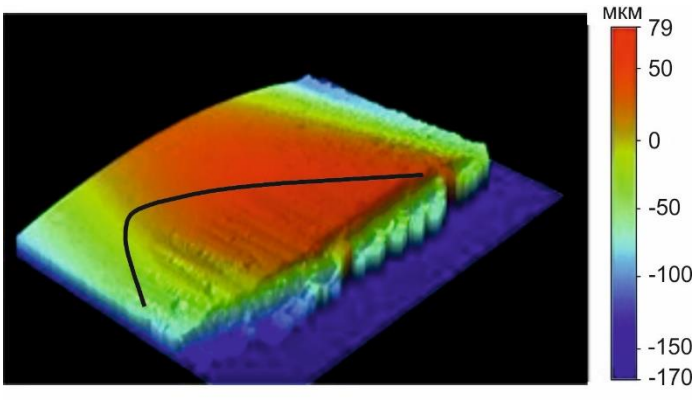

a

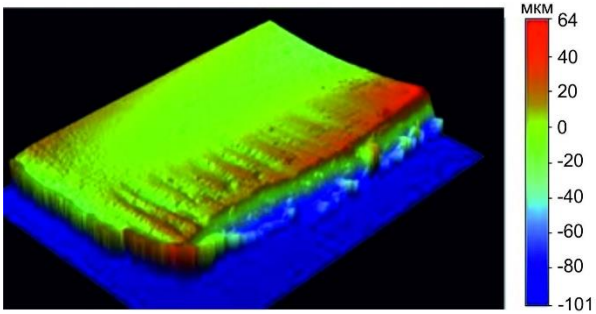

b

Figure 4 – 3*D* image of the wear area on the cutter surface (*a*) and 3*D* image of the wear area on the clearance face (*b*) of a PCNB cutter after machining ШХ15 steel, pointed to the straightened cutting edge

This circumstance should be taken into account when determining contact loads on the clearance face of the tool and calculating the components of the cutting force. Consider the profilograms obtained at different areas of contact between the worn clearance surface of the tool and the machined surface of part (Fig. 5).

The *X*-axis scanning direction is along the tool's straightened cutting edge, and the *Y*-axis scanning direction is along the cutting speed vector, i.e., the width of the wear chamfer. The profilograms show both the height of the depressions and the depth of the profile depressions on the worn surface and the frequency of their formation, which correlates well with the transverse feed rate of the workpiece during machining.

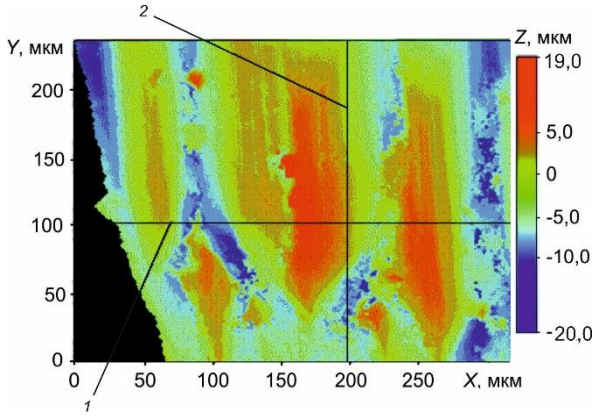
2
Y, мкм
200
150
100
50
0
Z, мкм
19,0
5,0
0
-5,0
-10,0
-20,0
0
50
100
150
200
250
X, мкм
1

a

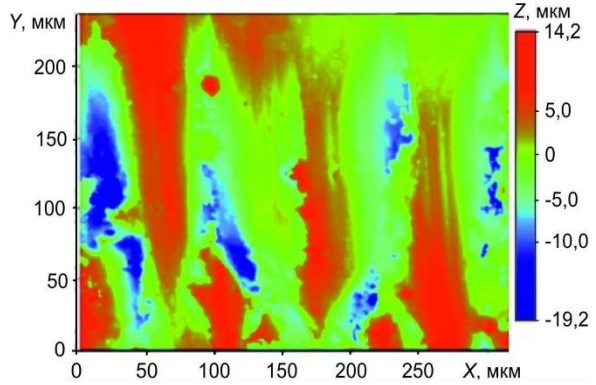
Y, мкм
200
150
100
50
0
Z, мкм
14,2
5,0
0
-5,0
-10,0
-19,2
0
50
100
150
200
250
X, мкм

b

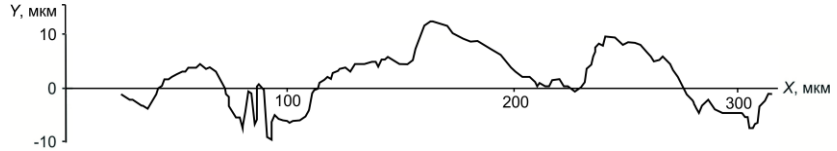
Y, мкм
10
0
-10
100
200
300
X, мкм

c

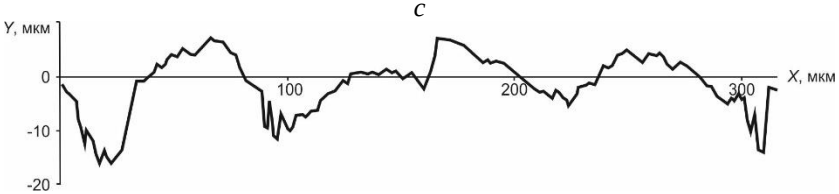
Y, мкм
0
-10
-20
100
200
300
X, мкм

d

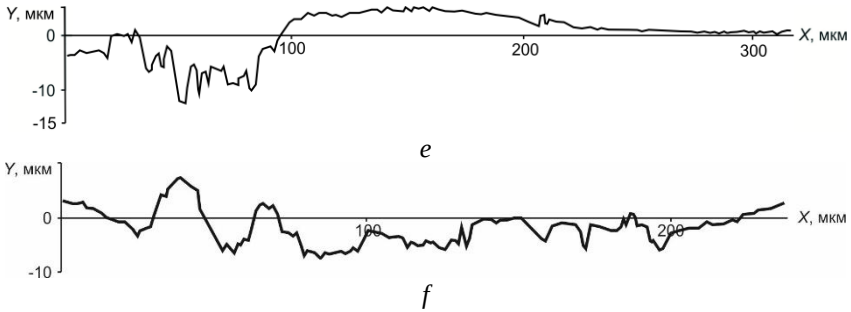

Figure 5 – Topogram of the contact surface (*a*, *b*), profilograms of irregularities in the directions of *X* (*c*, *d*), *Y* (*e*, *f*) by coordinates: *Y* = 105.3 μm (direction *1*) (*c*), *Y* = 102.4 μm (*d*), *X* = 199.0 μm (direction *2*) (*e*), *X* = 87.9 μm (*f*) (*a*, *c*, *e* – area *1*; *b*, *d*, *f* – area *2*)

The profilograms also show the maximum values of microroughness *Z* and the angles of inclination of the profile irregularities. Fig. 5 shows the tribograms and profiles (according to directions *1*, *2*) of the worn surface.

Analysis of the obtained data on the profile of the worn surface allows us to establish the ratio of the profile length to its projections in different parts of the worn surface.

Depending on the coordinate, the measured data characterize the profile of the worn surface both in the areas of plastic and elastic contact with the treated surface. The obtained data on the actual and nominal lengths and their ratio are summarized in Table 1.

Analyzing the difference in the actual bump profile along the wear zone along the cutting edge, we observe a longer bump length near the area where the main cutting edge cuts into the allowance material. The actual length of the profile in this direction is on average 1.37 times longer than the nominal length.

The difference between the lengths of the actual and nominal (100 μm) profiles in the direction from the front surface to the wear boundary in the same area is on average 1.62 times. The average deviations from the nominal length of the profile from the cutting edge to the wear boundary are 1.29 times. That is, a more developed wear surface is observed in the direction along the cutting edge.

Having obtained such data on the values of the profile lengths in each direction of the defined sections and on the segments by coordinates, we can find the integral values of the actual contact areas on each segment of the measured profile of the wear surface irregularities by solving the defined integral of the form:

$$A_{\Phi LxLy} = \int_{Lx_0}^{Lx_i} \int_{Ly_0}^{Ly_i} dLxdLy \,. \qquad (8)$$

Table 1 – Absolute and relative values of the profile length on individual sections of the wear surface

№	Coordinate *Y*	Site, μm	L_X, μm	*X*, μm	L_X/X
1	105,3	28–100	95	72	1,32
2		100–200	125	100	1,25
3		200–315	130	115	1,13
$\Sigma_{1\text{-}3}$		**28–315**	**350**	**287**	**1,22**
4	102,4	0–100	143	100	1,43
5		100–200	110	100	1,10
6		200–315	150	115	1,30
$\Sigma_{4\text{-}6}$		**0–315**	**403**	**315**	**1,28**
	Coordinate *X*	Site, μm	L_Y, μm	*Y*, μm	L_Y/Y
7	199,0	0–50	97	50	1,94
8		50–100	65	50	1,30
9		100–150	55	50	1,10
10		150–200	55	50	1,10
11		200–237	40	37	1,08
$\Sigma_{7\text{-}11}$		**0–237**	**312**	**237**	**1,32**
12	87,9	0–50	65	50	1,30
13		50–100	65	50	1,30
14		100–150	65	50	1,30
15		150–200	66	50	1,32
16		200–237	40	37	1,08
$\Sigma_{12\text{-}16}$		**0–237**	**301**	**237**	**1,27**

Similarly, the nominal rear surface on the same coordinate segments can be calculated by solving the integral:

$$A_{3xy} = \int_{x_0}^{x_i} \int_{y_0}^{y_i} dxdy \,. \qquad (9)$$

The obtained numerical values of the actual and nominal areas of the worn clearance face of the cutting tool calculated by formulas (8) and (9), respectively, and their relative values are summarized in Table 2.

Analyzing the data obtained, it should be noted that on the worn part of the tool with a round Kyborite PCBN cutting insert, the largest difference in the actual contact area with the machined surface compared to the nominal one is observed in

the zone of greatest wear, which is closest to the front surface, at a distance of ~ 100 μm.

Averaging the data obtained over the total length of the worn profile from the front surface to the boundary of the wear zone, the actual contact area exceeds the nominal one by 1.6 times.

To find the actual contact area along the entire contour of the wear zone, which can be represented as a curved triangle, let's try to solve the defined integral, in which the length of the profile in the direction of the cutting edge is indicated as the average value of the actual length Lx = 376.5 μm over the entire area from 0 to 315 μm, and Ly = 306.5 μm over the area from 0 to 237 μm.

Table 2 – Absolute and relative values of actual and nominal areas in individual sections of the wear surface profile

№	Coordinates	Site, μm		$A_Ф$, μm^2	A_H, μm^2	$A_Ф / A_H$
		X	*Y*			
1	*X* = 198,966 *Y* = 105,278	28–100	0–100	9215	3600	2,56
2		100–200	100–200	8125	5000	1,63
3		200–315	200–237	7150	5750	1,24
4		28–315	0–237	109200	68019	1,61
5	*X* = 87,873 *Y* = 102,380	0–100	0–100	9295	5000	1,86
6		100–200	100–200	7150	5000	1,43
7		200–315	200–237	9750	5750	1,70
8		0–315	0–237	121303	74655	1,62

In general, the integral equation is as follows:

$$A_{ФLxLy} = \int_{Lx_0}^{Lx_i} \int_{Ly_0}^{Ly_i} 0{,}5 dLx dLy \cdot \qquad (10)$$

According to the calculation, the actual area of the contact area is $A_{ФLxLy}$ = 0.058 mm^2, the nominal area is A_{HLxLy} = 0.037 mm^2.

4. CONCLUSIONS

As a result of the measurements and calculations, it was found that the presence of grooves on the worn rear surface of a tool equipped with a round Kyborite PCBN cutting insert when turning hardened steel ShKh–15 leads to an increase in the actual area of the contact area with the workpiece by 1.57 times compared to its nominal area.

However, it is necessary to take into account the fact that the projection of the worn part of the cutter will not always have a shape close to a triangle, and to carry out calculations in accordance with the actual wear contours.

Comparing the obtained ratios and taking them into account the increase in the length of the actual contours in the *Y* direction equal to 1.6, it can be argued that the data obtained in [7] on the ratio of the actual and nominal areas of the cutter wear surface have values that are at least 20% lower.

The obtained quantitative results reflect exclusively the ratio of contact surfaces as a result of the interaction of the tool material PCBN Kyborite with the machined hardened steel ShKh–15, but the described methodology for estimating the actual area of the worn area can be applied to other superhard polycrystals with a similar wear pattern. At the same time, for a more reasonable conclusion about the contact area, in addition to the surface profilogram of the plastic part of the contact, it is necessary to consider several profilograms of the surface of the elastic part, due to the fact that the height of micronorhomogeneities along this area decreases to its level on the unworn surface.

Given the use of a round insert, depending on the complexity of the workpiece profile, the actual wear area is determined not only by the total length of the main and auxiliary cutting edges, determined by the maximum values of the main and auxiliary angles in the cutter plan, but also by the size of the wear chamfer on the clearance face of the cutter and the degree of development of the microrelief of the contact area on the worn surface of the cutter.

References : 1. *Poletyka M. F.* Kontaktnye nahruzhky na rezhushchykh poverkhnostiakh ynstrumenta. – M. : Mashynostroenye, 1969. – 148 p.[in Russian]; **2.** *Rozenberg Yu. A.* Rezanie materialov : uchebnik dlja VUZov. – Kurgan : Izd. OAO Poligraf k-t», Zaural'e, 2007. – 294 p.; **3.** Vysokoproyzvodytelnaia chystovaia lezvyinaia obrabotka detalei yz stalei vysokoi tverdosty / *S. A. Klymenko, A. S. Manokhyn, M. Yu. Kopeikina i dr.*. – Kyiv : ISM im. V. N. Bakulia NAN Ukrainy, 2018. – 304 p.; **4.** *Demkyn N. B., Ryzhov E. V.* Kachestvo poverkhnosty y kontakt detalei mashyn. – M. : Mashynostroenye, 1981. – 244 p.; **5.** Tehnologicheskoe obespechenie i povyshenie ekspluatatsyonnyh svoystv detaley mashin i soedinenii / *A. G. Suslov, V. P. Fedorov, O. A. Gorlenko i dr.* – M. : Mashynostroenye, 2006. – 448 p.; **6.** *Bogdanovich P. N., Pryshak V. Ja., Bogdanovich S. P.* Trenie, smaska i iznos v mashinah : uchebnik dlja VUZov. – Minsk : Tehnologija, 2011. – 527 p.; **7.** *Manovytsky A. S., Klymenko S. An., Kopeikina M. Yu.* Opredelenye ploshchady zadnei poverkhnosty yznosa reztsa yz PKNB s radyusom pry vershyne pry tochenyy zakalennoi staly ShKh-15 // Sci. Letters of Acad. Soc. of Michal Baludansky. – 2019. – Vol. 7, № 1. – pp. 58–61; **8.** Sintez I spekanie sverhtverdyh materialov dlja proizvodstva instrumentov / *M. P. Bezhenar, A. A. Bochechka , G. D. Il'nitska i dr.* . – Minsk : Belarus. nauka, 2021. – 338 p.; **9.** *Chou Y. K., Evans C. J. Barash M. M.* Experimental investigation on CBN turning of hardened AISI 52100 steel // J. of Mat. Proces. Technol. – 2002. – 124. – pp. 274–283.; **10.** *Daicu R., Oancea G.* Methodology for Measuring the Cutting Inserts Wear / Symmetry. – 2022, 14/ – 469 p.; **11.** Comparison of Tool Wear, Surface Roughness, Cutting Forces, Tool Tip Temperature, and Chip Shape during Sustainable Turning of Bearing Steel / *H. Demirpolat, R. Binali, A.D. Patange et al*. // Materials. – 2023. – 16(12). – 4408.

Олександр Мановицький, Сергій Клименко, Сергій Клименко, Марина Копєйкіна, Київ, Україна

ФАКТИЧНА ПЛОЩА КОНТАКТНОЇ ДІЛЯНКИ НА ЗНОШЕНІЙ ЗАДНІЙ ПОВЕРХНІ РІЗЦЯ З КРУГЛОЮ РІЗАЛЬНОЮ ПЛАСТИНОЮ КИБОРИТУ

Анотація. *Для інструменту, оснащеного круглої різальної пластиною, запропонована залежність для розрахунку номінальної площі контактної ділянки по задній поверхні. Доведено, що фактична площа контактної ділянки інструменту суттєво відрізняється від номінальної за рахунок наявності системи мікронерівностей, що вносить помилку під час оцінки показників процесу обробки. На прикладі інструменту, оснащеного круглою різальною пластиною із полікристалічного кубічного нітриду бору (ПКНБ) киборіт, розглянуто підхід до визначення фактичної площі контакту задньої поверхні інструменту з оброблюваною деталлю із загартованої сталі під час чистового точіння. Показана можливість врахування впливу системи нерівностей на контактній ділянці інструменту, визначеної за параметрами її топографії, на розмір фактичної площини та визначено співвідношення фактичної та номінальної площ контактних ділянок інструменту. Встановлено, що в залежності від ступеню розвиненості мікрорельєфу співвідношення фактичної і номінальної площ контактної поверхні різця відрізняються, щонайменше, на 60%. Отримані кількісні результати відображають виключно співвідношення контактних поверхонь в результаті взаємодії інструменту, оснащеного ПКНБ киборіт, з оброблюваною деталлю із загартованої сталі ШХ-15, але описана методика визначення фактичної площі зношеної ділянки може бути застосована і для інструментів з іншими композитами з аналогічною картиною зношування. В той же час, для більш обґрунтованого висновку про площу контактних ділянок інструменту, крім профілограми поверхні пластичної частини контакту, необхідно розглядати декілька профілограм поверхні пружної частини ділянки контакту, у зв'язку з тим, що висота мікронерівностей на цій ділянці зменшується до її рівня на незношеній поверхні. Наведено, що фактична площа контактної ділянки пов'язана також із загальною сумарною довжиною головних і допоміжних різальних кромок, визначених максимальними значеннями головного та допоміжного кутів у плані інструменту, а також величиною фаски його зносу по задній поверхні.*

Ключові слова: *різальний інструмент; задня поверхня; киборит ПКНБ; контактна ділянка; нерівності; фактична площа контакту.*

UDC 621.923 **doi: 10.20998/2078-7405.2023.99.09**

TOPOGRAPHIC ADAPTABILITY IN THE DIAMOND GRINDING ZONE OF SUPERHARD MATERIALS

Vladimir **Fedorovich** [0000-0003-4440-3656], Yevgeniy **Ostroverkh** [0000-0002-8926-1324], Dmitry **Romashov** [0000-0001-6467-5726]

National Technical University «Kharkiv Polytechnic Institute», 2 Kyrpychova Street, Kharkiv 61002, Ukraine
Volodymyr.Fedorovych@khpi.edu.ua

Received: 08 November 2023 / Revised:17 November 2023 / Accepted: 22 November 2023 / Published: 01 December 2023

Abstract. *A comprehensive theoretical and experimental analysis of technological topographic adaptability is carried out, based on an idealized description of the topographic parameters of the working surface of the grinding wheel, their changes during its wear and experimental laser scanning of the working surface of the grinding wheel and the processed superhard material (SHM). It has been established that the protrusion height of diamond grains affects the intensity of destruction (removal) of stock through a change in the number of working grains and the actual contact area of the SHM with the working part of the grinding wheel surface. In a controlled grinding process, it is possible to stabilize the working height of the grains in any of the 3 stages of their wear intensity, equating this intensity with the intensity of removal of the intergranular bond. A method has been developed for determining the actual contact area of the working surface of the grinding wheel and changing its technological adaptability. It has been established that in the process of topographic adaptability, the actual contact area can change by several orders of magnitude, respectively, the specific pressure at the contact of diamond grains with the SHM will change, and, consequently, the nature and intensity of their mutual destruction.*
Keywords: *superhard polycrystalline material; diamond grains; working surface of the grinding wheel; microrelief of diamond grains; concentration of diamond grains in the grinding wheel.*

1. INTRODUCTION

The widespread use of superhard materials and the organization of mass production of cutting, smoothing, drawing, drilling and measuring tools from them require the development of highly efficient and precise methods and technology for their processing. The relevance of the problem being solved is dictated by the high labor intensity and low productivity of the SHM grinding process, the high consumption of expensive diamond grains of grinding wheels and, as a consequence, the high cost of processing. It is necessary to improve the reliability and quality of SHM tools, without which it is impossible to use them in automated production.

The process of diamond grinding of superhard materials is characterized by abnormally fast adaptability of the contacting surfaces, which is manifested in

changes in their topographic, structural-phase and energy characteristics. All this changes output parameters such as productivity, specific consumption of diamond grains, and the quality of the processed surface. Thus, adaptability as an objective phenomenon determines the efficiency of the SHM diamond grinding process.

2. APPLIED METHODS

Previously, the maximum height of the protrusion of grains from the diamond-retaining bond was taken as the main topographic parameter of the working surface of the grinding wheel (WSGW) [1]. It turns out (and this has been theoretically and experimentally proved) that the height does indirectly determine the value of the actual contact area, but this is a necessary but not a sufficient condition. The analysis showed that, other things being equal (granularity *z*, concentration *K*, grain grade, grinding modes) with the same grain height on different binders (different critical value of grain embedding, h_{cr}),the actual contact area may be different [2, 3]. Thus, the efficiency of the slimming process is determined not only by the working height of the grains on the WSGW, but also by the properties of the bond material, which have a twofold effect on the value of the actual contact area of the SHM with the WSGW [4]. The properties of the bond determine the value of the actual contact area not only due to the degree of diamond retention, but also due to the elastic (and sometimes plastic) pressing of diamond grains into the bond material, which also leads to a change in the actual contact area (further investigated by 3D modeling of the stress-strain state of the "SHM – grain – bond" system).

Previously, it was found that the maximum productivity of the process is achieved at the maximum height of the protrusion of the grains above the bundle, i.e. with a newly threaded grinding wheel [4, 5]. However, the analysis showed that the grinding of SHM does not require a high level of development of the WSGW at the macro level, since it does not determine the productivity due to the depth of grain penetration into the processed material (PM), and the volume of placement of grinding products is negligible. In this regard, the grain height *hp* should be selected only from the conditions of contact or non-contact of the metal bond with the material to be processed [6]. An increase in the working height of the grains inevitably leads to a decrease in the size of their embedding in the bond and, as a result, an increased consumption of diamond grains. A more in-depth study of the effect of grain height on the output of the grinding process found that an increase in h_w affects the processing productivity not due to the depth of grain penetration into the PM and an increase in the cutting parameters or a more favorable placement of grinding products, as in the case of processing other groups of materials, but due to a significant increase in pressure at the points of contact between the SHM and the grain and, as a result, a decrease in the number of cycles before destruction [7, 8].

It has been established that the height of the grain protrusion affects the intensity of destruction (removal) of stock through a change in the number of working grains and the actual contact area of the "SHM – WSGW". This feature takes place only in the treatment of SHM, when the introduction of grains into the processed material is practically absent, since their hardness is almost the same.

The number of working grains is determined by their concentration in the grinding wheel K and the working height of the grains h_w, i.e. the degree of their protrusion above the bond level:

$$n = f(h_w; K)$$

It has been established that the determining topographic parameter of the process of adaptability in the process of diamond grinding of SHM is the value of the actual contact area in the "WSGW – SHM" system.

The actual contact area also depends on the degree of wear of the grains Δh, i.e. on the mass nature of the formation of wear points on the grains. In a controlled grinding process, it is possible to stabilize the working height of the grains in any of the 3 stages of their wear intensity V_{worn}, equating this intensity with the intensity of the removal of the bind ($V_b = V_{worn}$) [9, 10]. At the same time, the lower the working height of the grains, the greater their number in contact, and the greater the degree of wear (wear pads) of most working grains. Specific loads per grain are reduced, the critical value of their embedding in the bundle is reduced and, as a result, the utilization rate of diamond grains is significantly increased.

To study the process of topographic adaptability, a comprehensive theoretical and experimental analysis of the 3D parameters of the topography of the working surface of the wheel and the treated surface was carried out, based on the theoretical description of the parameters of the relief of the working surface of the wheel and their change in the process of its wear, and experimental laser scanning of the WSGW and the surface of the SHM. A method has been developed for theoretical and experimental determination of the actual contact area in a system of surfaces that are fundamentally different in relief: discrete (WSGW) and quasi-continuous (SHM) in conditions where diamond grains are not embedded in the processed material.

Having established earlier [1] that the relative value of the actual contact area has a decisive influence on the intensity and nature of the mutual microdestruction of the elements of the "SHM–grain–bond" system, a theoretical analysis of the parameters of the grinding wheel and their changes as the grinding wheel adapts (wears) is carried out. The design model of the 3D grain-bond model is shown in Figure 1.

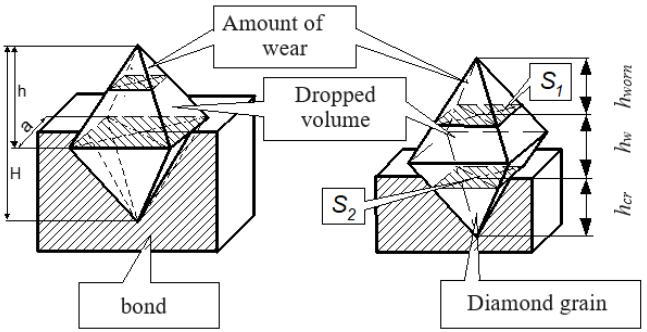

Fig.1. Computational model "Grain–bundle system"

Theoretical dependencies were obtained for calculating and tracking the change in the wear of the grinding wheel of such parameters as the number of grains on the grinding wheel (n) and the relative area of the bearing surface ($t_{rbsa)}$ dependingon the grain size of the wheel (l_{gs}), concentration (K), the properties of the bond material, the degree of wear of the grinding wheel, the working height of the grains (h_w) and the critical value of their integration into the bundle (h_{cr}):

$$n = \frac{(l_{gs} - h_{cr})S}{\left(\frac{16}{K}\right)^{\frac{2}{3}} l_{gs} S_{acs}} trbsa = \frac{l_{gs} - h_{cr} - h_w}{\left\lfloor\frac{16}{K}\right\rfloor^{2/3} 2 l_{gs}}, \quad (1)$$

where: S_{acs} is the average cross-sectional area of the grain.

These dependencies will be used in the development of the theoretical module of the expert system of the SHM grinding process.

It has been established that the relative reference area of the grain relief on the working surface of the wheel (t_{rbsa}) at 100% of the grain concentration in the absence of contact of the binder with the processed material cannot exceed 20.7%. The value of the relative area of the bearing surface of the WSGW, determined by the value of the actual contact area in the "WSGW–SHM" system, depends not only on the height of the protrusion of the grains (h_w), but also on the critical value of their embedding in the bundle (h_{cr}). With the same working height of the grains, the value of the actual contact area of the SHM with the WSGW will be different for different bundles.

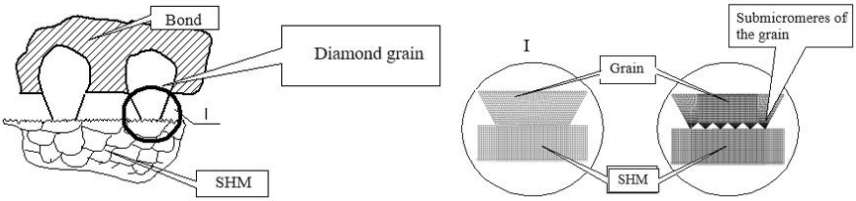

a) b)

c)

Fig.2 Design diagrams of the contact of the elements "SHM–grain–bundle": a – at the macro level; b, c – at the micro level (finite element mesh of the "grain–SHM" model).

The experimental study of the relief parameters of the WSGW was carried out by laser scanning of the working surface of the wheel. One of the most important advantages of this method is the ability to analyze the dynamics of changes in such an important parameter for the process under study as the relative reference area of the t_{rbsa} profile in a three-dimensional version and in computer mode. A method of theoretical, two-stage determination of the actual contact area of the WSGW with the SHM has been developed, based on the artificial replacement of the discrete surface of the grinding wheel with a solid one and taking into account the elastic deepening (deformation, indentation) of diamond grains into the bond and its change in the process of grinding wheel wear. At the first stage, the actual contact area of "WSGW–SHM" is calculated at the macro level through the relative area of the bearing surface, and then, taking it as the area of the contour, using the modernized method for calculating the parameters of the discrete relative bearing surface of the WSGW (b and γ), the actual contact area is calculated at the micro level "SHM – grain microrelief" according to the known dependencies of N.B. Demkin and I.V. Kragelsky [11] At the same time, as a characteristic the system does not use the modulus of elasticity of the contacting materials, but the modulus of elasticity of the metal bond. The computational models are shown in Figure 2.

A method for theoretical determination of the parameters of the topography of the WSGW (b and V) taking into account its discreteness, based on the artificial replacement of a discrete surface with a solid one. Options b and V The following are defined theoretically:

$$V = \frac{3Kl_{gs}\left(l_{gs}-h_{cr}-Kh_w\right)+0.75Kh_w^2}{l_{gs}^2-h_w l_{gs}} \tag{2}$$

$$b = \left[\frac{0.25K\left(l_{gs}-h_{cr}\right)}{l_{gs}} - \frac{0.25Kh_w}{2l_{gs}}\right]\left[\frac{l_{gs}-h_{cr}}{l_{gs}-h_{cr}-0.5h_w}\right]^V \tag{3}$$

The rounding radius of the vertices of the diamond grains is:

$$r = \frac{\left(0.0125K\left(l_{gs}-h_{cr}\right)\right)^2}{8\left(l_{gs}-h_{cr}-0.95h_w\right)} \quad (4)$$

where the designations correspond to (1).

It has been established that in the process of topographic adaptability, the actual contact area can change by several orders of magnitude, respectively, the specific pressure at the contact of diamond grains with the SHM will change, and, consequently, the nature and intensity of their mutual destruction.

3. RESULTS AND DISCUSSION

Figure 3b shows that the same value of the bearing area of the WSGW t_{rbsa} can be provided with significantly different values of h_w, i.e., by controlling the working height of the diamond grains, it is possible to control the value of tps, and, consequently, the intensity and nature of the destruction of the grains and the SHM.

However, the reduction of the working height of the grains, as noted above, leads to a decrease in the load on one grain, and, consequently, the contact pressures in the "SHM–grain" system also decrease, which, naturally, leads to the transformation of the nature of brittle self-sharpening of diamond grains into the process of their abrasion and a sharp decrease in the intensity of stock removal. An attempt to increase the pressure in the contact of the "SHM-grain" system by increasing the total load in the "SHM–WSGW" system by increasing the transverse feeding of S_{cf} or h_w can lead to the formation of defects on the treated surface of the SHM in the form of a network of microcracks.

Of all the factors that determine the size of the actual contact area, the concentration of diamonds in the grinding wheel remains the most controllable. By reducing the concentration, it is possible to reduce the number of grains in contact, increase the contact pressures in the "SHM–grain" system (without changing the total load on the processed SHM), resume the process of brittle self-sharpening (microcracks) of diamond grains and, as a result, intensify the removal of allowance.

If we analyze the obtained dependencies of the influence of the working height of the grains and the concentration of diamonds in the grinding wheel (Fig. 3a), we can state that the concentration of diamonds in the wheel is the most influential factor in the intensification of stock removal. This is convincingly proved (Fig. 3a) by the possibility of ensuring the same output (Q = 8 mm^3/min) for grinding wheels of 50% concentration and working height of grains h_w= 65 μm, or grinding wheel with 20% concentration and grain working height h_w = 30 μm.

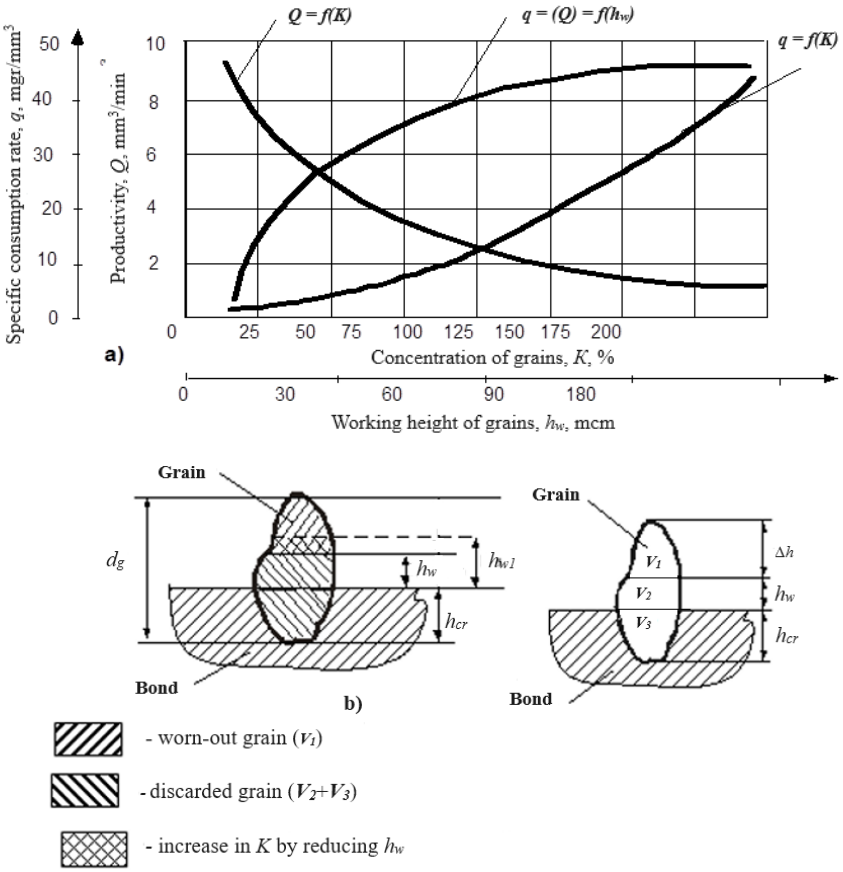

Fig.3. Schematic modeling of control of working height of grains (a) and wear of diamond grains (b)

It can be seen that if we reduce the working height of the grains$h_w$by half, then this is equivalent (for the value of t_{rbsa}) to an increase in the concentration of the grains by a factor of 2. Thus, if we determine from the dependence $Q = f(h_w)$ that the maximum performance for a 200/160 wheel will be at h_w= 140 μm, then to maintain the same t_{rbsa}at h_w = 20 μm, the height of h_w should be reduced by a factor of 7 or the concentration of diamond grains of the wheel should be no more than K = 14.2%. At the same time, under the same conditions, the specific consumption of diamonds is reduced by a factor of three. A schematic illustration of the analysis of

the influence of the working height of grains on the change in the ratio of the worn part of the grains and those that have fallen out of the bundle is shown in Figure 3 b.

Suppose that an increase in the concentration of diamonds in the grinding wheel corresponds to a proportional increase in the number of loading cycles in the "SHM–grain" contact and a similar decrease in pressure in the contact. Calculations have shown that when the load in the contact is doubled, which corresponds to a halving of the concentration of diamonds in the wheel, the number of cycles required to grind the stock with the SHM decreases by 10 times, and the number of cycles caused by the decrease in concentration decreases only by 2 times.

Reducing the concentration of diamonds in the wheel, even taking into account the reduction in the number of loading cycles in the "SHM–grain" contact, can increase the intensity of stock removal by 2–3 times only due to an increase in pressure in the contact.

Thus, it has been theoretically substantiated and experimentally proven that the concentration of diamonds in the wheel, the working height of the grains and the critical depth of their embedding in the bond are interrelated most important factors in the process of diamond grinding of SHM. A decrease in the concentration of diamonds in the wheel to the level of 5 – 20% with a corresponding decrease in the working height of the grains to the level of micro-irregularities of the bond and an increase in the modulus of its elasticity does not lead to a deterioration in the output indicators of the diamond grinding process of the SHM, since the value of the actual contact area of the WSGW with the SHM remains unchanged, but the specific consumption and processing costs are significantly reduced, and the degree of use of diamond grains increases.

When grinding SHM, the concept of coarse-grained and fine-grained wheels acquires a new special understanding, since in the process of microfracture of the allowance with SHM, not all the grain takes part, but only its submicrorelief (Fig. 2 c), since no grain is introduced into the PM. Coarse-grained grains with a well-developed sub-microrelief may be more effective in terms of stock removal than fine, but smooth, or ovalized grains. Therefore, even with a coarse-grained wheel, it is possible to carry out a precise finishing operation for the processing of SHM. Such a process can take place in case of mass formation of wear areas with very fine sub-microrelief on large grains. Such sub-microedges act as a finishing diamond paste with micro-edges rigidly fixed in the diamond grain.

It has also been established that in the case of SHM diamond grinding, the determining topographic parameter is not the macrorelief of the grinding wheel, but the sharpness of the submicroedges on the diamond grains. The protrusion height of the diamond grains from the bond and their concentration in the wheel are interrelated parameters through which the efficiency of the SHM diamond grinding process can be controlled. The value of the actual contact area in the "WSGW–SHM" system depends not only on the working height of the grain protrusion, but also on

the critical value of their embedding in the bundle, since at the same working height of the grains, the value of the actual contact area of the SHM with the WSGW will be different for different bundles. It has been theoretically substantiated and experimentally proven that the concentration of diamonds in the wheel, the working height of the grains and the critical depth of their embedding in the bond are the most important factors in the process of diamond grinding of SHM. Reducing the concentration of diamonds in the wheel to the level of 5 – 20% with a corresponding decrease in the working height of the grains to the level of micro-irregularities of the bond and increasing the modulus of its elasticity does not lead to a deterioration in the output indicators of diamond grinding of the SHM, since the value of the actual contact area of the WSGW with the SHM remains unchanged, but significantly reduces the specific consumption and cost of processing, increases the degree of use of diamond grains.

It is possible to control the efficiency of the diamond grinding process both at the pre-production stage, i.e. by selecting the optimal concentration of diamond grains in the wheel, and directly during the processing process – by changing the intensity of targeted dosed removal of the binder and the forced formation of a cutting submicrorelief on diamond grains [12].

It has been theoretically substantiated and experimentally proven that the concentration of diamonds in the wheel, the working height of the grains and the critical depth of their embedding in the bundle are interrelated most important factors in the process of diamond grinding of SHM.

The anisotropy of the physical and mechanical properties of diamond grains, which causes significantly different (up to 10 times) intensity of wear of their different facets, should be taken into account when analyzing changes in the parameters of the working surface of the wheel in the process of its wear, for example, when calculating the number of actually working grains, the value of the actual contact area in the "WSGW–SHM" system, and so on. confirms the correctness of this provision.

Dependencies have been obtained that link the working height of grains, their concentration with the number of grains on the WSGW and in contact with the SHM, the relative support surface area of the WSGW, the values of the actual contact area of the WSGW with the SHM, as well as their changes in the process of adaptability. These dependencies will be used in the theoretical module of the expert system of the SHM diamond grinding process [1].

Thus, a comprehensive theoretical and experimental analysis of the process of topographic adaptability was carried out, based on the theoretical description of the parameters of the topography of the working surface of the grinding wheel, their changes in the process of its wear and experimental laser scanning of the surface of the grinding wheel and SHM.

It has been established that the value of the actual contact area in the "WSGW–SHM" system depends not only on the working height of the protrusion of the grains, but also on the critical value of their embedding in the bundle, since at the same working height of the grains, the value of the actual contact area of the SHM with the WSGW will be different for different bundles. Theoretical dependencies were obtained to determine the number of grains on the WSGW and in contact with the SHM, the relative support surface area and the length of the profile of the WSGW, the value of the actual contact area of the WSGW with the SHM, as well as the dynamics of their change as the wheel wears out and the critical value of the grain embedding in the bundle changes. This makes it possible to theoretically assess the change in the topography parameters of the WSGW during the grinding process.

A method has been developed for determining the actual contact area of the WSGW with the SHM and its change in the process of adaptability, based on the artificial replacement of the discrete surface of WSGW with a continuous one and taking into account the elastic deepening of diamond grains into the binder. A two-stage method of 3D experimental-theoretical determination of the actual contact area of the WSGW with the SHM in the absence of grain penetration into the processed material and the absence of its contact with the bond is proposed, taking into account the sub-microrelief of diamond grains and SHM, the anisotropy of the properties of SHM crystallites and diamond grains, the elastic properties of the grinding wheel bond. At the first stage, the actual contact area "WSGW–SHM" is calculated at the macro level through the relative reference surface area of the wheel, and then, taking it as a contour, using the modernized method for calculating the parameters of the discrete relative support surface of the WSGW (b and γ), the actual contact area is calculated at the micro level "SHM – microrelief of grains" according to the known dependencies of N.B. Demkin and I.V. Kragelsky. The stiffness system uses the modulus of elasticity of the metal bond rather than the contacting materials.

Experimental determination of the actual contact area in the “WSGW–SHM” system can be performed based on the results of laser scanning of their surfaces and computer determination of the value of the relative support area.

4. CONCLUSIONS

It has been established that in the case of diamond grinding of SHM, the determining topographic parameter is not the macrorelief of the wheel, but the sharpness of the submicroedges on the diamond grains. The protrusion height of the diamond grains from the bond and their concentration in the wheel are interrelated parameters through which the efficiency of the SHM diamond grinding process can be controlled.

Theoretical dependencies have been obtained that describe the relationship and change of such parameters as the working height of the grains, the number of

grains at the WSGW and in the contact, their concentration in the diffuvial wheel, the relative reference length and the area of the WSGW profile, the actual contact area, and the specific load in the process of wear of the diamond wheel. It has been theoretically substantiated and experimentally proven that the concentration of diamonds in the wheel, the working height of the grains and the critical depth of their embedding in the bond are the most important factors in the process of diamond grinding of SHM. Reducing the concentration of diamonds in the wheel to the level of 5 – 20% with a corresponding decrease in the working height of the grains to the level of micro-irregularities of the bond and increasing the modulus of its elasticity does not lead to a deterioration in the output indicators of diamond grinding of the SHM, since the value of the actual contact area of the WSGW with the SHM remains unchanged, but significantly reduces the specific consumption and cost of processing, increases the degree of use of diamond grains.

References: 1. Modeling of the diamond grinding process by the finite element method [Electronic resource] : monograph / *Fedorovych V. O., Fedorenko D. O., Romashov D. V., Ostroverkh Y. V., Pupan L. I.*] ; National Technical University "Kharkiv Polytechnic Institute." –Kharkiv, 2023. 257 p. (in Ukrainian) – URI:https://repository.kpi.kharkov.ua/handle/KhPI-Press/64334. **2**. *Chi Y, Li H.* Simulation and analysis of grinding wheel based on Gaussian mixture model. Frontiers of Mechanical Engineering, 2012;7(4):427–432.DOI https://doi.org/10.1007/s11465-012-0350-3 **3**. *Frutani K, Ohguro N, et al*. In-process measurement of topography change of grinding wheel by using hydrodynamic pressure. International Journal of Machine Tool and Manufacture, 2002;42:1447–1453.https://doi.org/10.1016/S0890-6955(02)00073-1 **4.** *Ye R, Jiang X, Blunt L, Cui C, Yu Q.* The application of 3D-motif analysis to characterize diamond grinding wheel topography. Measurement, 2016;77:73–79.https://doi.org/10.1016/j.measurement.2015.09.005 **5.** *Amin A. Mokbel, T.M.A. Maksoud*, Monitoring of the condition of diamond grinding wheels using acoustic emission technique, Journal of Materials Processing Technology; 101 (2000) 292–297https://doi.org/10.1016/S0924-0136(00)00433-7. **6.** *K.-C. Fan, M.-Z.Lee, J.-I.Mou*, On-line non-contact system for grinding wheel wear measurement, International Journal Advanced Manufacturing Technology; 19 (2002) 14–22https://doi.org/10.1007/PL00003964. **7.** *Tönshoff HK, Peters J, Inasaki I, Paul T* (1992) Modelling and simulation of grinding processes. CIRP Annals –Manufacturing Technology 41 (2):677–688 https://doi.org/10.1016/S0007-8506(07)63254-5. **8.** *Verkerk J* (1977) Final report concerning CIRP cooperative work on the characterization of grinding wheel topography. Annals of the CIRP 26 (2):385–395. **9.** *Malkin S* (1989) Grinding technology: Theory and applications of machining with abrasives. Society of Manufacturing Engineers, USA. **10.** *Hegeman J* BJW (2000) Fundamentals of grinding: Surface conditions of ground materials. University of Groningen, Netherlands. **11.** *Kragelskii I.V., Dobychin M.N., Kombalov V.S.* Friction and Wear Calculation Methods, Oxford: Pergamon Press, 1982.– 454 p. **12.** *Qiao G, Dong G, Zhou M* (2013) Simulation and assessment of diamond mill grinding wheel topography. The International Journal of Advanced Manufacturing Technology 68 (9–12):2085-2093 https://doi.org/10.1007/s00170-013-4807-2

Володимир Федорович, Євгеній Островерх, Дмитро Ромашов, Харків, Україна

ТОПОГРАФІЧНА АДАПТИВНІСТЬ В ЗОНІ АЛМАЗНОГО ШЛІФУВАННЯ НАДТВЕРДИХ МАТЕРІАЛІВ

Анотація. *Широке застосування надтвердих матеріалів (НТМ) і організація масового виробництва з них ріжучого, шліфувального, волочильного, свердлильного і вимірювального інструменту вимагають розробки високоефективних і точних методів і технології їх обробки. Актуальність розв'язуваної проблеми продиктована високою трудомісткістю і низькою продуктивністю процесу шліфування НТМ, великою витратою дорогих алмазних зерен шліфувальних кругів і, як наслідок, високою вартістю обробки. Проведено комплексний теоретичний та експериментальний аналіз технологічної топографічної адаптивності, заснований на ідеалізованому описі топографічних параметрів робочої поверхні шліфувального круга, їх зміні при його зносі та експериментальному лазерному скануванні робочої поверхні шліфувального круга та оброблюваного надтвердого матеріалу. Встановлено, що висота виступання алмазних зерен впливає на інтенсивність руйнування (видалення) матеріалу заготовки через зміну кількості робочих зерен і фактичної площі контакту оброблюваного НТМ з робочою частиною поверхні шліфувального круга. У процесі контрольованого шліфування можна стабілізувати робочу висоту зерен на будь-якому з 3-х ступенів інтенсивності їх зносу, прирівнявши цю інтенсивність до інтенсивності зношування алмазоносної зв'язки круга. Розроблено методику визначення фактичної площі контакту робочої поверхні шліфувального круга з поверхнею НТМ та зміни її технологічної адаптивності. Встановлено, що в процесі топографічної адаптивності фактична площа контакту може змінюватися на кілька порядків, відповідно, буде змінюватися питомий тиск при контакті алмазних зерен з НТМ, а, отже, характер і інтенсивність їх взаємного руйнування. Отримано теоретичні залежності, що описують взаємозв'язок і зміну таких параметрів, як робоча висота зерен, число зерен на РПШК і в контакті, їх концентрація в алмазоносному шарі круга, відносна опорна довжина і площа профілю РПШК, фактична площа контакту, питоме навантаження в процесі зносу алмазного круга. Теоретично обґрунтовано і експериментально доведено, що концентрація алмазів у крузі, робоча висота зерен і критична глибина їх залягання в зв'язці є найважливішими факторами в процесі алмазного шліфування НТМ. Зниження концентрації алмазів в крузі до рівня 5 – 20% з відповідним зменшенням робочої висоти зерен до рівня мікронерівностей зв'язки і збільшенням модуля її пружності не призводить до погіршення вихідних показників алмазного шліфування НТМ, так як величина фактичної площі контакту РПШК з НТМ залишається незмінною, але значно знижує питомі витрати і вартість обробки, підвищує ступінь використання алмазних зерен.*

Ключові слова: *надтвердий полікристалічний матеріал; алмазні зерна; робоча поверхня шліфувального круга; мікрорельєф алмазних зерен; концентрація алмазних зерен у шліфувальному крузі.*

UDC 621.9.048.4 **doi: 10.20998/2078-7405.2023.99.04**

INVESTIGATION OF ELECTRO DISCHARGE MACHINING OF TOOL STEELS BASED ON THE ROUGHNESS OF THE MACHINED SURFACES

Zsolt **Maros** [0000-0001-5029-3559], Krisztina **Kun-Bodnár** [0000-0003-1904-4479], Vivien **Fekete**

University of Miskolc, 3515, Miskolc - Egyetemváros, Hungary
zsolt.maros@uni-miskolc.hu

Received: 08 November 2023 / Revised:12 November 2023 / Accepted: 19 November 2023 / Published: 01 December 2023

Abstract. *In electro discharge machining (EDM or spark erosion) the roughness of the machined surface plays a very important role in the applicability of the process. This paper deals with a comparative study of the electro discharge machining of tool steels based on the roughness characteristics of the machined surfaces. Another aim of the research is to investigate which tool materials (electrode material, copper, or graphite) are most effective to achieve the best possible surface microgeometry. Based on the data of the performed cutting experiments and the subsequent measurements, conclusions will be drawn regarding the machinability of the tested tool steels and the applicability of the electrode materials used.*
Keywords: *electrical discharge machining; copper, graphite electrodes; functional roughness parameters.*

1. INTRODUCTION

Thanks to the development of the materials to be machined, industry has started to work with materials of increasing hardness and strength, which would be extremely difficult or impossible to machine with traditional methods. This has led to the development of various non-traditional machining processes, one of the most important of which is electro discharge machining or spark erosion [1]. This process, which is suitable for machining electrically conductive, high hardness materials, allows the formation of spatial surfaces. Its popular field of application is the production of injection moulding tools.

Several papers deal with the examination of different tool materials, including copper, bronze and graphite electrodes [2, 3, 4]. Paper [5] presents a comparison of graphite and copper electrodes to analyse the efficiency of material removal. In present article, we investigate the machinability of different tool steels used for injection moulding machined with copper and graphite electrodes of plastic parts,

based on the roughness of the machined surfaces. In the literature, several people have already dealt with the roughness of EDM surfaces as a function of technological data [6, 7, 8, 9]. In this paper, we present our research results obtained during the examination of the microgeometric characteristics of EDM machined surfaces with copper and graphite electrodes.

The EDM surface is made up of overlapping, irregularly spaced craters (Fig. 1), the formation of which is influenced by a number of process parameters such as voltage, current, cycle time [1].

When using today's modern machine tools, most of these parameters are automatically generated by the machine tool and set to optimal values for processing. On EDM equipment, the optimization is based on the VDI grade, which is set by the machine operator before the start of machining. VDI stands for German Engineering Association (Verein Deutscher Ingenieure). This organization develops standard technical recommendations to help solve various technical processes and problems. The VDI 3400 standard deals with EDM. This recommendation groups machined surfaces into so-called VDI grades based on surface roughness from VDI 00 to VDI 45. The purpose of this is to standardize the surface characteristics of the parts, which is an essential aspect for engineers to design injection mould inserts produced by EDM. Today, the VDI scale is used worldwide in the tooling industry. The parameter is a surface roughness characteristic and complements and replaces the general surface roughness metrics.

The change of the roughness parameters was investigated as a function of the VDI grade of the machining. Similar studies have been reported in [10]. The implementation of the experiments and our measurement results are described below.

2. MICROSTRUCTURE OF THE EDM MACHINED SURFACE

The nature of EDM machined surface is different from that of a conventional machined surface. There is no directionality or groove corresponding to the federate. The machined surface is cratered. The roughness of the surface is created by the interaction of overlapping craters (Fig. 1). The dimensions of the craters depend on the characteristics of the spark discharge, the workpiece and electrode material.

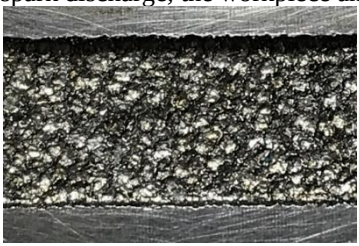

Figure 1 Microstructure of EDM machined surface

In the case of long-duration, low-energy discharges, wide and shallow craters are created because the discharge channel widens. Such a surface is shiny in spots. High-energy discharges of short duration create deep craters because there is not enough time to dissipate the generated heat. Such a surface looks homogeneous, has a silky, dull sheen. The energy content of the discharges can be controlled by changing the electrical parameters. Among the electrical parameters, current strength and pulse time have the greatest effect on surface roughness. However, these parameters cannot be set on modern machining machines, they are chosen by the machine itself depending on the specified VDI grade.

The roughness of EDM surfaces is now often only characterized by the VDI grade. At the same time, other roughness parameters are often also important from the point of view of operation. That is why it is important to choose the right roughness metrics. In our research, we examined the amplitude and material ratio parameters.

3. EXPERIMENTAL CONDITIONS

3.1 Machined materials and test pieces

During the experiment, the surfaces of four types of tool steel used for plastic injection moulding tools were machined by electro discharge machining. The chemical composition of the steels is shown in Table 1.

Table 1 – Chemical composition of plastic forming tool steels

Material	**C, %**	**Si, %**	**Mn,%**	**Cr, %**	**Mo, %**	**Ni, %**	**S %**
C45U (1.1730)	0.45	0.30	0,70				
40CrMnMo7 (1.2311)	0.40	0.30	1.50	1.90	0.20		
40CrMnMoS8-6 (1.2312)	0.40	0.40	1.50	1.90	0.20		0.08
45NiCrMo16 (1.2767)	0.48	0.23	0.40	1.30	0.25	4.00	

The test pieces were 100x120x20 mm, rectangular cross-section, non-heat treated plates, the surface of which was pre-ground for more efficient sparking. 5 mm deep cavities were made on these test pieces by EDM Figure 2). On one test

specimen was tested at 5 different VDI grades with both copper and graphite electrodes. The VDI grades set were 18, 21, 25, 29, 36.

Figure 2 – Test piece machined with EDM

3.2 Electrodes

To carry out the machining experiments, copper (red copper) and graphite electrodes were used for all test piece materials. The type of copper electrodes used was CuETP electrolytic copper and graphite of type ELOR-50-F, with a cross section of 55 x 15 mm.

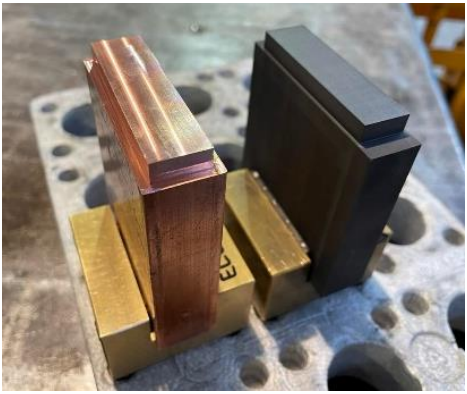

Figure 3 – Copper and graphite electrodes used for the experiments

3.3 Machine tools and measuring equipment

The machining experiments were carried out on a Neuar CNC-C50 type electro discharge machine. During the machining, the test pieces were clamped in a vice and the dielectric used was petroleum.

The surface roughness measurements of the machined cavities were carried out in the laboratory of the Institute of Manufacturing Science of the University of Miskolc, using an AltiSurf 520 three-dimensional surface topography machine. During this, we also measured the profile and spatial roughness parameters. In this article, we deal with the examination of profile parameters.

4. EVALUATION OF EXPERIMENTAL RESULTS

From the results of the EDM experiments, we can draw conclusions on the effect of the set VDI grade on the profile roughness parameters of the machined surface and the machining efficiency when machining different tool steels using copper and graphite electrodes.

4.1. Profile (2D), amplitude surface roughness parameter analysis

Figures 4 and 5 show the variation of the average surface roughness parameter R_a as a function of VDI grade for the tool materials tested, in the case of copper and graphite electrodes.

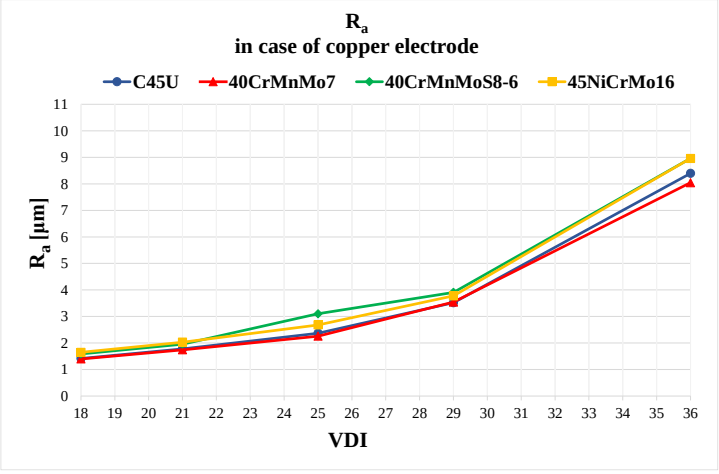

Figure 4 – Variation of R_a parameter as a function of VDI grade for copper electrode

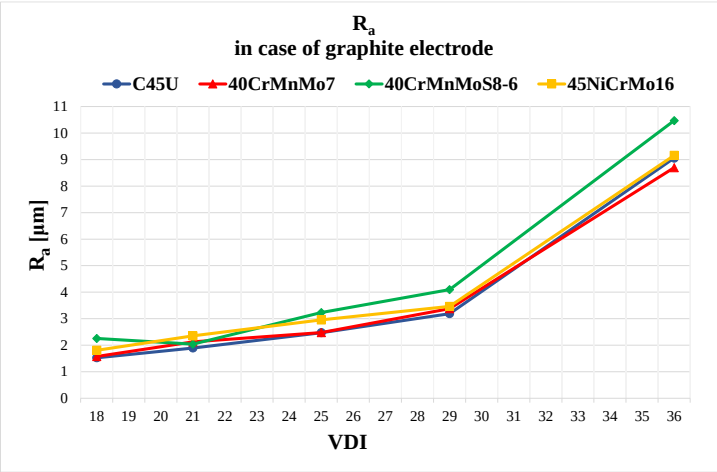

Figure 5 – Variation of R_a parameter as a function of VDI grade for graphite electrode

Figures 4 and 5 show that there is no significant difference in R_a between the different machined material grades. For both electrode materials, the lowest roughness values were obtained on the unalloyed C45U material grade and the worst roughness values were obtained on the 40CrMnMoS8-6 steel. The roughness of the surfaces produced with the copper electrode varied between R_a = 1.4-9 µm and with the graphite electrode between R_a = 1.5-10.5 µm, i.e. the two electrode materials also do not show significant values, although the roughness of the surfaces produced with the graphite electrode is mostly higher than that of the surfaces produced with the copper electrode.

Figures 6 and 7 describe the variation of the mean roughness depth R_z as a function of VDI grades. The general observations made for the R_a parameter are also valid here. The general statements made for the R_a parameter are also valid here. There are minor differences between the workpiece materials here as well, the mean roughness depth parameter R_z changes analogously to the R_a parameter depending on the VDI grade. For copper electrodes, R_z values ranged from 15.8 to 62.6 µm and for graphite from 16.7 to 70.3 µm. The values of R_z compared to R_a vary in the ratio $R_z \approx (6 \div 13) \cdot R_a$. This ratio is usually estimated by the manuals as $R_z \approx 8R_a$.

Figure 6 – Variation of parameter R_z as a function of VDI for copper electrode
Figure 6 – Variation of parameter R_z as a function of VDI for copper electrode
Figure 6 – Variation of parameter R_z as a function of VDI for copper electrode

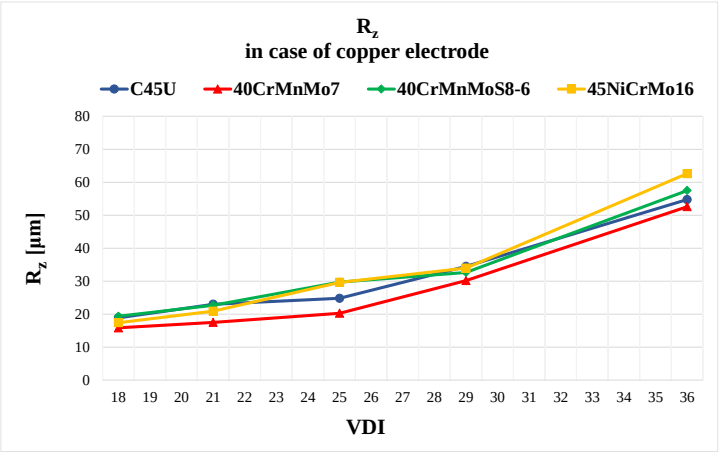

Figure 6 – Variation of parameter R_z as a function of VDI for copper electrode

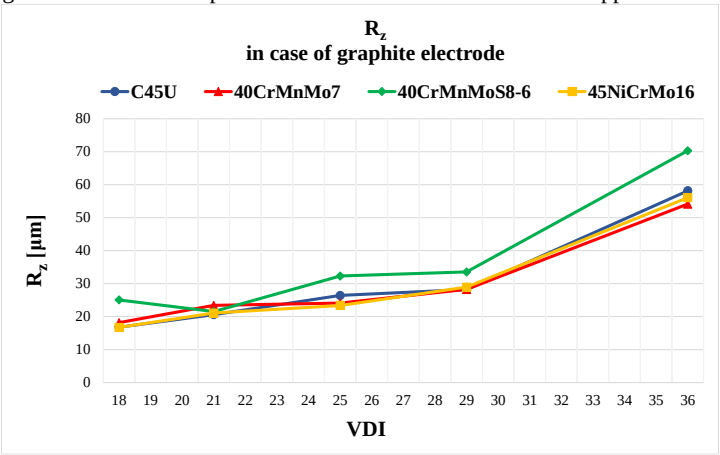

Figure 7 – Variation of parameter R_z as a function of VDI grade for graphite electrodes

Among the functional roughness parameters, the variation of the so-called material ratio parameter (R_{mr}) was investigated. The material ratio parameter R_{mr} is used to characterise the functional and wear properties of surfaces. The higher the percentage R_{mr} value of a given surface, the more favourable its functional properties. In our tests, the values of the material fraction parameter were determined at a depth of c = 10 µm. Figures 8 and 9 show the change in the material ratio parameters of surfaces made with copper and graphite electrodes in each VDI grade.

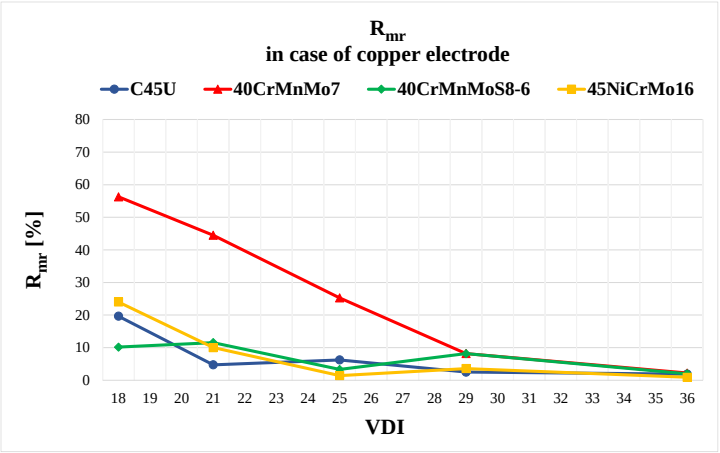

Figure 8 – Variation of R_{mr} parameter as a function of VDI grade for copper electrode

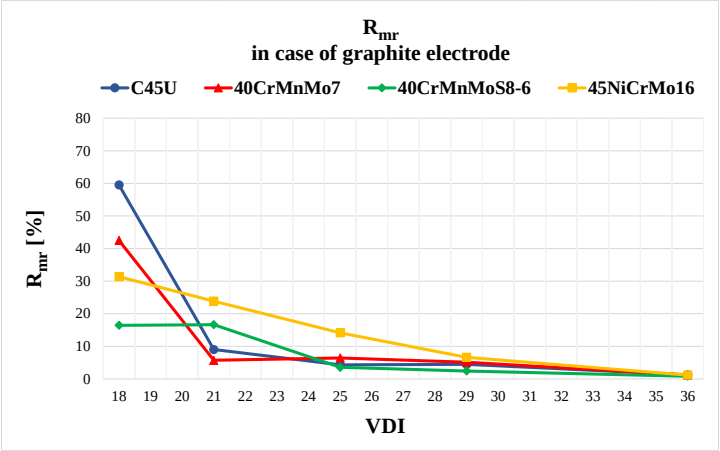

Figure 9 – Variation of R_{mr} parameter as a function of VDI grade for graphite electrode

In Figures 8 and 9, it can be observed that the best material ratio values are achieved at VDI 18 and that with increasing VDI grades, regardless of tool and workpiece material, the surface properties deteriorate and the material ratio parameter difference between steels decreases. In the case of copper electrodes, outstanding performance characteristics can be achieved when machining 40CrMnMo7 and, in the case of graphite, the same can be said for C45U and 45NiCrMo16.

4.1. Examination of machining times

We can draw conclusions about the productivity of the EDM process, i.e. the machining performance, from the machining time of each cavity. During the experiments, cavities with a cross-section of 55x15 mm and a depth of 5 mm were made by block EDM. Figures 10 and 11 show the machining time of the cavities made on the four types of tested tool steel workpieces as a function of the VDI degrees, in the case of copper and graphite electrodes.

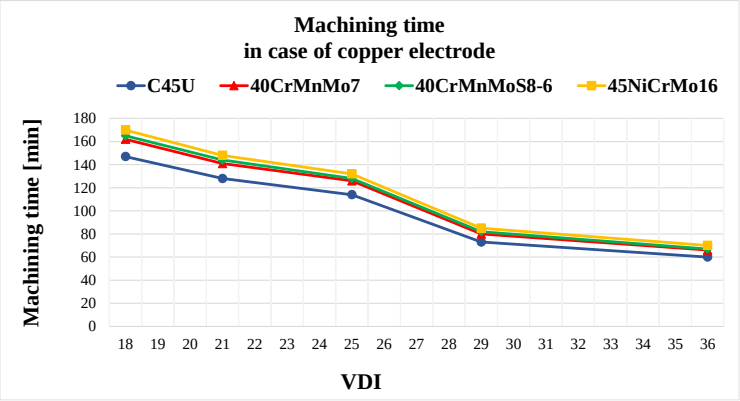

Figure 10 – Variation of machining times depending on the VDI grade in the case of a copper electrode

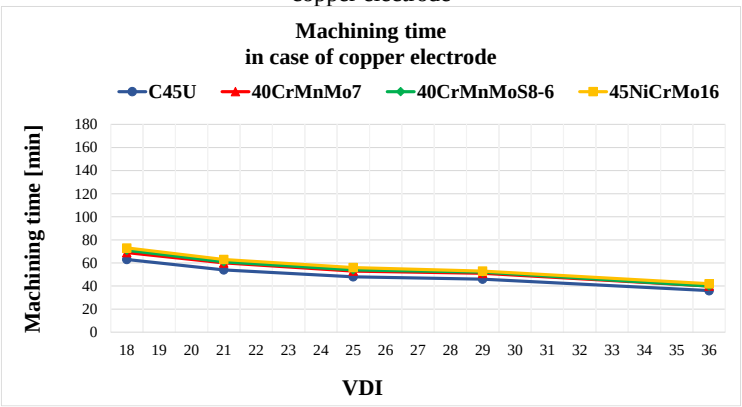

Figure 11 – Variation of machining times depending on the VDI grade in the case of a graphite electrode

From Figures 10 and 11, it can be seen that as the VDI grades increase, the machining time decreases, i.e., the machining becomes more productive. For the tool steels studied, for both copper and graphite electrodes, it can be said that the

proportion of alloying elements in the material being machined is related to the machining time. The less alloying elements the material tested contained, the shorter the time required for spark erosion. Accordingly, cavities made on unalloyed C45U steel took the least time to machine, and those made on 45NiCrMo16 steel with the most alloying elements took the longest. The most striking difference was observed between the two electrode materials The productivity of the graphite electrode is almost twice that of the copper electrode, which means that the spark cutting process takes significantly less time than with copper.

5. CONCLUSIONS

Summarising the results of the research work on the comparison of tool steels of different alloys machined by EDM, the following conclusions can be drawn:

- Regarding the amplitude roughness parameters (R_a and R_z), the surface roughness value deteriorates with increasing VDI grades. In the tested range, small roughness differences can be observed between the individual tool steels. Increasing the amount of alloying elements slightly worsens the surface roughness. Regarding the two types of electrode materials, it can be said that the roughness of the surfaces produced with a graphite electrode is usually greater than that produced with a copper electrode.
- In the case of EDM surfaces, the mean roughness depth R_z varied analogously to the average roughness R_a. Based on the measurement results, the relation $R_z \approx (6 \div 13) \cdot R_a$ can be written for their relationship.
- According to the material ratio parameter (R_{mr}) determined at a depth of c = 10 μm, the best operating and wear properties are achieved at VDI grade 18, which continuously deteriorate as the grade increases, and the results obtained on each tool target show a decreasing difference with increasing grades. The effect of the amount of alloying elements is more evident for the R_{mr} parameter than for the R_a and R_z parameters. For smaller alloying amounts, more favourable (higher) material ratio parameter values are obtained.
- In connection with the examination of the machining times, it can be said that increasing the VDI grades reduces the processing time, i.e. increases the material removal rate. From this point of view, the less alloyed materials were more machinable. Regarding the two electrode materials, a significant difference can be shown between graphite and copper. The material removal rate of graphite is much higher than that of copper, which means that the machining times for copper are about twice as long as for machining with a graphite electrode.

Summarizing our findings, it can be said that the surface roughness parameters deteriorate as the VDI grades increase (R_a and R_z increase, R_{mr} decreases). At the

same time, increasing the VDI grade reduces the machining time, i.e. increases productivity. No significant differences were found for the tool steel materials machined in the test. However, unalloyed or less alloyed steels could be machined more productively and with a better surface quality. In terms of roughness, the two electrode materials (copper and graphite) showed no significant differences, but the productivity of graphite was about twice that of copper electrodes. We intend to continue the research work by evaluating further profile and 3*D* roughness parameters.

References. **1.** *K. HHoS – T. Newman – S. Rahimifard – RD. Allen*: State of the art in wire electrical discharge machining (WEDM), International Journal of Machine Tools and Manufacture, Volume 44, Issues 12–13, October 2004, pp. 1247–1259, https://doi.org/10.1016/j.ijmachtools.2004.04.017 **2.** *A.A. Khan*: Electrode wear and material removal rate during EDM of aluminum and mild steel using copper and brass electrodes. Int. J. Adv. Manuf. Technol. 39, pp. 482–487 (2008). https://doi.org/10.1007/s00170-007-1241-3 **3.** *D'Urso, G., Maccarini, G. & Ravasio, C.* Influence of electrode material in micro-EDM drilling of stainless steel and tungsten carbide. Int. J. Adv. Manuf. Technol. 85, 2013–2025 (2016). https://doi.org/10.1007/s00170-015-7010-9 **4.** *V. Molnár, I. Sztankovics*: Analysis of Roughness Parameters Determining Tribological Properties in Hard Turned Surfaces, Hungarian Journal Of Industry And Chemistry 49:2 (2021) pp. 77–84. **5.** *F.L. Amorim Walter - L. Weingaertner*: The behaviour of graphite and copper electrodes on the finish die-sinking electrical discharge machining (EDM) of AISI P20 tool steel, J. Braz. Soc. Mech. Sci. & Eng. 29 (4) • Dec 2007, https://doi.org/10.1590/S1678-58782007000400004 **6.** *I Puertas - CJ Luis - L Alvarez*: Analysis of the influence of EDM parameters on surface quality, MRR and EW of WC–Co, Journal of Materials Processing Technology, Vol. 153–154, 10 November 2004, pp. 1026–1032, https://doi.org/10.1016/j.jmatprotec.2004.04.346 **7.** *S.H. Lee - X.P. Li*: Study of the effect of machining parameters on the machining characteristics in electrical discharge machining of tungsten carbide, Journal of Materials Processing Technology, Vol.115 (2001), pp. 344–358, https://doi.org/10.1016/S0924-0136(01)00992-X **8.** *E. L. Papazoglou - N. E. Karkalos - A. P. Markopoulos - P. Karmiris-Obratański*: On the Machining of Aluminium Alloy AL6063 with EDM, Cutting & Tools in Technological System, 2020, Edition 93, pp. 76–87, doi: 10.20998/2078-7405.2020.93.09 **9.** *M. Balanou - E. l. Papazoglou - A. P. Markopoulos - P. Karmiris-Obratański*: Experimental Investigation of Surface Topoghraphy of AL7075-T6 alloy Machined by EDM, Cutting & Tools in Technological System, 2021, Edition 94, pp. 3–10, doi: 10.20998/2078-7405.2021.94.01 **10.** *B. Mikó – Á. Drégelyi-Kiss – A. Poór*: Study of surface quality and electrode wear in EDM technology, In: *W, Zebala; I., Mankova* (szerk.) Development in Machining Technology, Cracow, Poland: Cracow University of Technology Tadeusz Kosciuszko, (2014) pp. 194–211.

Жолт Марош, Крістіна Кун-Боднар, Вів'єн Фекете, Мішкольц, Угорщина

ДОСЛІДЖЕННЯ ЕЛЕКТРОРОЗРЯДНОЇ ОБРОБКИ ІНСТРУМЕНТАЛЬНИХ СТАЛЕЙ ЗА ШОРСТКІСТЮ ОБРОБЛЮВАНИХ ПОВЕРХОНЬ

Анотація. *При електророзрядній обробці (електроерозійна або іскрова ерозія) шорсткість оброблюваної поверхні відіграє дуже важливу роль у застосовності процесу. Дана робота присвячена порівняльному дослідженню електророзрядної обробки інструментальних сталей на*

основі характеристик шорсткості оброблюваних поверхонь. Інша мета дослідження полягає в тому, щоб з'ясувати, які інструментальні матеріали (електродний матеріал, мідь або графіт) є найбільш ефективними для досягнення найкращої можливої мікрогеометрії поверхні. Що стосується параметрів амплітудної шорсткості (R_a і R_z), то значення шорсткості поверхні погіршується зі збільшенням марок VDI. У випробуваному діапазоні можна спостерігати невеликі відмінності шорсткості між окремими інструментальними сталями. Збільшення кількості легуючих елементів дещо погіршує шорсткість поверхні. Щодо двох типів електродних матеріалів можна сказати, що шорсткість поверхонь, отриманих за допомогою графітового електрода, зазвичай більша, ніж шорсткість, отримана мідним електродом. У випадку електроерозійних поверхонь середня глибина шорсткості R_z змінювалася аналогічно середній шорсткості R_a. За результатами вимірювань відношення $R_z \approx (6 \div 13)R_a$ можна записати для їх відносин. Відповідно до параметра співвідношення матеріалу (R_{mr}), визначеного на глибині c = 10 мкм, найкращі експлуатаційні та зносостійкі властивості досягаються на 18 рівні стандарту VDI, які безперервно погіршуються зі збільшенням рівня, а результати, отримані на кожній мішені інструменту, показують зменшувану різницю зі збільшенням рівня. Вплив кількості легуючих елементів більш очевидно для параметра R_{mr}, ніж для параметрів R_a і R_z. При менших кількостях легування виходять більш вигідні (більш високі) значення параметрів співвідношення матеріалів. У зв'язку з вивченням термінів механічної обробки можна сказати, що збільшення рівня VDI скорочує час обробки, тобто збільшує швидкість зняття матеріалу. З цієї точки зору, менш леговані матеріали були більш оброблюваними. Що стосується двох електродних матеріалів, то можна показати значну різницю між графітом і міддю. Швидкість видалення матеріалу графіту набагато вища, ніж у міді, а це означає, що час обробки з допомогою міді приблизно вдвічі довший, ніж для обробки графітовим електродом. На підставі даних проведених експериментів з обробляння і подальших вимірювань будуть зроблені висновки щодо оброблюваності випробовуваних інструментальних сталей і застосовності використовуваних електродних матеріалів.

Ключові слова: *електроерозійна обробка; мідні, графітові електроди; функціональні показники шорстості.*

UDC 621.9.048 **doi: 10.20998/2078-7405.2023.99.07**

ROUGHNESS INVESTIGATION OF SINGLE AND DOUBLE CUTTING MARKS ON FACE MILLED SURFACE

Antal **Nagy** [0000-0001-6160-4973], Janos **Kundrak** [0000-0002-6013-7856]

University of Miskolc, 3515, Miskolc - Egyetemváros, Hungary
antal.nagy@uni-miskolc.hu

Received: 03 November 2023 / Revised:14 November 2023 / Accepted: 22 November 2023 / Published: 01 December 2023

Abstract. *In machining with defined cutting edge tools, in some rotational tool processes (e.g. face milling) the tool edge may scratch the surface of the workpiece one more time, depending on the cutting conditions, during one revolution of the tool. As a result, the topographies with single or double cutting marks will be different from each other. The deviation, depending on its size, can also affect the functional performance (e.g. friction conditions) of the operating surfaces. In this article, face-milled topographies created with a symmetrical setting and with single or double milling marks are compared according to the magnitude of the roughness and the degree and nature of the inhomogeneity.*
Keywords: *face milling; surface roughness; back-cutting of milling tool; secondary material removal.*

1. INTRODUCTION

The aim of manufacturing is to create products and their parts with the required accuracy and surface quality so that structural, functional and other usage requirements can be achieved. Such expectations can be wear or corrosion resistance, sealing ability with or without sealing material, thermal and electrical conduction, possibility of coating, aesthetics, etc. In many cases these can be achieved by machining, where the tool separates the material of the workpiece, thereby creating chips and a new machined surface. The shape of the tool edge(s) is imprinted on the surface, creating a pattern specific to each cutting process [1]. In addition, many – often unknown – factors take place during the process (tool wear, change in chip cross-section, change in cutting force, vibrations, workpiece material heterogeneity, etc.) [2]. These machining process characteristics and phenomena that influence the formation of topography were described for turning in an Ishikawa diagram by Bajic et al. [3]. We supplemented this with a few points, considering the specifics of machining with rotating tools, which are circled on the graph (Figure 1). Many researchers study the effects of these parameters on roughness and countless articles are published about the results of their analyses.

In the case of machining with defined cutting edge tools, it is usually characteristic that during finishing the final topography is formed by the tool, leaving

a single impression of its edge(s) [4]. However, in machining with rotating tools (e.g. face milling), it happens that the tool edges cut the surface of the workpiece twice due to the movement conditions. In the beginning of the cutting, the edges separate material from the workpiece in each revolution [5], which is their front cutting movement. In this case, cycloid arcs are formed on the surface shifted by a feed distance. During the further feed movement, the same edges may scratch the already machined surface again during their return, during which further material separation, "re-cutting" occurs [6]. In this case double milling marks are formed on the surface [7]. In this case the texture consists of lozenge-like protrusions, and they become smaller as they move further away from the plane of symmetry – the path of the tool axis [6]. This occurs when the tool axis is perpendicular to the machined plane surface [6] and the length of the feed movement is greater than the radius of the tool.

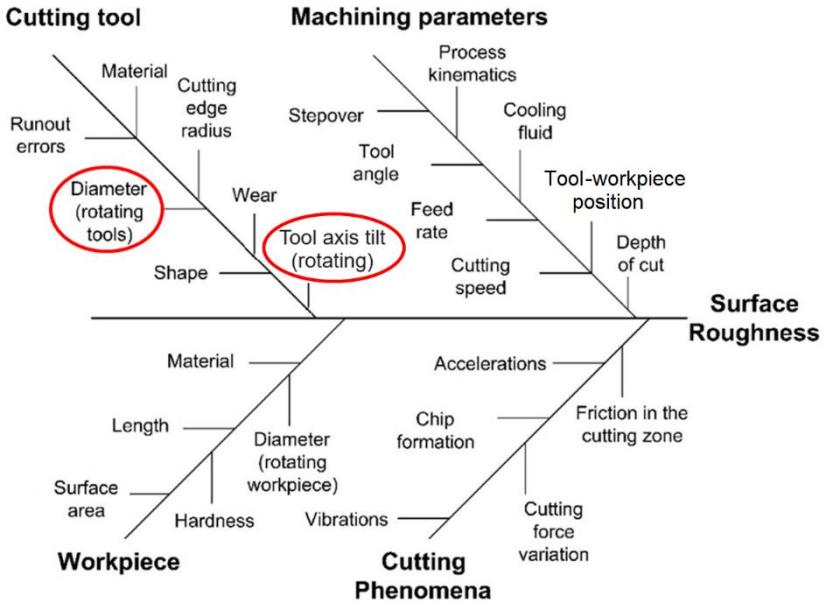

Figure 1 – Factors affecting surface roughness [3]

Milled surfaces having both single [8] and double [9] cutting marks are produced in industry for the same purpose of use, but these topographies have different characteristics. A lower roughness can be measured on the topography with double milling marks, where the degree of reduction is significantly affected by the phase difference (the ratio of the distance between a front-cutting and its nearest back-cutting mark measured in the symmetry plane and the feed), depending on the diameter of the

tool and the magnitude of the feed [7,10]. The roughness is also affected by the fact that the front- and back-cutting traces are not of the same depth, because of the bending of the tool due to the cutting forces and the elastic recovery of the workpiece material after cutting [11]. As the difference in depth decreases, the values of Ra and Rt decrease slightly [10].

No matter the texture, the face milled surface topography is various and its roughness is different when measured in various places, which was investigated on experimental surfaces [12,13] and on theoretical topographies produced analytically [14]. One of the main findings is that the profiles measured in the direction parallel to the tool advance are regularly repeated (periodic) with the feed distance. The roughness values are maximal in the symmetry plane, they decrease in other parallel planes the further away from it [12,15], and the degree of difference increases with increasing feed [16]. In perpendicular direction, the number of peaks increases on measured profiles further away from the symmetry plane, and their Ra and Rz values decrease.

In addition to the technological data and machining process characteristics, the roughness of the face milled surface topography is also influenced by the type of the texture; however, the topographical and functional effect of the secondary material separation is not known in sufficient depth. In this article, the aim of the study is to compare the topographic characteristics of the two types of patterns and to determine how the surface roughness and its deviations change due to the secondary material separation.

2. EXPERIMENTAL CONDITIONS

Milling experiments were carried out on a PerfectJet MCV-M8 vertical milling center. The workpiece material was C45 unalloyed carbon steel in a normalized state, on which the plane surfaces were machined on an area of 58×50 mm^2. They were cut with a Dijet SEKN 1203 AFTN type, JC5030 quality insert mounted on a Canela 0748.90.063 milling head, whose nominal diameter was D_t = 63 mm, the cutting edge angles were $\kappa_r = 45°$; $\gamma_o = 0°$; $\alpha_o = 20°$, and the width of the chamfer was 0.85 × 45° (Figure 2). We set the feed f_z = 0.4 mm/rev, the depth of cut a_p = 0.8 mm and the cutting speed v_c = 300 m/min. The tool axis was in a perpendicular position to the machined surfaces, so the range of the feed movement of the workpiece determined the formed impression. As the workpiece was moved until the tool axis line generated only front-cutting traces (Figure 2a), creating the M1 surface. However, the other workpiece was moved under the tool with a full length feed, where due to the motion conditions the edges scratched the surface twice (during front-cutting and back-cutting movement as well), producing surface M2 (Figure 2b). During the examination, we take into account that according to the directions of the cutting and feed speeds, two sides of the surfaces separated by a symmetry plane can

be distinguished; up-milling takes place on the workpiece from the start of cutting until the symmetry plane; after that, down-milling occurs. When evaluating the deviations and distributions of roughness values, the surface parts are marked with a superscript, where *U* is up-milled, *D* is down-milled.

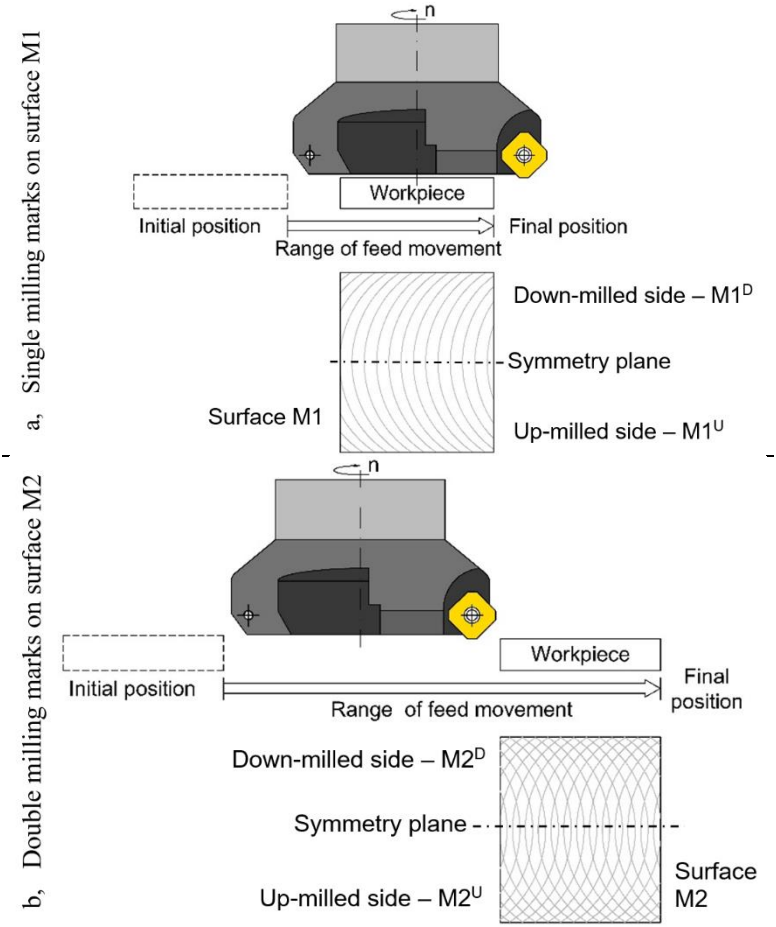

Figure 2 – Range of workpiece feed movement for creating topography having single (a) or double cutting marks (b)

This was followed by topography measurement on an AltiSurf 520 3*D* surface measuring device with a CL2 confocal chromatic sensor. To evaluate the roughness

deviations, 25 measurement points on the surface were determined in such a way that they designate examination planes parallel and perpendicular to the feed (Figure 3). These are important for milling regarding the kinematics and the position of the points. One of the planes in the feed direction is identical to the symmetry plane (path of the tool axis) (plane C), and the other parallel planes are taken at 10 mm distance between each other (planes A, B, D, E). The planes perpendicular to these (planes I–V) have a distance of 8 mm between each other. At the measurement points, profiles were measured in directions parallel and perpendicular to feed, and they were evaluated at 4 mm length with a section length of 0.8 mm.

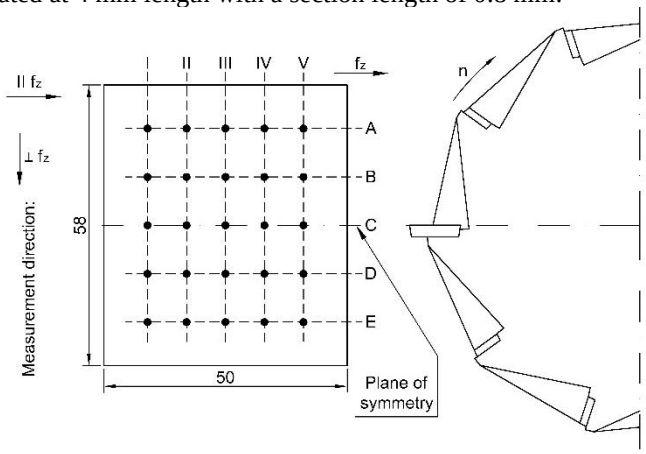

Figure 3 –Position of measurement points and planes on surfaces

Table 1 – R_a and R_z parameter values of profiles measured in feed direction

	Single cutting marks – Surface M1							**Double cutting marks – Surface M2**					
	I	**II**	**III**	**IV**	**V**	*ΔR*		**I**	**II**	**III**	**IV**	**V**	*ΔR*
Ra [µm]	2.48	2.53	2.51	2.50	2.51	*0.05*	**A**	1.64	1.48	1.52	1.52	2.09	*0.61*
	3.05	3.03	3.03	3.02	3.05	*0.03*	**B**	1.12	1.11	1.16	1.26	1.49	*0.38*
	3.20	3.19	3.21	3.21	3.17	*0.04*	**C**	2.82	2.93	2.99	2.91	2.87	*0.17*
	3.05	3.08	3.06	3.09	3.08	*0.04*	**D**	2.11	2.33	2.55	2.56	2.64	*0.53*
	2.57	2.58	2.60	2.60	2.65	*0.08*	**E**	2.25	2.46	2.40	2.37	2.43	*0.21*
ΔR	*0.72*	*0.66*	*0.70*	*0.71*	*0.66*			*1.70*	*1.82*	*1.83*	*1.65*	*1.38*	

Rz [μm]	10.52	10.24	10.25	10.25	10.58	*0.34*	**A**	8.49	8.49	7.61	7.18	8.82	*1.64*
	12.69	12.65	12.58	12.61	12.71	*0.13*	**B**	6.16	6.11	6.59	7.27	8.67	*2.56*
	13.07	13.04	13.21	13.24	13.20	*0.20*	**C**	10.70	11.33	11.44	11.15	11.12	*0.74*
	12.76	12.80	12.73	12.87	12.96	*0.23*	**D**	7.94	8.64	9.30	9.50	9.65	*1.71*
	10.90	10.88	10.86	10.99	11.14	*0.28*	**E**	8.77	9.63	9.22	9.49	10.88	*2.11*
ΔR	*2.55*	*2.80*	*2.96*	*2.99*	*2.62*			*4.54*	*5.22*	*4.85*	*3.97*	*2.45*	

3. RESULTS

We report the values of the average R_a and maximum R_z height of roughness profiles, which are the most frequently evaluated in industry, measured in the direction parallel to the feed (Table 1) and perpendicular to it (Table 2). In the tables, the degree of the deviations (ΔR) in each examination plane is given in italics.

Table 2 – R_a and R_z parameter values of profiles measured in the direction perpendicular to feed

	Single cutting marks – Surface M1							**Double cutting marks – Surface M2**					
	I	**II**	**III**	**IV**	**V**	*ΔR*		**I**	**II**	**III**	**IV**	**V**	*ΔR*
Ra [μm]	1.40	1.49	1.51	1.47	1.46	*0.11*	**A**	0.97	0.94	0.97	1.06	1.34	*0.40*
	0.57	0.62	0.63	0.63	0.63	*0.06*	**B**	0.54	0.55	0.56	0.53	0.51	*0.05*
	0.27	0.19	0.19	0.20	0.19	*0.08*	**C**	0.17	0.19	0.20	0.18	0.19	*0.03*
	0.64	0.63	0.63	0.63	0.62	*0.02*	**D**	0.49	0.52	0.51	0.59	0.58	*0.10*
	1.55	1.57	1.53	1.56	1.59	*0.06*	**E**	1.59	1.59	1.54	1.65	1.56	*0.11*
ΔR	*1.28*	*1.38*	*1.34*	*1.36*	*1.40*			*1.42*	*1.40*	*1.34*	*1.47*	*1.37*	
Rz [μm]	7.45	8.12	7.64	7.35	7.59	*0.77*	**A**	6.03	4.80	5.72	5.55	7.46	*2.66*
	4.01	4.12	3.80	3.71	3.79	*0.41*	**B**	3.43	3.35	3.47	3.19	3.07	*0.40*
	1.49	1.08	1.11	1.25	1.02	*0.47*	**C**	1.15	1.21	1.31	1.26	1.62	*0.47*
	3.92	3.74	3.80	4.03	3.75	*0.29*	**D**	3.22	3.07	2.65	3.28	3.44	*0.79*
	7.92	8.52	8.01	7.92	7.94	*0.60*	**E**	7.40	7.09	6.74	8.17	7.28	*1.43*
ΔR	*6.43*	*7.44*	*6.90*	*6.67*	*6.92*			*6.25*	*5.88*	*5.43*	*6.91*	*5.84*	

4. DISCUSSION

After completing the roughness measurements, we examined and compared the topographies made with the two types of textures, based on the data presented in Tables 1–2. During this, we analyzed the distribution and deviations of the measured roughness values in the examination planes on the surface according to the direction of measurement. On the topographies, the distribution is illustrated in Figures 4 and 6 with surface diagrams. The magnitude of the values and their deviations in the planes taken parallel (A–E) and perpendicular (I–V) to the feed are shown in Figures 5 and 7 with bar diagrams, where the height of the columns indicates the degree of the deviation.

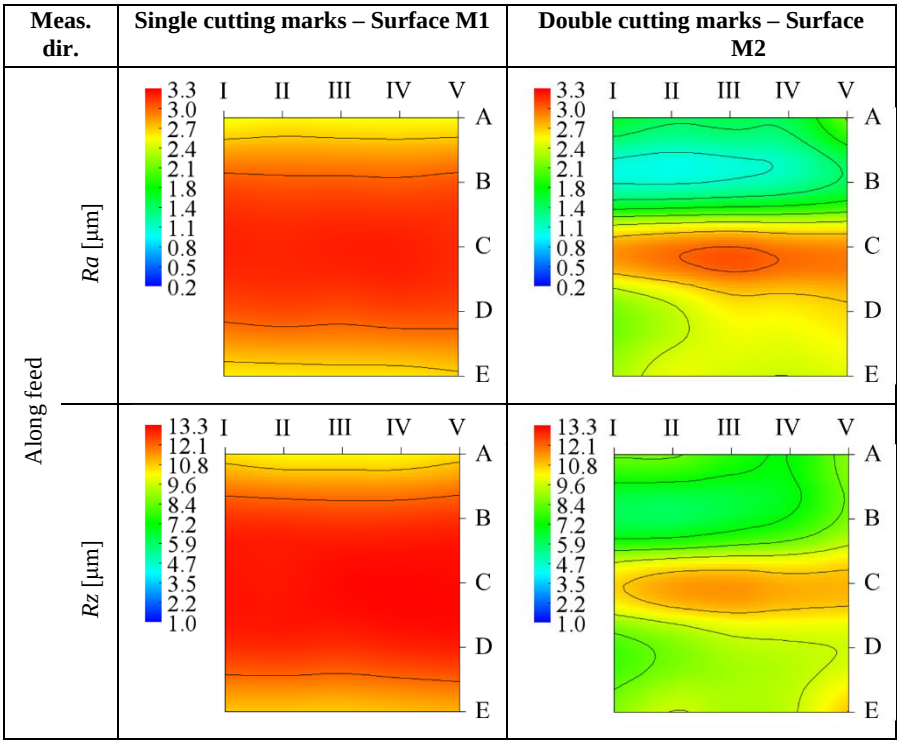

Figure 4 – Distribution of roughness values in the direction of the feed on the examined topographies

First, we analyze the R_a and R_z values of the profiles measured in the feed direction. On the surface with single milling marks (M1), the values in planes A–E parallel to the feed show negligible differences, which can be considered as the

standard deviation of the measurement results (Figure 5). The values are maximal in the symmetry plane C and they decrease in both directions further away from it (Figure 5). In the planes perpendicular to the feed (I–V), the deviations of the values are similarly between 21–25% (Table 1). Also, the distribution of values in these planes is the same (Figure 4). Negligible differences between the measured values can be seen on the $M1^U$ and $M1^D$ sides of the surface, at the same distance from the symmetry plane (Figure 5). Among the parameters, the values of R_z show greater variety compared to R_a (Figure 4).

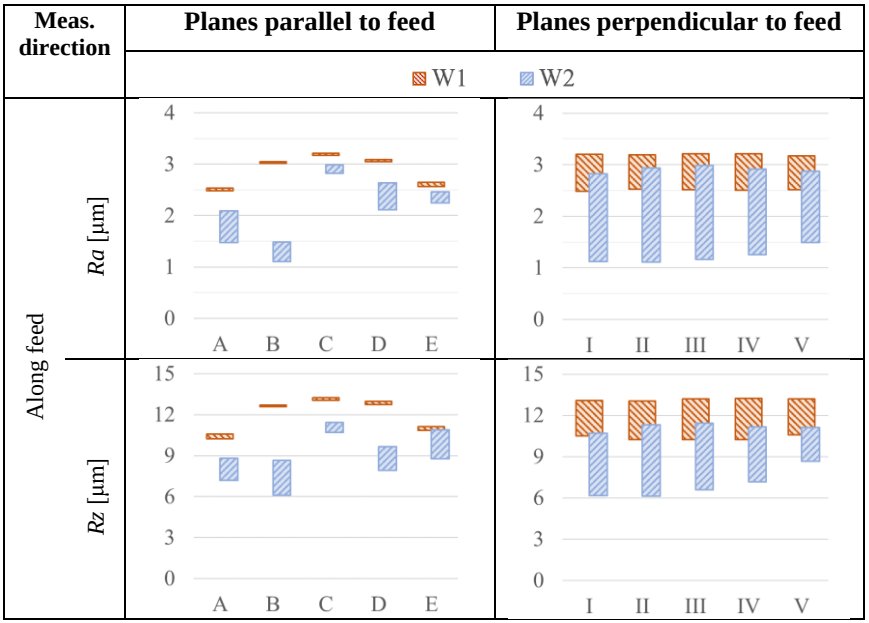

Figure 5 – Roughness values measured in feed direction and their deviations in the examination planes

As a result of the secondary material separation, the values of the investigated parameters in the planes parallel to the feed direction (A–E) decreased by 4–64% for Ra and 2–52% for R_z in the measurement points (Table 1). They are also maximal in plane C, and they decrease in both directions towards the edges of the investigated area (Figure 4). But as they are scarcely smaller in the middle plane than the values measured here on the M1 surface (by 9% on average for R_a, by 15.2% on average for R_z), then the further away from it the degree of decrease is significant; max. 64% for R_a, max. 52% for R_z (Figure 5). On this topography, we already see remarkable

deviations between the values of the two sides of the surface separated by the symmetry plane (Figure 5); the values on the down-milled ($M2^D$) side are higher than those on the $M2^U$ surface part. This observation is identical to the finding described in [18]. The largest deviation can be seen in plane A, on the up-milled side ($M1^U$, Fig. 5), where the degree of difference was also maximal (on the surface) and almost the same in our previous investigation [19]. In the numbered I–V planes, the deviation of the values is significantly larger compared to the differences calculated on the M1 surface, its extent is 1.5–2.5 times (Table 1). The distribution of values has also changed; further away from plane C in both directions, the values of points decrease but not in all cases (Figure 4). Ra parameter values showed more sensitivity to the variations in roughness on this surface. In summary, the roughness difference on the topography created with double milling marks is large and is significantly higher compared to the surface with a single impression (2.7 times in R_a and 1.87 times in R_z).

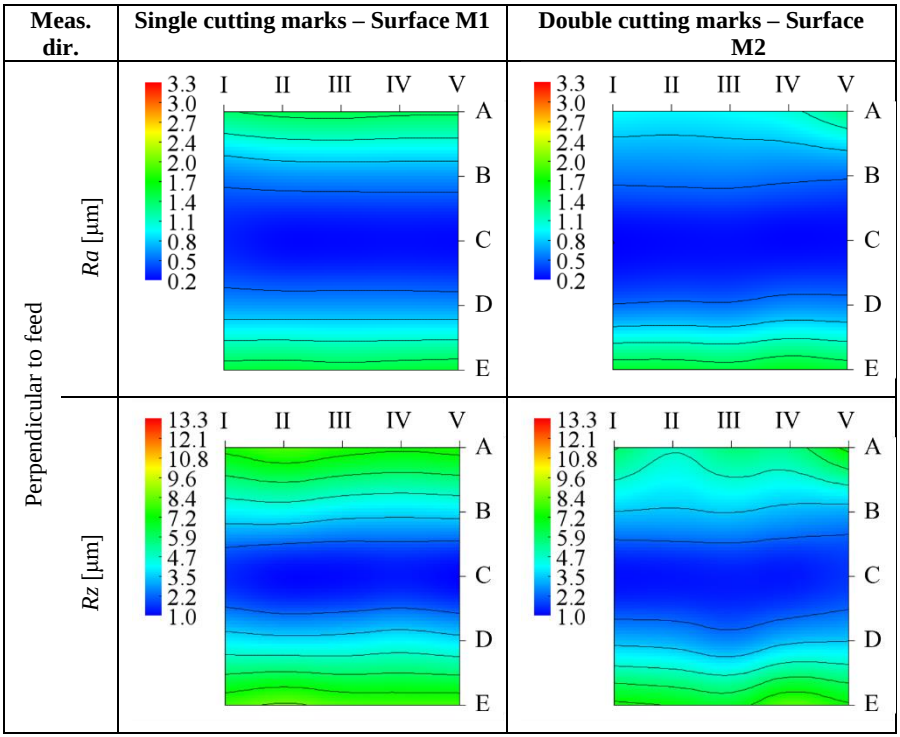

Figure 6 – Distribution of roughness values measured in the direction perpendicular to the feed on the examined topographies

Next, we evaluate the results of profiles measured in the direction perpendicular to the feed, starting with the M1 surface. The roughness values in the feed direction planes A–E are almost identical (Figure 7), the differences in them are ΔR_a = 0.02–0.11 μm, ΔR_z = 0.29–0.77 μm (Table 2). This contributes to the fact that the distance between adjacent measurement points taken in the feed direction is an integer multiple of the feed value, so profiles measured on the same plane that is parallel to the feed direction, are theoretically identical. The values of the R_a and R_z parameters examined on the topography are the lowest in the C symmetry plane and increase in two directions moving further away from it (Figure 7), similar to findings in [17]. The values and their distribution of the surface sides $M1^U$ and $M1^D$ are symmetrically almost identical to the symmetry plane (Figure 6). In the numbered (I–V) planes, as shown in Figure 7, the degree of deviations of the R_a values is almost the same (1.28-1.4 μm), in the case of the R_z parameter they are very similar (6.43–7.44 μm), the distributions are the same (Figure 6).

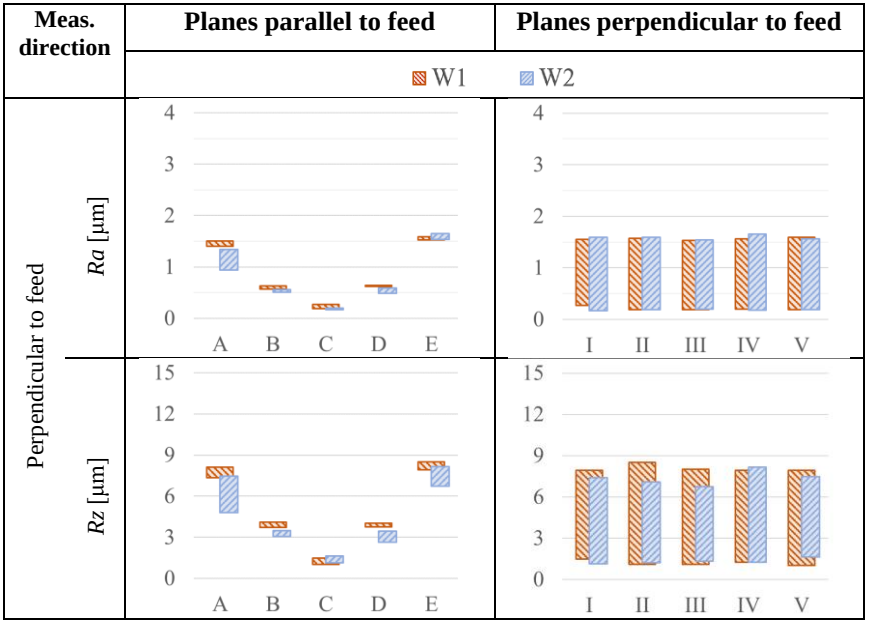

Figure 7 – Values measured in the direction perpendicular to the feed and their deviations in the examination planes

On the M2 topography with double milling marks, the values of points in planes B, C and D are minimally lower and the degree of deviations is similar compared to the same points on the M1 surface (Figure 7). On the other hand, in the extreme planes A and E, a greater degree of depreciation and larger deviations are characteristic, based on the comparison with the M1 surface (Figure 7). In the numbered (I–V) planes, the magnitude of deviations is slightly smaller compared to the M1 surface (Figure 7). However, the distribution of values has changed to the extent that higher values can be found on the $M2^U$ up-milled surface side (Figure 6), similar to the measurement results in the feed direction. The roughness deviations of the profiles measured in this direction are shown by the values of the R_z parameter with greater sensitivity than the values of R_a (Figure 7). Based on the measurement results (Table 2), we conclude that the roughness deviations of profiles measured in this direction are small.

5. CONCLUSIONS

In this article, the topography and roughness of plane surfaces face-milled with a symmetrical tool setting were examined, considering the effect of secondary material separation (back-cutting movement of the tool edge). The results can be summarized as follows.

- Based on the results of profile measurements in the feed direction, the values of R_a and R_z parameters on surfaces M1 and M2 are maximum in the symmetry plane and they decrease in both directions the further away from it (except that they increase in the extreme plane A). On the surface where secondary material separation occurred, the values decrease (minimally in the plane of symmetry, significantly towards the edges of the surface), while their deviations are larger.
- The results of the profile measurements in the direction perpendicular to the feed show that the values on the M1 and M2 surfaces are minimal in the symmetry plane and increase in two directions further away from it. In the case of secondary material separation, the decrease in roughness is small in most points, and the degree of deviations on the surface is greater. We find that by measuring the profiles in this direction, the change in roughness is less than when measured in the feed direction.
- The distribution of R_a and R_z values on the two – differently – machined surfaces differs regardless of the direction of measurement. While on the M1 topography with single cutting marks, the value decrease is almost the same on the up-milled ($M1^U$) and down-milled ($M1^D$) side of the surface further away from the symmetry plane, while on the surface with double milling marks (M2), the roughness values are higher on the up-milled side ($M2^U$).

- Different degrees of deviations can be measured on the face milled surfaces in the two measurement directions, so the tribological (e.g. friction) conditions may change if the milled surface in contact moves along these directions.
- During face milling, the secondary material separation changes the roughness values measured in different parts of the topography and their deviations. Under the investigated experimental conditions, the unevenness of the surface is best expressed by the R_z values measured in the feed direction.

References: 1. *Mitsyk, A., Fedorovich, V.* The nature of the formation of surface micro-roughness in vibration finishing and grinding processing. Cutting & Tools in Technological System. 2022. vol. 97, pp. 103 – 112. **2.** *Bali, J.* Forgácsolás (in Hungarian). Budapest: Tankönyvkiadó, 1985. **3.** *Bajić, D., Majce, I.* Optimisation of Parameters of Turning Process. International Scientific Conference on Production Engineering. vol. 47, Zagreb Lumbarda, Hrvatska. 2006. pp. 129 – 136. **4.** *Brown, C., Hansen, H., Jiang, X., Blateyron, F., Berglund, J., Senin, N., Bartkowiak, T., Dixon, B., Goic, G., Quinsat, Y., Stemp, W., Thompson, M., Ungar, P., Zahouani, E.* Multiscale analyses and characterizations of surface topographies. CIRP Annals - Manufacturing Technology. 2018. vol. 67. pp. 839 – 862. **5.** *Kundrak, J., Felhő, C.* 3D roughness parameters of surfaces face milled by special tools. Manufacturing Technology. 2016. vol. 16. № 3. pp. 532 – 538. **6.** *Hadad, M., Ramezani, M.* Modeling and analysis of a novel approach in machining and structuring of flat surfaces using face milling process. International Journal of Machine Tools & Manufacture. vol. 2016. vol. 105. pp. 32 – 44. **7.** *Ryu, S., Choi, D., Chu, C.* Roughness and texture generation on end milled surfaces. International Journal of Machine Tools and Manufacture. 2006. vol. 46. № 3-4. pp. 404 – 412. **8.** *Yin, Y., Du, S., Shao, Y., Wang, K., Xi, L.* Sealing analysis of face-milled surfaces based on high definition metrology. Precision Engineering. 2022. vol. 73. pp. 23 – 39. **9.** *Thanasuptawee, U., Thakhamwang, C., Siwadamrongpong, S.* Evaluation of face milling operation parameters on surface roughness of crankcase housing by two level factorial design with center points. Key Engineering Materials. 2018. vol. 780. pp. 105 – 110. **10.** *Franco, P., Estrems, M., Faura, F.* A study of back cutting surface finish from tool errors and machine tool deviations during face milling. International Journal of Machine Tools and Manufacture. 2008. vol. 48. № 1. pp. 112 – 123. **11.** *Torta, M., Albertelli, P., Monno, M.* Surface morphology prediction model for milling operations. The International Journal of Advanced Manufacturing Technology. 2020. vol. 106. pp. 3189 – 3201. **12.** *Varga, G., Kundrák, J.* Effects of technological parameters on surface characteristics in face milling. Solid State Phenomena. 2017. vol. 261. pp. 285 – 292. **13.** *Chuchala, D., Dobrzynski, M., Pimenov, D., Orlowski, K., Krolczyk, G., Giasin, K.* Surface roughness evaluation in thin EN AW-6086-T6 alloy plates after face milling process with different strategies. Materials. 2021. vol. 14. № 11. ArtNo. 3036. **14.** *Arizmendi, M., Jiménez, A.* Modelling and analysis of surface topography generated in face milling operations. International Journal of Mechanical Sciences. 2019. vol. 163. ArtNo. 105061. **15.** *Zhenyu, S., Luning, L., Zhanqiang, L.* Influence of dynamic effects on surface roughness for face milling process. The International Journal of Advanced Manufacturing Technology. 2015. vol. 80. № 9. pp. 1823 – 1831. **16.** *Felhő, C., Kundrák, J.* Topography of the machined surface in high performance face milling. Procedia CIRP. 2018. vol. 77. pp. 340 – 343. **17.** *Nagy, A., Kundrak, J.* Changes in the values of roughness parameters on face-milled steel surface. Cutting & Tools in Technological System. 2020. vol. 92. pp. 85 – 95. **18.** *Nagy, A., Kundrak, J.* Investigation of surface roughness characteristics of face milling. Cutting & Tools in Technological System. 2019. vol. 90, pp. 62 – 71. **19.** *Nagy, A., Kundrak, J.* Analysis of inhomogeneity of surfaces milled with symmetrical, down-milling, and up-milling settings. Development in Machining Technology: Scientific – Research Reports vol.10, Krakow, Poland: Cracow University of Technology. 2022. pp. 51 – 62.

ДОСЛІДЖЕННЯ ШОРСТКОСТІ ОДИНАРНИХ І ПОДВІЙНИХ СЛІДІВ РІЗАННЯ НА ТОРЦЬОВО ФРЕЗЕРОВАНІЙ ПОВЕРХНІ

Анотація. *При обробці за допомогою інструментів з певною різальною крайкою, в деяких процесах при використанні обертального інструменту (наприклад, торцьове фрезерування) крайка інструменту може ще раз протягом одного оберту інструменту, подряпати поверхню заготовки, залежно від умов різання. В результаті топографії з одинарними або подвійними відмітками різання будуть відрізнятися одна від одної. Відхилення, залежно від його розміру, також може вплинути на функціональні характеристики (наприклад, умови тертя) робочих поверхонь. У цій статті торцево-фрезеровані топографії, створені з симетричною установкою і з одинарними або подвійними фрезерними мітками, порівнюються відповідно до величини шорсткості, ступеня і характеру неоднорідності. За результатами вимірювань профілю в напрямку подачі значення параметрів R_a і R_z на поверхнях максимальні в площині симетрії і зменшуються в обидві сторони, чим далі від неї (за винятком того, що збільшуються в крайній площині). На поверхні, де відбулося відокремлення вторинного матеріалу, величини шорсткості зменшуються (мінімально в площині симетрії, ближче до країв поверхні), при цьому їх відхилення більші. Розподіл значень R_a і R_z на двох – по-різному – оброблюваних поверхнях відрізняється незалежно від напрямку вимірювання. У той час як на топографії M1 з одинарними мітками різання зменшення значення майже однакове на фрезерованій (M1U) і фрезерованій (M1D) стороні поверхні, більш віддаленій від площини симетрії, тоді як на поверхні з подвійними фрезерними мітками (M2) значення шорсткості вищі на фрезерованій стороні (M2U). На торцевих фрезерованих поверхнях можна вимірювати різні ступені відхилень у двох напрямках вимірювання, тому трибологічні (наприклад, тертя) умови можуть змінитися, якщо фрезерована поверхня, що контактує, рухається в цих напрямках. Під час торцевого фрезерування вторинне розділення матеріалу змінює значення шорсткості, виміряні на різних ділянках рельєфу, та їх відхилення. У досліджуваних експериментальних умовах нерівність поверхні найкраще виражається значеннями R_z, виміряними в напрямку подачі.*

Ключові слова: *торцеве фрезерування; шорсткість поверхні; зворотне різання фрезерного інструменту; видалення вторинного матеріалу.*

UDC 621.9.08 **doi: 10.20998/2078-7405.2023.99.06**

LASER MEASUREMENTS IN CUTTING PROCESSES

Miklós **Béres** [0000-0002-0185-5321], Gyula **Varga** [0000-0002-1956-790X]

University of Miskolc, 3515, Miskolc - Egyetemváros, Hungary
mechbere@uni-miskolc.hu

Received: 08 November 2023 / Revised:15 November 2023 / Accepted: 20 November 2023 / Published: 01 December 2023

Abstract. *Laser measurements are used chiefly for experiments during metal cutting. The recent development of laser technology offers chances that are advisable to take advantage of machine manufacturing. This article presents some measuring applications for metal cutting. Its purpose is to show separate literature on each technology to provide insight into the possibilities of laser measurements.*
Keywords*: metal cutting; laser measurement; in-process monitoring; LDV; optical sensors.*

1. INTRODUCTION

In production systems, the maintenance of efficient productivity plays a prominent role. The technological processes in machine manufacturing technology have become more diverse in recent decades, and countless new procedures appear every day (Research and Markets [1–5]).

Zaghal and Benke [6] report on determining reliable area sizes for 3D roughness measurement in their work. In their article, Zhou, J., et al. [7] and Zhou, H., et al. [8] analyse in detail the activities related to laser polishing. Lavrinenko et al. [9] present a review study entitled “Modern Developments Related to the Directed Impact on the Cutting Surface of a Diamond Abrasive Tool and its Contact Zone in the Processes of Machining (review)". In their article, they examine in detail the activity of laser sharpening evaluation on diamond wheels [10–11], and also analyse the laser surface roughness measurement [12].

The driving force behind the increase in indicators is reducing production time. At the same time, this phenomenon also affects traditional technological processes. These production processes must also meet quality, reliability and increased productivity [13–14]. Increasing the machining speed is a promising way to speed up the different production steps. However, it also raises new problems. In-situ metrology in production systems improves accuracy and reduces machining time by eliminating repositioning and setting operations [15]. Various monitoring methods and techniques help to achieve these goals. These procedures are increasingly crucial in individual production technology operations [16]. This article does not intend to deal with the various monitoring techniques. However, we must

note that the respective areas are slowly separating. Some condition monitoring procedures monitor the machine tool (MCM), while others focus directly on the tool. The former mainly focuses on condition-based maintenance (CBM) [17–20], providing data that can complement a risk-based maintenance strategy (RBM) (offering a severe economic advantage for users). Other monitoring techniques maximise the valuable working time spent on quality production by examining the tool condition. [21–23]. Predictive maintenance uses analytical models to analyse data from sensors that estimate the condition of a part, machine or process. Predictive maintenance procedures benefit from machine data collection and more frequent sampling, while condition-based monitoring applications benefit from multiple sensing inputs [24–25]. At the same time, the condition-based inspection often acts as an early warning system. In parallel with the systems that monitor the tool's condition, we can observe the material separation process separately. This third control strategy is closely related to the previous controls [11], [14].

Today, we have many different sensors and measurement methods at our disposal. However, each has limitations, so the measurement is still burdened with errors [26–27]. The more sensitive the measurement method (for example, laser) is to the physical signal, the more accurately it can reproduce the phenomenon under investigation. From this point of view, they, therefore, offer a definite advantage [28]. At the same time, they may require complicated installation, their area of use may be limited, or their investment costs may be high, so they have not become widespread [29-30]. It can be said for almost all optical sensors, the only exception perhaps being the use of CCD detectors [31]. Using a laser as a measuring tool was still considered expensive almost a decade ago. Today, however, the situation has changed.

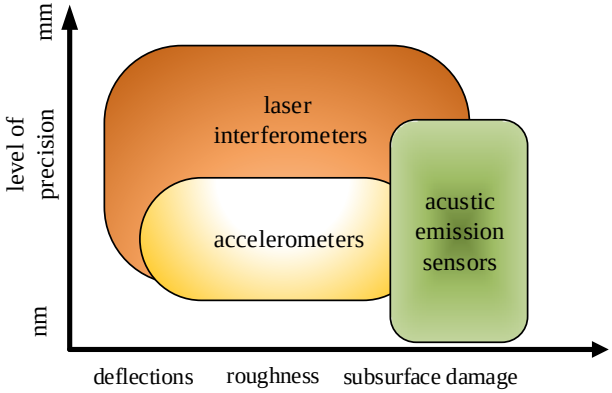

Figure 1. Applicability of laser interferometers compared to accelerometers and acoustic emission sensors

The laser as a measuring device was a costly procedure nearly a decade ago [32]. However, due to the significant reduction in production costs and their intensive use in the electronics industry, their scope of application has widened. Laser devices are still developing at a tremendous pace today. This trend applies to lasers, high-resolution cameras, smart devices, and microcontrollers performing local computing tasks [33]. New application areas come to the fore through the miniaturisation and embedding of measuring devices.

An example of such a device is the multi-beam, integrated semiconductor laser developed by Li et al. [34]. Compared to previous devices, this new six-beam laser chip reduces the loss caused by detection time and increases signal stability. Li's development is beneficial for measuring vibrations in the low-frequency range, with an amplitude of up to a few 100 μm/s, a resolution and quality similar to commercially available LDVs. Subprocesses of the cutting cycle and events that occur (even unexpectedly) require additional attention, as they sensitively affect the accurate evaluation of the measurements. In the case of laser measurements, it happened, for example, that the displacement signal was sometimes "lost" (drop-out) in the transition phase of the cutting cycle [35–36]. In the case of measurements carried out with a Laser Doppler Vibrometer, the reflected signal may become low in intensity and fall below the acceptable level. As a result, the measurement signal itself disappears or becomes non-processable.

The shape of the tool is also an influencing factor. If it gets in the way of the laser, it causes a (sometimes significant) abnormality in the reflected signal. Such a phenomenon can be experienced, for example, in drilling [36].

The mentioned reasons partly explain the common practice that laser measuring devices are usually not used alone but together with other sensors [35], [37–41]. At the same time, laser devices may be required as an additional signal source or to clarify the dynamic model of the system. This is especially true during cutting.

Figure 1. (based on [42]) provides some information about the applicability of laser interferometers used in ultra-precision machining as a function of accuracy and control parameters.

2. LASER MEASUREMENTS IN TURNING

Turning is often the subject of investigation as a traditional machining process. Many proven measurement methods have been developed for its study. However, the power consumption calculated based on the current consumption of the main spindle is used as the input parameter that forms the basis of condition monitoring. The power consumption strategy is used primarily in performance-based TCM (Tool Condition Monitoring) to identify the end-of-life condition of a tool. The

disadvantage at the same time is that it is less suitable for effectively detecting tool breakage and other similar sudden events [43].

In the case of turning, more superficial measurements are made with the help of a laser. Its early consumption, which is still present today, is the tachometer. First, its implementation is simple, so we can even measure the signal taken from the chuck with it. Urbikain and his colleagues also used the laser this way when they carried out measurements on a CNC lathe centre, investigating the practical implementation possibilities of the SSV (spindle speed variation technique) [44]. In the experiments, the measurement of energy consumption ensured the balance between better stability limits and acceptable spindle behaviour. Accurate speed data was required for feedback. This data was provided by the laser - successfully.

We should mention its other use as a surface scanning method. A procedure used not only for turning but also for other cutting operations. A procedure used to check both the tool and the machined surface. In their recently published article, Ádám Kiss and his colleagues looked for answers to the causes of self-excited vibrations during turning [45]. They obtained the dynamic behaviour of the vibrations generated during the machining process by comparing the results from the measurement of the roughness of the machined surface with the theoretical correlations. For this purpose, an industrial laser differential displacement meter was used to measure the deviation of the surface from the ideal geometry. In the case of most surfaces, the ratio of regular reflection and diffuse reflection is a function of surface roughness. Therefore, the reflected light pattern carries information about the quality of the surface. During their measurements, the sensor provided sufficient accuracy for detection. As a limitation, the laser spot is not an ideal point but an ellipse. Since the sensor measures the average of the surface roughness - moreover, not symmetrically - this effect appears as a moving average along the measurement line. Spot asymmetry is often encountered when the instrument uses a semiconductor laser. In such a case, the measurement distance must be considered. In the case of spatial-mode semiconductor solid-state lasers (SD), the semiconductor laser beam, at a suitable distance both in the direction perpendicular to the active layer and parallel to it, can only seem Gaussian [46] or Lorenz distributed [47]. Therefore, the measurement distance is always problematic for these measurements - due to the type of laser.

A similar laser application was included earlier in a series of experiments by Wong and his research group [48]. In their article, they presented an optical method that uses the scattering pattern of reflected laser light to track the condition of the tool in case of roughing. During the measurement, the light beam of a low-power He-Ne gas laser was reflected from the workpiece's surface. The scattered light was recorded with a digital camera and then analysed using appropriate image processing techniques. The average of the resulting pattern and its standard deviation for the intensity image were examined. This method can detect a roughness

corresponding to 1/8 of the laser wavelength. Of course, to analyse the tool's wear, the quality of the surface, the optical parameters, and the tool degradation had to be matched. According to their experience, surface quality, tool wear and optical characteristics are not always consistent because they depend on many factors. The scattered laser pattern itself does not correlate with tool wear, but the intensity distribution of the pattern does – but only in a limited range of wear.

Self-excited vibrations were investigated by Prasad et al., but already during a series of experiments with LDV. In their study [38], they looked for the connection between the workpiece's vibration, the tool's wear, and the texture of the machined surface. During face turning, the vibration in the feed direction was measured with a laser. An FFT spectrum was formed from the received signal and then evaluated. By carrying out the measurements on different materials, with the sharp, the less worn, and finally, the blunt tool, they found that as the tool's wear progressed, the vibration amplitudes also increased in the frequency range - as expected. The further increase in vibration was attributed to the ever-increasing friction between the workpiece and the cutting tool, which is also a consequence of tool wear.

In another paper by Prasad, the cutting temperature and the dynamic characteristics of the vibration signals were analysed simultaneously [39]. LDV was used to extract the vibration data in the feed direction during orthogonal cutting, and the temperature was measured by infrared thermography. They aimed to create an experimental database to detect and monitor tool wear. Their experiments showed a relationship between vibrations, cutting temperature and tool wear, depending on the speed.

The article by Venkata Rao et al. [40] is related to turning but also touches on the next chapter, in which the authors analysed the effects of cutting speed, feed and tip radius of the cutting insert in hole turning. Vibrations in this process are especially problematic when the tool is still at the beginning of the hole machining and most of it is located outside the hole. The vibration of the workpiece was also monitored with the LDV. The roughness and wear parameters were compared with the vibration amplitudes by recording the FFT spectrum of the signal.

During hole turning, laser measurements were also performed in cases where the machining process is aided by externally generated vibrations [49]. Chern and Liang used a piezo crystal oscillator to vibrate the tool in the feed direction. They aimed to improve the crossing holes and reduce the surface roughness. At the intersection of the holes, even significant burrs can form, which, for example, cause problems with flow technology in the case of valves. In their tests, the laser played an additional role. The vibration amplitudes were analysed with a laser displacement meter. Its sampling frequency was 50kHz, while the frequency that excites the tool could be changed to 14kHz, so very high frequencies could also be tested.

3. LASER INSPECTION DURING DRILLING

Recently, several articles have been published about using LDV during drilling [36],[49–50], but it is by no means a commonly used method. Unlike previous material separation operations, drilling is even less common to use a laser as a sensor signal source. Nevertheless, this measurement method's advantages can be seen precisely during this cutting process.

Electronic non-contact measurement techniques, such as inductive and capacitive displacement sensors, offer limited possibilities for non-contact measurement. These are limited only to close measurements and are sensitive to thermal expansion. So, they must be arranged in two pairs for acceptable measurement [35]. With drilling, direct control of the cutting process is impossible – as it cannot be directly observed. Thus, only indirect measurement procedures help understand the process's phenomena during cutting, even when creating a TCM strategy. It is advisable to examine the tool's vibrations; for instance, individual chip removal steps can be better observed by measuring the tool itself [51].

Chern and Liang repeated the same vibration tests performed in hole turning for small diameter holes. The measuring range of the laser displacement meter (50kHz) made it possible to measure the excitation in the higher frequency range correctly.

During measurements during drilling, it was clearly observed that until (with fixed cutting parameters) the drill bit begins to cut with its total diameter, the individual temporal phases have a specific time and frequency range [50].

Balaji et al. deal with the effect of cutting speed, feed and groove angle on drilling tool life (wear) [52]. His study examined the tool's vibrations during drilling on a universal lathe with a Laser Doppler vibration meter. He determined the relationship between the vibration amplitudes and wear, groove angle, surface quality, and vibration parameters based on the measured data.

4. LASER MEASUREMENTS IN MILLING

Milling is the cutting operation that has been/is being researched the most due to its versatility. This is why we often come across laser devices during examinations. In their early work [53], Ryabov et al. used a laser to measure tool wear during the process and to detect medium and large tool defects. The measurement of noisy signals obtained under natural cutting conditions was based on laser displacement sensors, and two laser sensors were used simultaneously. The tool's cutting-edge shape was checked with the two lasers. In addition, the received signals were fed into the control system and used as a synchronisation signal for speed control. According to their experience, the reflection's characteristics depend on the light dispersion properties of the surface and the direction of the incident light

beam. Based on the results obtained during practical measurements, average and worn surfaces can be clearly distinguished through the light intensity patterns resulting from the difference in the surface. However, they do not differ significantly in their dispersion properties.

The article by Tatar and Grin also analyses tool vibrations during high-speed milling [35]. Since, in the case of high-speed cutting when measuring spindle vibration, low-vibration signal transmission, disturbances in the bearings, and magnetic disturbances in the motor make classical measurements unreliable, a new sensor was chosen. The task was solved with a non-contact laser sensor placed near the tool. In experiments, LDV measured the speed of a given point of the tool and its displacement, thanks to the built-in system. This possibility is a real advantage in the lower frequency range. At the same time, due to the appearance of pseudo-vibrations and transverse vibrations from the shape of the tool shank, they had to perform additional measurements.

The topic of the work by Faassen et al. was self-excited vibrations occurring during high-speed milling [54]. While others use constant parameters for the entire spindle speed range to describe the machine dynamics and the behaviour of the cutting process, they proposed a model that also considers the spindle speed to construct the stability maps. In this model, the dynamics of the machine also play a role. To measure the dynamic behaviour of the main spindle-tool holder-tool system and determine the effect of the spindle speed on this behaviour, FRF (Frequency Response Function) tests were performed with an impulse hammer. Measurements were made with a stationary and rotating spindle, where the vibrations were recorded with a twin-sensor industrial laser (LTS – Laser Twin Sensor) surface inspection sensor. They could establish a frequency response characteristic in the range of 750–1750 Hz through laser measurement. The previous experiments were supplemented with microphone measurements to refine the stability limits.

Rantatalo's measurements were also made on a milling machine [55]. His method was primarily aimed at analysing the vibrations of the main spindle. In his complex work, he searched for an answer to the effect of the main spindle as a rotating element on the system's stability. Its solution is general, so it can also be used with other chucked devices.

The dynamic effect of the main spindle on cutting was also dealt with by Österlind and his research group [56], but unlike others, he used the method of in-process modal analysis (OMA – Operational Modal Analysis). For static measurements, the transfer functions were prepared with an impulse hammer, and then the parameters during the operation were recorded with an OMA. They also used several different sensors in their experiments. The vibrations of the workpiece, the tool holder and the table were measured with accelerometers. In contrast, the tool's response to vibrations was measured with a laser Doppler vibration meter. The

measurement results were used to analyse the stability map of the system, examining the changes that occurred during cutting.

Self-excited vibrations have been a topic of interest to researchers for a long time. For example, in a previous article, Nakagawa et al. discuss the effects of vibrations generated during the milling of hardened steel materials on the surface quality [57]. Since the previously discussed eddy current sensor had both placement and dynamic disadvantages (detection threshold in the lower frequency range), the displacement of the milling tool tip was measured with an LDV. During measurement, two LDVs simultaneously monitored the operation and the mutually perpendicular displacements of the tooltip. They tried to correct the instrument's relative measurement error by placing it relatively far from the measurement point. During their experiments, with the help of high-resolution measurements, they identified two different types of self-excited vibrations. It was possible to observe the change in the unstable regions of the stability map.

The dynamic properties of the machine tool-tool-workpiece system were also investigated by Norman et al., during which LDV was used to predetermine the dynamic parameters of the system [58]. Since the stiffness of the machine tool itself changes due to the changing working conditions (e.g. due to the variable bearing stiffness depending on the speed), they prepared a test bench for their tests. The effects of various factors affecting the system's dynamics were checked. The response data measured with the LDV were monitored by examining different load cases. So, the system's transfer function was defined in such a way that the main spindle axis was in rotation all the time - i.e. during work. The results of their experiments confirmed the advantage of testing with non-contact methods that the disadvantages observed with traditional sensors, such as the mass load of the accelerometers or the error caused by the damping of the pulse hammerhead, do not occur during the measurement. The measurements can, therefore, be performed even while the tool is rotating so that the changes in the system's transfer functions determined at different rotation speeds can be monitored.

5. COMMON EXPERIENCES WITH LASER MEASUREMENTS

As with all sensor types, measurement errors with laser sensors are caused by the conditions of their installation since the measured speed signal is relative. During machining experiments for research purposes with the LDV measuring instrument, it is a problem that the device (due to its dimensions) can often only be used mounted on a stand [36], [59]. So, vibrations originating from the laser's "capture" conditions also appear at the output of the LDV [60–61]. However, isolation from the environment, which is an obvious solution, requires careful preparation. In addition, it is complicated to eliminate low frequencies, so this problem cannot be solved effectively. The author and several colleagues used an

optical vibration-free table during his measurements in several different measuring setups. He experienced vibrations independent of the choice of stand and originating from the characteristics and design of the measuring device [62].

The idea of Halkon and Rothberg [63] offers a simple solution to the relativity of the speed signal as a source of error. It has been proven in practice that if an accelerometer is paired with a second one mounted anywhere on the instrument and aligned in the laser beam, it solves this problem well. In their experiments, the instrument was supplemented with two traditional acceleration sensors that measure the vibration in the laser's direction. If they measure in the same direction and are axisymmetric to the laser beam, the amplitude and phase spectra of the instrument's vibrations can be well corrected. However, in addition to favourable experiences, the correction may be impaired by the transverse sensitivity of the acceleration sensor. Regardless, it is not only the relativity of the measurement that causes problems but also the polarised coherence of the laser light. By itself, the interference pattern would be an applicable property, for example, if it were a matter of examining the quality of the surface. In the case of a light wave with this property, if the light illuminates an optically rough surface - and most surfaces are like this - then each small surface element will act as a point source of coherent light. Due to the uncorrelated light waves created in this way, a granular pattern of dark and light spots is formed on the detector due to the superposition. The sensor is several such, i.e. collects a spot pattern with one sampling shape, and the current output of the photodiode will be proportional to the sum of these instantaneous intensity distributions [64].

If the spot pattern changes space and time (for example, a rapid movement of the target perpendicular to the measurement direction or a sudden rotation), the Doppler signal - and thus the output of the detector – is modulated by the change in the pattern [65-66]. Therefore, the formation of pattern noise can be explained by the fact that the point illuminated by the laser during the vibration was not the same point during the entire movement period [67].

Nevertheless, in the case of vibration testing, it is a distinct disadvantage because the sample fluctuates almost randomly [35–36], [41]. The effect of the change in granularity on the measured signal can be reduced by averaging the measurements [68–69]. However, spurious vibrations arising from the "repetition" of the pattern due to rotation are still visible in the spectrum. Their name used in international literature is pseudo-oscillations [69–70]. Therefore, if the laser scans a workpiece or tool rotating at high speed, we will get disturbing peaks and higher-order harmonics in the frequency spectrum due to the effect [64–65], [69].

For the simplest solution to this problem, it seems that making an "optically smooth" surface for the measurements can be a good solution [35], [41], [58]. That is, on the one hand, a clean and, on the other hand, smooth polished surface must be created for good reflection. However, making such preparations or ensuring this

condition permanently is not always possible. The question is similar to the speckle noise phenomenon occurring in remote sensing (or laser-based remote sensing – LIDAR – Light Detection and Ranging). Courville, although not working in the field of metal cutting, draws attention in their work to the fact that a single LDV with two properly positioned detectors in one line can simultaneously record two measurements, which will have independent speckle noise [71]. To reduce the noise of the spot, he recommends separating the signals in the frequency range and averaging the measurement series recorded with several sensors simultaneously. In this way, they can also record the orthogonal polarisation of light.

Vass and his fellow researchers developed an algorithm operating in a time domain to improve the reflected light's signal/noise ratio [72]. According to their experiments, if the spot pattern of the reflected light differs significantly from the majority of the samples in the signal (examined over time), i.e. the amplitude distribution of the sample does not follow the usual dispersion of the signal and shows an extreme deviation from the average. The peakedness (kurtosis) can be used to detect the disturbance. If outliers exceed a limit, they can be automatically removed. Hosek, who compared the effectiveness of this method with several techniques, also similarly limits the vibration amplitudes [66]. The disadvantage of the kurtosis method is that it is primarily suitable for detecting random and out-of-average scattering noise.

An additional, simple solution is to eliminate noise smearing errors caused by rotation is almost self-evident – if the cutting conditions permit – the measurement must be performed on the stationary tool [36], [40], [49], [51]. However, this limitation cannot be a condition for developing a condition-monitoring strategy.

6. SUMMARY

In summary, it can be said that laser measuring devices are used in different ways for different types of machining. Lasers came to the fore primarily for surface inspection and determining the dynamic behaviour of the machine system or process. The use of lasers in drilling among the machine manufacturing technological processes is still waiting to be discovered in contrast to milling or turning, which are well and effectively researched areas.

Interferometric measuring devices are more accurate than other laser measuring techniques, but their more complicated construction makes them more sensitive to the conditions. The triangular measuring technique, which is well-proven in practice, can also be used adequately for measurements during cutting. It is a method often used for research, but during production, it is currently used almost only in cases of positioning and coordinate measurement.

It is typical that the laser measuring technique is only one component of a more complex measuring system and takes on a complementary role alongside other types of measuring devices.

Indeed, the cutting or machining conditions are not always favourable for measuring methods where environmental effects can strongly influence the measurement results. However, with its advantages, laser technology can increasingly provide a suitable answer to the problems that arise during cutting.

ACKNOWLEDGEMENT

Project no. NKFI-125117 has been implemented with support from the National Research, Development and Innovation Fund of Hungary, financed under the K_17 funding scheme.

References: 1. The machine tool industry: three trends affecting it globally. [Online]. Available: https://www.etmm-online.com/the-machine-tool-industry-three-trends-affecting-it-globally-a-721307/. [Accessed: 03-Sep-2019]. **2.** *Ahmad, M. I., Yusof, Y., Daud, M. E., Latiff, K., Kadir, A. Z. A., Saif, Y.:* Machine monitoring system: a decade in review. International Journal of Advanced Manufacturing Technology, Vol 108, No 11–12., pp. 3645–3659, 2020. **3.** *Yi-Cheng, H., Chang-Chih, L., Po-Chou, C.:* Prognostic diagnosis of the health status of an air-turbine dental handpiece rotor by using sound and vibration signals. Journal of Vibroengineering, Vol 18, No 3, pp. 1514–1524, 2016. **4.** *Nath, C.:* Integrated Tool Condition Monitoring Systems and Their Applications: A Comprehensive Review. Procedia Manufacturing, Vol 48, pp. 852–863, 2020. **5.** *Kovač, P., Mankova, I.:* A review of machining monitoring systems. Journal of Production Engineering, Vol 14, No 1, pp. 8–13, 2011. **6.** *Zaghal, J.; Benke, M.*: Determination of Reliable Area Sizes for 3d Roughness Measurement, Cutting & Tools in Technological System, 98 pp. 3–12, 10 p., 2023. **7**. *Zhou, J., Han, X., Li, H., Liu, S., Shen, S., Zhou, X., Zhang, D.*: In-situ laser polishing additive manufactured AlSi10Mg: Effect of laser polishing strategy on surface morphology, roughness and microhardness, Materials 14, pp. 393, 2021. **8.** *Zhou, H., Zhou, H., Zhao, Z., Li, K., Yin, J.*: Numerical simulation and verification of laser-polishing free surface of S136D die steel, Metals 11, p. 400, 2021. **9.** *Lavrinenko, V., Fedorovich, V., Ostroverkh, Y., Solod, V.*: Modern Developments Related to the Directed Impact on the Cutting Surface of a Diamond Abrasive Tool and its Contact Zone in the Processes of Machining (review), Cutting & Tools in Technological System 98 pp. 13–28, 16 p.,2023. **10.** *Wei Zhou, Genyu Chen, Mengyang Gao, Mingquan Li*: Laser sharpening evaluation of diamond wheels based on 3Drecognition, Diamond and Related Materials, Vol 129, No 11, 109354, 2022. **11.** *Longzhou Dai, Genyu Chen, Mingquan Li, Shangyong Yuan*: Efficient and precision dressing of arc-shaped diamond grinding wheel by laser dressing and electrical discharge dressing, Diamond and Related Materials. Vol 125, No 5, 108978, 2022. **12.** *Molnar, V.*: Designation of Evaluation Area in Measuring 3D Surface Roughness, Cutting & Tools in Technological System 93, pp.56–64., 2020. doi:10.20998/2078-7405.2020.93.07 **13.** *Landers, R., Ulsoy, G., Furness, R.:* Process Monitoring and Control of Machining Operations. in Hurmuzlu, Y., Nwokah, O. D. I., The Mechanical Systems Design Handbook: Modeling, Measurement, and Control, (1st ed.), Ch 6, pp. 99–117, CRC Press, 2002. **14.** *Djurdjanovic, D., Mears, L., Niaki, F. A., Haq, A. U., Li, L.:* State of the Art Review on Process, System, and Operations Control in Modern Manufacturing. Journal of Manufacturing Science and Engineering, Transactions of the ASME, Vol 140, No 6, ASME, 2018. **15.** *Nishiguchi, T., Koizumi, Y., Maeda, Y., Masuda, M., Nagayama, K., Okamura, K.:* Improvement of Productivity in Aspherical Precision Machining with In-situ Metrology. CIRP Annals, Vol 40, No 1, pp. 367–370, 1991. **16.** *Zhou, Z., Yao, B., Xu, W., Wang, L.*: Condition monitoring towards energy-efficient manufacturing: a review. International Journal of Advanced Manufacturing Technology, Vol 91, No 9–12, pp. 3395–3415, 2017. **17.** *Goyal D.,*

Pabla, B. S.: Condition based maintenance of machine tools - A review. CIRP Journal of Manufacturing Science and Technology, Vol 10, pp. 24–35, 2015. **18.** *Greenough, R. M., Grubic, T.:* Modelling condition-based maintenance to deliver a service to machine tool users. The International Journal of Advanced Manufacturing Technology, Vol52, pp. 1117–1132, 2011. **19.** *Chikuruwo, M. N. H., Maregedze, L., Garikayi, T.:* Design of an automated vibration monitoring system for condition-based maintenance of a lathe machine (Case study). in 2016 International Conference on System Reliability and Science, ICSRS 2016 - Proceedings, pp. 60–63, 2017. **20.** *Tandon, N., Parey, A.:* Condition Monitoring of Rotary Machines. in Wang, L., Gao, R. X., Condition Monitoring and Control for Intelligent Manufacturing, Springer Series in Adv. Man. (SSAM), pp. 109–136, 2006. **21.** *Elbestawi, Mo A., Dumitrescu, M., Ng, Eu-Gene:* Tool Condition Monitoring in Machining. in Wang, L., Gao, R. X., Condition Monitoring and Control for Intelligent Manufacturing, Springer Series in Adv. Man. (SSAM), pp. 55–82, 2006. **22.** *Ulsoy, A., G.:* Monitoring and Control of Machining. in Wang, L., Gao, R. X., Condition Monitoring and Control for Intelligent Manufacturing, Springer Series in Adv. Man. (SSAM), pp. 1–32, 2006. **23.** *Ghani, J. A., Rizal, M., Nuawi, M. Z., Ghazali, M. J., Haron, C. H. C.:* Monitoring online cutting tool wear using low-cost technique and user-friendly GUI. Wear, Vol 271, No 9–10, pp. 2619–2624, 2011. **24.** *Požar, T., Možina, J.:* Enhanced ellipse fitting in a two-detector homodyne quadrature laser interferometer. Measurement Science and Technology, Vol 22, No 8, 2011. **25.** *Cho, S., Binsaeid, S., Asfour, S.:* Design of multisensor fusion-based tool condition monitoring system in end milling. The International Journal of Advanced Manufacturing Technology, Vol 46, pp. 681–694, 2010. **26.** *Kuntoglu, M., Aslan, A., Saglam, H., Pimenov, D. Y.:* Optimization and Analysis of Surface Roughness Flank Wear and 5 Different Sensorial Data via Tool Condition Monitoring System in Turning of AISI 5140. Sensors, Vol 20, 2020. **27.** *Dimla, D. E. Snr.:* Sensor signals for tool-wear monitoring in metal cutting operations – a review of methods. International Journal of Machine Tools and Manufacture, Vol 40, No 8, pp.1073-1098, 2000. **28.** *Powell, R. L., Stetson, K. A.:* Interferometric Vibration Analysis by Wavefront Reconstruction. Journal of the Optical Society of America, Vol 55, No 12, pp. 1593-1598, 1965. **29.** *Sadílek, M., Kratochvíl, J., Petru, J., Čep, R., Zlamal, T., Stančeková, D.:* Cutting tool wear monitoring with the use of impedance layers. Tehnicki Vjesnik, Vol 21, No 3, pp. 639–644, 2014. **30.** *Donati, S., Norgia, M.:* Overview of self-mixing interferometer applications to mechanical engineering. Optical Engineering, Vol 57, No 5, pp 13, 2018. **31.** *Kurada, S., Bradley, C.:* A review of machine vision sensors for tool condition monitoring. Computers in Industry, Vol 34, No. 1. Elsevier, pp. 55–72, 1997. **32.** *Randall, R. B.:* Vibration based Condition Monitoring. John Wiley & Sons Ltd, Chichester, UK, 2011. **33.** *Downey, J., Bombiński, S., Nejman, M., Jemielniak, K.:* Automatic multiple sensor data acquisition system in a real-time production environment. Procedia CIRP, Vo. 33, pp. 215–220, 2015. **34.** *Li, Y., Zhu, J., Duperron, M., O'Brien, P., Schüler, R., Aasmul, S., de Melis, M., Kersemans, M., Baets, R.:* Six-beam homodyne laser Doppler vibrometry based on silicon photonics technology. Optics Express, Vol 26, No 3, pp. 3638-3645, 2018. **35.** *Tatar, K., Gren, P.:* Measurement of milling tool vibrations during cutting using laser vibrometry. International Journal of Machine Tools and Manufacture, Vol 48, No 3–4, pp. 380–387, 2008. **36.** *Béres, M., Paripás, B.:* Measuring of drill bit vibration by laser Doppler methods. IOP Conference Series: Materials Science and Engineering, Vol 448, No 1, 2018. **37.** *Rizal, M., Ghani, J. A., Nuawi, M. Z., Haron, C. H. C.:* An embedded multi-sensor system on the rotating dynamometer for real-time condition monitoring in milling. The International Journal of Advanced Manufacturing Technology, Vol 95, pp. 811–823, 2018. **38.** *Prasad, B. S., Sarcar, M., Ben, S.:* Development of a system for monitoring tool condition using acousto-optic emission signal in face turning-an experimental approach. The International Journal of Advanced Manufacturing Technology, Vol 51, No 1, pp. 57–67, 2010. **39.** *Prasad, B. S., Prabha, K. A., Kumar, P. V. S. G.:* Condition monitoring of turning process using infrared thermography technique – An experimental approach. Infrared Physics & Technology, Vol 81, pp. 137–147, 2017. **40.** *Rao, K.V., Murthy, B., Rao, N. M.:* Experimental study on tool condition monitoring in boring of AISI 316 stainless steel. Proceedings of the Institution of Mechanical Engineers, Part B: Journal of Engineering Manufacture, Vol 230, No 6, pp.1144–1155, 2016. **41.** *Tatar, K., Rantatalo, M., Gren, P.:* Laser vibrometry measurements of an optically smooth rotating spindle. Mechanical Systems and Signal Processing, Vol 21, No 4, pp. 1739–1745, 2007. **42.** *Lee, Y.,*

Dornfeld, D. A.: Application of Open Architecture Control System in Precision Machining. 31st CIRP International Seminar on Manufacturing Systems, Berkeley, CA, May 1998. **43.** *Bhuiyan, M. S. H., Choudhury, I. A.:* Review of Sensor Applications in Tool Condition Monitoring in Machining. Comprehensive Materials Processing, Vol. 13, pp. 539–569, 2014. **44.** Urbikain, G., Olvera, D., de Lacalle, L. N. L., Elías-Zúñiga, A.: Spindle speed variation technique in turning operations: Modeling and real implementation. Journal of Sound and Vibration, Vol 383, pp. 384–396, 2016. **45.** *Kiss, A. K., Bachrathy, D., Stepan, G.:* Laser scanned patterns of machined surfaces. Procedia CIRP, Vo. 77, pp. 355–358, 2018. **46.** *Sun, H.:* Modeling the near-field and far-field modes of single spatial mode laser diodes. Optical Engineering, Vol 51, No 4, 2012. **47.** *Naqwi, A., Durst, F.:* Focusing of diode laser beams: a simple mathematical model. Applied Optics, Vol 29, pp. 1780–1785, 1990. **48.** *Wong, Y. S., Nee, A. Y. C., Li, X. Q., Reisdorf, C.:* Tool condition monitoring using laser scatter pattern. Journal of Materials Processing Technology, Vol 63, No 1–3, pp. 205–210, 1997. **49.** *Chern, G. L., Liang, J. M.:* Study on boring and drilling with vibration cutting. International Journal of Machine Tools & Manufacture, Vol 47, No 1, pp. 133–140, 2007. **50.** *Béres, M., Paripás, B.:* Fúrószár rezgéseinek mérése lézer Doppler módszerrel. Proc. XXXI. MicroCAD International Multidisciplinary Scientific Conference, University of Miskolc, Hungary, 20–21 April 2017. **51.** *Béres, M., Paripás, B.:* Measurements of vibration by laser Doppler method in the course of drilling. Lecture Notes in Mechanical Engineering, Vol 0, No. 1, pp. 199–208, 2018. **52.** *Balaji, M., Murthy, B. S. N., Rao, N. M.:* Optimization of Cutting Parameters in Drilling of AISI 304 Stainless Steel Using Taguchi and ANOVA. Procedia Technology, Vol 25, pp. 1106–1113, 2016. **53.** *Ryabov, O., Mori, K., Kasashima, N., Uehara, K.:* An In-Process Direct Monitoring Method for Milling Tool Failures Using a Laser Sensor. CIRP Annals. – Manufacturing Technology, Vol 45, No 1, pp. 97–100, 1996. **54.** *Faassen, R. P. H., Van de Wouw, N., Oosterling, J. A. J., Nijmeijer, H.:* Prediction of regenerative chatter by modelling and analysis of high-speed milling. International Journal of Machine Tools and Manufacture, Vol 43, No. 14, pp. 1437–1446, 2003. **55.** *Rantatalo, M.:* Non-contact measurements and modelling of milling machine tool vibrations. Ph.D. thesis/ LuleÂ University Technol., ISSN: 1402–1757, 2006. **56.** *Österlind, T., Frangoudis, C., Archenti, A*.: Operational modal analysis during milling of workpiece, fixed on a stiffness controllable joint. Journal of Machine Engineering, Vol 13, 2013. **57.** *Nakagawa, H., Kurita, Y., Ogawa, K., Sugiyama, Y., Hasegawa, H.:* Experimental analysis of chatter vibration in end-milling using laser Doppler vibrometers. International Journal of Automation Technology, Vol 2, No 6, pp. 431-438, 2008. **58.** *Norman, P., Bäckström, M., Rantatalo, M., Svoboda, A., Kaplan, A.:* A sophisticated platform for characterization, monitoring and control of machining. Measurement science and technology, Vol 17, No 4, pp. 847, 2006. **59.** *Béres, M., Paripás, B.:* Comparison of two laser interferometric methods for the study of vibrations, in Vehicle and Automotive Engineering, Part of the Lecture Notes in Mechanical Engineering book series (LNME), pp. 205–216. Springer, 2017. **60.** *Majár, J., Béres, M., Kovács, E.:* Effect of Different Supports on the Systematic Errors in Laser Doppler Measurements. Proc. MultiScience – XXXIII. microCAD, International Multidisciplinary Scientific ConferenceUniversityofMiskolc, 23–24. May 2019. **61.** *Munoa, J., Beudaert, X., Dombovari, Z., Altintas, Y., Budak, E., Brecher, C., Stepan, G.:* Chatter suppression techniques in metal cutting. CIRP annals, Vol 65, No 2, pp. 785–808, 2016. **62.** *Norgia, M., Melchionni, D., Pesatori, A.:* Self-mixing instrument for simultaneous distance and speed measurement. Optics and Lasers in Engineering, Vol 99, pp. 31–38, 2017. **63.** *Halkon, B. J., Rothberg, S. J.:* Taking laser Doppler vibrometry off the tripod: correction of measurements affected by instrument vibration. Optics and Lasers in Engineering, Vol 91, pp. 16–23, 2017. **64.** *Halliwell, N. A.:* The laser torsional vibrometer: a step forward in rotating machinery diagnostics. Journal of sound and vibration, Vol 190, No 3, pp. 399–418, 1996. **65.** *Rothberg, S. J., Allen, M. S., Castellini, P., Di Maio, D., Dirckx, J. J. J., Ewins, D. J., … , Vignola, J. F.:* An international review of laser Doppler vibrometry: Making light work of vibration measurement. Optics and Lasers in Engineering, Vol 99, pp. 11–22, 2017. **66.** *Hosek, P.:* Algorithm for signal drop-out recognition in IC engine valve kinematics signal measured by laser Doppler vibrometer. Optics & Laser Technology, Vol 44, No 4, pp. 1101–1112, 2012. **67.** *Drain, L. E.:* The laser Doppler techniques. Chichester, 1980. **68.** *Bell, J. R., & Rothberg, S. J.:* Laser vibrometers and contacting transducers, target rotation and six degree-of-freedom vibration: what do we really measure? Journal of Sound and Vibration,

Vol 237, No 2, pp. 245–261, 2000. **69.** *Rothberg, S. J., Baker, J. R., Halliwell, N. A.:* On Laser Vibrometry of Rotating Targets: Effects of Torsional and In-Plane Vibration. Journal of Laser Applications, Vol 2, No 1, pp. 29–36, 1990. **70.** *Martin, P., Rothberg, S.:* Introducing speckle noise maps for laser vibrometry. Optics and Lasers in Engineering, Vol 47, No 3–4, pp. 431–442, 2009. **71.** *Courville, S. W.:* Toward orbital seismology: theory for speckle noise reduction in laser Doppler vibrometer measurements on distant rough surfaces. Colorado School of Mines ProQuest Dissertations Publishing, No 27662723, 2019. **72.** *Vass, J., Šmíd, R., Randall, R. B., Sovka, P., Cristalli, C., Torcianti, B.:* Avoidance of speckle noise in laser vibrometry by the use of kurtosis ratio: Application to mechanical fault diagnostics. Mechanical Systems and Signal Processing, Vol 22, No 3, pp. 647–671, 2008.

Міклош Береш**,** Дьюла Варга, Мішкольц, Угорщина

ЛАЗЕРНІ ВИМІРЮВАННЯ В ПРОЦЕСАХ РІЗАННЯ

Анотація. *Метрологія на місці у виробничих системах підвищує точність і скорочує час обробки за рахунок виключення операцій перепозиціонування і установки. Досягти цих цілей допомагають різні методи і прийоми моніторингу. Ці процедури набувають все більшого значення в окремих технологічних операціях виробництва. Деякі процедури моніторингу стану контролюють верстат, тоді як інші зосереджуються безпосередньо на інструменті. Перший в основному зосереджений на технічному обслуговуванні на основі стану, надаючи дані, які можуть доповнити стратегію технічного обслуговування на основі оцінки ризику (пропонуючи серйозну економічну перевагу для користувачів). Інші методи моніторингу максимізують дорогоцінний робочий час, витрачений на якісне виробництво, досліджуючи стан інструменту. Сьогодні в нашому розпорядженні є безліч різних датчиків і методів вимірювання. Однак кожен з них має обмеження, тому вимірювання все одно обтяжене похибками. Чим чутливіший метод вимірювання (наприклад, лазерний) до фізичного сигналу, тим точніше він може відтворити досліджуване явище. З цієї точки зору вони, таким чином, мають певну перевагу. Нові сфери застосування виходять на перший план завдяки мініатюризації та вбудовуванню вимірювальних приладів. Прикладом такого пристрою є багатопроменевий, інтегрований напівпровідниковий лазер. У порівнянні з попередніми пристроями, цей новий шестипроменевий лазерний чіп зменшує втрати, спричинені часом виявлення, і підвищує стабільність сигналу. Розробка дуже вигідна для вимірювання вібрацій в низькочастотному діапазоні, з амплітудою до 100 мкм/с, роздільною здатністю і якістю, подібними до комерційно доступних LDV. Лазери вийшли на перший план насамперед для поверхневого контролю та визначення динамічної поведінки машинної системи або процесу. Використання лазерів у свердлінні серед технологічних процесів машинобудування все ще чекає свого відкриття, на відміну від фрезерування або токарної обробки, які є добре та ефективно дослідженими галузями. Інтерферометричні вимірювальні прилади більш точні, ніж інші лазерні вимірювальні методи, але їх більш складна конструкція робить їх більш чутливими до умов. Трикутна методика вимірювання, яка добре зарекомендувала себе на практиці, також може бути адекватно використана для вимірювань під час різання. Це метод, який часто використовується для досліджень, але під час виробництва в даний час він використовується майже тільки у випадках позиціонування та вимірювання координат.*

Ключові слова: *різання металу; лазерне вимірювання; технологічний моніторинг; LDV; оптичні датчики.*

UDC 621.9.048 **doi: 10.20998/2078-7405.2023.99.10**

PURPOSE AND TECHNOLOGICAL PROPERTIES OF GRANULAR MEDIA FOR VIBRATION FINISHING AND GRINDING PROCESSING

Andrii **Mitsyk** [1][0000-0002-3267-8065], Vladimir **Fedorovich** [2][0000-0001-7015-8653], Yevgeniy **Ostroverkh** [2][0000-0002-8926-1324]

[1]Volodymyr Dahl East Ukrainian National University (Severodonetsk)
[2] National Technical University «Kharkiv Polytechnic Institute», 2 Kyrpychova Street, Kharkiv 61002, Ukraine
Volodymyr.Fedorovych@khpi.edu.ua

Received: 15 August 2023 / Revised:20 September 2023 / Accepted: 25 October 2023 / Published: 01 December 2023

Abstract. *The purpose and characteristics of granular working media used in vibration processing operations are given. It is indicated that the purpose of granular media is their contact interaction with the processed part surface under conditions of various energy parameters. This interaction is accompanied by elastic-plastic deformation, micro-cutting, adhesion and mechanic-chemical processes. Indicators of technological and operational properties for various types of granular media are given, including the intensity of material removal from the processed surface, cutting ability, wear resistance and achieved surface roughness. The physical and technological parameters of granular media have been established, including deformability, hardness during finishing and hardening operations and surface roughness of the media granules. The influence of the parameters of processing media granules on the productivity of vibration treatment has been determined. It is shown that such parameters are the binding of the granules material, its wear resistance, grain material, granulation and the shape of individual granules. It is noted that the choice of granule sizes depends on two main factors such as: the necessity to obtain a given roughness and high productivity of vibration operations. It was revealed that to ensure high surface cleanliness, the use of small granules of the medium is required, but to obtain high productivity, the use of large granules is required. Approximate dependencies have been determined that relate the size and weight of granules of the processing medium and the processed parts. It is indicated that the best results in achieving high quality of the processed surface and sufficient productivity are provided by granular media with a shape close to a sphere. It is noted that granules in the form of cones, pyramids, prisms and other forms are used for the successful processing of hard-to-reach places in the form of small holes, straight and sharp angles in the interface of the surface of parts, niches or pockets. Such granules are specially manufactured from a mixture of grinding powders of various grain sizes and an inorganic binder based on clays. The features of the physical and technological parameters of processing media are given.*

Key words: *vibration treatment; granular medium; processed parts, physical and technological parameters; productivity of vibration processing.*

1. GENERAL PROVISIONS

In metalworking industries, the granular media are used for finishing and grinding processing of various range parts during various types of vibration treatment [1, 2]. The technological operations include cleaning, washing, finishing-grinding, polishing, hardening and drying ones. Table 1 provides some examples of the use of granular media for various vibration finishing and grinding operations in production processes for the manufacture of parts [3].

2. PURPOSE AND CHARACTERISTICS OF GRANULAR MEDIA

The general purpose of granular media is to carry out contact interaction with the processed surface of parts under conditions of various energy parameters, accompanied by elastic-plastic deformation, micro-cutting, as well as adhesive and mechanic-chemical processes [4].

Table 1

Application of Granular Media for Vibratory Finishing-grinding Operations

№	Vibratory finishing and grinding operations	Composition and characteristics of processing medium granules, granulation
1	Cleaning castings from molding materials, removing flash and scale	Steel and cast iron sprockets, 15...50 mm
		Steel die-cut, 5...20 mm
		Mixture of sprockets and steel die-cuts with grinding wheels, 15...25 mm
		A mixture of scrap grinding wheels of various hardness
		Cast sprockets
		A mixture of mineral ceramic granules TsM-332 with grinding powder
		Mixture of steel balls and abrasive powder, 3...8 mm
2	Deburring with a base thickness of 0.15...0.2 mm, rounding of sharp edges, rough and fine grinding to $R_a = 0.32$ μm	Scrap waste from abrasive and grinding wheels, 8...40 mm
		Mineral ceramic grinding granules TsM-332, 8...25 mm
		Die cutting, chopped wire, needles, 3...15 mm
		Mixture of mineral-ceramic granules with abrasive powder, 8...25 mm

		Porcelain balls, 6...10 mm
		Glass balls, 2...14 mm
		Metal stamping with added abrasive materials
3	Polishing, glossing, finishing, hardening, stabilizing treatment	Polished steel balls 100Cr6 (DIN 17230), 3...6 mm
		Wooden cubes, felt wads, leather scraps, nut shells with the addition of polishing pastes
4	Washing parts from various types of contaminants	Rubber granules, 5...15 mm
5	Drying parts after cleaning and rinsing	Wood chips, crushed corn cobs

To carry out the mentioned technological operations, the granular medium must have certain technological properties. According to the above classification, each type of granular media is characterized by certain indicators of technological and operational properties. In particular, for abrasive granules hey are:

– intensity of material removal from the processed surface;

– cutting abilities;

– wear resistance;

– roughness of the processed surface.

The concept of "material removal rate" is measured in weight or volume units of material removal over a certain period of time [1–3].

Cutting ability is characterized by the ratio of the mass of material removed from a unit of surface per unit of time:

$$R = \frac{\sum_{i=1}^{S} Q_i}{t \sum_{i=1}^{S} S_{q_i}},$$

where Q_i – removal of material from the sample; S_{q_i} – sample surface area, cm^2; t – processing time, min.

The specific consumption of abrasive granules is the difference in mass or volume of consumed abrasive per unit time before and after processing, that is:

$$J_m = M_o - M_k ,$$

where J_m – mass of worn abrasive; M_o and M_k – mass of abrasive granules before and after treatment.

The processing coefficient (specific material removal) is characterized by the ratio of the mass of material removed from a unit surface of the sample to the mass of the consumed abrasive:

$$K_0 = \frac{\sum_{i=1}^{S} Q}{J_m \sum_{i=1}^{S} S_{q_i}} .$$

The wear resistance of abrasive granules is the ratio of the mass of worn material per unit time to the initial mass of the processed granules, expressed as a percentage:

$$J_{\text{sp.}} = \frac{J_m}{M_o} 100\% .$$

An important parameter of abrasive granules is the roughness of the processed surface, including the established roughness. It represents the surface roughness formed under constant processing conditions over a period of time, after which no change in roughness occurs [5].

3. PHYSICAL AND TECHNOLOGICAL PARAMETERS OF GRANULAR MEDIA

For metal granular media, important parameters are: deformability; hardness when performing finishing and hardening operations; roughness of the working surface of the medium granules [1].

When performing finishing operations, especially hardening ones, the durability of metal granules, maintaining the integrity of the working surfaces and their roughness, that is, the absence of chips, chipping, cracks, etc., becomes important. The presence of the mentioned defects may be accompanied by damage to the processed surface and deterioration of its relief.

For metal granules, the density of the material is essential. As the density of the granule material increases, the processing intensity increases due to an increase in the contact forces of interaction between the granules and the surface being processed. In addition to steel balls, granules from non-ferrous metals and alloys, as well as cast iron, are used as metal granules.

Depending on the material, non-metallic granular media are divided into polymer and organic. The polymer are used in washing operations, applying mechanic-chemical coatings, etc. The granules of these media must be oil- and water-resistant, acid- and alkali-resistant. They must have sufficient hardness and wear resistance under abrasion conditions. Examples include granules of polystyrene, fabric-based laminate, rubber, polyurethane and others. Granules made from materials of organic origin are used in the operations of washing, drying and lapping, fine surface finishing, and applying mechanic-chemical coatings. These media are often saturated with various types of pastes and powders in order to increase mass and impart polishing properties [6].

A distinctive feature of granules of organic origin is their low density, leading to a decrease in the intensity of the process. As a result, they resort to making the granules heavier by "interspersing" metal bodies of various shapes into them.

Pasty abrasive media is a flexible tool used for processing of complex surfaces, internal channels and grooves. In terms of content, it is a viscoelastic polymer filled with abrasive. The processing operations are carried out by moving the medium relative to the surface being treated.

The paste-like abrasive medium consists of a plastic semi-solid binder and abrasive grains. The pressure of the moving medium is 65 ... 2060 N/cm^2. Materials with different mechanical properties can be subjected to this treatment.

Silicon carbide, boron carbide, aluminum oxide, and diamond are used as abrasive grain materials. Grains ranging in size from 5 to 1525 μm are used. With the use of a large-grain abrasive, the processing intensity increases, while a smaller-grain abrasive helps reduce surface roughness and provides access to small-diameter holes.

The depth of micro-cutting when processing with abrasive paste depends on the applied pressure, the density of the paste and the size of the abrasive grains.

During the processing, the abrasive granules are destroyed and dulled, and the ground material becomes part of the abrasive medium.

The service life of the paste depends on a number of factors:

– initial amount of paste when loading;

– type and size of abrasive grains;

– paste flow speed;

– part configurations.

4. INFLUENCE OF GRANULAR MEDIUM PARAMETERS ON VIBRATION PROCESSING PRODUCTIVITY

In the practice of vibration treatment, it has been shown that its performance is influenced by such parameters of the granular medium as the binding of the granule material, its wear resistance, grain material, granulation and the shape of individual granules [3].

The bond of abrasive materials can be different - ceramic and made on the basis of organic binders (phenolic resin plastic, vulcanite, etc.).

Its effect on the vibration treatment process is similar to the effect of grinding wheels when grinding metal products on machine tools and consists in facilitating chipping of dull grains.

Research has shown that when using a ceramic binder, it is possible, by changing the size of the granules and processing modes, to obtain the necessary results, practically eliminating vibration processing with granules made on the basis of organic binders. This made it possible to use any high-performance chemically active solutions during all vibration operations [7]. When using granules only with a ceramic binder, the range of granular media used in vibration processing areas is significantly reduced, that makes it easier to organize the work of the workshop.

The hardness of the binder provides the necessary wear resistance of abrasive granules. With excessively soft ligaments, rapid destruction of granular media occurs and the accompanying clogging of the reservoir, which leads to a decrease in the productivity of vibrating machines.

From the point of view of wear of granular media, media with granule hardness VT and CT should be considered the most rational. However, when working with them, the surface may become greasy, which can be eliminated by using special working solutions [8].

Granular mineral ceramic media from the TsM-332 (microlite) brand are more resistant to abrasion. Their wear resistance compared to granules of hardness M is 200...350 times higher.

The material of the granular medium during vibration treatment has a relatively insignificant effect on both the metal removal and the resulting micro-roughness of the processed part. The interaction forces during vibration processing are insignificant, so there is practically no destruction of grains. The wear of the medium granules occurs mainly due to the chipping of grains from the binder. This effect ensures self-sharpening of the grinding bodies during processing.

The grain size of the granular processing medium has a great effect on metal removal and the micro-roughness of the obtaned surface in various vibration processing operations.

The granulation of the processing medium, in combination with the modes and its circulation in the vibrating machine reservoir, is one of the main factors determining the amount of metal removed from the surface of parts per unit of time. Metal removal depends not only on the size of the granules, their shape, weight and processing modes, but also on the design, sizes, material and weight of the processed part [9].

In many cases, it is possible to prescribe the required granulation of the processing medium with sufficient accuracy for practice without additional experiments. However, these decisions are often preliminary; they require redetermination when adjustment the technological process of vibration treatment, depending on the constructive features of the parts being processed. First of all, such features include the presence of pockets, small-diameter holes, grooves and other elements that make it difficult for granules to access the treated surfaces.

Therefore, when choosing the granulation of processing media, the shape and material of their granules, the type of technological process, the required productivity, design and final cleanliness of the surface of the processed parts are taken into account. The most widespread granulation of processing media is in the range of 3...50 mm [10].

The choice of granule sizes depends on two main factors: the need to obtain a given roughness and high productivity of vibration operations. To ensure high surface cleanliness, the use of small granules of the medium is required, and to obtain high productivity, large granulations are required. In addition, it is necessary to take into account that metal removal depends on the number of granules that are simultaneously placed on the processed part surface and strike it simultaneously or with a slight lag.

There is no direct proportionality between the size of the medium granules and metal removal. With small granulation, the number of impacts increases, while the force of interaction between the granules and the part decreases. In some cases, metal removal by medium-weight granules turns out to be higher than by heavy-weight granules.

It has been established that the dimensions and weight of the granules of the processing medium and the processed parts are interconnected by the following approximate dependencies:

$$\frac{P_{\text{part.}}}{P_{\text{gran.}}} > 30\,; \quad L_{\text{gran.}} = \frac{l_{\min}}{5}\,,$$

where $P_{\text{part.}}$ and $P_{\text{gran.}}$ – weight of the part and granules; $L_{\text{gran.}}$ – medium granule size; $l_{\min}$ – the smallest linear dimension of the part.

The shape of the granules of the processing medium is extremely diverse. It can vary from sharp-edged crap of grinding wheels and granules made of TsM-332 (microlite) material with sharp edges to well-rolled granules of spherical or elliptical shape. In the initial stage of work, when the granules still have sharp edges, marks and nicks may appear on the parts. To achieve high grades of surface cleanliness of the processed part, it is necessary to use either granules that have worked in rough operations for a time sufficient to round off sharp edges, or to specially process them until the sharp spots are rounded off.

The best results in achieving high quality of the processed surface and sufficient productivity are provided by granular media with a shape close to a sphere. The main disadvantage of such granules is the impossibility of processing hard-to-reach places in the form of small holes, straight and sharp corners in the mating surfaces of parts, niches, and pockets. In these cases, specially made granules are used in the form of cones, pyramids, prisms and other shapes. To improve their cutting properties, such granules are made from a mixture of grinding powders of various grain sizes and an inorganic binder based on clays.

5. CONCLUSIONS

1. An important condition for the implementation of the vibration treatment process is the presence of a granular processing medium. In domestic and foreign practice, it has been established that medium granules have a decisive effect on achieving surface quality and process productivity.

2. The choice of granular medium is made depending on the purpose of the operation being performed, the material and configuration of the processed part, as well as the vibration processing method used.

3. When choosing granular media, it is necessary to take into account the requirement for the quality of the surface being processed and the minimum cost of the treatment process, limiting the range of granular media for the purpose of ease of acquisition, preparation for use, as well as sorting and storage in metalworking production conditions.

References: **1.** Osnovy vibracijnoi' tehnologii': navchal'nyj posibnyk / *Lubens'ka L.M., Kalmykov M.O., Jasunik S.M.* Lugans'k: Vyd-vo SNU im. V. Dalja, 2009. 284 p. [in Ukraine] **2.** *Kartashov I.N., Shainskij M.E., Vlasov V.A.* Obrabotka detalej svobodnymi abrazivami v vibrirujushhih rezervuarah. Kiev: Vishha shk., 1975. 188 p. [in Russian] **3.** Ozdobljuval'no-abrazyvni metody obrobky: pidruchnyk / *L.M. Lubens'ka, V.B. Strutyns'kyj, Jasunik S.M., M.O. Kalmykov*. Kyi'v – Lugans'k: «Noulidzh», 2011. 268 p. [in Ukraine] **4.** Instrument dlja obrobki detalej vil'nimi abrazivami: monografija / *M.O. Kalmykov, T.O. Shumakova, V.B. Strutins'kij, L.M. Lubens'ka*. Kyiv – Luhans'k: «Noulidzh», 2010. 214 p. [in Ukraine] **5.** Nadtverdi abrazyvni materialy v mehanoobrobci: encyklopedychnyj dovidnyk / *V.I. Lavrinenko, M.V. Novikov*; za zag. red. M.V. Novikova. Kyi'v: INM im. V.M. Bakulja NAN Ukrai'ny, 2013. 456 p. [in Ukraine] **6.** *Kundrák J., Morgan M., Mitsyk A.V.,*

Fedorovich V.A., Grabchenko A.I. Mathematical simulation of the vibration treatment of parts in a liquefied abrasive working medium. The International Journal of Advanced Manufacturing Technology, pp. 5377 – 5398 (2022). https://doi.org/10.1007/s00170-022-08843-8 **7.** *Bereshhenko A.A.* Vibrohimicheskaja obrabotka uglerodistyh i legirovannyh stalej: dis. … kand. him. nauk: 05.17.03 / Institut obshhej i neorganicheskoj himii AN USSR. Kiev, 1980. 132 p. [in Russian] **8.** *Mitsyk A.V., Fedorovich V.A.* Process otdelochno-zachistnoj vibroobrabotki i parametry, vlijajushhie na ego proizvoditel'nost'. Cutting & Tools in Technological System. Kharkiv, NTU «KhPI». 2013. № 83. pp. 184 – 194. [in Russian] **9.** *Mitsyk A.V.* Rozvytok vibracijnoi' ozdobljuval'no-zachyshhuval'noi' obrobky v seredovyshhi vil'nyh abrazyvnyh granul. Visnyk SNU im. V. Dahl. Sjevjerodonec'k, SNU im. V. Dahl, 2021. № 1 (265). pp. 68 – 74. [in Ukraine] https://doi.org/10.33216/1998-7927-2021-265-1-68-74 **10.** *Mitsyk A.V., Fedorovich V.A., Grabchenko A.I.* Interaction of the abrasive medium with the treated surface and the process of metal removal during vibration treatment in the presence of a chemically active solution. Cutting & Tools in Technological System. Kharkiv, NTU «KhPI». 2021. № 94. pp. 42 – 48. https://doi.org/10.20998/2078-7405.2021.94.05

Андрій Міцик, Володимир Федорович, Євгеній Островерх, Харків, Україна

ПРИЗНАЧЕННЯ ТА ТЕХНОЛОГІЧНІ ВЛАСТИВОСТІ ГРАНУЛЬОВАНИХ СЕРЕДОВИЩ ДЛЯ ОЗДОБЛЮВАЛЬНО-ЗАЧИЩУВАЛЬНОЇ ВІБРАЦІЙНОЇ ОБРОБКИ

Анотація. *Наведено призначення та характеристика гранульованих робочих середовищ, що використовуються на операціях віброобробки. Вказано, що призначення гранульованих середовищ полягає в їхній контактній взаємодії з оброблюваною поверхнею деталі в умовах різних енергетичних параметрів. Така взаємодія супроводжується пружнопластичною деформацією, мікрорізанням, адгезійними та механохімічними процесами. Наведено показники технологічних та експлуатаційних властивостей для різних видів гранульованих середовищ, серед яких інтенсивність зйому матеріалу з оброблюваної поверхні, різальні здібності, зносостійкість, досягнута шорсткість поверхні. Встановлено фізико-технологічні параметри гранульованих середовищ, у тому числі деформаційну здатність, твердість при виконанні оздоблювально-зміцнювальних операцій, шорсткість поверхні гранул середовища. Визначено вплив параметрів гранул обробних середовищ на продуктивність вібраційної обробки. Показано, що такими параметрами є зв'язка матеріалу гранул, його зносостійкість, матеріал зерна, грануляція та форма окремих гранул. Зазначено, що вибір розмірів гранул залежить від двох основних факторів: необхідності отримання заданої шорсткості та високої продуктивності вібраційних операцій. Виявлено, що для забезпечення високої чистоти поверхні потрібно застосування гранул середовища малих розмірів, а для отримання високої продуктивності застосування гранул великої грануляції. Встановлено орієнтовні залежності, що зв'язують розміри та вагу гранул обробного середовища та оброблюваних деталей. Вказано, що найкращі результати досягнення високої якості обробленої поверхні та достатньої продуктивності дають гранульовані середовища за формою близькі до сфери. Зазначається, що для успішної обробки важкодоступних місць у вигляді дрібних отворів, прямих та гострих кутів у поєднанні поверхні деталей, ніш, кишень використовуються спеціально виготовлені із суміші шліфувальних порошків різної зернистості та неорганічної зв'язки на основі глин, гранули у вигляді конусів, пірамід, призм та інших форм. Надано особливості фізико-технологічних параметрів обробних середовищ.*

Ключові слова: *віброобробка; гранульоване середовище; фізико - технологічні параметри; продуктивність віброобробки.*

UDC 621.91.01 **doi: 10.20998/2078-7405.2023.99.03**

ARITHMETIC MEAN HEIGHT AND MAXIMUM HEIGHT OF THE ROUGHNESS PROFILE IN HONING WITH DIFFERENT FEEDS

István **Sztankovics** [0000-0002-1147-7475]

University of Miskolc, 3515, Miskolc - Egyetemváros, Hungary
istvan.sztankovics@uni-miskolc.hu

Received: 03 November 2023 / Revised:11 November 2023 / Accepted: 23 November 2023 / Published: 01 December 2023

Abstract. *The achievable surface quality is an important factor even in roughing procedures; however, it is most relevant in finishing. Two commonly measured and analysed characteristics of the machined surface roughness profile are the Arithmetic Mean Height and the Maximum Height of the Roughness Profile. In this paper these parameters were studied in bore honing. Cutting experiments were carried out, where the feed rate and the applied honing tool are varied. After the evaluation of the measured 2D surface profiles, the following conclusions were drawn: the effect of the feed rate is not linear; the lowest values of the analysed roughness parameters were achieved by the application of 50 mm/rev. feed rate and a honing tool with 80 grain size and ceramic binder; the difference between the studied roughness parameters was 6.5-8.0-fold.*
Keywords: *arithmetic mean height of roughness profile; cutting; experiments; honing; maximum height of roughness profile.*

1. INTRODUCTION

The study of the achievable surface quality is an important task in machining, most importantly in finish procedures. A part of the evaluation of the machined surface quality is the analysis of the geometric errors on the surface, which can be done by the investigation of 2D roughness parameters. It is necessary to specify the optimal process parameters to optimize surface roughness [1,2]. Though much research is ongoing in this field [3,4], it is not an easy task to give the optimal setup parameters. It is also a difficult task in abrasive machining. A part of this is the study of the cutting tool, where the change in the area and the maximum stress with a change in the grain concentration are established [5]. Yang et al. found, that increasing the grain size results in increased surface roughness by more than four times [6]. The radial and axial speed had little effect on the roughness in their work. Szabó showed that by changing the grain material it is possible to effectively influence the amount of material removed from the workpiece in a unit of time [7]. In their work, Sabri et al showed that by changing the material (and especially the grain size) of the honing tool, the final surface roughness and topography of the

machined workpieces can be favourably influenced [8]. It was found that a higher elastic modulus of the bond can increase the strength of abrasive material, which provides an increase in grinding performance and a reduction in the specific consumption of grains [9]. Goelden et al. proved with their simulation and experimental work that the prescribed roughness can be achieved with fewer strokes by increasing the pressure [10]. The abrasive cutting process is also affected by the selected binder of the tool [11,12].

In this paper, the Arithmetic Mean Height and the Maximum Height of the Roughness Profile are studied in bore honing by changing the feed rate and the material of the tool. The values of these parameters were measured and analysed.

2. EXPERIMENTAL CONDITIONS AND METHODS

The aim of the experiments was to study the effect of several parameters (pressure, feed, grain size) on the surface roughness in bore honing. The values of the analysed parameters were chosen according to the rules of 23 full factorial design of experiments.

The machining was done with the different setups on a WMW 270/700 honing machine, which was provided by Belcord Kft. in Eger, Hungary (their help is greatly appreciated). The honing experiments were carried out on sleeves with EN-GJL-250 lamellar cast iron alloy material, 192 mm bore length and 88 mm inner diameter. Three kinds of honing tools were used, which had Al_2O_3. The specifications of the different honing tools can be seen in Table 1.

Among the cutting parameters, the cutting speed (v_c) was fixed to 200 m/min and the applied pressure on the honing stone (p) was adjusted to 10 bar. The feed per revolutions (v_f) was set to 25 mm/rev, 50 mm/rev and 75 mm/rev. The resulted setups and the set parameters can be seen in Table 2.

Table 1 – Honing tool characteristics

Mark	Grain size	Binder	Structure
I	80	ceramic	medium dense
II		synthetic resin	dense
III	240		

Table 2 – Experimental setups

Setup number	1	2	3	4	5	6	7	8	9
Bore length [mm]	192	192	192	192	192	192	192	192	192
Bore diameter [mm]	88	88	88	88	88	88	88	88	88
Cutting speed	200	200	200	200	200	200	200	200	200

[m/min]									
Pressure [bar]	10	10	10	10	10	10	10	10	10
Feed rate [mm/rev.]	25	25	25	50	50	50	75	75	75
Honing tool no.	1	2	3	1	2	3	1	2	3

Measurements were carried out on the workpieces after the cutting experiments with a Mitutoyo SJ-301 Surftest roughness measurement device. The roughness profiles were registered on three generatrix of each bore. The measured profiles were evaluated with the AltiMap Premium 6.2.7487 surface analysis software. The analysed parameters of the 2D (linear) profile were (ISO 21920:2021):

- *Ra* – Arithmetic Mean Height of the roughness profile [µm]
- *Rz* – Maximum Height of the roughness profile [µm]

3. EXPERIMENTAL RESULTS

The experiments were carried out and the surface profiles are measured for each setup. Figure 1 shows the roughness profile of the machined surfaces after the machining with 25 m/min feed were carried out with the three tools. Figure 2 presents the three different results in case of 50 m/min feed. Lastly, the roughness profiles corresponding to the 75 m/min feed can be seen in Figure 3.

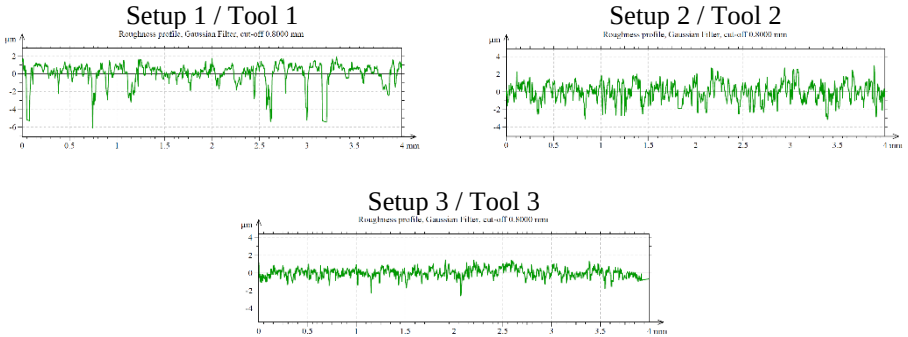

Figure 1 – Roughness profiles measured after machining with 25 m/min feed rate

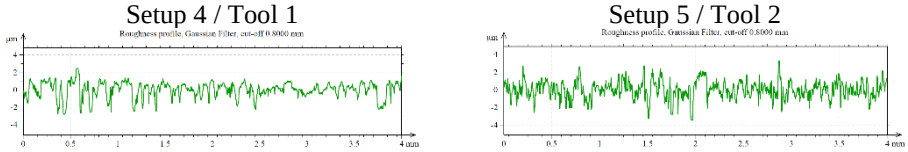

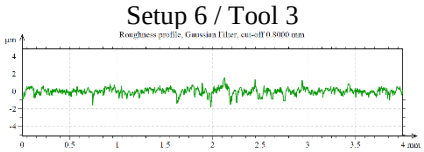

Figure 2 – Roughness profiles measured after machining with 50 m/min feed rate

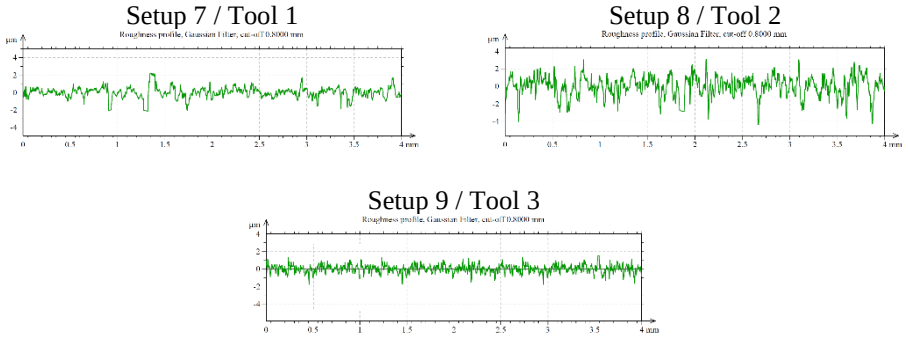

Figure 3 – Roughness profiles measured after machining with 75 m/min feed rate

Table 2 – Measurement results

Setup		1	2	3	4	5	6	7	8	9
R_a [µm]	1	0.86	0.80	0.40	0.67	0.79	0.31	0.98	1.02	0.50
	2	0.68	0.82	0.42	0.68	0.77	0.31	0.80	0.99	0.31
	3	0.68	0.74	0.25	0.69	0.80	0.28	0.75	0.89	0.36
	Mean	0.74	0.79	0.36	0.68	0.79	0.30	0.84	0.97	0.39
R_z [µm]	1	6.17	5.06	3.16	4.67	5.02	2.16	7.44	7.33	3.70
	2	6.01	5.31	2.97	4.09	5.41	2.13	5.97	6.23	1.99
	3	5.17	5.08	1.91	3.89	4.79	2.10	7.23	6.70	2.48
	Mean	5.78	5.15	2.68	4.22	5.08	2.13	6.88	6.75	2.72

The resulted profiles were evaluated, and the analysed roughness values were determined for each setup. Then the mean values of the three measurements of R_a and R_z were calculated for each setup These values are shown in Table 2.

4. DISCUSSION

The evaluation of the results follows the assessment of the measurements. Figure 4 presents the Arithmetic Mean Height of the roughness profile in function of the feed rate and the used honing tool. As the feed rate increased from 25 mm/rev. to 50 mm/rev. and lastly 75 mm/rev, an interesting phenomenon could be noticed.

Among these three setup parameters, the middle value resulted the lowest R_a in all three types of honing tools. The increase of v_f from 50 mm/rev. to 75 mm/rev. results in a 20% increase in R_a, while the decrease of the studied setup parameter resulted in a 10% increase in this roughness parameter. This suggest that the effect of the feed rate is not linear contrary to other finish machining procedures as bore turning. Therefore the choice of feed rate for honing procedure is a complex task and further considerations must be taken into account in the process planning. The effect of the proper choice of honing tool material is more significant. If a coarser grain structure is applied, the roughness will be higher in both type of applied binders. However, if the finer grains are applied, a nearly two-fold decrease in the R_a value can be expected. This relation is expected since the size of the grains corresponds to the size of the micro-scratches generated on the machined surface.

Figure 5 shows the alteration of Maximum Height of the roughness profile in function of the feed rate and the selected honing tools. The trend of the change is similar to the previously described alteration. However, the application of synthetic resin instead of a ceramic binder led to higher R_a values in feeds of 25 mm/rev. and 75 mm/rev., yet the R_z values became lower. This suggest that the selected binder affects the chip removal, this leading to a different shaped surface profile as it can be seen in Figure 1-3. In the studied parameter range, the difference between R_a and R_z was 6.5-8.0-fold. This differs from the usually applied ratio of 5 in machining with defined cutting edged tools.

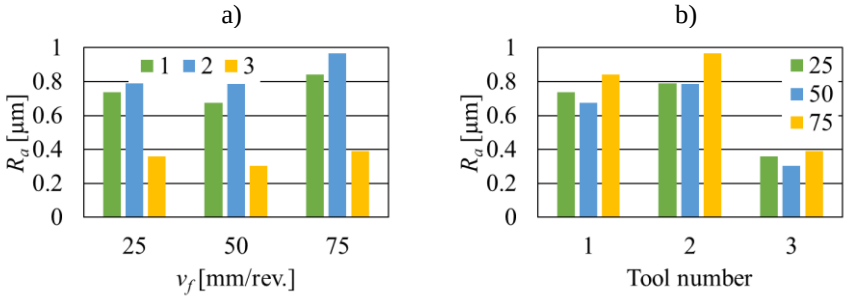

Figure 4 – Arithmetic Mean Height of the roughness profile in function of feed rate (a) and applied tool (b)

a) b)

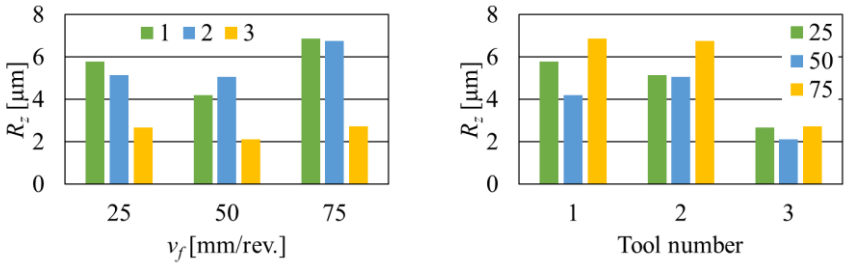

Figure 5 – Maximum Height of the roughness profile
in function of feed rate (a) and applied tool (b)

5. CONCLUSIONS

The study of the expectable machined surface roughness is needed particularly in finish procedures. Honing is a widely used chip-removal procedure in the production of good quality bores due to its advantageous characteristics. In this paper, the Arithmetic Mean Height and the Maximum Height of the roughness profile are analysed. Cutting experiments were carried out by the application of different kinds of honing tools and feed rate. The machined surfaces were measured and evaluated.

The following conclusions can be highlighted after the evaluation of the experimental results:

- The effect of the feed rate on the studied roughness parameters is not linear.
- Minimal values of the analysed roughness parameters were got using 50 mm/rev. feed rate and a honing tool with 80 grain size and ceramic binder.
- The difference between R_a and R_z was 6.5-8.0-fold.

References: 1. *Sapit, A. B., Shather, S. K., & Abed, F. N.* (2020). Enhancement of the performance surface roughness of wire cutting process by additives Nano [AL_2O_3]. Periodicals of Engineering and Natural Sciences, 8(2), pp. 933–941. **2.** *Ferencsik, V., & Varga, G.* (2022). The effect of burnishing process on skewness and kurtosis of the scale limited surface. Rezanie I Instrument V Tehnologiceskikh Sistemakh / Cutting And Tool In Technological Systems, (97), pp. 83–90. **3.** *Ferencsik, V., & Varga, G.* (2022). The Influence of diamond burnishing process parameters on surface roughness of low-alloyed aluminium workpieces. Machines, 10(7), 564. **4.** *Nagy, A., & Varga, G.* (2022). Analyzing the effect of the tool pass number and the direction of sliding burnishing on surface roughness. Rezanie I Instrument V Tehnologiceskikh Sistemakh / Cutting And Tool In Technological Systems 97 pp. 70–82. **5.** *Kundrak, J., Fedorovich, V., Pyzhov, I., Ostroverkh, Y., & Pupan, L.* (2022, September). Numerical Simulation of Grain Concentration Effect on Output Indicators of Diamond Grinding. In Grabchenko's International Conference on Advanced Manufacturing Processes (pp. 165–175). Cham: Springer International Publishing. **6.** *Yang, C. Y., Wang, Z., Su, H., Fu, Y. C., Zhang, N. H., & Ding, W. F.* (2023). Numerical analysis and experimental validation of surface roughness and morphology in honing of Inconel 718 nickel-based superalloy. Advances in Manufacturing, 11(1), pp. 130–142. **7.** *Szabó, O.* (2014).

Examination of material removal process in honing. Acta technica corviniensis – bulletin of engineering, 7, pp. 35–38. **8.** *Sabri, L., Mezghani, S., El Mansori, M., Zahouani H.* (2011). Multiscale study of finish-honing process in mass production of cylinder liner. Wear, Volume 271, Issues 3–4, pp. 509–513. **9.** *Kundrák, J., Fedorovich, V., Markopoulos, A. P., Pyzhov, I., & Ostroverkh, Y.* (2022). Theoretical Assessment of the Role of Bond Material during Grinding of Superhard Materials with Diamond Wheels. Machines, 10(7), 543. **10.** *Goeldel, B., El Mansori, M., & Dumur, D.* (2013). Simulation of roughness and surface texture evolution at macroscopic scale during cylinder honing process. Procedia CIRP, 8, pp/ 27–32. **11.** *Fedorovich, V., Fedorenko, D., Pyzhov, I., & Ostroverkh, Y.* (2021). Modeling the influence of metal phase in diamond grains on self-sharpening of grinding wheels on ceramic bonds. Rezanie I Instrument V Tehnologiceskikh Sistemakh / Cutting And Tool In Technological Systems, (94), pp. 92–101. **12.** *Lavrinenko, V., Fedorovich, V., Ostroverkh, Y., & Solod, V.* (2023). Modern developments related to the directed impact on the cutting surface of a diamond abrasive tool and its contact zone in the processes of machining. Rezanie I Instrument V Tehnologiceskikh Sistemakh / Cutting And Tool In Technological Systems, (98), pp. 13–29.

Іштван Станкович, Мішкольц, Угорщина

СЕРЕДНЬО АРИФМЕТИЧНЕ І МАКСИМАЛЬНЕ ЗНАЧЕННЯ ВИСОТИ ПРОФІЛЮ ШОРСТКОСТІ ПРИ ХОНІНГУВАННІ З РІЗНИМИ ПОДАЧАМИ

Анотація. *Досяжна якість поверхні є важливим фактором навіть при чорнових процедурах, однак найбільш актуальна вона при обробці. Дві загальноприйняті та проаналізовані характеристики профілю шорсткості оброблюваної поверхні – це середня арифметична висота та максимальна висота профілю шорсткості. Механічна обробка проводилася за допомогою різних установок на хонінгувальному верстаті. Експерименти з хонінгування проводилися на гільзах з пластинчастого чавуного сплаву EN-GJL-250, довжиною отвору 192 мм і внутрішнім діаметром 88 мм. Використовувалися три види хонінгувальних інструментів, на основі Al_2O_3. Серед параметрів різання, швидкість різання (v_c) була зафіксована на рівні 200 м/хв, а прикладений тиск на хонінгувальний брусок (р) був відрегульований до 10 бар. Подача на оберт (v_f) була встановлена на 25 мм/об, 50 мм/об і 75 мм/об. Вимірювання проводилися на заготовках після проведених експериментів з різання приладом для вимірювання шорсткості Mitutoyo SJ-301 Surftest. Профілі шорсткості були зареєстровані на трьох твірниках кожного отвору. Виміряні профілі були оцінені за допомогою програмного забезпечення для аналізу поверхні AltiMap Premium 6.2.7487. Проаналізовані параметри 2D (лінійного) профілю були (ISO 21920:2021): R_a – середня арифметична висота профілю шорсткості [мкм], R_z – максимальна висота профілю шорсткості [мкм]. У даній роботі ці параметри були вивчені при хонінгуванні отворів. Були проведені експерименти з різанням, де варіюється швидкість подачі і застосовуваний хонінгувальний інструмент. Після оцінки виміряних 2D профілів поверхні були зроблені наступні висновки: вплив швидкості подачі не є лінійним; найнижчі значення аналізованих параметрів шорсткості були досягнуті застосуванням швидкості подачі 50 мм/об та хонінгувального інструменту з розміром зерна 80 та керамічного в'яжучого; Різниця між досліджуваними параметрами шорсткості становила 6,5–8,0 разів.*

Ключові слова: *середнє арифметичне значення висоти профілю шорсткості; різання; експерименти; хонінгування; максимальна висота профілю шорсткості.*

UDC 621.923.7 **doi: 10.20998/2078-7405.2023.99.05**

ANALYTICAL ANALYSIS OF THE THEORETICAL SURFACE ROUGHNESS IN THE CASE OF BURNISHING OF CYLINDRICAL WORKPIECE

Viktoria **Ferencsik** [0000-0002-8673-1095]

University of Miskolc, 3515, Miskolc - Egyetemváros, Hungary
ferencsik.viktoria@uni-miskolc.hu

Received: 02 November 2023 / Revised:09 November 2023 / Accepted: 18 November 2023 / Published: 01 December 2023

Abstract. *In the last decade, ensuring the highest possible surface quality of manufactured parts has been given a major priority, so more and more emphasis is being placed on the examination and development of finishing treatments that can effectively ensure increasingly stringent surface roughness. For this purpose, diamond burnishing - which is a widely used cold plastic technology - can be used productively as it can improve the surface roughness of the material. But even though due to the development of engineering technology, new possibilities and methods are constantly being developed to examine individual material structure changes, the ability to plan the surface roughness is very difficult. This paper focused on the determination of theoretical roughness to establish a mathematical model that can predict and analyse the relationship between experimental process parameters and surface roughness parameters. To validate the model, real experiments were performed, where the surface roughness were measured before and after the application of burnishing process on low alloyed aluminium shaft pieces.*
Keywords: *mathematical model; modified Hertz theory; contact theory; problems of contact mechanics*.

1. INTRODUCTION

The calculation of theoretical roughness has a long history in the case of cutting operations [1– 6], in longitudinal turning, which is most like the kinematics of surface burnishing as Fig. 1 shows, the theoretical roughness can be determined analytically as a combination of the rotational and axial linear feed of the workpiece.

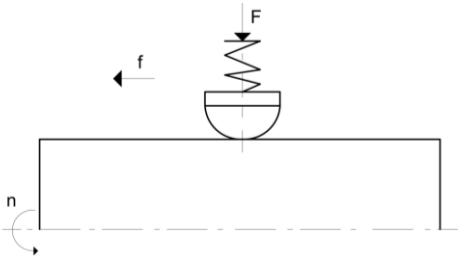

Figure 1. Schematic illustration of burnishing [7]

But the effectiveness of diamond surface burnishing and the plastic deformation process itself are influenced by many parameters, even to a critical degree. For example, inappropriately selected burnishing force can generate lower compressive and, in extreme cases, tensile residual stress, thus reducing the wear resistance and service life of the surface. To optimise the process, many researchers have worked on modelling surface roughness and stress state, which can be used to estimate the burnishing efficiency of a given material grade.

Cui et al. [8] found that their model based on Hertz theory can be used as a good approach for estimating surface roughness when applying excessive burnishing forces to Inconel 718 material grade. Vaishya et al. [9] also started from the use of the Hertz theory in the case of machining Stavax material quality with TiC burnishing tool and primarily investigated the effect of the burnishing force. The results of the experimental and theoretical values showed a good approximation and according to their claim, the deviation was caused by just the assumptions made during the development of the model, however, these uncertain factors were not named. Felhő and Varga [10] determined the theoretical roughness for diamond burnishing of 30CrMo4 material, which they compared with both finite element modelling and real experimental results, and their work was greatly influenced by the modified Hertz theory of Bouzid et al. [11].

In his work, Korzynksi [12] compared several models applicable to surface burnishing and showed that classical burnishing models are only valid for so called surface hardening burnishing. They are suitable for determining the tool indentation depth, but do not consider the stereometric condition of the initial surface, which has a significant influence on the surface roughness after burnishing. Felhő [13] presents in his publication the possibilities of analytical modelling of theoretical roughness for different machining processes. He points out also one of the obvious disadvantages of these calculations is that they ignore many factors that can influence the real surface roughness: the cutting/burnishing forces and the associated vibrations of the machining system, the roughness of the tool, etc.

To explain the contact mechanical relations between bodies with circular surfaces (sphere, cylinder), several models have been developed, such as Johnson-Kendall-Roberts model, Bradley model, Derjaguin-Müller-Toporov model, but based on my experience in literature research, the most preferred solution is to use Hertz theory, so the relation developed for normal contact of elastic solids. In this paper, the approach of Ponomarjov et al. [14] with Hertz-theory is combined to determine the theoretical roughness of burnished EN AW-2011 cylindrical workpiece.

2. ANALYTICAL MODEL OF SURFACE ROUGHNESS

The contact of deformable solids is a common phenomenon in nature and in engineering practice, and plays an important role in physics, biology, astrophysics, nanoindentation, etc. [15, 16]. But the examination of deformations and stresses at the point of contact of the components is one of the most complicated chapters in modern elasticity. The theory of deformation of elastic bodies was founded by Hertz and it has been a milestone in modern contact mechanics since it was published publicly in 1882. It describes the contact mechanism of two solid bodies in the range of linear elasticity and negligible deformations [14].

In the case of burnishing process, the use of this theory is justified because burnishing is a chipless manufacturing technology, so the depth of cut as a parameter cannot be interpreted. However, in order to analytically determine the theoretical roughness, it is necessary to calculate the so-called normal indentation depth of the tool (Figure 2 – δ), as this already enables the use of the modelling method which is correctly applied in turning. Figure 2 schematically shows that during the burnishing process, the tool with the radius "R_1" penetrates the material of the workpiece and generates an indentation depth "δ" in the axial width "2a" under the influence of the force "*F*".

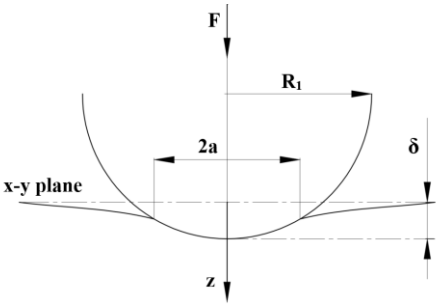

Figure 2. Theoretical illustration of surface burnishing

Hereinafter, I briefly summarize the treatment of the spherical burnishing tool and the outer axial workpiece with Hertz-theory, which is also based on the thought process of Johnson-Kendall-Roberts and Ponomarjov.

According to the Hertz contact theory the radii of the two contacting balls are R_1 and R_2 respectively, it can be seen on the left side in Figure 3. On the right side of it, "*r*" denotes the distance of the moving point from the force, "w_1" and "w_2" denote the displacement of the bodies in the directions "z_1" and "z_2", then the convergence of the given points can be described as follows:

$$\delta = (z_1 + w_1) + (z_2 + w_2) \quad (1)$$

In this way, contact the points for which it is satisfied that:

$$z_1 + z_2 = \delta - (w_1 + w_2) \quad (2)$$

From Fig. 3:

$$R_1^2 - r^2 = (R_1 - z_1)^2 = R_1^2 - 2R_1 r + {z_1}^2 \quad (3)$$

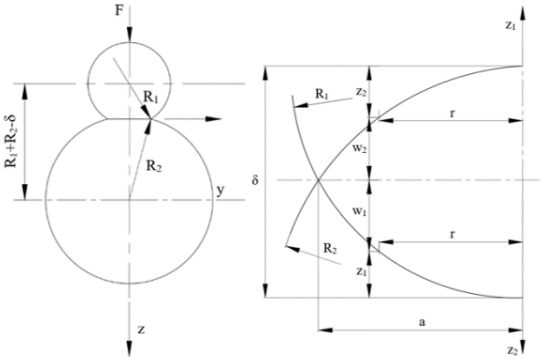

Figure 3. Approach distance of contacting bodies

"z_1^2" is a second-order small value, negligible, thus:

$$z_1 = \frac{r^2}{2R_1}; z_2 = \frac{r^2}{2R_2} \quad (4)$$

The distance of the approaching points after contact can be expressed as follows:

$$w_1 + w_2 = \delta - (z_1 + z_2) = \delta - \frac{r^2}{2}\left(\frac{1}{R_1} + \frac{1}{R_2}\right) \quad (5)$$

As Fig. 4 shows, when machining an axial workpiece with a spherical tool, the surface pressure is distributed over an ellipsoidal surface and is proportional to the ordinates of the ellipsoid.

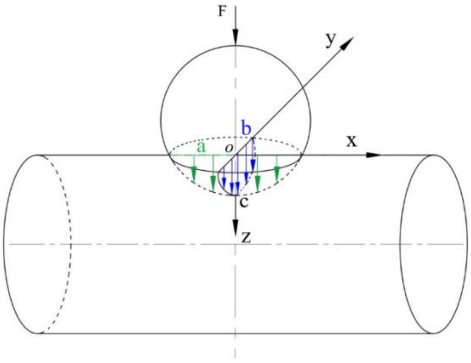

Figure 4. Pressure distribution during burnishing axial workpiece

The equation of ellipsoid must be applied:

$$\left(\frac{x}{a}\right)^2 + \left(\frac{y}{b}\right)^2 + \left(\frac{z}{c}\right)^2 = 1 \tag{6}$$

As the pressure distribution on the contact area is axisymmetric about x-y axes and the maximum pressure is located at the centre of the contact area (O), the pressure distribution supposed to be semi-ellipsoid, so:

$$w_1 + w_2 = \delta - \frac{x^2}{2R_1} - \frac{y^2}{2}\left(\frac{1}{R_1} + \frac{1}{R_2}\right) \tag{7}$$

Under this semi-ellipsoidal load, on S_c contact surface the vertical displacement of the elliptical contact point "w" can be expressed as follows using the elastic material parameters:

$$w_1 = k_1 \int_{S_c} \frac{p}{r} dS \; ; w_2 = k_2 \int_{S_c} \frac{p}{r} dS \tag{8}$$

Relation for the calculation of elastic material parameters "k_1" and "k_2":

$$k_1 = \frac{1-\nu_1^2}{E_1} ; k_2 = \frac{1-\nu_2^2}{E_2} \tag{9}$$

While, according to Fig. 4, the pressure distribution can be obtained as (10):

$$p = p_0 \frac{c}{a} = p_0 \sqrt{1 - \left(\frac{x}{a}\right)^2 - \left(\frac{y}{a}\right)^2} \tag{10}$$

And, given the corresponding force balance equation:

$$p_0 = \frac{3F}{2ab\pi} \tag{11}$$

Based on the relationships described so far, the calculation for major (a) and minor semi-axis (b) of the ellipse and the value of the approach distance [14–17]:

$$a = \alpha \sqrt[3]{\frac{3}{4}\frac{2R_1R_2}{R_1+2R_2}\left(\frac{1-\vartheta_1^2}{E_1} + \frac{1-\vartheta_2^2}{E_2}\right)^2 F} \tag{12}$$

$$b = \beta \sqrt[3]{\frac{3}{4}\frac{2R_1R_2}{R_1+2R_2}\left(\frac{1-\vartheta_1^2}{E_1} + \frac{1-\vartheta_2^2}{E_2}\right)^2 F} \tag{13}$$

$$\delta = \gamma \sqrt[3]{\frac{9}{128}\frac{R_1+2R_2}{2R_1R_2}\left(\frac{1-\vartheta_1^2}{E_1} + \frac{1-\vartheta_2^2}{E_2}\right)^2 F^2} \tag{14}$$

α, β and γ are coefficients, which can be calculated from Table 1 [16] with equation (15):

$$cos\theta\ p = \frac{R_1}{R_1+2R_2} \quad (15)$$

Table 1. Table of coefficients values [18]

θ	**0°**	**10°**	**20°**	**30°**	**35°**	**40°**	**45°**	**50°**
α	∞	6.612	3.778	2.397	2.397	2.136	1.926	1.754
β	0	0.319	0.408	0.493	0.530	0.576	0.604	0.641
γ	-	0.851	1.220	1.550	1.550	1.637	1.709	1.772
θ	**55°**	**60°**	**65°**	**70°**	**75°**	**80°**	**85°**	**90°**
α	1.611	1.486	1.378	1.284	1.202	1.128	1.061	1.00
β	0.678	0.717	0.759	0.802	0.846	0.893	0.944	1.00
γ	1.828	1.875	1.912	1.944	1.967	1.985	1.996	2.00

Table 2 summarizes the applied parameters and the calculated values for this idealised elliptical contact area.

Table 2. Applied parameters and results of analytical calculation

F **[N]**	***R₁*** **[mm]**	***R₂*** **[mm]**	**ν₁**	**ν₂**	***E₁*** **[N/mm²]**	***E₂*** **[N/mm²]**	**Θ (°)**	**δ [μm]**
20	3.5	21.5	0.07	0.33	$11.43 \cdot 10^5$	$7 \cdot 10^4$	85	
α (°)	**β (°)**	**γ (°)**	***k₁***		***k₂***	***a*** **[mm]**	***b*** **[mm]**	**2.34**
1.061	0.944	1.996	$2.77 \cdot 10^{-7}$		$4.04 \cdot 10^{-6}$	0.0924	0.0822	

The value of the roughness height factor (R_t) resulting from the application of surface burnishing is influenced by the surface roughness created by the previous operation, the burnishing feed (v_f), the penetration depth of the burnishing tool (δ), and the so-called furrow depth (h), which represents the maximum of the theoretical roughness peaks created during burnishing, as illustrated in Figure 5 [11, 18].

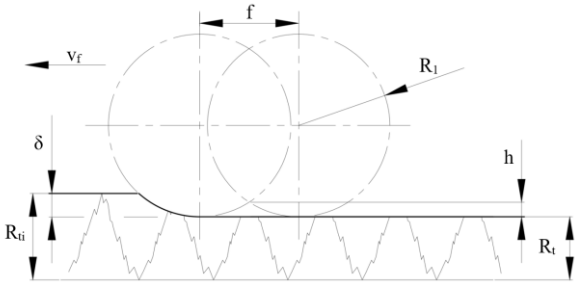

Figure 5. The relationship between the theoretical maximum furrow depth and the indentation depth when using a small burnishing feed [11]

This factor is determined by calculating the intersection point of two tool impressions that are one unit feed apart – assuming that its value is smaller than the normal indentation depth - according to formula (16).

$$h = \frac{125f^2}{R_1} \tag{16}$$

Knowing the normal indentation depth and the furrow depth, the theoretical maximum roughness can be determined, so the distance between the highest and lowest point of the profile:

$$R_t = R_{t_i} - \delta + h \tag{17}$$

3. REAL MACHINING EXPERIMENTS

For validating theoretical investigation, the real burnishing experiment were carried out on EN AW-2011 low alloyed aluminium shaft. Burnishing operations were preceded by finishing turning set at f_1 = 0.2 mm/rev and then f_2 = 0.15 mm/rev feed rate with an E400 universal lathe. Then, the burnishing was carried out with the same machine using a PCD spherical burnishing tool (r = 3.5 mm) and the kinematic viscosity of the applied manual dosing oil was v = 70 mm^2/s, while the burnishing speed was v = 50.54 m/min, the burnishing force F = 20 N and feed rate is v_f = 0.001 mm/rev.

Surface roughness measurements – before and after burnishing – were conducted on an Altisurf 520 3D surface topography measuring device. A CL2 confocal chromatic sensor was used, the cut-off was 0.8 mm and Gauss filter was applied. The measurement results were evaluated with Altimap Premium.

4. RESULTS AND DISCUSSION

This publication dealt with the analytical determination of the surface roughness generated by diamond burnishing applied to the external cylindrical surface. Considering the many uncertainty factors (stiffness of the machine system, vibrations, roughness of the tools, etc.), the author tried to apply the correct mathematical model in the case of the contact mechanics problem of spherical and cylindrical bodies, studying the Hertz- and Jhonson-Kendall-Roberts-theory, combining it with Ponomarjov's approach. The value obtained during the theoretical determination of the indentation depth of the tool– which is of prime importance –

was 2.34 μm, while in the real case it was 3.62 μm. The two values come close enough to form the basis of further theoretical and experimental investigations.

It is important to note that the procedure in question and the related analytical models were applied primarily in the case of metallic material qualities, while the present study focuses on the examination of non-metallic material.

My future plans include using the analytical model to create a finite element simulation model and then validating these results with real burnishing experiments.

References: 1 *P. Bernardos, G.C. Vosniakos*: Prediction surface roughness in machining – review**,** International Journal of Machine Tools and Manufacture 43, pp. 833–844. 2003. **2** *I. Sztankovics, J. Kundrak*: Theoretical Value and Experimental Study of Arithmetic Mean Deviation in Rotational Turning, Rezanie i instrument v tehnologiceskikh sistemakh / Cutting and tool in technological systems, 96, pp. 73-81. 2022. **3** *V. Molnar, I. Sztankovics*: Analysis of Roughness Parameters Determining Tribological Properties in Hard Turned Surfaces, HUNGARIAN JOURNAL OF INDUSTRY AND CHEMISTRY 49, pp. 77–84. 2021. **4** *J. Kundrak, A.P. Markopoulos, T. Makkai, N.E. Karkalos, A. Nagy*: Multi-Objective Optimization Study in Face Milling of Steel, Proceedings of the International Symposium for Production Research pp. 3–15. 2018. **5** *C. Felho, G. Varga*: Theoretical roughness modelling of hard turned surfaces considering tool wear, Machines 10, .pp. 1–18. 2022. **6** *I. Sztankovics, I. Pasztor*: Preliminary Analysis of Surface Topography in Tangential Turning, Rezanie i instrument v tehnologiceskikh sistemakh/Cutting and tool in technological systems, 97, pp. 155–163. 2022. **7** *M. Korzynski*: Modelling and experimental validation of the force-surface roughness relation for smoothing burnishing with a spherical tool, International Journal of Machine Tools & Manufacture 47, pp.1956–1964. 2007. **8** *P. Cui, Z. Liu, X. Yao, Y. Cai*: Effect of Ball Burnishing Pressure on Surface Roughness by Low Plasticity Burnishing Inconel 718 Pre-Turned Surface, Materials 15, pp. 1–14. 2022. **9** *R.O. Vaishya, V. Sharma, V. Mishra, A. Gupta, M. Dhanda, R.S. Walia, M. Kumar, A.D. Oza, D.D. Burduhos-Nergis, D.P. Burduhos-Negris:* Mathematical Modelling and Experimental Validation of Surface Roughness in Ball Burnishing Process, Coatings 12, pp. 1–15. 2022. **10** *C. Felho, G. Varga*: CAD and FEM Modelling of Theoretical Roughness in Diamond Burnishing, International Journal of Precision Engineering and Manufacturing 23, pp. 375–384. 2022. **11** *W. Bouzid, O. Tsoumarev, K. Sai*: An Investigation of Surface Roughness of Burnished AISI 1042 steel, International Journal of Manufacturing Technology 24, pp. 120–125. 2004. **12** *M. Korzynski*: A Model of Smoothing Slide Ball-Burnishing and an Analysis of the Parameter Interaction, Journal of Materials Processing Technology 209, pp. 625–633. 2009. **13** *C. Felho*: Analytical Modelling of Theoretical Roughness for Some Typical Machining Process in the Mechanical Engineering Industry, Multidisciplinary Sciences 12, pp. 164–185 (in Hungarian). 2022. **14** *S.D. Ponomarjov, V.L. Bidermann, K.K. Liharjev, V.M. Markusin, N.N. Malinyin, V.I. Feodoszjev*: Strength Calculations in Mechanical Engineering 3, Technical Publisher Budapest, pp. 369–417 (in Hungarian). 1965. **15** *C.E. Wu, K.H. Lin, J.Y. Juang:* Hertzian Load-Displacement Relation Holds for Spherical Indentation on Soft Elastic Solids Undergoing Large Deformations, Tribology International 97, pp. 71–76 2006. **16** *Z. Guo, M. Hao, L. Jiang, D. Li, Y. Chen, L. Dong*: A Modified Hertz Model for Finite Spherical Indentation Inspired by Numerical Simulations, European Journal of Mechanics/A Solids 83, pp. 1–13. 2020. **17** *K. Han, D. Zhang, C. Yao, L. Tan, Z. Zhou, Y. Zhao:* Analytical Modelling of Through Depth Strain Induced by Deep Rolling, Journal of Strain Analysis 00, pp. 1–12. 2021. **18** *M.R. Stalin John, A. Welsoon Wilson, A. Prasad Bhardwaj, A. Abraham, B.K. Vinayagam*: An investigation of ball burnishing process on CNC lathe using finite element analysis, Simulation Modelling Practice and Theory 62, pp. 88–101. 2016.

Вікторія Ференчик, Мішкольц, Угорщина

АНАЛІТИЧНИЙ АНАЛІЗ ТЕОРЕТИЧНОЇ ШОРСТКОСТІ ПОВЕРХНІ В РАЗІ ВИГЛАДЖУВАННЯ ЦИЛІНДРИЧНОЇ ЗАГОТОВКИ

Анотація. *В останнє десятиліття забезпечення максимально можливої якості поверхні виготовлених деталей стало основним пріоритетом, тому все більше уваги приділяється вивченню та розробці фінішної обробки, яка може ефективно забезпечити найнижчу шорсткість поверхні. Для цієї мети можна продуктивно використовувати алмазне вигладжування, яке є широко використовуваною технологією холодної пластичної деформації, оскільки воно може покращити шорсткість поверхні матеріалу. Але, незважаючи на те, що у зв'язку з розвитком інженерних технологій постійно розробляються нові можливості і методи вивчення індивідуальних змін структури матеріалу, можливість планування шорсткості поверхні дуже ускладнена. Ця робота була присвячена визначенню теоретичної шорсткості для створення математичної моделі, яка може передбачати та аналізувати взаємозв'язок між параметрами експериментального процесу та параметрами шорсткості поверхні. Для валідації моделі були проведені реальні експерименти, під час яких вимірювалася шорсткість поверхні до і після застосування процесу вигладжування на низьколегованих алюмінієвих валах. Враховуючи безліч факторів невизначеності (жорсткість системи верстата, вібрації, шорсткість інструментів тощо), авторка спробувала застосувати правильну математичну модель у випадку задачі контактної механіки сферичних і циліндричних тіл, вивчаючи теорію Герца і Джонсона-Кендалла-Робертса, поєднуючи її з підходом Пономарьова. Значення, отримане при теоретичному визначенні глибини вдавлення інструменту, що має першорядне значення, становило 2,34 мкм, тоді як у реальному випадку – 3,62 мкм. Ці дві величини досить близькі, щоб лягти в основу подальших теоретичних і експериментальних досліджень. Важливо відзначити, що дана процедура і пов'язані з нею аналітичні моделі були застосовані в основному у випадку якості металевих матеріалів, в той час як дане дослідження зосереджено на дослідженні неметалічних матеріалів. Подальші плани авторки включають використання аналітичної моделі для створення моделі імітації скінченних елементів, а потім перевірку цих результатів за допомогою реальних експериментів з полірування.*

Ключові слова: *математична модель; модифікована теорія Герца; теорія контакту; задачі контактної механіки.*

UDC 621.9. **doi: 10.20998/2078-7405.2023.99.11**

PROBABILISTIC APPROACH TO CALCULATING THE RATIONAL THICKNESS OF THE TOOL`S CUTTING INSERT FOR HEAVY MACHINE TOOLS

Galyna **Klymenko** [0000-0002-1022-6324], Viktor **Kovalov** [0000-0001-5091-5856], Yana **Vasylchenko** [0000-0002-4566-8827], Dmytro **Korchma** [0009-0000-1875-6285], Roman **Boroday** [0009-0009-6730-9540]

Donbass State Engineering Academy (DSEA), bul. Mashinostroiteley, 39, Kramatorsk, Ukraine
wasilchenko.ua@gmail.com

Received: 10 November 2023 / Revised:19 November 2023 / Accepted: 23 November 2023 / Published: 01 December 2023

Abstract. *The paper proves that the development of regulations for the operation of cutting tools on heavy machine tools, the formation of objective functions for optimising the parameters of machining parts should be carried out based on a given level of reliability of the cutting tool. In this case, a large number of indicators are used to determine the tool's reliability, durability and maintainability separately. Based on statistical and theoretical studies of the probabilistic nature of the properties of the cutting tool and the parameter of load distribution on it, quantitative dependencies between the parameters of the scattering of properties and the thickness of the tool plate of a prefabricated tool were obtained. The stochastic nature of the machining process on heavy machine tools causes a large dispersion of the properties of the machined and tool materials and other machining parameters. This leads to the need for a probabilistic approach to determining the design and technological parameters of the cutting tool. The reliability of a prefabricated cutter depends on both its load and the bearing capacity of the tool structure, which is the ultimate stress that characterises the strength of the structure. Using a probabilistic approach to calculating the thickness of the cutting plate of the cutters, a correction factor for the thickness was determined taking into account the level of reliability of the tool. The level of reliability was understood as the probability that the maximum stress arising under the action of the load will not exceed the bearing capacity. Typical structures that are most commonly used at modern heavy engineering enterprises were investigated. The law of distribution of cutting forces was determined on the basis of statistical data on the operation of carbide cutters. The thickness of the cutting element was calculated for the Rayleigh load distribution law, determined on the basis of statistical data on cutting forces during turning for different cutter designs. The distribution of the bearing capacity of the tool material of the tool inserts was determined on the basis of laboratory tests.*

Keywords: *cutting tool; reliability; failure probability; load-bearing capacity; cutting insert; cutting force.*

1. INTRODUCTION

Increasing the level of automation of existing metal-cutting equipment requires special attention to the stability of workpiece processing and the reduction of machine downtime, including that caused by cutting tool failures. This is especially important for heavy-duty CNC machines, the cost of which is very high

[1–2]. Therefore, the problem of increasing the reliability of cutting tools for heavy machine tools has become particularly relevant [3]. The process of cutting tool

operation is a complex technological system, and a number of indicators are used to assess its reliability [4–6]. The cutting tool is an integral part (the most vulnerable element) of the technological system of machining. The level of reliability of the technological system of turning cutters for heavy machine tools and its maintenance process is determined to a greater or lesser extent by all indicators of the reliability of the tool operation process.

Assessing the reliability of prefabricated turning cutters for heavy machine tools is essential not only at the stage of their operation but also at the stage of their design [7]. The development of regulations for the operation of cutting tools on heavy machine tools, the formation of objective functions for optimising the parameters of machining parts should be carried out based on a given level of reliability of the cutting tool. In this case, a large number of indicators are used to determine the reliability, durability and maintainability of the tool separately. The distribution of the tool life characterises the reliability of the cutting blade and does not allow solving the problem of ensuring reliable operation of the tool, including other structural elements of the prefabricated cutter. The availability factor can serve as a comprehensive indicator of the reliability of a prefabricated tool as a system [4].

The reliability of a prefabricated cutter depends on both its load and the bearing capacity of the tool structure, which is the ultimate stress that characterises the strength of the structure. If the reliability of a prefabricated tool is less than its rational level, it is necessary to change its structural elements, for example, the thickness of the cutting insert, which mainly determines the strength of the tool [8-10]. A design calculation method is often used, according to which the required reliability is incorporated into the designed structure in advance.

2. APPLIED METHODS

Testing of cutting tools in both laboratory and production environments demonstrates the stochastic nature of the cutting forces that occur during workpiece processing, as well as the random variation of the cutting tool properties themselves. To take into account the probabilistic nature of tool operation, information on the distribution laws of both tool loads and tool bearing capacity is required.

For elastic systems, within which a prefabricated cutter is considered, the dependence of the maximum stresses S on the load q in general form is

$$S = K_C q,$$

where K_C –is a coefficient that depends on the dimensions of the tool's cross-sections.

The level of reliability is defined as the probability that the maximum stress arising from the load will not exceed the bearing capacity:

$$H=P(R>S),$$

where H – reliability level, P - event probability, R - load-bearing capacity, S - effective maximum voltage.

If the law of distribution of cutting forces is known, then using the rules for finding the law of distribution of functions of a random argument, it is possible to find the law of distribution of maximum stresses acting in the cutter structure

$f_1(S)$. $f_1(S)=\frac{1}{K}f_3\left(\frac{S}{K}\right)$

The law of distribution of cutting forces is determined on the basis of statistical data on the operation of carbide cutters (Fig. 1), which does not negate Rayleigh's law.

The reliability or probability of failure-free operation can be determined:

$$H=\int_{-\infty}^{\infty} f_2(R)\left[\int_{-\infty}^{\infty} f_1(S)dS\right]dR \quad (1)$$

or

$$H=\int_{-\infty}^{\infty} f_1(S)\left[\int_{S}^{\infty} f_2(R)dR\right]dS \quad (2)$$

Substituting the known f1(S) and f2(R) in (1) or (2), integrating with the given level of reliability H_{giv}, we obtain the expression for determining the K_C:

$$K_C=\varphi(a_1, a_2,..., a_n, H_{giv}),$$

where $a_1, a_2,..., a_n$ –parameters of the load distribution laws and load-bearing capacity are known in advance. Knowing the K_C, it is possible to find the cross-sectional dimensions of a toolholder or cutting insert.

When turning parts, a large number of random factors are observed to act on them, subject to different distribution laws. It was found that the load is distributed according to Rayleigh's law

$$f_3(q)=\frac{q}{a^2}e^{\left[-\frac{q^2}{2a^2}\right]}, \quad (3)$$

where a, q are the parameters of the Rayleigh distribution law, and the carrying capacity according to the normal law

$$f(R)=\frac{1}{\sqrt{2\pi}\,\sigma_R}e^{\left[-\frac{(R-m_R)^2}{2\sigma_R^2}\right]}, \qquad (4)$$

where m_R, σ_R – parameters of the law of normal distribution,

In accordance with (3) and (4), the level of reliability of the structure is determined:

$$H=\int_{-\infty}^{\infty} f_3(q)\left[\int_{-\infty}^{R} f_1(S)dS\right]dR=\int_{-\infty}^{\infty} f_2(R)F_1(R)dR. \qquad (5)$$

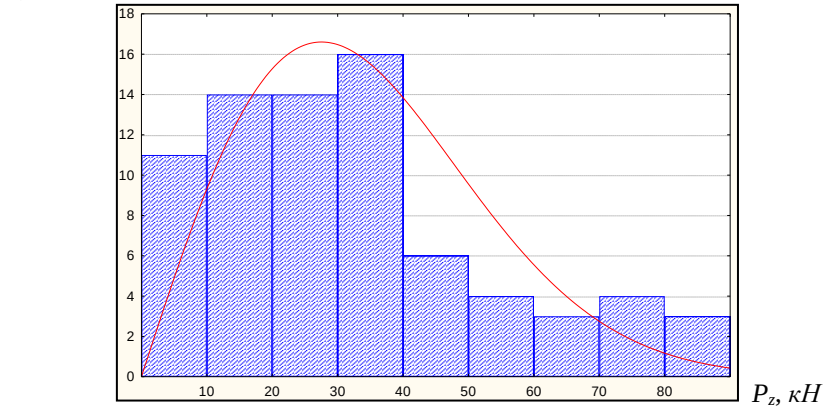

a

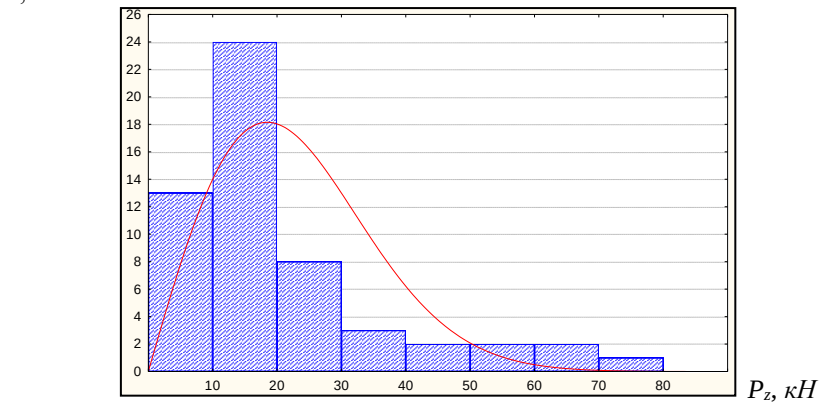

b

Figure 1 Distribution of the cutting force component P_z during turning on heavy-duty lathes: a - with D_{max} = 2500 mm, b - with D_{max} = 1250 mm.

$$f(R)=\frac{1}{\sqrt{2\pi}\,\sigma_R}e^{\left[-\frac{(R-m_R)^2}{2\sigma_R^2}\right]}, \qquad (6)$$

where m_R, σ_R – parameters of the normal distribution law,

In accordance with (1) and (2), the level of reliability of the structure is determined:

$$H=\int_{-\infty}^{\infty} f_3(q)\left[\int_{-\infty}^{R} f_1(S)dS\right]dR=\int_{-\infty}^{\infty} f_2(R)F_1(R)dR. \qquad (7)$$

Substituting (5) and (6) into (7), we obtain :

$$H=1-\frac{1}{\sqrt{1+\frac{\pi\sigma_R^2}{2K^2m_q^2}}}e^{\left(-\frac{1}{\frac{4K^2m_q^2}{\pi m_R^2}+\frac{\sigma_R}{m_R}}\right)}. \qquad (8)$$

After transformations, this expression becomes the following:

$$(1-H)^2\left(1+\frac{\pi m_R^2\left(\frac{\sigma_R}{m_R}\right)^2}{2K^2m_q^2}\right)=e^{\left(-\frac{1}{\frac{4K^2m_q^2}{\pi m_R^2}+\frac{\sigma_R}{m_R}}\right)}. \qquad (9)$$

With a small variability of σ_R/m_R, we obtain the approximate dependence for determining K_h

$$K_h=\frac{m_R}{2m_q}\sqrt{-\frac{\pi}{\ln(1-H)}}. \qquad (10)$$

To determine the thickness of the plate for the average values of the parameters (reliability level 0.5), three-dimensional models of turning cutters were developed in SolidWorks. We studied the typical schemes of plate fastening, which are most often used at modern machine-building enterprises (Fig. 2).

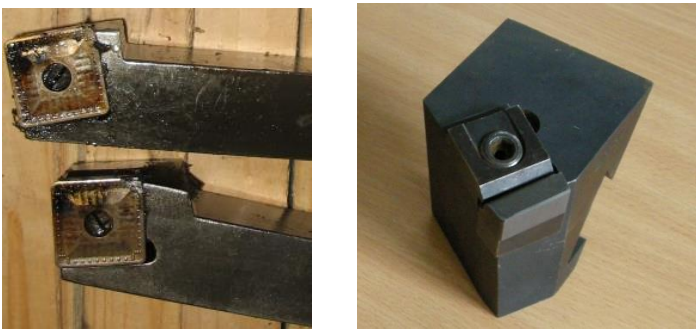

Figure 2 Designs of turning cutters for turning parts on heavy machine tools

The insert thicknesses for the carbide cutters for a reliability level of 0.5 were calculated using the finite element method with the ANSYS software package. The cutting forces were taken from a range of the most frequent ones encountered when machining parts on heavy-duty lathes.

3. RESULTSAND DISCUSSION

Examples of the stresses that arise for calculating the geometric parameters of the cutting element of a turning cutter at the design stage for given loading conditions are shown in Figs. 3, 4.

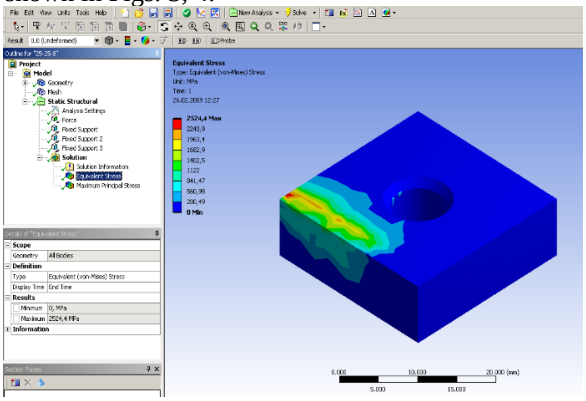

Figure 3 Distribution of equivalent stresses occurring in a square-shaped cutting insert

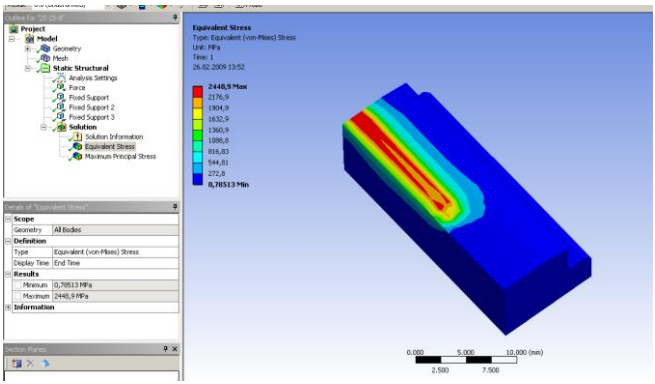

Figure 3 Distribution of the equivalent stresses that occur in the insert

For the Rayleigh load distribution law, we calculated the thickness of the cutting insert (Fig. 4) under different types of stresses arising during preliminary turning of parts on heavy machine tools.

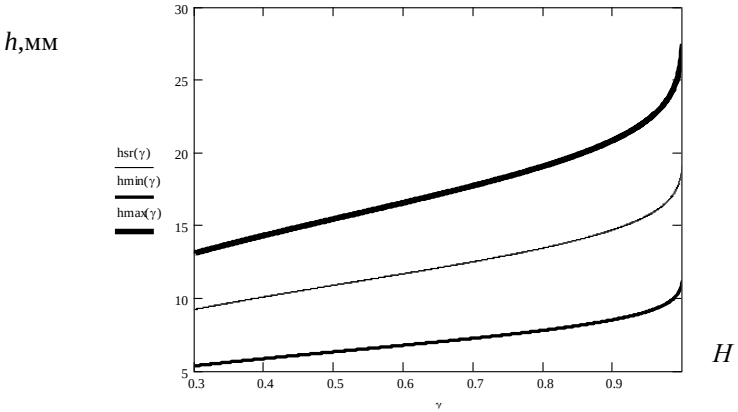

Figure 4. Dependence of the cutting element thickness on the reliability level *H*

The probabilistic approach to calculating the thickness of a prefabricated cutter insert made it possible to determine correction factors for the thickness of the insert depending on the level of reliability, which take into account the distribution parameters of both the properties of the cutting tool and its load.

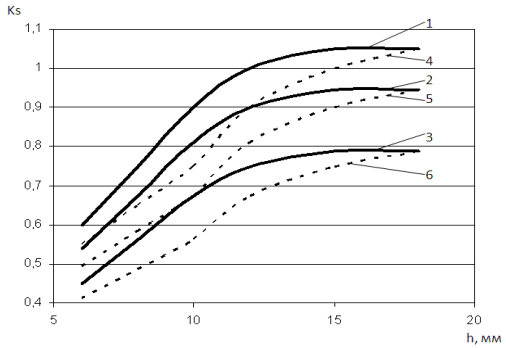

Figure 5 Fragment of a map for selecting a feed correction factor depending on the thickness of the insert*1* - height of the toolholder *H* = 40 mm, reliability level 0.65; *2* - height of the toolholder *H* = 40 mm, reliability level 0.8; *3* - height of the toolholder *H* = 40 mm, reliability level 0.9; *4* - height of the toolholder *H* = 63 mm, reliability level 0.65; *5* - height of the toolholder *H* = 63 mm, reliability level 0.8; *6* - height of the toolholder *H* = 63 mm, reliability level 0.9

Software and comprehensive standardisation maps for heavy machine tools were developed and implemented to select tool operation regulations based on the level of reliability of the operation process, which for the first time take into account the design of the machine and tool, the level of tool reliability and tool consumption.

4. CONCLUSIONS

For the first time, on the basis of statistical and theoretical studies of the probabilistic nature of the properties of a cutting tool and the parameter of load distribution on it, quantitative dependencies between the parameters of scattering properties and the thickness of the cutting plate of a prefabricated cutter were obtained. It is proved that ensuring the reliability of a cutting insert of the level 0.8 requires an increase in its thickness by 30% compared to the calculated values for the average load.

References: 1. *Yang Tian , Zhifeng Liu , Xinpeng Xu, Guang Wang, Qiwei Li, Yang Zhou and Jiangli Cheng* Systematic review of research relating to heavy-duty machine tool foundation systems. Advances in Mechanical Engineering 2019, Vol. 11(1) pp. 1–16 , https://journals.sagepub.com/doi/10.1177/1687814018806106. **2.** *Qin Guo* Reviews on the machining and measurement of large components Advances in Mechanical Engineering 2023, Vol. 15(9) https://doi.org/10.1177/16878132231191381 **3**. *Mohamad Gaddafee, Satish Chinchanikar,* An Experimental Investigation of Cutting Tool Reliability and its Prediction Using Weibull and Gamma Models*:* A Comparative Assessment, Materials Today: Proceedings, Volume 24, Part 2, 2020, pp. 1478–1487, ISSN 2214-7853, https://doi.org/10.1016/j.matpr.2020.04.467 **4.** *Klymenko G. Kvashnin V.* Reliability assurance technological systems exploitation of heavy lathe Cutting & tool in technological system 2019; 91: pp. 78-86 https://doi.org/10.20998/2078-7405.2019.91.08 **5.** *Letot, C., Serra, R., Dossevi, M. et al*. Cutting tools reliability and residual life prediction from degradation indicators in

turning process. Int J Adv Manuf Technol 86, pp. 495–506 (2016). https://doi.org/10.1007/s00170-015-8158-z **6.** *Liu, Erliang & An, Wenzhao & Xu, Zhichao & Zhang, Huiping.* (2020). Experimental study of cutting-parameter and tool life reliability optimization in inconel 625 machining based on wear map approach. Journal of Manufacturing Processes. 53. pp. 34-42. https://doi.org/10.1016/j.jmapro.2020.02.006 **7.** *Wardany, Tahany & Elbestawi, Mohamed.* (1997). Prediction of tool failure rate in turning hardened steels. The International Journal of Advanced Manufacturing Technology. 13. pp. 1–16. https://doi.org/10.1007/BF01179225 **8.** *Karimi, B., Niaki, S.T.A., Haleh, H. et al.* Reliability optimization of tools with increasing failure rates in a flexible manufacturing system. Arab J Sci Eng 44, 2579-2596 (2019). https://doi.org/10.1007/s13369-018-3309-9 **9.** *Bakša, Tomáš & Kroupa, Tomáš & Hanzl, Pavel & Zetek, Miroslav.* (2015). Durability of Cutting Tools during Machining of Very Hard and Solid Materials. Procedia Engineering. https://doi.org/10.1016/j.proeng.2015.01.511 21. **10.** *Jaydeep M. Karandikar, Ali E. Abbas, Tony L. Schmitz,* Tool life prediction using Bayesian updating. Part 2: Turning tool life using a Markov Chain Monte Carlo approach, Precision Engineering, Volume 38, Issue 1, 2014, pp. 18-27, ISSN 0141-6359, https://doi.org/10.1016/j.precisioneng.2013.06.007 .

Галина Клименко, Віктор Ковальов, Яна Васильченко, Дмитро Корчма, Роман Бородай, Краматорськ, Україна

ІМОВІРНІСНИЙ ПІДХІД ДО РОЗРАХУНКУ РАЦІОНАЛЬНОЇ ТОВЩИНИ РІЖУЧОЇ ПЛАСТИНИ ІНСТРУМЕНТУ ДЛЯ ВАЖКИХ ВЕРСТАТІВ

Анотація. *У статті доведено, що розробка регламентів експлуатації різальних інструментів на важких верстатах, формування цільових функцій оптимізації параметрів обробки деталей повинні здійснюватися виходячи із заданого рівня надійності різального інструменту. При цьому використовується велика кількість показників, що визначають окремо безвідмовність, довговічність та ремонтопридатність інструменту. На основі статистичних і теоретичних досліджень імовірнісного характеру властивостей різального інструменту і параметра розподілу навантаження на нього отримані кількісні залежності між параметрами розсіювання властивостей і товщиною інструментальної пластини збірного інструменту. Стохастичний характер процесу обробки на важких верстатах зумовлює великий розкид властивостей оброблюваних і інструментальних матеріалів та інших параметрів обробки. Це призводить до необхідності імовірнісного підходу до визначення конструктивно-технологічних параметрів різального інструменту. Надійність роботи збірного різця залежить як від його навантаження, так і від несучої здатності конструкції інструменту, яка є граничним напруженням, що характеризує міцність конструкції. Використовуючи імовірнісний підхід до розрахунку товщини ріжучої пластини різця, було визначено поправочний коефіцієнт на товщину з урахуванням рівня надійності інструменту. Під рівнем надійності розуміли ймовірність того, що максимальне напруження, яке виникає під дією навантаження, не перевищить тримальної здатності. Досліджувалися типові конструкції, які найчастіше використовуються на сучасних підприємствах важкого машинобудування. Закон розподілу сил різання визначався на основі статистичних даних про роботу твердосплавних різців. Товщина ріжучого елемента розраховувалася для релеївського закону розподілу навантаження, визначеного на основі статистичних даних про сили різання при токарній обробці для різних конструкцій різців. Розподіл тримальної здатності інструментального матеріалу пластин визначено на основі лабораторних випробувань.*

Ключові слова: *різальний інструмент; надійність; ймовірність відмови; тримальна здатність; різальна пластина; сила різання.*

UDC 621.923 **doi: 10.20998/2078-7405.2023.99.12**

SURFACE TEMPERATURES AND VACATION BURNS OCCURRING DURING GRINDING OF CEMENTED GEARS WITH TWO DISHED WHEELS ON DIFFERENT PARTS OF THE MACHINED INVOLUTE PROFILE

Volodymyr **Tonkonogyi** [1][0000-0003-1459-9870], Oleksiy **Yakymov** [1][0000-0003-2096-4555], Liubov **Bovnegra** [1][0000-0003-0429-2816], Fedir **Novikov** [2][0000-0001-6996-3356]

[1]Odesa Polytechnic National University, 1, Schevchenko av., Odesa, 65044, Ukraine
[2]Simon Kuznets Kharkiv National University of Economics, 9-A Nauky Av., Kharkiv 61166, Ukraine
novikovfv@i.ua

Received: 09 November 2023 / Revised:16 November 2023 / Accepted: 25 November 2023 / Published: 01 December 2023

Abstract. *To increase grinding productivity with the provision of specified physical and mechanical properties of the surface layer of the surface layer of the processed part it is necessary to know the temperature on the surface of the workpiece, since its value depends on the depth of the defective surface layer. In the work theoretically justified the difference of surface temperatures in the initial (at the base), in the middle (on the dividing circle) and final (at the top) points of involute profile of the gear tooth when grinding with two disc wheels on the zero scheme. The difference in temperature at different points of the processed tooth profile is justified by the fact that at different parts of the trajectory of the movement of the heat source acts a different number of thermal pulses. These pulses have different duration and time intervals between the actions of these pulses in different points of the involute profile are also different. The number of thermal actions on a fixed point of the machined profile depends on the length of the heat source, and the duration of heating of the surface at this point is determined by the width of the heat source. The duration of cooling depends on the location of the point on the involute profile. Mathematical models have been developed to calculate the temperatures at different parts of the trajectory of the rolling path of a disc grinding wheel on the tooth being machined. Each of these formulas contains two sums. The first sum determines the temperature increase at a fixed point of the tooth profile under repeated exposure to thermal pulses during the forward stroke, and the second sum - during the reverse stroke. Mathematical models are based on the principle of superposition of thermal fields. It is found that the temperature in the middle part of the tooth is 40% less than at the tooth apex and 20% less than at the tooth base. The engineering method of distribution of the total allowance by passes at multi-pass gear grinding with two dished wheels according to the zero scheme has been developed. The method is based on the experimental dependence of the depth of the defect layer on the depth of cutting, which has a linear character. In the work, calculations were made on the allowance distribution in the initial, middle and final points of the involute tooth profile. The calculations showed that in order to prevent burns on the final machined surface, grinding in different parts of the machined profile should be performed with a different number of passes. The smallest number of passes on the separating circle, and the largest - on the top of the tooth. The proposed methodology of distribution of allowances by passes can be used at the stage of design of gear grinding operation (for optimization of modes) and at the stage of machining (for diagnostics of the*

operation). It is theoretically substantiated that calculations of allowance distribution by passes should be made only for the tooth head. To increase grinding productivity with provision of the specified physical and mechanical properties of the surface layer of the processed part it is necessary to know the temperature on the surface of the workpiece, as its value depends on the depth of the defective surface layer. In the work theoretically justified the difference in surface temperatures in the initial (at the base), in the middle (on the dividing circle) and final (at the top) points of involute profile of the gear tooth when grinding with two disk wheels on the zero scheme. The difference in temperature at different points of the processed tooth profile is justified by the fact that at different parts of the trajectory of the heat source acts a different number of thermal pulses. These pulses have different duration and time intervals between the actions of these pulses in different points of the involute profile are also different. The number of thermal actions on a fixed point of the machined profile depends on the length of the heat source, and the duration of heating of the surface at this point is determined by the width of the heat source. The duration of cooling depends on the location of the point on the involute profile. Mathematical models have been developed to calculate the temperatures at various parts of the rolling path of a dished grinding wheel on a machined tooth. Each of these formulas contains two sums.
Keywords: *dished wheels; zero scheme; tempering burns; multi-pass grinding.*

1. INTRODUCTION

The rapid development of mechatronics is not accompanied by a marked reduction in the need for gears. The continuous development of technology leads to increasingly stringent requirements for gears. The requirements for minimizing the weight and size of gears are coupled with the need to be able to operate at high speeds, transfer high loads and at the same time provide increased operational reliability and durability. To meet these requirements, gears must be manufactured to 3 - 4 degrees of accuracy, and the working surfaces of their teeth must have high hardness (HRC 60-62). Surface hardness of teeth is provided by chemical-thermal treatment, after which the gear ring warps. To eliminate errors caused by deformation of the teeth and warping of the crown and to ensure the required accuracy of manufacturing of gears is possible only by grinding. The grinding process is accompanied by thermal impact on the machined surface [1, 2], causing the appearance of burns (structural changes) and residual tensile stresses [3, 4], which reduce the durability of the gear wheel in terms of contact endurance by 3 - 5 times, and in terms of bending endurance by 1.4 - 1.6 times. In spite of this, gear grinding is still an indispensable method of finishing.

Gear grinding with two disc wheels allows to obtain gear wheels of 3-4 degrees of accuracy with surface roughness R_a = 1.0 - 0.3 mkm [5, 6]. At the zero method of grinding with two disc wheels the wheels are set parallel to each other at a distance equal to the length of the common normal) [7, 8]. The advantage of the "zero method" of gear grinding over the "15-degree method" is the absence of a "mesh" on the grinding surfaces of the teeth. The main disadvantage of the process of grinding with disc-shaped wheels according to the zero-degree scheme is high thermal stress. To predict the possibility of thermal defects, it is necessary to study the mechanism of heat generation during gear grinding. Modeling of thermal

processes occurring during grinding of involute tooth profiles is devoted to works [9 – 11]. The authors of [12, 13] studied the mechanism of heat generation during gear grinding. Gear grinding is characterized by periodically alternating stages of heating and cooling of each point of the machined surface. In [14], formulas for calculating the surface temperature at each of these stages were obtained. The structure of these formulas includes the requirement that at the moment of the end of the heating stage, the instantaneous temperature distribution is the initial condition for modeling the temperature field at the cooling stage. The formulas for temperature calculation proposed in [14] are valid only for profile gear grinding. The zero-point gear grinding scheme with two disc wheels is widely used in aircraft engine building and shipbuilding, despite the fact that the production of machines operating under this scheme has been discontinued due to their low productivity. It can be stated that abrasive high-precision hobbing is currently experiencing a crisis associated with the search for new effective methods, technologies and tools that increase its productivity [15 – 17].

Goal of the work – development of engineering methodology of allowance distribution at multi-pass grinding of cemented spur gears with two dished wheels according to the zero scheme, providing the given physical and mechanical characteristics of quality of surface layers of the final-machined teeth.

2. RESEARCH METHODOLOGY

Theoretical studies were carried out on the basis of scientific fundamentals of mechanical engineering technology, metal science, thermal physics of cutting. To investigate the quality of the surface layer of the working surfaces of gear wheels, their microhardness was measured, and the detection of burns was carried out by color defectoscopy. Cylindrical spur gears (m=2 mm; z=20) made of 12X2H4A steel (E3310X (USA), X12Ni5 (Germany), SNC815 (Japan), 13NiCr14 (France), 655N13 (England), 12Ch2N4A (Bulgaria), 12H2N4A (Poland), 16420 (Czech Republic)) were investigated. The heat treatment of the gears consisted of cementation in a solid carburetorizer at 900 ºC to a depth of 1.1÷ 1.3 mm, high tempering at 650 ºC, double hardening at 850 ± 20 ºC and at 800 ± 20 ºC, cold treatment in liquid nitrogen and tempering at 150 ± 10 ºC. The gears were machined on a Maag SS ½ X gear grinding machine with disk grinding wheels 24A F60 K 10 V5 using a zero scheme (Fig. 1).

The distribution of microhardness along the depth of the surface layer was determined on the PMT-3 device by the "oblique slices" method. The teeth-samples were obtained as follows. On a lathe with abundant cooling with emulsion, the toothed crown was separated from the hub. After cutting, the crown was broken into individual teeth. After burn etching, oblique flat cuts were made on the tooth

specimens at an angle of 2º30′ ± 10′ at the tooth base, near the dividing circle and at the tooth apex (Fig. 2 a, b, c, respectively).

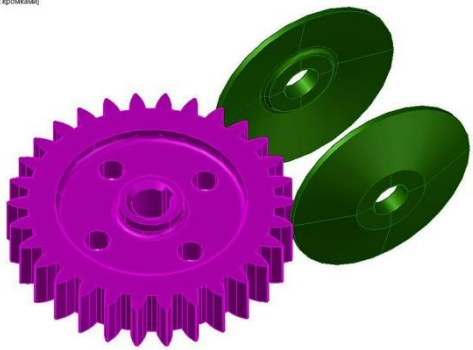

Figure 1 – Zero grinding method

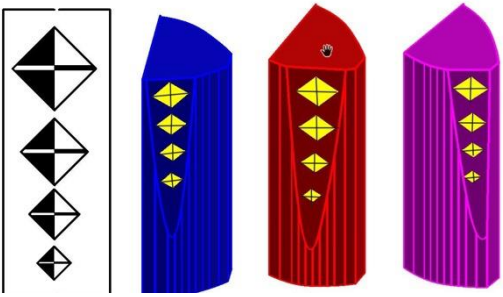

Figure 2 – Microhardness measurement locations on oblique sections made at the tooth base (a), in the area of the dividing circumference (b), on the tooth head (c) using the PMT-3 instrument

The roughness height of the flat slices corresponded to roughness class 13 R_z = 1.00 ÷ 0.05 mkm). Etching for burn-in detection was performed in four steps: 1) etching at room temperature in aqueous solution of ammonium sulfate (100 ÷ 150 g/l) for 15 ÷ 30 s followed by rinsing in cold water; 2) etching at room temperature in aqueous solution of hydrochloric acid (50 ÷ 100 g/l) for 60 s followed by rinsing in cold water; 3) neutralization at room temperature in aqueous solution of sodium carbonate (30 ÷ 50 g/l) for 1 ÷ 3 min; 4) anticorrosion treatment in aqueous solution of sodium nitrate (200 ÷ 250 g/l) for 1 ÷ 3 min.

The dark-etching zone is a tempering product, has an underestimated hardness compared to the base metal and is a ferrite-carbide mixture. Hardness was measured on a PMT-3 microhardness tester by pressing a diamond tip in the form of a regular tetrahedral pyramid with a dihedral angle at the apex of 136º at a load of 100 g into the surface of an oblique slice and measuring the linear quantity of

the diagonal of the resulting imprint. The hardness number was calculated by dividing the load by the surface area of the indentation, assuming that the angles of the indentation correspond to the angles of the pyramid. Microhardness measurements on oblique slices were made at four points equidistant from each other at equal distances of 50 mkm (Fig. 2).

3. RESEARCH RESULTS

A characteristic feature of the zero method of gear grinding is the different intensity of heat generation in different parts of the rolling path of the disc wheel along the involute profile of the tooth. The difference of temperatures formed on different fragments of the rolling trajectory is explained by the fact that different thermal processes occur in different points of the involute profile due to different amounts of thermal influences on these points, different time intervals between interactions, and different durations of influences. Fig. 3 shows three points of contact between the disk grinding wheel and the tooth being machined, one of which is located at the base of the tooth (Fig. 4), one near the dividing circle (Fig. 5), and one at the head of the tooth (Fig. 6). The dimensions of the contact patch of the disc wheel with the tooth of the wheel change continuously during the running-in process.

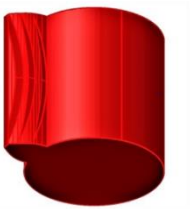

Figure 3 – Contact spots of the dished wheel with different parts of the involute tooth profile

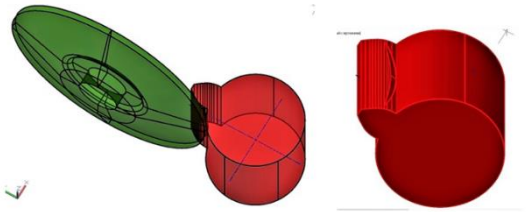

a b

Figure 4 – Contact area between the dished grinding wheel (a) and the lower part of the involute tooth profile (b)

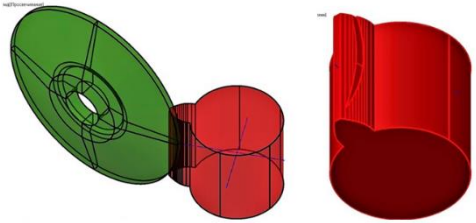

a b

Figure 5 – Contact area between the dished grinding wheel (a) and the involute tooth profile in the area of the dividing cylinder (b)

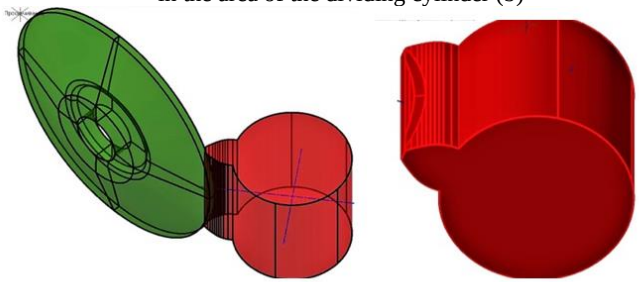

a b

Figure 6 – Contact spot between the dished grinding wheel (a) with the upper part of the involute tooth profile (b)

When running the abrasive tool over the tooth in the direction of the trough, the area of the spot decreases, and when running in the direction of the tooth apex, the area of the spot increases. This is due to the variability of the involute radius of curvature within the height of the machined tooth: it is the largest at the tooth apex and the smallest at the tooth base (Fig. 7, Fig. 8).

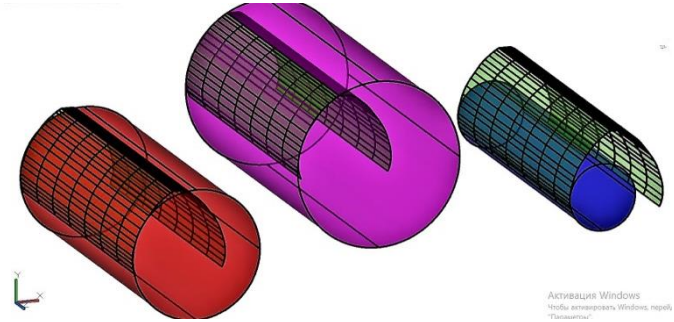

Figure 7 – Straight circular cylinders imitating fragments of involute tooth profile on the head, stem and middle part of the tooth.

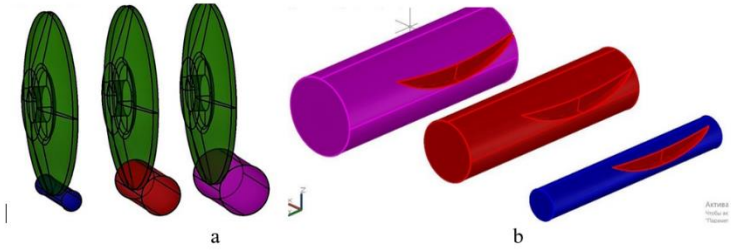

a b

Figure 8 – Contact spots of the dished grinding wheel (a) with cylinders simulating the involute tooth profile on the head (purple), stem (blue) and in the area of the dividing cylinder (red) (b)

In Fig. 9 – Fig. 11 show the actual shape of the contact spot of the dished grinding wheel with the tooth to be machined (its length is X).

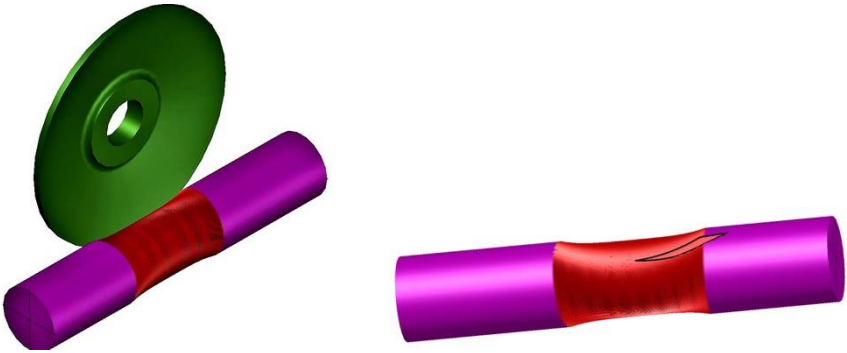

a b

Figure 9 – Actual contact patch of the dished wheel (a) with the cylinder simulating involute profile on the tooth head, taking into account the displacement of the tool from the previously machined area in the direction of the feed rate by the value of the running-in path (b).

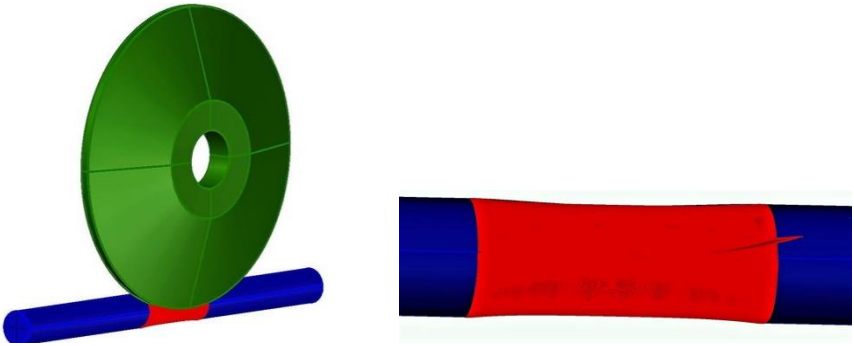

a b

Figure 10 – Actual contact patch of the dished wheel (a) with the involute cylinder at the tooth base, taking into account the pre-machined section of the gear width with subsequent tool displacement in the longitudinal feed direction (b).

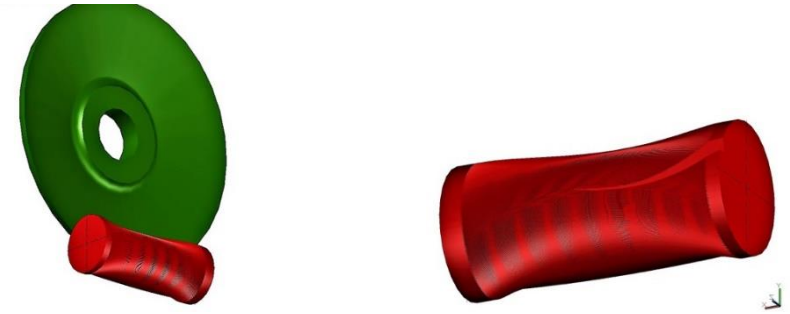

a b

Figure 11 – Actual contact patch of the dished wheel (a) with the cylinder simulating an involute profile in the area of the dividing circle, taking into account the displacement of the tool from the machined area in the working feed direction by an amount corresponding of the value to the running-in path (b).

Usually in technical literature, the contact spot is taken as a segment with maximum thickness in the center and length equal to 2X. This is due to the fact that when the wheel contacts the workpiece, the presence of a transition area (cutting zone) and a previously machined surface on the tooth is usually not taken into account. This leads to distortion of the shape and significant overestimation of the contact area. If the boundaries of the contact spot of the abrasive tool with the tooth of the gear are taken as the boundaries of the thermal source, the latter in the process of grinding the tooth on the zero scheme will repeatedly pass over each point of the machined surface and met with the areas of the heat conducting space, preheated on the previous running-in movements. The points located on different parts of the machined surface perceive different amounts of thermal influences: the point located on the tooth head experiences 7 heatings (Fig. 12, Fig. 13), the point on the dividing circle - 5 (Fig. 14, Fig. 15), and the point on the tooth base is heated 3 times (Fig. 16, Fig. 17). Within the tooth height, the probability of thermal defects has a variable character and in most cases takes the maximum values at its head [18, 19].

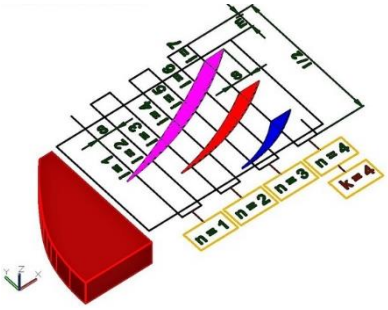

Figure 12 – Schematic of the point under the heat source during four double break-in movements of the dished wheel on the tooth being machined when the heat source is located on the tooth head.

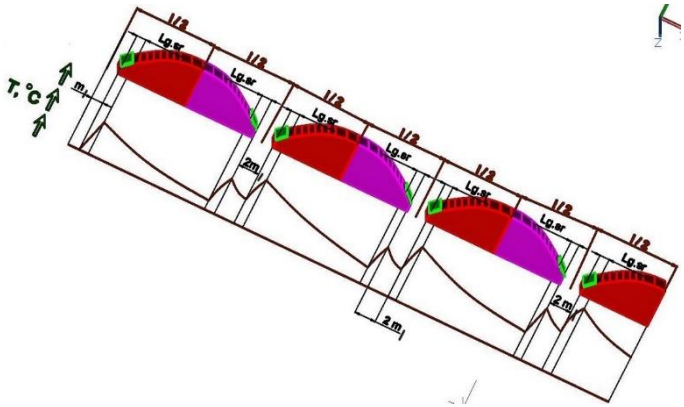

Figure 13 – Change of surface temperature at the point located on the tooth head for the total time of four double break-in movements of the dished wheel on the machined involute profile

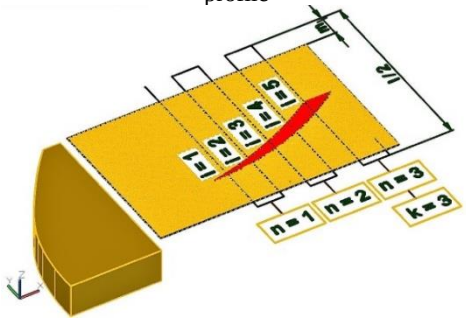

Figure 14 – Schematic of passing the point under the heat source for the time of three double break-in movements of the dished wheel on the tooth when the heat source is located on the dividing circle

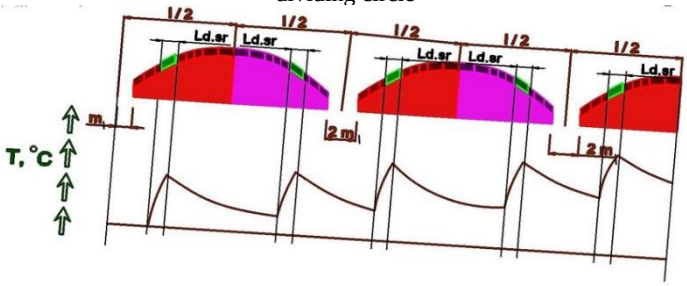

Figure 15 – Change of surface temperature at the point located in the crop circle area for the total time of three double break-in movements of the dished wheel on the machined involute profile

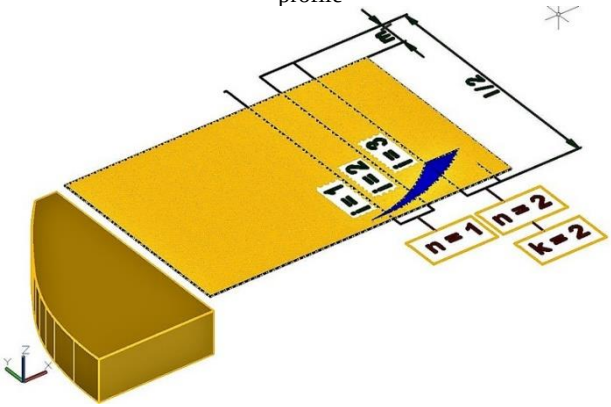

Figure 16 – Schematic of the point under the heat source for the time of two double break-in movements of the dished wheel on the tooth when the heat source is located near the tooth base.

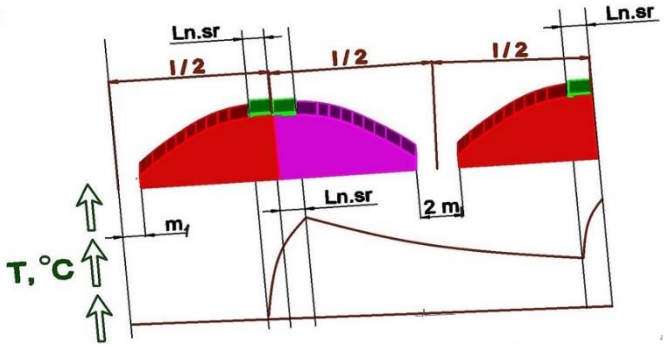

Figure 17 – Variation of surface temperature at a point located at the tooth base for the total time of two double break-in movements of a dished wheel along an involute profile.

For theoretical substantiation of localization of thermal defects on the tooth head it is necessary to be able to make calculations of temperatures on different parts of tooth side surfaces, arising during grinding with disc-shaped wheels according to the zero-pass scheme, taking into account repeated heat exposure on each point of the machined surface. As a basis for modeling the temperature fields in multi-pass grinding, we will use a one-dimensional thermophysical scheme in which a point of the heat conducting medium is subjected to repeated heating. Fig. 13 shows the scheme of a point passing under a fixed planar heat source of width L_g.sr located near the tooth apex. The following

designations are adopted in the scheme: *l*/2 - length of forward or reverse break-in movements, numerically equal to the sum of the tooth height and the value of the abrasive tool exit beyond the machined tooth m_1:

$$l/2 = m + 1{,}25m + m_1,$$

where *m* is the modulus of the gear wheel; *l* is the length of the full break-in movements, equal to the sum of the lengths of the forward and reverse strokes.

On Fig. 13 shows the heating scheme of a point as it passes 7 times under a planar heat source located near the tooth apex.

From Fig. 12 and Fig. 13, it can be seen that the number of point passes under the heat source depends on its length *X* and the magnitude of the longitudinal feed *S*.

The number of heated points increases with increasing contact patch size and with decreasing longitudinal feed. The duration of heated point increases with increasing width of the heat source L_g.sr:

$$L_g.sr = \frac{1}{2\cdot k}\cdot \sum_{i=1}^{2\cdot k} L_g \cdot i; \tag{1}$$

$$L_g.i = \sqrt{2\cdot r\cdot t_i - t_i^2} \quad \text{for } 1 \le i \le 2\cdot k; \tag{2}$$

where *r* is the radius of curvature of the edge of the dished grinding wheel; $r = 0.4\cdot m$; t_i - thicknesses of layers removed by the abrasive tool during one break-in movements in different parts of the contact patch:

$$t_1 = \left(\rho_g + r\right) - \Delta_1; \tag{3}$$

ρ_g – radius of curvature of the involute at the tooth head;

$$t_i = \left(\rho_{g.i-1} + r\right) - \Delta_1 \quad \text{for } 2 \le i \le 2\cdot k; \tag{4}$$

$$\Delta_i = \sqrt{\left(\rho_{g.i-1} - t_i + r\right)^2 + \theta_i^2} \quad \text{for } 1 \le i \le 2\cdot k; \tag{5}$$

$$\rho_{g.i} = \rho_g - \sum_{i=1}^{2\cdot k} t_i; \tag{6}$$

$$\theta_i = \frac{2\cdot\left(R_{kr} - r\right) - \sqrt{\left[2\cdot\left(R_{kr} - r\right)\right]^2 - 4\cdot\left(X_g - i\cdot S\right)^2}}{2}; \tag{7}$$

R_{kr} is the radius of the grinding wheel; X_g – length of the contact spot of the circle with the tooth on the head:

$$X_g = \sqrt{2 \cdot \rho_g \cdot t_0 - t_0^2}; \quad (8)$$

t_0 - cutting depth;

$$2 \cdot k = \frac{X_g - S}{S}. \quad (9)$$

On Fig. 13 shows the pattern of temperature rise in a single point of the machined surface as it moves under a flat stationary heat source located on the head of the tooth being machined.

The formula for calculating temperatures, which takes into account the multiplicity of thermal effects on a separately taken point of the lateral surface of the tooth when the heat source is located near the apex of the tooth, is as follows:

$$T_k = \frac{2 \cdot \psi \cdot q_g}{\sqrt{c \cdot \rho_m \cdot \lambda}} \cdot \sum_{n=1}^{k} \left[\sqrt{\frac{(k-n) \cdot I - 2m_1}{V_{obk}}} \cdot ierfc\left(\frac{t_0}{2 \cdot \sqrt{a} \cdot \frac{(k-n) \cdot I + I - 2m_1}{V_{obk}}} \right) - \right.$$

$$\left. - \sqrt{\frac{(k-n) \cdot I + I - 2m_1 - L_g.sr}{V_{obk}}} \cdot ierfc\left(\frac{t_0}{2 \cdot \sqrt{a} \cdot \sqrt{\frac{(k-n) \cdot I + I - 2m_1 - L_g.sr}{V_{obk}}}} \right) \right] +$$

$$+ \frac{2 \cdot \psi \cdot q_g}{\sqrt{c \cdot \rho_m \cdot \lambda}} \cdot \sum_{n=1}^{k} \left[\sqrt{\frac{(k-n) \cdot I + L_g.sr}{V_{obk}}} \cdot ierfc\left(\frac{t_0}{2 \cdot \sqrt{a} \cdot \sqrt{\frac{(k-n) \cdot I + L_g.sr}{V_{obk}}}} \right) - \right.$$

$$\left. - \sqrt{\frac{(k-n) \cdot I}{V_{obk}}} \cdot ierfc\left(\frac{t_0}{2 \cdot \sqrt{a} \cdot \sqrt{\frac{(k-n) \cdot I}{V_{obk}}}} \right) \right], \quad (10)$$

where $a = \lambda / \left(c \cdot \rho_m \right)$ – thermal conductivity of the material to be processed, m^2/S; ψ – coefficient showing how much of the work is converted to heat; ρ_m, c, λ –density (kg/m^3), heat capacity ($I / \left(kg \cdot {}^oC \right)$ and thermal conductivity $I / \left(m \cdot S \cdot {}^oC \right)$ of the material to be processed respectively; q_g – heat flux density formed on the tooth head, W/m^2; V_{obk} – run-in speed, m/s;

$$V_{obk} = \frac{2 \cdot n'}{1000} \cdot tg \left(arccos \frac{r_\omega \cdot \cos \alpha_{t\omega}}{r_\omega + 1{,}2 \cdot m \cdot m_1} \right) \cdot R_p ; \quad (11)$$

n' – number of double rolling movements per minute; R_p – radius of the pitch circle of the machined wheel;

$$r_\omega = R_p = \frac{r_0}{\cos 20^o} = \frac{m \cdot z_1}{2} ; \quad (12)$$

z_1 – number of teeth on the machined wheel; m – wheel module; m_1 – the value of grinding wheel out of the tooth head when break-in movements; r_0 – radius of the main circumference of the wheel; $\alpha_{t\omega}$ – angle pressure.

Formula (10) contains two sums, one of which forms the temperature increase at a fixed point of the surface under the heat source during the crimping movements in the direction of the tooth-space, and the second sum provides the temperature increase during the break-in movements to the side of the apex of the tooth.

On Fig. 14 and Fig. 15 show one-dimensional thermophysical schemes, which are the basis for modeling the temperature field. In these schemes, a point of the heat conducting medium is subjected to multiple heating due to its multiple passages under a flat heat source of wide $L_d.sr$ located in the region of the dividing circumference. Fig. 15 illustrates the nature of the temperature field in the region of the dividing circumference formed during multi-pass gear grinding with a dished grinding wheel using the zero method. The formula for calculating the temperatures based on Fig. 14 and Fig. 15 is as follows:

$$T_k = \frac{2 \cdot \psi \cdot q_d}{\sqrt{c \cdot \rho_m \cdot \lambda}} \times$$

$$\times \sum_{n=1}^{k}\left[\sqrt{\frac{(k-n)\cdot l + L_d.sr}{V_{obk}} + \frac{l}{2\cdot V_{obk}}}\cdot ierfc\left(\frac{t_0}{2\cdot\sqrt{a}\cdot\sqrt{\frac{(k-n)\cdot l + L_d.sr}{V_{obk}} + \frac{l}{2\cdot V_{obk}}}}\right) - \right.$$

$$\left. - \sqrt{\frac{(k-n)\cdot l}{V_{obk}} + \frac{l}{2\cdot V_{obk}}}\cdot ierfc\left(\frac{t_0}{2\cdot\sqrt{a}\cdot\sqrt{\frac{(k-n)\cdot l}{V_{obk}} + \frac{l}{2\cdot V_{obk}}}}\right)\right] +$$

$$+ \frac{2\cdot\psi\cdot q_d}{\sqrt{c\cdot\rho_m\cdot\lambda}}\cdot\sum_{n=1}^{k}\left[\sqrt{\frac{(k-n)\cdot l + L_d.sr}{V_{obk}} + \frac{l}{2\cdot V_{obk}}}\cdot ierfc\left(\frac{t_0}{2\cdot\sqrt{a}\cdot\sqrt{\frac{(k-n)\cdot l + L_d.sr}{V_{obk}}}}\right) - \right.$$

$$\left. - \sqrt{\frac{(k-n)\cdot l}{V_{obk}}}\cdot ierfc\left(\frac{t_0}{2\cdot\sqrt{a}\cdot\sqrt{\frac{(k-n)\cdot l}{V_{obk}}}}\right)\right]. \qquad (13)$$

Schemes of formation of temperature increases in the point moving along the trajectory of break-in movements of the dished grinding wheel on the tooth of the processed wheel and periodically passing under a fixed flat heat source, located near the base of the tooth, are shown in Fig. 16 and Fig. 17. Fig. 17 illustrates the nature of temperature change at this point in the process of grinding the tooth. The formula for calculating the temperatures based on Fig. 16 and Fig. 17 is as follows:

$$T_k = \frac{2\cdot\psi\cdot q_d}{\sqrt{c\cdot\rho_m\cdot\lambda}}\times$$

$$\times \sum_{n=1}^{k}\left[\sqrt{\frac{(k-n)\cdot l + 2L_n.sr}{V_{obk}}}\cdot ierfc\left(\frac{t_0}{2\cdot\sqrt{a}\cdot\frac{(k-n)\cdot l + 2L_n.sr}{V_{obk}}}\right) - \right.$$

$$-\sqrt{\frac{(k-n)\cdot l + L_n.sr}{V_{obk}}}\cdot ierfc\left(\frac{t_0}{2\cdot\sqrt{a}\cdot\sqrt{\frac{(k-n)\cdot l + L_n.sr}{V_{obk}}}}\right)\Bigg] +$$

$$+\frac{2\cdot\psi\cdot q_d}{\sqrt{c\cdot\rho_m\cdot\lambda}}\cdot\sum_{n=1}^{k}\Bigg[\sqrt{\frac{(k-n)\cdot l + L_n.sr}{V_{obk}}}\cdot ierfc\left(\frac{t_0}{2\cdot\sqrt{a}\cdot\sqrt{\frac{(k-n)\cdot l + L_n.sr}{V_{obk}}}}\right) -$$

$$-\sqrt{\frac{(k-n)\cdot l}{V_{obk}}}\cdot ierfc\left(\frac{t_0}{2\cdot\sqrt{a}\cdot\sqrt{\frac{(k-n)\cdot l}{V_{obk}}}}\right)\Bigg]. \qquad (14)$$

The Fig. 18 – Fig. 20 show the results of calculations of the lengths of the contact spots X of the processed gear, the number of passes of the point under the heat source $2\cdot k$ and temperatures T in points 1 (in the upper part of the tooth head), 2 (in the area of the dividing circumference) and 3 (in the area of the tooth base) at grinding of gears ($z = 20$, $m = 2$ mm, $m = 8$ mm) from cemented steel 18X2H4MA with a dished wheel mm on the zero pattern at modes: $t_0 = 0.05$ mm; $n' = 112$ min^{-1}; $S = 1.5$ mm; $S = 3$ mm.

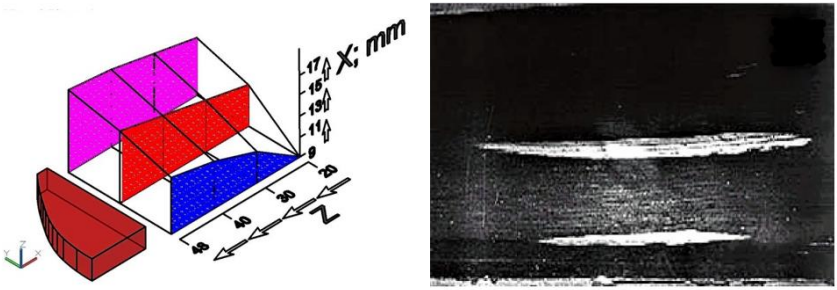

a b

Figure 18 – Increase in the length of the contact patch of a dished wheel with a gear tooth as it moves from the tooth base to its head for modulus *m*=2 mm and tooth counts 20< *z* <48: (a) calculated data; (b) experimental data [18]

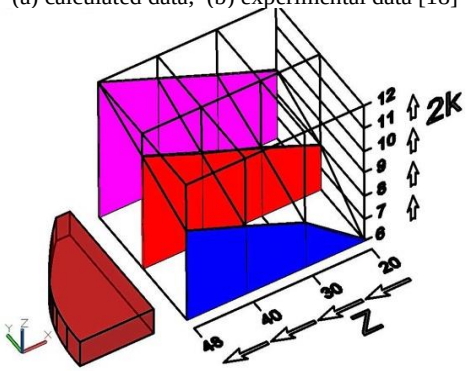

Figure 19 – Increase in the number of passes *2k* of the heat source over a fixed point of the machined surface at displacement of this point from the tooth base to its head for module *m*=2 mm and tooth counts 20< *z* <48

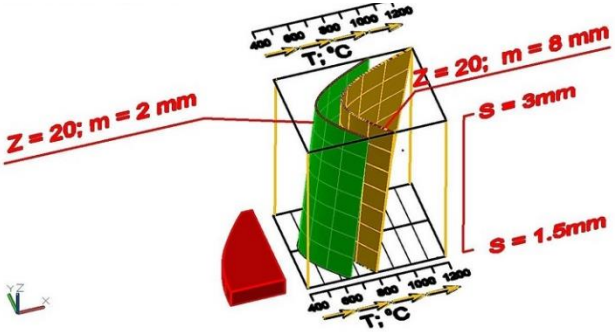

Figure 20 – Calculated temperatures formed during grinding of gear wheels (*z*=20; *m*=2 mm; *m*=8 mm) from cemented steel 18X2H4MA with a dished wheel according to the zero scheme on modes: *t*=0.05 mm; *n*`=112 1/min;
1.5 mm < *S* < 3.0 mm

The experimental determination of the contact area of a dished wheel with an involute tooth profile involved putting the tool into engagement with the wheel and measuring the resulting trace [18]. In this case, the contact area did not take into account the presence of a transition area (cutting zone) and a previously machined surface on the tooth being machined. In order to take into account these features of the shaping process, the gear wheel was pre-machined to a part of the width of its tooth crown corresponding to the studied phase of meshing of the tool with the wheel, then the tool was taken out of meshing and shifted in the direction

of longitudinal feed by the value of the break-in movements path. The grinding wheel left a trace on the tooth to be machined (Fig. 18, b).

Fig. 12 shows that in the process of break-in movements of the dished wheel in the direction of the tooth apex there is an increase in the length of the contact spot of the abrasive tool with the machined material.

In multi-pass grinding, the point at the base of the tooth absorbs fewer thermal influences than the point at the head. As the number of teeth increases, the number of contacts between the grinding wheel working surface and the fixed point of the involute profile being machined increases. Fig. 20 shows that the temperature in the middle part of the tooth profile is 35 % to 45 % less than at the head and 18 % to 22 % less than at the stem.

From Fig. 20, it can be seen that as the modulus m and longitudinal feed *S* increase, an increase in temperature *T* is observed.

At gear grinding with dished wheels, the dependence of the depth of the defective (tempered) layer h_d on the cutting depth *t* has a linear character (Fig. 21) [20].

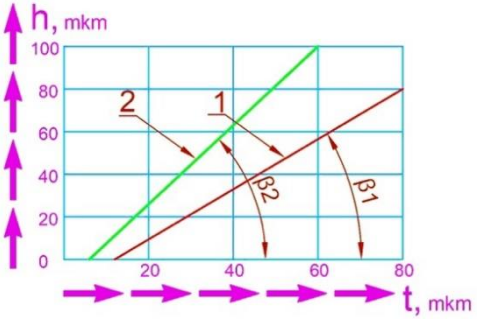

Figure 21 – Dependence of the depth of the defect layer on the grinding depth on machines operating with two dished wheels according to the "zero" (straight line 1) and "15-degree" (straight line 2) schemes.

Figure 22 –15- and 20-degree grinding method.

The graphs show that at the 15-degree grinding scheme (Fig. 22), temper burns begin to form at shallower cutting depths, and the process of propagation of critical temperatures deep into the workpiece proceeds more intensively compared to the "zero" scheme (Fig. 1). If the depths of the tempered layers $h_{d.a}$ and $h_{d.b}$ formed with cutting depths ta and t_b are determined experimentally, it is possible to determine the angle tangent of the line $tg\beta$, which defines the graph $h_d=f(t)$ (Fig. 23). The cutting depth t_0, at which no vacation burns, can be determined from the relations: $tg\beta = h\boldsymbol{d.b}\,/(t\boldsymbol{b} - t_0)$; $t_0 = (t\boldsymbol{b} \times tg\beta - h\boldsymbol{d.b})\,/\,tg\beta$.

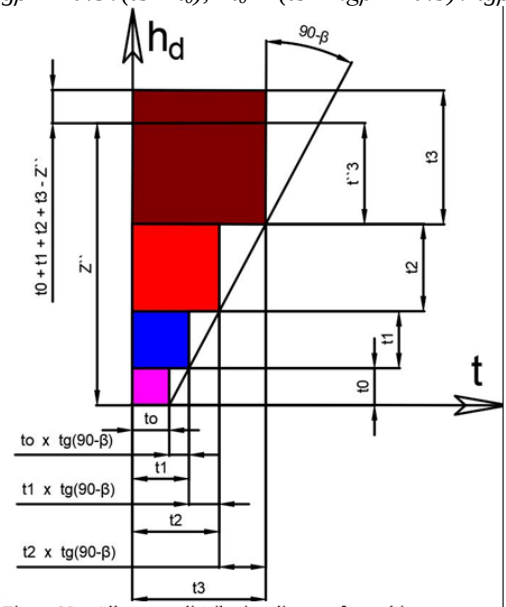

Figure 23 – Allowance distribution diagram for multi-pass gear grinding

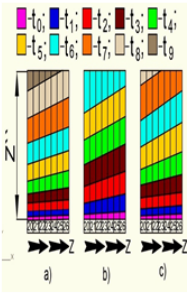

Figure 24 – Allowance distribution $z^{//}$ by passes calculated at the apex (a), on the dividing circle (b), and at the tooth base (c) for the tooth number range $20 < z < 26$ and constant modulus m=2 mm

Knowing the cutting depth t_0, at which no vacation burns are formed, and the angle β, it is possible to calculate the cutting depths for multi-pass grinding that satisfy the condition: the depth of burn propagation must not exceed the allowance remaining for subsequent passes. The depth of cut at different grinding passes is calculated by the formula: $\boldsymbol{ti} = ti\text{-}1 + \boldsymbol{ti\text{-}1} \times \mathrm{tg}(90^{o} - \beta)$, $i \geq 1$.

The numbering of the cutting depths at different grinding passes in Fig. 23 corresponds to the sequence of their calculation and does not coincide with the order of layer-by-layer removal of the allowance $z^{//}$. The sum of calculated cutting

depths t_i must be equal to the value of the total allowance $z^{//}$. If the sum of cut thicknesses of the machined material exceeds the allowance $z^{///}$, the last calculated depth of cut t_3 must be corrected downward $t_3^{///}$ (Fig. 23).

Fig. 24 shows the distribution of the total allowance $z^{//}$ by passes. Fig. 24 shows that different sections of the involute tooth profile require different numbers of grinding passes to prevent the appearance of temper burns: 10 - at the tooth apex (a), 7 - at the dividing circle (b), 9 - on the tooth base (c). The calculations of cutting depths t_i were carried out according to the method given in [20]. The obtained results can be explained by the fact that according to the graph (Fig. 20) the lowest heat stress in the area of the dividing circumference, so grinding can be carried out with greater cutting depths and, consequently, with a smaller number of passes. The highest heat stress is at the tooth apex, so more passes will be required to prevent vacation burns. Burns result in sharp hardness variations along the depth of the structurally altered layer. The greater the depth of penetration of the critical temperature deep into the part, the greater the reduction in microhardness at the surface. The higher the heat stress of grinding, the more intense the martensite tempering and the deeper the vacation burn. In order to reduce the depths of distribution of the vacation burn, it is necessary to reduce the depths of cutting when distributing the total allowance over grinding passes, and this leads to an increase in the number of technological transitions and, as a consequence, to an increase in the processing time and the cost of production of gears.

4. CONCLUSIONS

1. A mathematical model has been developed that allows calculations of surface temperatures during grinding of gear wheels with two dished wheels on a zero scheme.

2. Calculations have established that the temperatures and depths of penetration of critical temperatures, causing structural changes in the processed material, deep into the workpiece at different points of the trajectory of the grinding circumference break-in movements over the tooth are different: the farther from the dividing circle, the higher the grinding temperature and the thicker the depth of the defective layer.

3. The engineering methodology for determining the depths of cut at multi-pass grinding on the machines operating two dished wheels on the zero pattern is developed.

References: 1. *Ryabchenko S.V., Silchenko Ya.L., Fedorenko V.T., Polonsky L.G., Yanovsky V.A.* Quality analysis of surfacemachined with CBN disks. Machining in Mechanical Engineering: Transactions. Zhitomir: ZhSTU, 2015. Issue 15. 167-177. **2.** *Ren Xiao Zhong, Hu Hai Feng*. Analysis on the Temperature Field of Gear Form Grinding. Innovative Solutions in Materials Science and Engineering, 01 Sep 2014, Vol. 633-634,

Issue 2, pages 809-812. DOI: 10.4028/www.scientific.net/AMM.633-634.809 URL: http://www.scientific.net/AMM.633-634.809 **3.** *Jin T, Yi J, Peng S.* Determination of burn thresholds of precision gears in form grinding based on complex thermal modeling and Barkhausen noise measurements. Int J Adv Manuf Technol. 2017. 88(1-4). 789-800. **4.** *Guerrini G., Lerra F., Fortunato A.* The Effect of Radial Infeed on Surface Integrity in Dry Generating Gear Grinding for Industrial Production of Automotive Transmission Gears. J. Manuf. Process. 2019. 45. 234-241. Doi: 10.1016/j.jmapro.2019.07.006 **5.** *Larshin, V., Babiychuk, O., Lysyi, O., Uminsky, S.* Discontinuous Generating Gear Grinding Optimization. Lecture Notes in Mechanical Engineering, 2022, LNME, pp. 263-272, 2022. https://doi.org/10.1007/978-3-031-06025-0_26 https://www.scopus.com/authid/detail.uri?authorId=57217107788 **6.** *Ryabchenko S. V.* COG-WHEEL GRINDING WITH ABRASIVE CUBIC BORON NITRIDE DISKS. Vestnik Bryanskogo gosudarstvennogo tekhnicheskogo universiteta. 2018. №11(72). pp. 67–72. DOI:10.30987/article_5be14a35530b65.64215370 **7.** *Ryabchenko S.V., Polonskiy L.G., Golovnya V.D., Yanovskiy V.A., Kozyar Ya.A.* Shlifovaniye zubchatykh kolos krugami iz kubicheskogo nitrida bora. Vísnik ZHDTU. Seríya: Tekhníchní nauki 2017. No 2(80). pp. 68–72. DOI: https://doi.org/10.26642/tn-2017-2(80)-68-72 http://nbuv.gov.ua/UJRN/Vzhdtu_2017_2%281%29_13 **8.** *Sokolova I.D., Svitka A.S.* Analiz metodov shlifovaniya zubchatykh kolos na sovremennom oborudovanii. Innovatsionnaya nauka. Mezhdunarodnyy nauchnyy zhurnal. 2016. №9. pp. 83–87. [in Russian] **9.** *Shuying Yang, Weifang Chen, Su Nong, Lei Dong, Houyun Yu*. Temperature field modeling in the form grinding of involute gear based on high-order function moving heat source. Journal of Manufacturing Processes. Volume 81, September 2022. 1028–1039. https://doi.org/10.1016/j.jmapro.2022.07.014 **10.** *Jun Yi, Tan Jin, Wei Zhou, Zhaohui Deng*. Theoretical and experimental analysis of temperature distribution during full tooth groove form grinding. Journal of Manufacturing Processes, Volume 58, October 2022. pp. 101–115. https://doi.org/10.1016/j.jmapro.2020.08.011 **11.** *Jin Tan, Yi Jun, Li Ping*. Temperature distributions in form grinding of involute gears. Int J Adv Manuf Technol. 2017 (88). 2609–2620. **12.** *Lishchenko, N.* Profile gear grinding temperature determination. Transactions of Kremenchuk Mykhailo Ostrohradskyi National University. 2018. 100–108. https://doi.org/10.30929/1995-0519.2018.1.100-108 **13**. *Su J., Ke Q., Deng X. et al.* Numerical simulation and experimental analysis of temperature field of gear form grinding. Int J Adv Manuf Technol. 2018. 97. 2351–2367. https://doi.org/10.1007/s00170-018-2079-6 **14.** *Lishchenko N.V., Larshin V.P.* Profile Gear Grinding Temperature Reduction and Equalization. Journal of Engineering Sciences, Volume 5, Issue 1 (2018). A1-A7 DOI: 10.21272/jes.2018.5(1).a1 **15.** *Guerrini G., Landi E., Peiffer K., Fortunato A.* Dry Grinding for Sustainable Automotive Transmission Production. J. Clean. Prod. 2018. 176. 76–88. Doi: 10.1016/j.jclepro.2017.12.127. **16.** *Pashchenko E.O., Kukharenko S.A., Riabchenko S.V., Bychykhin V.M., Shatokhin V.V.* Development of the Technology for Manufacturing and Introducing a New Class of Tools with CVD-Diamond for Grinding High-Precision Gear Wheels of Special Reducer Units. Sci. Innov. 2020. V.16, No 1. https://doi.org/10.15407/scin16.01.069. **17.** *Riabchenko S., Lavrinenko V., Sheiko M., Paschenko E.* Elaboration of technology tor making the European nomenclature high-porous abrasive wheels of monocrystalline corund using a precision instrument of superhard materials for turbo-building of Ukraine Science and Innovation: Academic and Research Journal. Kyiv: National Academy of Sciences of Ukraine. 2018, volume 14(5). 49–56. **18.** *Ryabchenko S.V.* Shlifovaniye zubchatykh kolos tarel'chatymi krugami. Oborudovaniye i instrument dlya professionalov : mezhdunarodnyy informatsionno-tekhnicheskiy zhurnal (seriya: Metalloobrabotka). Khar'kov: Informatsionno-izdatel'skiy dom «Tsentr Inform». 2014. No 2. 44–48. [in Russian] **19**. *Jin T, Yi J* (2016) Investigation on the grinding force, power and heat flux distributions along the tooth profile in form grinding of gears. In: Proceedings of the ASME 2016 international manufacturing science and engineering conference MSEC2016, 27 June – 1 July 2016, Blacksburg, Virginia, USA. **20.** *Novikov F. V., Zhovtobryukh V. A., Gusarev V. S., Naddachin V. B., Yakimov A. A., Andilakhay A. A., Sergeyev A. S., Novikov D. F.* Innovatsionnoye razvitiye sovremennykh tekhnologiy : monografiya. – Dnepr: LIRA. 2021. 280 p. [in Russian].

Володимир Тонконогий, Олексій Якимов, Любов Бовнегра, Одеса, Україна
Федір Новіков, Харків, Україна

ПОВЕРХНЕВІ ТЕМПЕРАТУРИ І ПРИПІКАННЯ ВІДПУСТКИ, ВИНИКАЮЧІ ПІД ЧАС ШЛІФУВАННЯ ЦЕМЕНТУЮЧИХ ЗУБЧАТИХ КОЛІС ДВОМА ТАРІЛЬЧАСТИМИ КРУГАМИ, НА РІЗНИХ ДІЛЯНКАХ ОБРОБЛЮВАНОГО ЕВОЛЬВЕНТНОГО ПРОФІЛЮ

Анотація. *Для підвищення продуктивності шліфування із забезпеченням заданих фізико-механічних властивостей поверхневого шару оброблюваної деталі необхідно знати температуру на поверхні заготовки, оскільки від її величини залежить глибина дефектного поверхневого шару. У роботі теоретично обґрунтовано відмінність поверхневих температур у початковій (біля основи), у середній (на ділильному колі) і кінцевій (біля вершини) точках евольвентного профілю зуба шестірні при шліфуванні двома тарілчастими кругами за нульовою схемою. Відмінність температур у різних точках оброблюваного профілю обґрунтовується тим, що на різних ділянках траєкторії переміщення теплового джерела діє різна кількість теплових імпульсів. Ці імпульси мають різну тривалість та проміжки часу між діями цих імпульсів у різних точках евольвентного профілю теж різні. Кількість теплових дій на фіксовану точку оброблюваного профілю залежить від довжини теплового джерела, а тривалість нагрівання поверхні в цій точці визначається шириною теплового джерела. Тривалість охолодження залежить від місця розташування точки на евольвентному профілі. Розроблено математичні моделі для розрахунку температур на різних ділянках траєкторії обкатування тарілчастого шліфувального круга по оброблюваному зубу. Кожна з цих формул містить дві суми. Перша сума визначає збільшення температури у фіксованій точці профілю зуба при багаторазовій дії на неї теплових імпульсів при прямих ходах, а друга сума – при зворотних ходах. Математичні моделі ґрунтуються на принципі суперпозиції теплових полів. Встановлено, що температура в середній частині зуба на 40% менше, ніж у вершини зуба і на 20% менше, ніж у його основи. Розроблено інженерну методику розподілу загального припуску за проходами для багатопрохідного зубошліфування двома тарілчастими кругами за нульовою схемою. Методика ґрунтується на експериментальній залежності глибини дефектного шару від глибини різання, що має лінійний характер. У роботі виконано розрахунки з розподілу припуску в початковій, середній та кінцевій точках евольвентного профілю зуба. Розрахунки показали, що для запобігання появі припікань на остаточно-обробленій поверхні шліфування на різних ділянках оброблюваного профілю повинно здійснюватися з різним числом проходів. Найменша кількість проходів на ділильному колі, а найбільша – біля вершини зуба. Запропонована методика розподілу припуску за проходами може бути використана на етапі проектування операції зубошліфування (для оптимізації режимів) і на етапі механічної обробки (при діагностиці операції). Теоретично обґрунтовано, що розрахунки з розподілу припуску за проходами слід здійснювати тільки на головці зуба.*

Ключові слова: *тарілчасті круги; нульова схема; припікання відпалу; багатопрохідне шліфування.*

UDC 536:621.9 (075.8) **doi: 10.20998/2078-7405.2023.99.13**

STUDYING THE INFLUENCE OF THERMOMECHANICAL PHENOMENA ON GRINDED SURFACE QUALITY PARAMETERS OF PRODUCTS MADE FROM HARD-TO-PROCESS MATERIALS

Anatoliy **Usov** [0000–0002–3965–7611], Yuriy **Zaychyk** [0000–0002–8577–1095]

Odesa Polytechnic National University, 1, Schevchenko av., Odesa, 65044, Ukraine
usov_a_v@op.edu.ua

Received: 11 November 2023 / Revised:18 November 2023 / Accepted: 26 November 2023 / Published: 01 December 2023

Abstract. *Grinded surface quality state of products made from hard-to-process materials is formed under the influence of thermomechanical phenomena during final machining operations. But grinding causes the formation of burns, cracks, and tensile stresses in surface layers of products. These defects significantly influence reliability and durability of products during their operation. High thermal tension of diamond-abrasive processing leads to the fact that thermophysics of these processes is dominating in formation of quality characteristics of processed surface. Existing grinding methods for products made from hard-to-process materials do not allow to fully eliminate defects that occur in surface layer. Among the factors that conduce these defects are inevitable fluctuations of processing allowance, microheterogenity of the material characterized by the size of grain, packaging defects, structural transformations and dislocations, product warping during thermal treating, insufficiently studied thermomechanical phenomena. The mentioned effects accompany grinding process and cause burn marks, microcracks, structural transformations, residual stresses. Exploration of thermomechanical phenomena that form the quality of surface layer considering preceding machining operations of products, determining their influence on cracks and burns formation based on quality analysis of thermal and stress states and make up the objective of this research. This paper proposes more efficient models for studying quantitative connections between technological system parameters, physical and mechanical properties of processed materials, their structure, and thermomechanical processes during grinding. We have developed optimal technological parameters for processing metals and alloys prone to defects in surface layer based on determined relationships. Such defects encompass defects like cracks, burns, and chips.*

Keywords*: grinding; processed surface quality; thermomechanical phenomena; model; defects; technological parameters; defects-free processing criteria.*

1. INTRODUCTION

The development of study of surface quality leads to the establishment of functional dependencies between technological system parameters, instrument properties, processing modes, roughness, hardening, existence of cracks and burns, precision of product surface, and materials. Determining relationships between the most important properties of products (durability, fatigue and long-term strength,

contact rigidity, magnetic properties, etc.) made from hard-to-process materials and technological parameters (surface microrelief, microhardness, presence of microcracks and chips, spreading depth of hardened layer) is an important task of machine building technology.

Studying only mechanical processing influence on the operational properties of product is insufficient because preceding processing types (thermal, thermomechanical, thermochemical, etc.) and especially preparation of workpieces contribute significantly to the alternation of surface layer properties exposed to further mechanical processing. The Development of the technological heredity problem is a base of scientific and practical trends in machine building technology aiming to enhance operational qualities of machines details applying technological methods during manufacturing.

Review of the literature. The most widespread final machining operation is grinding which ensures high precision and high manufacturing productivity. But also grinding may cause burns, cracks, and tensile stresses in surface layers of products which affect their reliability and durability during operation [1] [2] [3] [4]. The problem of surface layer quality enhancement can be solved with following approaches:

- Selection of proper grinding modes and appropriate instrument characteristics for particular material.
- Usage of grinding wheels and belts with intermittent working surface.
- Applying system with automatic regulation of cutting power.
- Cutting fluids significantly decreases thermal tension of grinding operation and thus decreasing the probability of burn marks and cracks.

But application of mentioned methods within current manufacturing technology and considering composite materials cannot fully exclude defects that appear in surface layer. This is magnified by processing allowance fluctuations, material heterogeneity, product warping, thermal defects during processing.

High thermal tension of diamond-abrasive processing determines the dominating role of thermal physics of this process in surface layer quality characteristics. This thesis is confirmed by research of a wide range of scientists regarding concrete problems of such processes [5] [6] [7] [8]. Among the most noted results in this trend are the following works: [9] – influence of thermal physics on processed surface quality, [10] – thermal nature of surface quality during grinding; control of thermal physics applying intended process interruption, [11] – influence of thermal physics on stressed state of processed surface, [12] – influence of geometrical form of product and grinding technological parameters on surface layer quality, [13], [14] – determination of grinding temperature that is a consequence of

thermal interaction between abrasive grains like heat sources, research of grinding process using similarity theory methods, influence of cutting fluids on thermal physics and quality characteristics of grinded products.

Problem statement. Research of thermomechanical phenomena that form surface layer quality considering preceding machining operations, determining the influence of them on cracks and burns occurrence basing on quantitative analysis of thermal and stressed state and make up the sense of this paper.

In this scientific work we propose more efficient models for studying quantitative relationships between the parameters of technological system parameters, physical and mechanical properties of processed metals, presence technological defects in the surface layer, structure and thermomechanical processes which accompany grinding operation. Optimal technological parameters for processing metals and alloys (prone to defects occurrence) that are being developed based on established relationships.

Research methods and materials. One of the concrete results of this scientific work is the establishment of grinding defects formation patterns depending on heredity and processed material type, its heterogeneity and methods for their removing employing proper technological system. Grinding of machine details is followed by thermal and mechanical phenomena which interact between each other and define surface layer quality. Quantitative description of these phenomena requires the choice of definite models. Considering interconnections of processes during grinding it becomes obvious that stress-strained state of the surface layer is determined mainly by temperature. If we use the model of thermoelastic body that reflects the interconnection of mechanical and thermal phenomena in finite thermal flows, then we can significantly progress in the research of thermomechanical phenomena accompanying grinding process [15].

2. RESULTS

For further studying of the kinetics of thermomechanical processes we will use the following system of differential equations [16] as primary theoretical foundation. This system describes the interaction between deformation field and temperature fileld:

$$G\Delta\vec{U}_j + \left(\lambda_t + G\right) graddiv\vec{U}_j - \rho\frac{\partial^2\vec{U}_j}{\partial\tau^2} + \mathrm{P}_j = \alpha_t\beta_t gradT \tag{1}$$

$$\Delta T - \frac{1}{a}\frac{\partial T}{\partial\tau} - \eta l\frac{\partial}{\partial\tau} div\vec{U}_j = -\frac{W}{\lambda} + C_q^{-2}\frac{\partial^2 T}{\partial t^2} \tag{2}$$

where λ_t, G – are Lamé constants; $\beta_t = 3\lambda_t + 2G$; ρ - processed material density; α_t – temperature coefficient of metal linear extension; $a = \lambda / C_v$ –

temperature diffusivity coefficient; λ - thermal diffusivity coefficient; C_v – dimensional thermal capacity; $\vec{U}$ (Φ, τ) – total displacement vector of internal Φ (x, y, z) in surface layer under the action of thermomechanical forces following grinding process; $l = 1 + \tau_r \delta/\delta$ (τ - relaxation time); $\eta = \alpha_t \beta_t T(\Phi, \tau) / \lambda$; W – thermal source power; C_q – heat spread rate in processed material; τ - time; P_j – cutting forces.

$$grad T(x, y, z) = \frac{\partial T}{\partial x}\vec{i} + \frac{\partial T}{\partial y}\vec{j} + \frac{\partial T}{\partial z}\vec{k}$$

$$div\vec{U}_j = \frac{\partial U}{\partial x} + \frac{\partial U_y}{\partial y} + \frac{\partial U_z}{\partial z}$$

As thermal effects prevail over force phenomena, we can ignore the component responsible for the transformation of mechanical energy into thermal energy in the thermal conductivity equation. Thus, we can come to thermal conductivity equation of hyperbolic type. To solve the equation system (1), (2) in explicit way we will ignore the influence of inertial components and the limitation of thermal spreading rate. Moreover, we will consider the flat problem to omit the analytical difficulties connected with spatial thermoelasticity problems solution. This step is acquitted because for the research of thermomechanical state of grinded surfaces it is important to consider the information about temperature and deformation spreading along the depth and in the direction of instrument movement as the source of thermal emission in processing zone.

The analysis of the scaled schemes of grinding wheel interaction with processed surface showed that the curvature of the wheel and of the product (in limits of contact zone) insignificantly affects the geometrical schema of the wheel and product interaction. That's why when building the calculations schema, we assume that product can be presented as partially homogeneous half-plane. This assumption enables us to study thermomechanical processes during grinding of products with several types of coating with thickness Δa_K which are applied to main matrix. Such schema determines thermal and strained conditions for layer coupling along splitting border - a_K.

During material smelting and during technological process the following effects and phenomena may occur: structural heterogeneities as phase transformations of unstable structures, grain films, heredity austenite grains borders, carbide lining, cementite grid, dents, flocks, and other defects. In our model we will consider such defects as inclusions and cracks in surface layer.

The calculation schema for the problem of determining thermomechanical state during grinding of products with heterogeneities as inclusions and cracks in surface layer is described on fig. 1.

The system of equations that determine thermal and stress-strained state of

processed product surface includes [17]:

a) Equation of non-stationary thermal conductivity

$$\frac{\partial T}{\partial \tau} = a^2 \left(\frac{\partial^2 T}{\partial x^2} + \frac{\partial^2 T}{\partial y^2}\right) \tag{3}$$

b) L'ame elasticity equations in displacements

$$\frac{\partial \theta}{\partial x} \cdot \frac{1}{1-2\mu} + \Delta \vec{U} = b^T \frac{\partial T}{\partial x}; \quad \vec{U} = \frac{U}{2G}; \quad \vec{V} = \frac{V}{2G}; \tag{4}$$

$$\frac{\partial \theta}{\partial y} \cdot \frac{1}{1-2\mu} + \Delta \vec{U} = b^T \frac{\partial T}{\partial y}; \quad b^T = \frac{4G(1+\mu)}{1-2\mu} \alpha t \tag{5}$$

c) initial conditions

$$T(x, y, o) = 0 \tag{6}$$

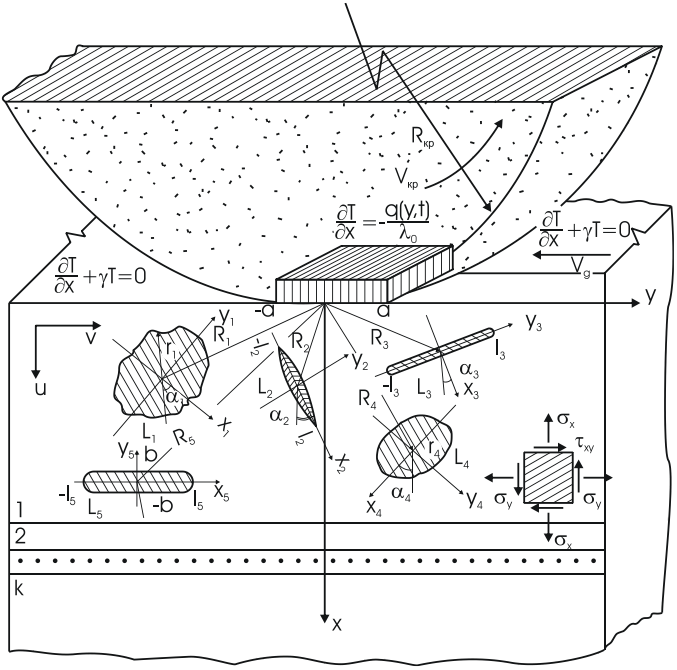

Fig.1. Calculation schema for defining thermomechanical state during grinding of products which contain heterogeneities in surface layer.

d) border conditions

$$\frac{\partial T}{\partial x} = -\frac{q(y,t)}{\lambda}, \quad |y| < a;$$

$$-\frac{\partial T}{\partial x} + jT = 0, \quad |y| > a;$$

$$\sigma_x(x,y,t)\big|_{x=0} = \tau_{xy}(x,y,t)\big|_{x=0} = 0 \qquad (7)\ (8)\ (9)$$

e) for layer coupling

for temperature fields for strain fields

$$T^{k-1}(a_k - 0, y, \tau) = T^{k}(a_k + 0, y, \tau) \quad V_j^{k-1}(a_k - 0, y) = V_j^{k}(a_k + 0, y) \qquad (10)$$

To consider the constructional peculiarities of the grinding wheels we need to apply the following boundary conditions:

$$q(y,\tau) = \frac{c\sqrt{\tau}}{\lambda}[H(y) - H(y - 2a^*)] \sum_{k=0}^{n} \sigma(y + kl - v_{kp}\tau) \qquad (11)$$

where $H(y)$ — Heaviside step function; $\sigma(y)$ — Dirac delta function; n — number of grains that go through the contact zone by time $\tau = \frac{\sqrt{\pi t_{шл}}}{v_{kp}}$; λ — product's material thermal conductivity; $c\sqrt{\tau}$ — thermal flow from a single grain; v_g, v_{kp}, $t_{шл}$ grinding modes, $2a^*$ — arc length of contact between wheel and product; l^* — distance between cutting grains.

We have obtained theoretically and confirmed by the experiment maximal values of instant temperature T_M and temperature from single grains to a constant component T_K. These values will be used as criterial for predicting burn-like defects appearance conditions and their depth.

The existence of stress concentrators like preceding machining operations defects in the surface layer of grinded products complicates the research for crack formation reasons. That's why to determine the limited balanced state of strained surface layer we need to insert values of the components of stresses and deformations at the corner apex into classic strength criterion. Such approach is used in fracture mechanics [18], [19], where newly formed strength criteria are the invariants in the models of continuum mechanics and in models which consider structural peculiarities of the material. From the existing criteria in fracture mechanics which are divided into energetic, power and strained, the most proper for our case are power criteria which are related to the definition of stress intensity factor [19]. In the most general case, the distribution of strains near 0 point of crack-like defect contour is presented as a superposition of triple deformations which correspond to main types of crack surface displacement. They are: normal separation (I), transverse (II) and lateral (III) displacements.

Stress intensity factors K_I, K_{II}, K_{III} serve as a measure for the singularity of stresses near the apex of crack-like defect. The critical value of the stress intensity K_C is a characteristic of the material. When the load causes stress intensity to become critical, then crack-like defect transforms into primary crack. Critical stress is inversely proportional to the square root from the initial length of crack-like defect [19]:

$$\sigma_C = \frac{K_{1C}}{\sqrt{\pi l}}$$

where *2l* is the initial length of the crack-like defect and index 1 means that this is the first stage of destruction.

Grinding is a multifactor process. Physical and mechanical properties of processed metal, its structure, grinding modes (fig. 2) and grinding wheels characteristics, conditions for preliminary treating with impregnating compounds and cutting fluids characteristics influence product's surface layer quality during grinding [20].

That's why to ensure the quality of processed surfaces we need select processing modes, cutting fluids, and instrument characteristics corresponding to established functional relationships between physical and mechanical properties of materials and grinding process parameters. At the same moment grinding temperature T (x, y, τ) and thermal flow q(y,τ), stresses $\sigma_{p\,max}$ and cutting forces P_Y, P_Z, intensity factor $K_1(S, \alpha, \sigma_{p\,max})$ shall not exceed their limit values which ensure required quality of the surface layer.

Let's consider the following system of bounding inequations obtained by the solution of problems (3) – (11). This fact allows us to develop the algorithm for selecting technological parameters that ensure required quality of processed surfaces.

During the exploration of kinetics of temperature field of the product considering peculiarities of single grains we have established that it consists of regular (constant) and instant (impulse) components. Impulse component – T_M describes temperature state of the metal under the grain. Constant component – TK characterizes metal temperature in the processing zone as a result of cumulative action from instrument grains.

Despite the short duration of instant temperature action and its fast descend along the depth it takes part in forming of structural stressed state of thin surface layer of the product. That's why

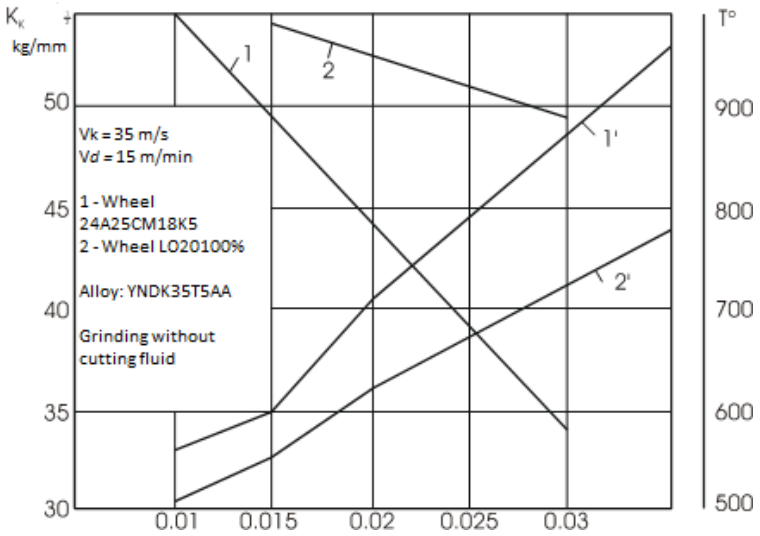

Fig .2. Influence of the grinding depth on the intensity of cracks formation during processing of UNDK magnets in state of α-phase.

bounding inequations for values of the temperature itself and its spreading depth will be correspondingly equal to:

$$T(x,y,\tau)=\frac{C}{2\pi\lambda}\sum_{k=0}^{n}H(\tau-\frac{kl}{V_{kp}})H(\frac{L+kl}{V_{kp}})\int_{\gamma_1}^{\gamma_2}f(\tau,\tau')d\tau'\le[T]_M \quad (12)$$

$$T([h],0,\tau)=\frac{C}{2\pi\lambda}\sum_{k=0}^{n}H(\tau-\frac{kl}{V_{kp}})H(\frac{L+kl}{V_{kp}})\int_{\gamma_1}^{\gamma_2}\psi(\tau,\tau')d\tau'\le[T]_{СП} \quad (13)$$

where

$$\psi(\tau,\tau')=\exp\left[-\frac{V_\partial(kl-V_{kp}\tau')}{2a}-\frac{V_\partial^2(\tau-\tau')}{4a}-\frac{(kl-V_{kp}\tau')^2+[h]^2}{4a(\tau-\tau')}\right] \quad (14)$$

$[T]_{ср}$ – acceptable temperature of structural transformations of given metal; [h] – limit acceptable depth of structural transformations.

In some cases the loss of quality of the surface layer becomes significant only when structural transformations spread to a certain depth. Its value is determined by operational conditions and indirectly by technical conditions. Limit values of such depth are determined by the zone of deep heating, sic constant component of the temperature field. Bounding inequations in this case have the following form:

$$T_k(o,y,\tau)=\frac{CV_{kp}}{\pi\lambda l\sqrt{V_g}}\int_0^{\tau}\int_{-e}^{e}\frac{x(r,t)e^{-\frac{(y-r)^2}{4(\tau-t)}}}{2\sqrt{\pi(\tau-t)}}\left\{\frac{1}{\sqrt{\pi(\tau-t)}}+\gamma e^{\gamma^2(\tau-t)}\left[1+\Phi(\gamma\sqrt{\tau-t})\right]\right\}drdt \quad (15)$$

$$T_k([h],0)=\frac{CV_{kp}}{\pi\lambda l\sqrt{V_g}}\int_0^{\sqrt{Dt_{\text{ø}\ddot{\text{e}}}}}\sqrt{[h]^2+y'^2}\,e^{-\frac{V_{\partial}y'}{2a}}K_{1/2}\left(\frac{V_{\partial}}{2a}\sqrt{y'^2+[h]^2}\right)dy'\le[T]_{np} \quad (16)$$

$$T_k^{\max}(L,0)\frac{CV_{kp}a}{\lambda lV_g^2}\sqrt{\frac{a}{\pi}}\left[1-\exp\left(-\frac{V_{\partial}\sqrt{Dt_{\text{ø}\ddot{\text{e}}}}}{a}\right)\right]\le[T]c.n. \quad (17)$$

In the last inequation we used limit temperature on the surface (X = 0) as bounding factor.

Grinding cracks formation depends on the value of temporal stresses which originate in the surface layer under the influence of thermomechanical phenomena accompanying this process. Maximum stress originates in the zone of intensive cooling. That's why the structure of controlling inequation in this case will be the following [21]:

$$\sigma_{\max}(x,\tau)=2G\frac{1+\nu}{1-\nu}\alpha_t T_k^{\max}erf\left(\frac{x}{2\sqrt{a\tau}}\right)\le[\sigma]_{\text{i}\div} \quad (18)$$

The phenomenological approach in the estimation of cracks formation of metals during don't consider many technological factors. Particularly the influence of thermal treating modes for these materials and their structure defectivity related to preceding machining operations. That's why we need more "sensitive" limiting inequation. The structure of such inequation shall include functional connections of technological parameters of diamond-abrasive processing and shall consider technological heredity.

We can use the limitation of stress intensity factor with established relationships with technological parameters in mentioned above role. The main criterion of crack resistance for metals is the coefficient K_{1C} [22]:

$$K_1=\frac{1}{\pi\sqrt{l}}\int_{-l}^{l}\sqrt{\frac{l+t}{l-t}}\{\sigma_{xx},\sigma_{yy}\}dt\le K_{1C} \quad (19)$$

where $2l$ – linear size of structural defect.

Defect-free grinding of materials with low mechanical characteristics is possible if we limit cutting forces, particularly tangential component – P_Z and decrease friction coefficient between the abrasive and processed metal - ρ.

Thus, from the study about the influence of cutting forces on the stressed state in the surface layer we can build another one auxiliary condition for defect-free grinding:

$$P_z \le \frac{\pi\sqrt{Dt_{\text{øë}}}}{KP^2 \sin\pi\theta}\left[[\tau]_C - \frac{E\rho\sqrt{Rt}}{2(1-\nu^2)\sqrt{R}}\right] \quad (20)$$

where [τ] – limit value of the tangent stress on the displacement; $\theta = \frac{1}{\pi} arctg \frac{1-2\nu}{2\rho(1-\nu)}$. ρ – minimal possible value of the friction coefficient between the abrasive and processed metal provided by the application of cutting fluids and impregnating compounds; $K = P_Y / Pz$ – relationship factor.

Using known value of crack resistance coefficient K_{1C} of the processed material [23], size of the "weakest" structural parameter *l*, we can determine the range of technological parameters which ensure limit value of thermal flow when structural defects balance is preserved:

$$q^* = \frac{P_z V_{kp} \alpha_b}{\sqrt{Dt_{\text{øë}}}} \le \frac{\sqrt{3}\lambda K_{1C}}{Hl\sqrt{\pi l}\,\delta^*} \quad (21)$$

The conditions of the defect-free grinding can be implemented using the information about the structure of processed metal. Thus, in case of prevailing character of structural imperfections with length 2l, their regular location related to contact zone between instrument and product we can use the balance condition in defect as criterial relationships:

$$l_0 < \frac{K_C^2}{\pi\left[GT_k(1+\nu)\alpha_t\right]^2} \quad (22)$$

In this formula the technological part lies in the connection between contact temperature value T_K and grinding modes and instrument characteristics (4.4.6).

Obtained inequations uncover the relationship of limit characteristics of temperature and power fields with controlling technological parameters. They define the area of combinations of technological parameters (modes, cutting fluids, grinding wheel characteristics) which ensure the required quality of processed surfaces.

Based on the obtained criterial relationships we developed the algorithm for providing surface layer quality of products during grinding considering maximum processing productivity (Fig. 3).

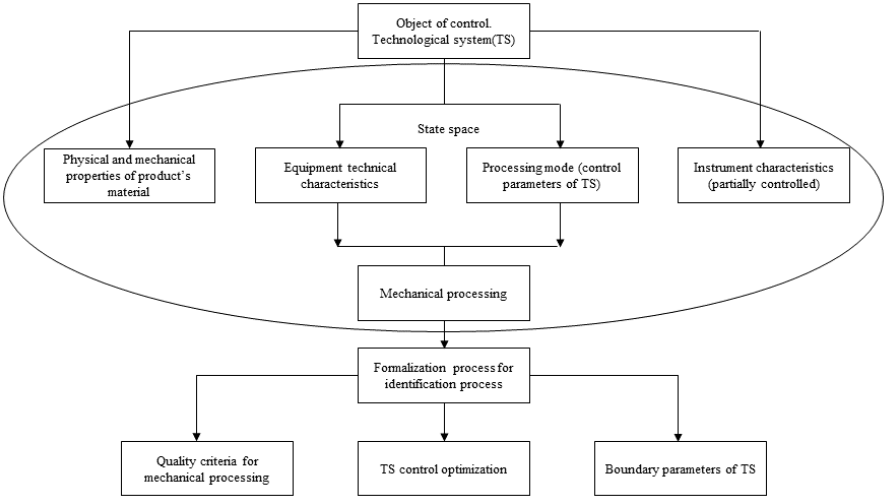

Fig.3 Algorithm for providing quality of mechanical processing corresponding to optimal accepted parameters of technological system.

3. CONCLUSIONS

Prevention of grinding cracks during the processing of products made from hard-to -process materials which have low mechanical properties and anisotropy depends on the right choice of grinding wheel characteristics, proper modes (which provide defect-free processing considering manufacturing technological process and morphology).

Obtained technological criteria proposed in form of bounding inequations (by the limit values of the grinding temperatures, burn mark depth, cutting forces, thermal flow, stress intensity) make possible to find the area of combinations of technological parameters – cutting fluids, grinding wheel characteristics which provide the required quality of products.

We developed the algorithm for providing quality working surfaces of products made from hard-to-process materials prone to defects formation during grinding.

References: 1. *V. O. Dziura and P. O. Marushchak*, Technological methods for ensuring the quality parameters of surfaces of bodies of rotation and their profilometric control, Ternopil: FOP Palyanytsya, 2021, p. 170. **2.** *D. M. Stepanov, N. V. Gonchar, E. V. Kondratyuk, P. R. Tryshyn*, Features of finishing processing of complex-profile and thin-walled aviation parts with brush polymer-abrasive tools, Zaporizhzhia: NU "Zaporizhzhia Polytechnic", 2022, p. 200. **3.** *V. G. Lebedev, E. A. Lugovskaya, A. V. Ovcharenko* , Experimental studies of the process of grinding martensitic-aging steel N18K9M5T, Technologies in mechanical engineering, №. 27, pp. 69–78, 2017. **4.** *F. Novikov, V. Polyansky*, Determination of conditions for improving the quality of machining by temperature criterion, Perspective

technologies and devices, № 17, pp. 99–105, 2020. **5.** *O. E. Semenovskiy*, Improving the manufacturability of manufacturing complex-profile parts. Series Technical sciences. **6.** *Y. M. Kusyj*, Naukovo-prykladni osnovy tekhnolohichnoho uspadkuvannia parametriv yakosti dlia zabezpechennia ekspluatatsiinykh kharakterystyk vyrobiv, Lviv, 2021. [in Ukrainian] **7.** *A. A. Levchenko*, Influence of technological heredity in the production of spare parts on the water supply of parts and their wear resistance, Problems of Technology, no. 2, pp. 23–28, 2006. **8.** *O. V. Yakimov, A. V. Usov, P. T. Slobodyanyuk, D. V. Iorgachov*, Thermophysics of machining, Odesa: Astroprint, 200, p. 256. **9.** *A. G. Derevyanchenko, T. V. Kozhukhar, S. K. Volkov*, Complex system for recognition of classes of defects of surfaces and structures of materials, Technologies in mechanical engineering, no. 12, pp. 98–108, 2017. **10.** *A. A. Matalin*, Yssledovanye temperatur shlyfovanyia stalnыkh yzdelyi. V knyhe "Kachestvo poverkhnosty y dolhovechnost detalei mashyn", Kh: Monography, 2007. [in Russian] **11.** *A. V. Yakimov, Y. A. Naparin, A. N. Parshakov*, Prychyni voznyknovenyia shlyfovochnikh treshchyn., Vestnik Mashynosrojeniya, no. 8, pp. 46–49, 1974. [in Russian] **12.** *S. A. Popov, N. P. Malevskiy, L. M. Tereshenko*, Almazno-obrazivnaya obrabotka metallov i tverdykh splavov, Moscow: Mashinostrojeniye, 1977, p. 263. [in Russian] **13.** *A. V. Yakimov*, Modelirovanije termomekhanicheskikh protsesov pri shlifovanii neodnorodnikh materialov, in Teplofizika tekhnologicheskikh protsesov, Toljatti, 1988. [in Russian] **14.** *A. V. Usov, A. V. Yakimov, E. A. Kormiltsna, F. M. Salkovskiy*, Prichyny poyavlenija defektov pri shlifovanii magnitotverdykh splavov, Tekhnologija elektrotekhnicheskogo proizvodstva, vol. 1, no. 4, p. 3, 1998. [in Russian] **15.** *A. V. Usov, A. V. Yakimov, I. P. Sazonov*, Vliyanije termomekhanicheskikh napryazheniy na treshinoobrazovanije pri shlifovanii tsementiruemikh splavov, in Sovremennyje problemi rezaniya instrumentami iz sverkhtverdykh materialov, Kharkiv, 1981. [in Russian] **16.** *Y. S. Podstrygach, Y. M. Kolyako*, Obobshennaya termomekhanika, Kyiv: Naukova dumka, 1976, p. 312. [in Russian] **17.** *G. Y. Popov*, Selected works, Vols. 1,2, Odessa: VMV, 2007. **18.** *N. G. Stashchuk*, Problems of mechanics of elastic bodies with crack-like defects, Kyiv: Naukova Dumka, 2009, p. 324. **19.** *V. V. Panasyuk*, Limiting equilibrium of fragile bodies with cracks, Kyiv: Naukova Dumka, 2008, p. 248. **20.** *G. A. Oborsky, A. F. Dashchenko, A. V. Usov, D. V. Dmitrishin*, Modeling of systems, Odessa: Astroprint, 2013, p. 664. **21.** *B. Boly, J. Weiner*, Theory of temperature stresses, Moskow: Mir, 1964, p. 427. **22.** *Y. S. Podstrygach, Y. M. Kolyano*, Neustanovivsheisya temperaturnyje polya i napryazheniya v tonkikh plastinakh, Kyiv: Naukova Dumka, 1972, p. 308. [in Russian] **23.** *V. I. Pokhmurskiy, Y. I. Kruzhanivskiy*, Mekhanika ruynuvannya i mitsnist materialiv, vol. 10, Lviv - Ivano-Frankivsk, 2006, p. 1193. [in Ukrainian].

Анатолій Усов, Юрій Зайчик, Одеса, Україна

ДОСЛІДЖЕННЯ ВПЛИВУ ТЕРМОМЕХАНІЧНИХ ЯВИЩ НА ПАРАМЕТРИ ЯКОСТІ ШЛІФОВАНИХ ПОВЕРХОНЬ ДЕТАЛЕЙ ІЗ СКЛАДНО ОБРОБЛЮВАНИХ МАТЕРІАЛІВ

Анотація. *Стан якості шліфованої поверхні виробів із складно оброблюваних матеріалів формується під впливом термомеханічних явищ, що супроводжують фінішну операцію. Але застосування шліфування пов'язане з появою припіків, тріщин, розтягуючих напружень в поверхневих шарах деталей, що істотно впливає на надійність і довговічність цих деталей в процесі їх експлуатації. Висока теплоємність алмазно-абразивних процесів обробки призводить до того, що теплофізика цих процесів часто є домінуючою у формуванні якісних характеристик оброблюваної поверхні. Існуючі способи шліфування деталей з важкооброблюваних матеріалів не дозволяють повністю усунути дефекти, що виникають в поверхневому шарі. Цьому сприяють: неминучі коливання припусків через помилки в попередніх операціях механічної обробки; Недостатньо вивчені мікронеоднорідність самого матеріалу, що характеризується зернистістю, дефектами упаковки, зміщенням і структурними перетвореннями, короблення деталей при термічній і подібній обробці, термомеханічними явищами, які супроводжують*

процес шліфування і в результаті яких на оброблюваних поверхнях з'являються припіки, мікротріщини, структурні перетворення, залишкові напруження. Предметом даної роботи є дослідження термомеханічних явищ, що формують якість поверхневого шару, з урахуванням попередніх видів обробки виробів, встановлення їх впливу на утворення тріщин і припіків на основі кількісного аналізу теплового і напруженого станів. У представленій роботі запропоновані більш ефективні моделі для дослідження кількісних співвідношень між параметрами технологічної системи, фізико-механічними властивостями оброблюваних металів, їх структурою і термомеханічними процесами, що відбуваються в поверхневому шарі деталей, що шліфуються. На основі встановлених співвідношень розроблено оптимальні технологічні параметри обробки металів і сплавів, які значно схильні до появи дефектів поверхневого шару, таких як тріщини, відколи, припіки.

Ключові слова: *шліфування; якість обробленої поверхні; термомеханічні явища; модель; дефекти; технологічні параметри; критерії бездефектної обробки*.

UDC 621.914.22 **doi: 10.20998/2078-7405.2023.99.14**

INFLUENCE OF RADIAL DEPTH OF CUT ON INITIAL CONDITIONS OF OSCILLATIONS DURING END-MILLING OF THIN-WALLED PARTS

Sergei **Dyadya** [0000-0002-7457-7772], Olena **Kozlova** [0000-0002-3478-5913], Pavlo **Tryshyn** [0000-0002-3301-5124], Eduard **Brukhno** [0000-0001-5526-073X], Denys **Yakhno** [0009-0009-2816-9397]

National University «Zaporizhzhya Polytechnic», Zaporizhzhya, Ukraine
kozlova@zntu.edu.ua

Received: 14 November 2023 / Revised:20 November 2023 / Accepted: 25 November 2023 / Published: 01 December 2023

Abstract. *Milling is widely used in mechanical engineering and other industries. Optimization of this process can lead to improved quality of machined parts, increased productivity and reduced wear of equipment. The paper investigates an important aspect of the milling process, namely the influence of radial depth of cut on the properties of the tool-part technological system (TS) and the amplitude of vibrations during machining. Vibrations can be a direct cause of reduction of quality and accuracy of machined parts. When the amplitude of vibrations increases, their impact on accuracy becomes critical. The analysis of studies of up and down end-milling with different radial depths of cut in the third speed zone of oscillations shows that with increasing radial depth of cut the cutting time and maximum thickness of the cut layer increases. This affects the length of the cutting surface and the character of the workpiece oscillations during up and down-milling. The length of the cutting surface determines how many waves of accompanying free oscillations of the TS and with what intensity will leave their trace on the cutting surface. In up-milling, the thickness of the cut layer increases with increasing radial depth of cut, while the amplitude of the accompanying free oscillations TS and their period decrease. At down milling the thickness of the cut layer decreases, and the amplitude of accompanying free oscillations of the TS and their period increase. A common characteristic feature of up and down-milling is the shaping of the machined surface in the cutting zone with a small thickness of the cut layer. In up-milling, this area is at the beginning of cutting, when the oscillation conditions are the same for all radial cutting depths. Therefore, the machined surfaces after up-milling with different radial cutting depths have close values of pitch and undulation height. At down-milling with increasing radial depth of cut, the amplitude of accompanying free oscillations of the TS in the profiling zone increases. This leads to an increase in the pitch and height of undulations on the machined surface. When milling in the third speed oscillation zone, it is necessary to select the radial depth of cut so that the cutting time is less than the period of the accompanying free oscillations of the TS. This will avoid undesirable oscillations and improve the quality of machining. The paper provides important results and recommendations for optimizing the milling process, considering the influence of radial depth of cut on TS properties and vibration amplitude. These findings may be useful for professionals working in the field of cutting materials processing to improve the efficiency and quality of production processes.*

Keywords: *milling; up and down-feed; radial depth of cut; accompanying free oscillations of the technological system; cutting time; thickness of the cut layer.*

1. INTRODUCTION

Ensuring accuracy and productivity in the production of workpieces are the main tasks of machine-building companies. At the same time, the main focus is on preventing the causes that adversely affect them.

One of these causes is cutting vibrations. At small vibration amplitudes they are not taken into account when selecting cutting modes and tool geometry. At large vibration amplitudes their influence on accuracy becomes decisive. Various methods are used to control vibration intensity. In heavy milling, the machine's own drives are used to suppress vibrations. They are controlled based on signals received from an external accelerometer located near the centre point of the tool. The measured acceleration is fed back to an additional control loop to regulate cutting speed and feed rate [1]. In multiaxial milling of hollow fan blades, the vibration stability of the tool depends on its motion. The use of optimization of cutting parameters on the basis of a single-line motion makes it possible to analyses the dynamic responses to different positions of the tool cutting edge and to select stable milling areas [2, 3]. Machining on the previous tool track leads to regenerative chatter. To break them, cutters with different geometries are used. Milling cutters with variable pitch create a phase shift of the current oscillation trajectory of the workpiece during cutting relative to the trace on the cutting surface from the previous cut [4 – 6]. But depending on the milling process, they can perform worse than milling cutters with a uniform pitch. Improved performance of variable-pitch milling cutters can be guaranteed by taking into account the reflected dynamic behaviour of the machine-tool-workpiece system. Cutter behaviour is tuned along stability margins at selected spindle speed ranges [7].

2. EXPERIMENTS AND DISCUSSION OF RESULTS

The studies focus on the effects of free oscillations, forced oscillations and self-oscillations [8]. The latter have the greatest impact on machining accuracy and tool life. But in [9] it is shown that at small cutting time in the process of end milling self-oscillations do not occur. In this case, the accompanying free oscillations of the TS "tool - workpiece". As free oscillations, they depend on the properties of the TS and, unlike self-oscillations, on the initial conditions. In milling, the properties of the TS and the initial conditions of oscillations depend on cutting modes and tool geometry.

This paper presents the results of research into the influence of radial depth of cut on the accompanying free oscillations of the TS during up and down end-milling of a thin-walled part. Cutting at these feed directions is performed according to two fundamentally different schemes. But in both cases the thickness of the cut layer is

variable (Fig. 1). In up-milling, it increases from the tool plunge until it leaves the workpiece (Fig. 1, a). In down milling, it decreases from the tool plunge until it leaves the workpiece (Fig. 1, b) [10].

Figure 1 - Cutting patterns for up (a) and down (b) end-milling [10]
a_e – radial cutting depth; a_{max} – maximum thickness of the layer to be cut; S_z - feed per tooth

The studies were carried out on an experimental bench [11] when milling a St. 3 sample with a single-tooth carbide milling cutter ∅54 мм. Axial depth of cut – a_p = 4 mm, feed per tooth – S_z = 0,1 mm/tooth, spindle speed – n = 280 rpm, radial cutting depth – a_e = 0.1; 0.3; 0.5 mm. Stiffness of thin-walled plate – j_{pl} = $2{,}98 \cdot 10^6$ N/m, free oscillation frequency – f_{fo} = 512 Hz. Free oscillation frequency of the cutter – f_{fr} = 1315 Hz, cutter stiffness – $j_{fr} = 34 \cdot 10^6$ N/m.

Cutting speed v = 47 m/min (n = 280 rpm) is recommended when machining difficult-to-machine materials. These materials are used to produce aircraft engine parts. This speed falls into the third speed zone of oscillations [11], in which the intensity of oscillations is high. Milling in this zone was chosen to better illustrate the effect of radial depth of cut on the vibration amplitude and properties of the TS.

During the experiments, oscillograms of oscillations of the thin-walled part and profilograms of the machined surfaces were recorded. They are shown in Fig. 2 – 5. The oscillogram fragments and profilograms were used to determine the parameters of oscillations of the workpiece during cutting, pitch and height of undulations on the machined surface. When determining the period and amplitude of the accompanying free oscillations, the Savitsky-Goley filter was used to straighten the oscillogram fragment.

The oscillograms of the oscillations of the workpiece using the electro-contact device showed areas of contact breakage during cutting and the absence of friction between the cutter and the specimen.

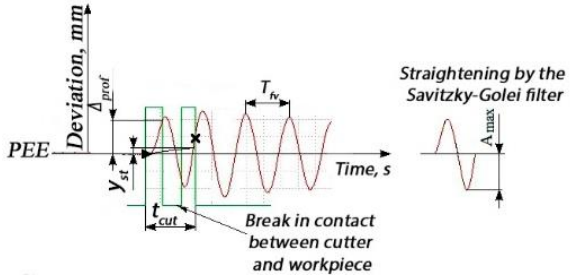

a_e = 0.1 mm

a

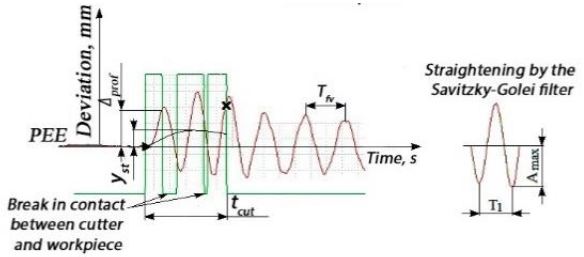

a_e = 0.3 mm

b

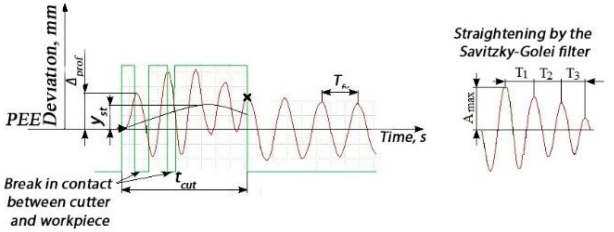

a_e = 0.5 mm

c

Figure 2 - Fragments of oscillograms of workpiece oscillations during up milling with different radial depth of cut.

► - tool plunging; x – tool exit from the workpiece; PEE - position elastic equilibrium of the part; A_{max} – maximum amplitude of the accompanying free vibrations of the workpiece when cutting; t_{cut} - cutting time; y_{st} – static deflection of the workpiece from the radial component of the cutting force P_y; T_{fv}- free vibration period of the part; T_1, T_2, T_3 – periods of accompanying free oscillations of the TS, Δ_{prof} – deviation from the PEE of the first wave of accompanying free oscillations during counter milling

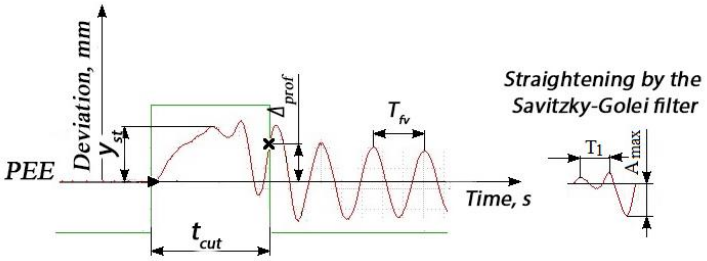

a_e = 0.1 mm

a

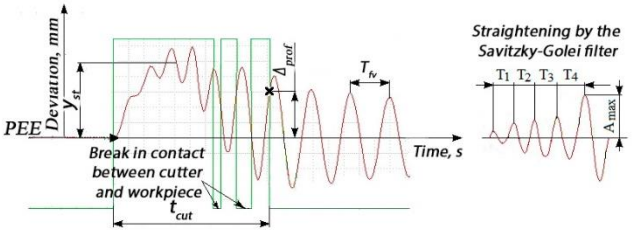

a_e = 0,3 mm

b

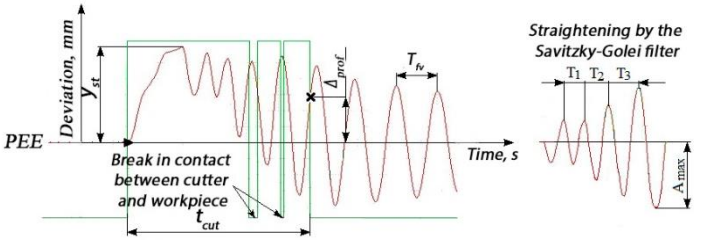

a_e = 0,5 mm

c

Figure 3 - Fragments of oscillograms of workpiece oscillations during down milling with different radial depth of cut

Δ_{prof} – deviation from the elastic equilibrium position of the last wave of accompanying free oscillations during down milling

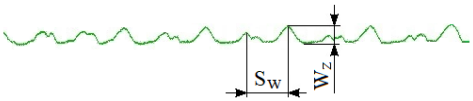

a_e = 0.1 mm

a

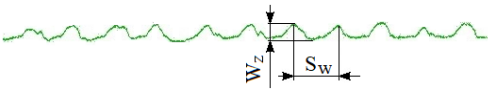

a_e = 0.3 mm

b

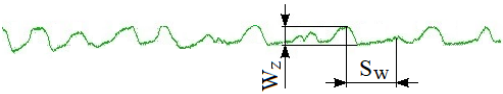

a_e = 0.5 mm

c)

Figure 4 - Profilograms of machined surfaces after up milling with different radial depth of cut

S_w – waviness pitch; W_z – waviness height

a_e = 0.1 mm

a

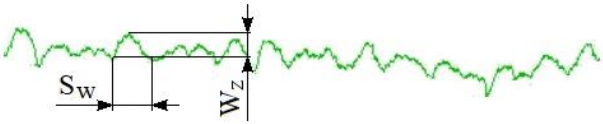

a_e = 0.3 mm

b

a_e = 0.5 mm

c

Figure 5 - Profilograms of machined surfaces after down milling with different radial depth of cut

Tables 1-3 show the values of parameters of workpiece oscillations during cutting, pitch and height of undulations of machined surfaces after up and down milling.

Table 1- Measurement results of oscillogram fragments after up milling

a_e, mm	t_{cut}, 10^{-3} s	y_{st}, mm	A_{max}, mm	Δ_{prof}, mm	T_{fv}, 10^{-3} s/ f_{fv}, Hz	T_1, 10^{-3} s/ f_{fv}, Hz	T_2, 10^{-3} s/ f_{fv}, Hz	T_3, 10^{-3} s/ f_{fv}, Hz
0,1	2,2	0,009	0,065	0,061	1,95/512	-	-	-
0,3	4,12	0,026	0,076	0,070	1,95/512	1,72/581	-	-
0,5	7,0	0,042	0,086	0,068	1,95/512	1,6/625	1,6/625	1,28/781

Table 2 - Measurement results of oscillogram fragments after down milling

a_e, mm	t_{cut}, 10^{-3} s	y_{st}, mm	A_{max}, mm	Δ_{prof}, mm	T_{fv}, 10^{-3} s/ f_{fv}, Hz	T_1, 10^{-3} s/ f_{fv}, Hz	T_2, 10^{-3} s/ f_{fv}, Hz	T_3, 10^{-3} s/ f_{fv}, Hz	T_4, 10^{-3} s/ f_{fv}, Hz
0,1	4,68	0,084	0,051	0,055	1,95/512	1,12/892	-	-	-
0,3	8,04	0,144	0,101	0,088	1,95/512	1,08/925	1,12/892	1,48/675	1,68/595
0,5	9,24	0,181	0,122	0,099	1,95/512	1,04/961	1,2/833	1,52/657	-

Table 3 - Step and height of undulations of the machined surface after up and down milling

a_e, mm	Feeding direction			
	Up milling		Down milling	
	S_w	W_z	S_w	W_z
0,1	2,05	0,065	0,61	0,036
0,3	2,13	0,061	0,94	0,075
0,5	2,13	0,066	1,27	0,102

In end milling, the thickness of the cut layer is determined by the feed rate on the tool tooth. Its maximum thickness depends on the radial depth of cut (Fig. 6).

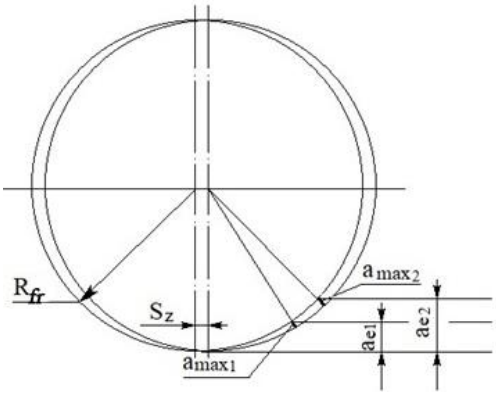

Figure 6 - Maximum thickness of the cut layer – a_{max} at different radial cutting depths – a_e

S_z - feed rate per cutter tooth; R_{fr} – cutter radius; a_{max1} – maximum thickness of the cut layer at cutting depth a_{e1}; a_{max2} – maximum thickness of the cut layer at cutting depth a_{e2}

Fragments of oscillograms shown in Fig. 2–3 show that the effect of radial depth of cut on the cutting process is related to cutting time.

When cutting with a radial depth of a_e = 0.1 mm, the oscillogram fragment for counter milling (Fig. 2, a) shows oscillations that have no period due to the short cutting time. At down milling with the same cutting depth, oscillations that have a period are recorded on the oscillogram fragment (Fig. 3, a). In this case, the amplitude of oscillations is smaller than in up milling due to the start of cutting from the greatest thickness of the cut layer.

When cutting with a radial depth of a_e = 0.3 mm, the cutting time increases and on the fragment of the oscillogram during up milling (Fig. 2, b), the accompanying free oscillations of the TS have a period. At the same time, the maximum thickness of the cut layer is insufficient to damp the oscillations. Therefore, their amplitude increases. At down milling with the same cutting depth, the number of waves accompanying free oscillations and their amplitude increase in the fragment of the oscillogram (Fig. 3, b). The period of these oscillations is shorter during down milling than during up milling.

During the cutting time with radial depth of a_e = 0.5 mm at up milling there is an increase in the amplitude of accompanying free oscillations of the TS at minimum thickness of the cut layer and its subsequent decrease with increasing thickness of the cut layer (Fig. 2, c). The period of accompanying free vibrations is also variable

when milling with variable thickness of the cut layer. It decreases as the thickness of the layer to be cut increases. At down milling with a radial cutting depth of a_e = 0.5 mm, the maximum thickness of the cut layer increases and in the fragment of the oscillogram (Fig. 3, c) the accompanying oscillations of the TS start later than at cutting with a depth of a_e = 0.3 mm. When the thickness of the sheared layer decreases, the amplitude of the accompanying free oscillations increases and negative damping is observed, when the amplitude A of the accompanying free oscillations of the TS increases according to the exponential law [12]:

$$A = A_0 e^{\beta t} \cos(\omega t + \varphi_0), \quad (1)$$

where A_0 – initial amplitude;
β – attenuation factor;
ω - cyclic frequency;
φ_0 - initial phase of oscillation.

Fig. 7 shows the graphs of dependence of the maximum amplitude of accompanying free oscillations of the TS during up and down milling on the radial depth of cut.

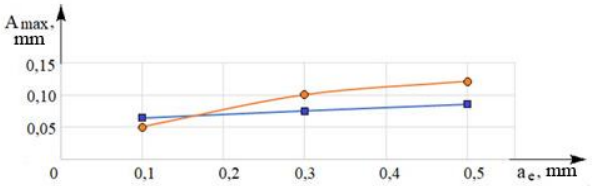

● – maximum amplitude of accompanying free oscillations of the TS during down milling;
■ – maximum amplitude of accompanying free oscillations of the TS during up milling;

Figure 7 - Effect of radial depth of cut – a_e on the maximum amplitude of the accompanying free vibrations TS A_{max}

In addition to the influence on the character of accompanying free oscillations of the TS during up and down milling, the radial depth of cut affects the elastic pushback of the workpiece associated with the action of the radial component of the cutting force P_y (Fig. 8). It is greater in down milling, when cutting starts from the greatest thickness of the layer to be cut.

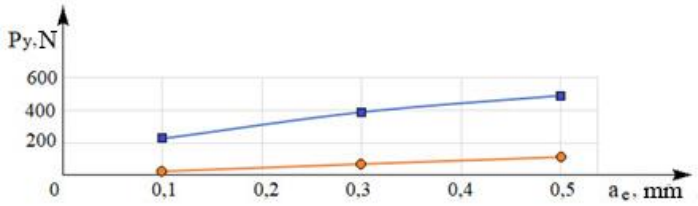

● - radial component of cutting force during up milling;
■ - radial component of cutting force during cross milling.

Figure 8 - Effect of radial depth of cut – a_e on the radial component of the cutting force P_y

Different cutting schemes for up milling and down milling affect the properties of the tool-piece technological system. The stiffness of the tool-piece system is higher in down milling than in counter-cut milling. Therefore, the oscillation periods of the workpiece during down milling are shorter than during up milling. The number of waves on the cutting surface is greater in down milling than in up milling.

Despite the above mentioned differences in the cutting process during up milling and down milling, there is one common feature between them. In both cases, the shaping zone of the machined surface is located in the cutting area with the minimum thickness of the cut layer.

In up milling, the depth of the forming depression is determined by the deviation from the elastic equilibrium position (PEE) of the first wave of the accompanying free oscillations TS – Δ_{prof}. It has close values when milling with different radial depths of cut. Therefore, machined surfaces after up milling with different radial depths of cut have similar values of S_w pitch and W_z waviness height.

At down milling, the depth of the forming depression is determined by the deviation from the PEE last wave of the accompanying free oscillations of the TS – Δ_{prof}. Increasing the amplitude of accompanying free oscillations at the section with minimum thickness of the cut layer with increasing radial depth of cut increases the value of Δ_{prof}. Therefore as the radial depth of cut increases the pitch S_w and the waviness height W_z of the machined surface increase during down milling.

3. CONCLUSIONS

The performed studies show that the influence of radial cutting depth on the properties of the technological system “tool-piece” and the amplitude of accompanying free oscillations of the TS is related to the cutting time and the

maximum thickness of the cut layer, which increase with increasing radial depth. At down milling it affects the time of occurrence of accompanying free oscillations of the TS and their amplitude, which increases according to the exponential law. At up milling, the amplitude of accompanying free oscillations of the TS at the beginning of cutting with a small thickness of the cut layer increases, but with increasing thickness of the cut layer it decreases.

Differences in the character of cutting vibrations are related to the variable thickness of the cut layer and different cutting patterns in up and down milling.

The common characteristic feature of up and down milling is the shaping of the machined surface in the cutting area with the minimum thickness of the cut layer. In up milling, the oscillations at the beginning of cutting at different radial cutting depths occur under the same conditions. Therefore, the pitch and height of the waviness on the machined surface have close values. In down milling, the amplitude of the accompanying free oscillations of the TS at the tool exit increases with increasing radial depth of cut. Therefore, with increasing radial depth of cut, the pitch and height of waviness on the machined surface increases after down milling.

When milling in the third speed zone of oscillations, the radial depth of cut should be chosen so that the cutting time is less than the period of the accompanying free oscillations of the TS in order to eliminate the negative effect of oscillations on the machined surface.

References: **1**. *Munoa J, Beudaert X, Erkorkmaz K, et al*. Active suppression of structural chatter vibrations using machine drives and accelerometers. CIRP Annals. 2015; 64(1):385–388. **2**. Zhou X, Zhang DH, Luo M, et al. Toolpath dependent chatter suppression in multi-axis milling of hollow fan blades with ball-end cutter. The International Journal of Advanced Manufacturing Technology. 2014;72 (5-8):643–651. **3**. *Yilong L, Baohai W, Ming L, Dinghua Z* Modeling and cutting path optimization of shallow shell considering its varying dynamics during machining. 15th CIRP Conference on Modelling of Machining Operations, 31. 2015;521 – 526. **4**. *Budak E.* An analytical design method for milling cutters with nonconstant pitch to increase stability – Part I: Theory; Part II: Application, Trans. ASME Journal of Manufacturing Science and Engineering, 125;2003:29–38. **5**. *Stepan G., Hajdu D, Iglesias, A, Takacs D, Dombovari Z* Ultimate Capability of Variable Pitch Milling Cutters. CIRP Ann., 2018;67(1): 373–376. **6**. *Zhan D, Jiang S, Niu J, Sun Y* Dynamics Modeling and Stability Analysis of Five-Axis Ball-End Milling System with Variable Pitch Tools. Int. J. Mech. Sci., 2020;182:105774. **7**. *Stepan G, Hajdu D, Iglesias A, et al*. Ultimate capability of variable pitch milling cutters. CIRP Annals. 2018;67(1):373-376. **8**. *Schmitz TL, Smith KS.* Machining Dynamics. Springer US; 2009. **9**. *Dyadya S, Vnukov Y, Kozlova O, Trishyn P* Regularities of Oscillations During Turning and End Milling. Advanced Manufacturing Processes V. Selected Papers from the 5th Grabchenko's International Conference on Advanced Manufacturing Processes (InterPartner-2023), September 5–8, 2023, Odessa, Ukraine, 136-144. **10**. *Mazur MP, Vnukov YuM, Grabchenko AI, Dobroskok VL, Zaloga VO, Novosolov YuK, Yakubov FYa* Osnovi teoriyi rizannya materialiv. Lviv:Novij Svit-2000, 2020:471 p. [in Ukrainian] **11**. *Vnukov Yu. N, Dyaya SI, Kozlova Ye. B, Logominov VA, Chernovol N.N*. Self-oscillations when milling thin-walled elements of parts. Zaporizhzhia: ZNTU; 2017. 208 p. **12**. *Strelkov S.P.* Vvedenie v teoriyu kolebanij. Moscow.: Izd-vo Nauka;1964: 438 p. [in Russian].

Сергій Дядя, Олена Козлова, Павло Тришин, Едуард Брухно, Денис Яхно,
Запоріжжя, Україна

ВПЛИВ РАДІАЛЬНОЇ ГЛИБИНИ РІЗАННЯ НА ПОЧАТКОВІ УМОВИ ВИНИКНЕННЯ КОЛИВАНЬ ПІД ЧАС КІНЦЕВОГО ФРЕЗЕРУВАННЯ ТОНКОСТІННИХ ДЕТАЛЕЙ

Анотація. *Фрезерування широко застосовується в машинобудуванні та інших галузях промисловості. Оптимізація цього процесу може призвести до поліпшення якості оброблених деталей, підвищення продуктивності та зниження зносу обладнання. У статті досліджується важливий аспект процесу фрезерування, а саме вплив радіальної глибини різання на властивості технологічної системи «інструмент – деталь» (ТС) та амплітуду коливань у процесі обробки. Вібрації можуть бути безпосередньою причиною зниження якості та точності оброблених деталей. При зростанні амплітуди коливань їхній вплив на точність стає критичним. Виконаний аналіз досліджень зустрічного і попутного кінцевого фрезерування з різними радіальними глибинами різання в третій швидкісній зоні коливань показує, що зі збільшенням радіальної глибини різання збільшується час різання і максимальна товщина шару, що зрізається. Це впливає на довжину поверхні різання і характер коливань деталі під час зустрічного і попутного фрезерування. Від довжини поверхні різання залежить, скільки хвиль супроводжувальних вільних коливань ТС і з якою інтенсивністю залишать свій слід на поверхні різання. Під час зустрічного фрезерування зі збільшенням радіальної глибини різання товщина шару, що зрізається, збільшується, а амплітуда супроводжуючих вільних коливань ТС і їхній період зменшуються. При попутному фрезеруванні товщина шару, що зрізається, зменшується, а амплітуда супроводжуючих вільних коливань ТС і їхній період збільшуються. Загальною характерною особливістю зустрічного і попутного фрезерування є формоутворення обробленої поверхні в зоні різання з малою товщиною шару, що зрізається. При зустрічному фрезеруванні ця ділянка припадає на початок різання, коли умови коливання однакові для всіх радіальних глибин різання. Тому оброблені поверхні після зустрічного фрезерування з різними радіальними глибинами різання мають близькі значення кроку і висоти хвилястості. При попутному фрезеруванні зі збільшенням радіальної глибини різання збільшується амплітуда супроводжуючих вільних коливань ТС у зоні профілювання. Це призводить до збільшення кроку і висоти хвилястості на обробленій поверхні. Під час фрезерування в третій швидкісній зоні коливань необхідно підбирати радіальну глибину різання так, щоб час різання був меншим за період супроводжуючих вільних коливань ТС. Це дасть змогу уникнути небажаних коливань і поліпшити якість обробки. Стаття надає важливі результати та рекомендації для оптимізації процесу фрезерування, враховуючи вплив радіальної глибини різання на властивості ТС та амплітуду коливань. Ці висновки можуть бути корисними для фахівців, які працюють у галузі обробки матеріалів різання, для підвищення ефективності та якості виробничих процесів.*

Ключові слова: *фрезерування; зустрічна і попутна подача; радіальна глибина різання; супроводжуючі вільні коливання технологічної системи; час різання; товщина шару, що зрізається.*

CONTENT

Felhő Cs. Analysis of the effect of varying the cutting ratio on force components and surface roughness in face milling……3

Sztankovics I., Pásztor I.T. Alteration of the cutting force components in tangential turning**……...**12

Manovytsky O., Klymenko S., Klymenko S., Kopeikina M. Actual contact area on the worn clearance face of the cutter with the round kyborite insert……21

Fedorovich V., Ostroverkh Y., Romashov D. Topographic adaptability in the diamond grinding zone of superhard materials……34

Maros Z., Kun-Bodnár K., Fekete V. Investigation of electro discharge machining of tool steels based on the roughness of the machined surfaces..... 46

Nagy A., Kundrak J. Roughness investigation of single and double cutting marks on face milled surface……. 58

Béres M., Varga G. Laser measurements in cutting processes……. 71

Mitsyk A., Fedorovich V., Ostroverkh Y. Purpose and technological properties of granular media for vibration finishing and grinding processing…… 85

Sztankovics I. Arithmetic mean height and maximum height of the roughness profile in honing with different feeds…… 94

Ferencsik V. Analytical analysis of the theoretical surface roughness in the case of burnishing of cylindrical workpiece**……** 101

Klymenko G., Kovalov V., Vasylchenko , Korchma D., Boroday R. Probabilistic approach to calculating the rational thickness of the tool`s cutting insert for heavy machine tools…….110

Tonkonogyi V., Yakymov O., Bovnegra L., F. Novikov F. Surface temperatures and vacation burns occurring during grinding of cemented gears with two dished wheels on different parts of the machined involute profile……119

Usov A., Zaychyk Y. Studying the influence of thermomechanical phenomena

on grinded surface quality parameters of products made from hard-to-process materials……140
Dyadya S., Kozlova O., Tryshyn P., Brukhno E., Yakhno D., Influence of radial depth of cut on initial conditions of oscillations during end-milling of thin-walled parts……153

Наукове видання

РІЗАННЯ ТА ІНСТРУМЕНТИ
в технологічних системах

Міжнародний науково-технічний збірник

Випуск № 99

Укладач *д.т.н., проф. І.М. Пижов*
Оригинал-макет *А.М. Борзенко*
Відп. за випуск *к.т.н., проф. Є.В. Островерх*

В авторській редакції

Матеріали відтворено з авторських оригіналів

Підп. до друку 12.12.2023.Формат 60x84 1/16. ПапірСоруРарег.
Друк - ризографія. Гарнитура Таймс. Умов.друк.арк. 10,93. Облік.вид.арк. 11,0. Наклад 30 прим.
1-й завод 1-100. Зам. № 1149. Ціна договірна.

Видавничий центр НТУ «ХПІ»
Свідоцтво про державну реєстрацію ДК № 116 від 10.07.2000 р.
61002, Харків, вул. Кирпичова, 2